Transcription factor GATA6 and ISC gene SMOC2 in the regulation of BMP pathway in intestinal adenoma

Elisa Montagni

TESI DOCTORAL UPF - 2015

Director

Eduard Batlle Gómez, PhD

Tutor

Antonio García de Herreros Madueño, PhD

Institute for Research in Biomedicine, Barcelona

Colorectal Cancer Laboratory

INSTITUTE FOR RESEARCH IN BIOMEDICINE

IRB BARCELONA

Experimental and Life Science Department

upf. Universitat Pompeu Fabra Barcelona

Acknowledgements

The last 5 years have been so intense and significant that I have the duty to mention some of the people that mainly contributed to this experience.

First of all, I would like to thank IRB Barcelona and my supervisor Eduard for selecting me and providing me a great place to work. Thank you Eduard for receiving me in your lab, for your guidance and giving me the opportunity to conduct top quality research with amazing tools.

Many thanks to all the members of ex- and current Batlle lab (Elena, Daniele, Enza, Alex, Diana, Marta, Clara, Xavi, Carme, Mark, Sergio, Francisco, Carles, Peter, Gemma, Jordi, Gavin, Anna, Isabella, Guiomar, Elisa “grande”). I learned something from all of you. Thanks for support and patience from my first silent year to my fifth noisy year!

In particular, special thanks go to:
Francisco, for adopting me as “lab older brother” since the first day, for daily scientific speculations, for psychological support and infinite availability.
My right-hand person, Xavi, for fun, support and great team work… thanks for your competence and for taking so much care of my work.
The histology team, Marta, Begoña and Alicia, for your competence, your care and for sharing ups and downs.
Enza, for lightening the working days and for self-confidence injections… (and I’m infinitely grateful for your help when my flat was falling apart right during the thesis writing!).
Peter, for support and patience.
Gavin, for selecting me as collaborator and for training me with high throughput experiences!
Finally, during the writing of the thesis, I could count on the precious help of Eduard, Elena, Francisco, Mark and Xavi for text corrections.

Un grazie speciale va a chi ha rappresentato il “punto di partenza”, a chi mi ha iniziato a questo lavoro con passione, onestà e pazienza: la mia Sis Michi e Silvanetta.

Thanks to my “PhD studies background”: this amazing city, Barcelona, so vibrant and surprising. It made me feel home and meet lovely people.

In particular, two people shared with me each step of this intense experience: Gius and Const, thank you for your genuine friendship.

Grazie agli AMICI di sempre (Lalli, Simo, Marco, Ale, Giò, Giù e Marghe) per esserci quando serve, per sdrammatizzare, per creare un nido protettivo.

Grazie infinite al mio angelo custode: Dá, non ci sono parole per spiegare quanto siamo forti insieme. Infinito affetto, supporto, aiuto, empatia e divertimento. Ricambio dicendo che questa tesi è anche un po’ tua.

Infine grazie di cuore alla mia famiglia, a chi c’è e a chi non c’è più. Grazie per l’educazione che mi avete trasmesso e le possibilità che mi avete offerto. Grazie per la fiducia incondizionata e per dare immenso valore alle mie scelte. Grazie per spingermi sempre a guardare avanti senza recriminare il passato. Grazie per essere così forti e uniti.

Abstract

The first chapter identifies the transcription factor GATA6 as negative regulator of a transcriptional circuit dedicated to prevent the expansion of Adenoma Stem Cells (AdSCs) during the onset of colorectal cancer (CRC). In particular, we show that GATA6 directly activates the expression of the WNT pathway component *LGR5* and represses BMP levels in adenoma by competing with the β-catenin/TCF4 complex for the binding to *BMP4* enhancer regions. As a result of this mechanism, two compartments are established within an adenoma: a BMP positive differentiated cell zone and a BMP negative undifferentiated cell zone, where AdSCs reside. Genetic deletion of *Gata6* increases BMP levels in the AdSC compartment, inhibiting self-renewal and intestinal tumorigenesis. These findings represent a key contribution to understand the mechanisms that regulate tumor hierarchy and reveal for the first time the existence of a niche that protects AdSCs from BMP signals.

The second chapter focuses on the functional characterization of *Smoc2*, a novel Intestinal Stem Cell (ISC) gene. We generated genetic mouse models in order to overexpress or ablate *Smoc2* in the intestine. We found that SMOC2 acts as a BMP inhibitor in the intestine and that it is not only restricted to epithelial Stem Cells (SCs) but it is also expressed by the stroma. Although it is dispensable for normal ISC maintenance and intestinal homeostasis, high levels of SMOC2 are required for tumorigenesis. Indeed, *Smoc2* overexpression leads to spontaneous development of hamartomas and enhances adenoma formation in mice with an *Apc* mutant background; inversely, *Smoc2* deficiency decreases

tumorigenesis and prolongs survival of *Apc* mutant mice. In particular, we observed that SMOC2-mediated BMP inhibition positively affects Insulin-like Growth Factor (*Igf1*) expression in adenoma endothelial cells (ECs). Our data suggest that SMOC2 could enhance tumor-associated inflammation through BMP-mediated *Igf1* regulation in the stroma.

Resumen

El primer capítulo describe la identificación del factor de transcripción GATA6 como regulador negativo de un circuito transcripcional fisiológico dedicado a reprimir la expansión de las células madre de los adenomas (Adenoma Stem Cells o AdSCs) en el inicio de la tumorogénesis colorrectal. De manera específica, mostramos como el factor GATA6 activa directamente la expresión del componente de la ruta de WNT, *LGR5*, y también directamente reprime niveles de hormona BMP (Bone Morphogenetic Protein) a través de la competición directa con el complejo beta-catenina-TCF4 por la unión a regiones enhancer del gen *BMP4*. Como resultado de este circuito transcripcional que hemos descubierto, en los adenomas se generan dos compartimentos, una zona positiva para la señalización mediada por BMP que contiene las células diferenciadas de los adenomas, y un área negativa para BMP, donde residen y se expanden las AdSCs. La ablación genética de *Gata6* incrementa los niveles de BMPs en el compartimento de las AdSCs, inhibiendo la autorenovación de las mismas y por ende la tumorogénesis. Este descubrimiento representa una aportación clave para entender los mecanismos que regulan la jerarquía tumoral y revelan por primera vez la existencia de un nicho que protege las AdSCs de las señales de BMP.

El segundo capítulo describe la caracterización funcional de *Smoc2*, uno de los genes identificados en el laboratorio dentro del programa genético específico de las células madre del intestino (Intestinal Stem Cells o ISCs). Durante el transcurso de la tesis

doctoral, hemos generado modelos animales de ratón que permiten manipular la expresión de *Smoc2* (sobreexpresión y depleción). A través de la caracterización de estos modelos animales demostramos que SMOC2 actúa como un inhibidor de la señalización mediada por BMP el intestino, y que se expresa no solamente en las ISCs, sino también en el estroma. Si bien *Smoc2* es dispensable para la homeostasis intestinal y el mantenimiento del pool de células madre, se requieren elevados niveles de SMOC2 durante la tumorogénesis intestinal. La sobreexpresión de *Smoc2* en el epitelio intestinal da lugar al desarrollo espontáneo de hamartomas. Asimismo, aumenta la formación de adenomas en un fondo genético que presenta mutaciones en el gen supresor de la tumorogénesis intestinal *Apc*. De manera inversa, la ablación genética de *Smoc2* disminuye la formación de tumores y prolonga la supervivencia de ratones con el gen *Apc* mutado. Concretamente, hemos observado que la inhibición de la ruta de BMP mediada por SMOC2 afecta la expresión de *Igf1* (Insulin-like Growth Factor 1) en células endoteliales de adenomas. Nuestros datos sugieren que SMOC2 promueve la inflamación asociada al tumor a través de la regulación de la ruta de BMP que a su vez controla la expresión de *Igf1* en el estroma tumoral.

Preface

The body of this thesis is composed of two result chapters, preceded by an introduction and followed by discussion and conclusion sections. The experimental work was carried out in the Colorectal Cancer laboratory at the Institute for Research in Biomedicine (IRB) located at the Parc Científic de Barcelona (PCB).

The first chapter is based on a scientific article that, at the time of this thesis submission, was published in the journal Nature Cell Biology. First author of this work is Gavin Whissell who presented it in his doctoral thesis at the moment of the first submission for publication. Since then, we have been going through a long experimental revision that lasted 8 months, which I took care of. This included the planning, execution and analysis of a large proportion of the experimental work. In particular, I was involved in experiments using cell lines and primary cell cultures. This first chapter describes the identification of transcription factor GATA6 as a mediator of a transcriptional circuit that targets BMP and regulates the expansion of AdSCs. This circuit contributes to the establishment of hierarchies in adenoma, with high BMP expression defining differentiated tumor cell zones, and low BMP zones defining the SC compartment. Through repression of BMP signaling, GATA6 maintains the AdSC compartment and ensures tumor progression.

The second chapter describes my main thesis project that started five years ago. At that time, the first ISC signatures had been generated and *Lgr5* was the only gene known to specifically mark ISCs. Our laboratory had a great interest in dissecting the functions

encoded by specific SC genes. In particular, we decided to focus on SMOC2, a secreted extracellular matrix protein implicated in the regulation of BMP pathway during invertebrate development. The accumulating evidence supporting the crucial role of BMP signaling for intestinal homeostasis, led us to hypothesize that SMOC2 could be a BMP inhibitor directly secreted by the SCs to regulate BMP levels in the surrounding niche and maintain homeostasis. We demonstrated the involvement of SMOC2 in the negative regulation of BMP signaling, however its biological function emerged to be more complex than hypothesized. In fact, we observed that SMOC2 exerts pro-inflammatory and pro-tumorigenic roles in the intestine by targeting the stromal compartment. The lack of functional antibodies against SMOC2 denied us the possibility to detect the protein and its spatial range of action. To explore its function we undertook several experimental approaches, which mainly focused on the generation of different genetic mouse models and *ex vivo* primary stem cell cultures. The specific mechanism of action of SMOC2 is still currently unclear, however we hope that through the use of the tools generated during this thesis, we will soon be able to uncover the function of this gene in the intestine.

Index

Introduction

1. Adult stem cells (SCs) and tissue homeostasis

Evolution from single cell-organisms to multicellularity entailed the appearance of differently specialized types of cells and the consequent need for a hierarchical organization in order to maintain the tissue homeostasis. The concept behind tissue hierarchy involves the separation between tissue maintenance and tissue function. Hierarchy is achieved through the existence of tissue-specific pools of long-lived undifferentiated cells that maintain the tissue. These cells have the potential to generate short-lived specialized cells, which in turn exert the appropriate functions of a given tissue.

The cells responsible for tissue maintenance are termed adult SCs and they act as a repair system for the body by replenishing adult tissue. The classical definition of adult SC requires it to possess two properties: self-renewal and multipotency. Self-renewal identifies the ability to go through numerous cycles of cell division while maintaining the undifferentiated state. Multipotency refers to the ability to give rise to different types of specialized cell types.

Differentiated cells represent the major component of the tissue and exert all the required physiological functions. Yet, these cells are short-lived and need to be replenished by the SC activity in order to maintain the tissue homeostasis.

The rate of division of SCs and differentiated cells determines the turnover of the tissue. Tissues exposed to constant environmental insult, such as the intestine, skin and the hematopoietic system, have rapid cycling SC pools, whereas tissues such as liver,

muscle, pancreas and brain activate their SC population only upon severe stress.

As the SCs are generally less abundant than their progeny, they often give rise to an intermediate pool of highly proliferative cells termed transit-amplifying (TA) cells. TA cells are committed progenitors with low self-renewal capability that undergo several cycles of expansion before undergoing differentiation (**Figure 1**).

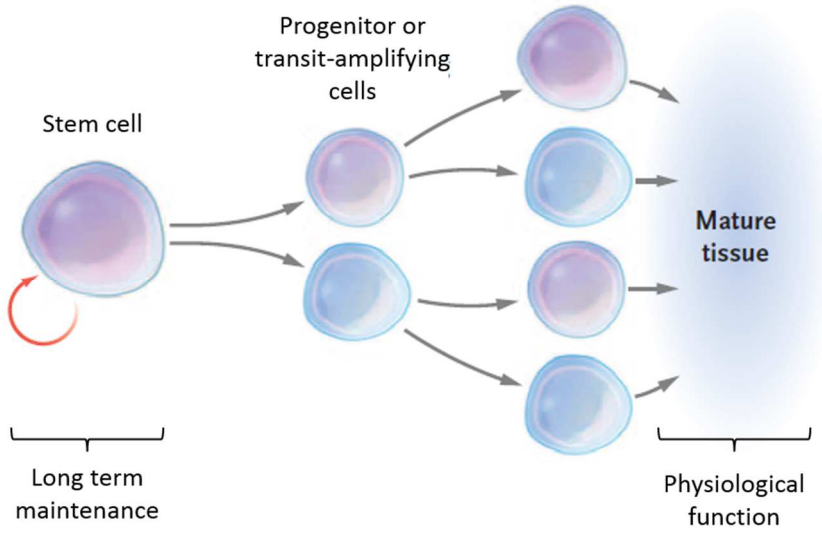

Figure 1: Schematic representation of a hierarchically organized tissue. SCs reside at the top of the hierarchy. They have the ability to self-renew and differentiate in to multiple lineages. Before differentiating into mature functional cells, the direct descendants of the SCs (progenitor cells or TA cells) undergo several rounds of division in order to expand the compartment. Adapted from (Jordan et al., 2006).

1.1 Adult SC self-renewal

1.1.1 Asymmetric and symmetric SC division

In order to accomplish self-renewal and potency, SCs can undergo asymmetric or symmetric cell division.

Upon asymmetric cell division, a SC generates one daughter cell with a SC fate and one daughter cell that undergoes differentiation (**Figure 2 A, left panel**). Asymmetric cell division implies that SCs would be unable to expand in number, an essential process during development or after injury.

Thus, there is an alternative mechanism, the symmetric cell division, that leads to the generation of daughter cells that acquire the same fate (either stem or differentiated) (**Figure 2 A, right panel**).

Both mechanisms ensure the maintenance of the stem and differentiated cell populations (**Figure 2 B**) and can be used depending on the needs of the tissue (Morrison and Kimble, 2006).

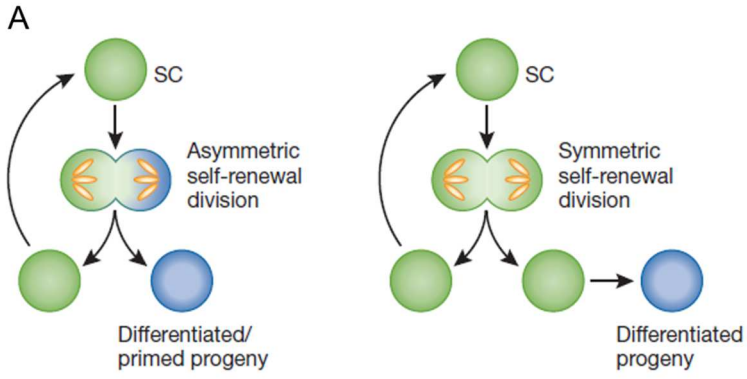

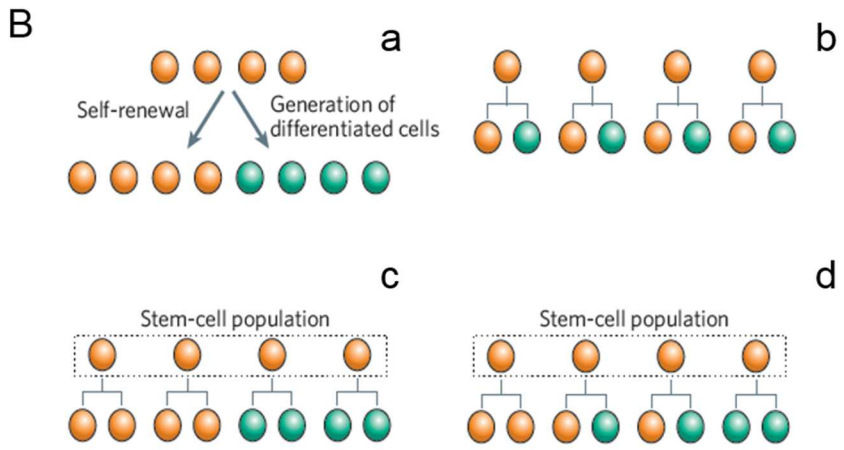

Figure 2: Asymmetric and symmetric SC division. A. In asymmetrical cell divisions, cell fate specification is coupled to mitosis and involves unequal partitioning of cellular components to the resulting daughter cells (left panel). In symmetrical cell divisions, cellular components are equally distributed to the two daughter cells that result to be identical (right panel). From (Fuchs and Chen, 2013). B. (a) SCs (orange) must accomplish the dual task of self-renewal and generation of differentiated cells (green). (b-d) Possible SC strategies to maintain a balance between SCs and differentiated progeny. From (Morrison and Kimble, 2006).

1.1.2 The SC niche

Most SCs can divide by either asymmetric or symmetric division and the balance between these two models is controlled by developmental and environmental cues that ensure tissue homeostasis.

In particular, the SC niche represents a defined anatomical compartment that provides signals to the SCs in the form of secreted and cell surface molecules that control the rate of SC proliferation, determine the fate of SC daughters, and protect SCs from exhaustion or death (Jones and Wagers, 2008; Schofield, 1978). First of all, the signals coming from the niche regulate SC self-renewal, survival and maintenance. Second, the particular spatial relationship between SCs and support cells can polarize SCs within the niche to promote asymmetric SC divisions. Moreover, adhesion between SCs, supporting stromal cells and the extracellular matrix (ECM) anchors SCs within the niche in close proximity to self-renewal and survival signals. Thus, the SC niche provides structural support, trophic support, topographical information and the appropriate physiological signals to regulate SC function in both invertebrate and vertebrate organisms (Jones and Wagers, 2008).

In general, the SC niche is composed by stromal support cells; ECM proteins that provide structure, organization and mechanical signals to the niche; blood vessels that carry systemic signals and provide a conduit for recruitment of inflammatory and other circulating cells into the niche; and neural inputs that might similarly communicate distant physiological signals to the stem cell microenvironment (**Figure 3**).

Finally, increasing evidence implicates deregulation of the SC niche as a cause of many pathologies associated with tissue degeneration (Visnjic et al., 2004), ageing (Boyle et al., 2007; Conboy et al., 2005) and tumorigenesis (Corre et al., 2007; Zhu et al., 2002).

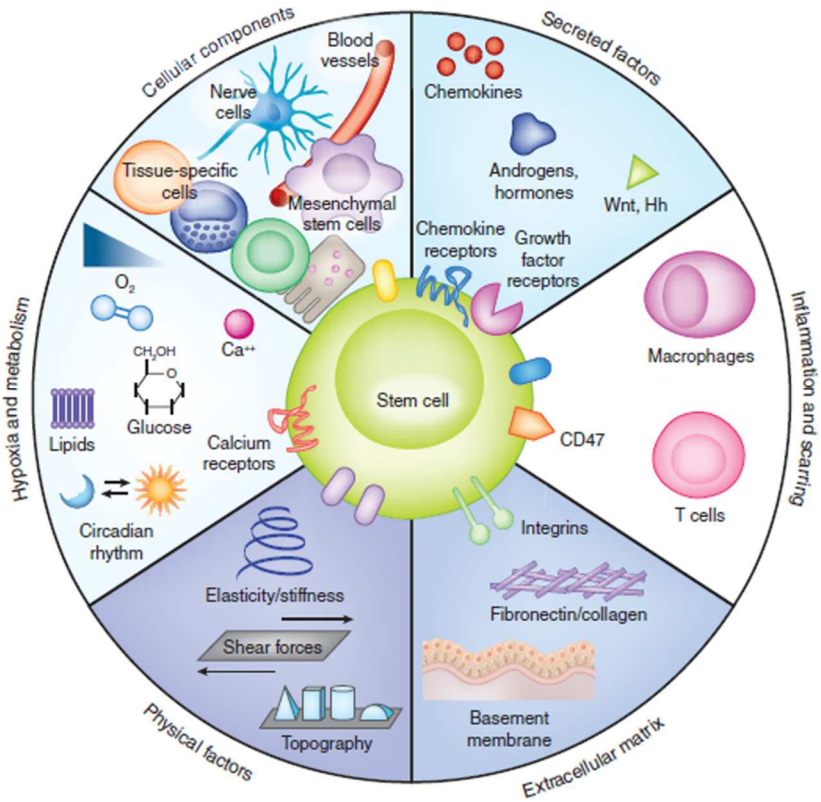

Figure 3: Components of the SC niche. The SC niche is a complex and dynamic structure that transmits and receives signals through cellular and non-cellular mediators. The niche includes different cellular components (stromal cells, immune cells and the vascular network), soluble factors, extracellular matrix, neural inputs, physical parameters and metabolic control. From (Lane et al., 2014).

1.2 Experimental strategies to determine SC populations

1.2.1 Transplantation assay

The term “stem cell” is based on the strict criterion of extensive clonal self-renewal capability. This definition derives from the hematopoietic field where *in vivo* transplantation assays are available to assess replicative potential. The concept behind this approach in based on the purification of a determined bone marrow cell population and its consequent transplantation into a host mouse that has been previously depleted of the Hematopoietic Stem Cells (HSCs) by irradiation treatment. The expected result is that only HSCs will be able to fully regenerate the bone marrow functionality for extended periods of time. This approach has been particularly useful to identify the difference between long term HSCs and short term HSCs (Ficara et al., 2008). However, similar *in vivo* reconstitution assays do not yet exist for many adult tissues and thus it is not possible to clearly prove self-renewal in those organs by this classic approach.

1.2.2 Label retention and quiescence

Label retention was once considered a hallmark of tissue SCs (Duvillié et al., 2003; Mackenzie and Bickenbach, 1985; Morris and Potten, 1994; Terskikh et al., 2012).

In order to identify label-retaining cells (LRCs), replicating DNA was labeled by administration of radioactive thymidine or Bromodeoxyuridine (BrdU). Tissues were then stained and cells that still retained their labels months or years after labeling were considered to be SCs (Potten and Hendry, 1975). This paradigm was based on the notion that SCs should persist in tissues and

divide only rarely to protect their genome. Nevertheless, recent works performed in skin and intestine have shown that LRCs are not the only SCs (Barker et al., 2007; Claudinot et al., 2005; Li and Clevers, 2010) demonstrating that quiescence and label retention are not innate properties of all tissue SCs.

1.2.3 Lineage tracing

In some rapidly regenerating tissues (most notably the intestine), clonal marking techniques can prove life-long self-renewal in the absence of transplantation and firmly establish the identity of SCs.
Lineage tracing is a technique that consists of genetically labeling a cell population and following the label in its progeny. The most utilized system for lineage tracing is based on the Cre recombinase fused to the ligand binding domain of the estrogen receptor: the Cre-ER^{T2} fusion protein. The expression of this protein is driven by a gene specific for a certain cell population (stem, progenitor or differentiated cells). Animals engineered with this allele are then treated with the ER^{T2} agonist 4-OH Tamoxifen that specifically activates the nuclear translocation of the Cre recombinase in the cells expressing the gene of interest. The reporter allele usually consists of an ubiquitous promoter followed by a transcriptional stop signal which prevents the transcription of the reporter gene. Commonly, the stop signal is a tandem of three polyadenylation sequences flanked by loxP sites. Upon 4-OH Tamoxifen treatment, the Cre is induced and the stop signal is removed allowing the expression of the reporter (**Figure 4 A**). In this experimental setting, only the population that expresses the gene driving the recombinase will be initially labeled. In the long term, all the progeny derived from the initially labeled population will also bear

the reporter expression. In particular, if the Cre is driven by a differentiation gene, no population will be labeled in the long term as the labeling will be lost as the cells die. Like the SCs, progenitor cells are often multipotent and may give rise to several different mature lineages. However, they can be distinguished from true stem cells by the fact that their clonal labeling will be transient and will not last for the life of the animal. In contrast, SCs will produce labeled offspring permanently (**Figure 4 B**). Therefore, when the labeling permanently persists in all the cells composing the tissue, it can be concluded that the gene of interest marks adult SCs.

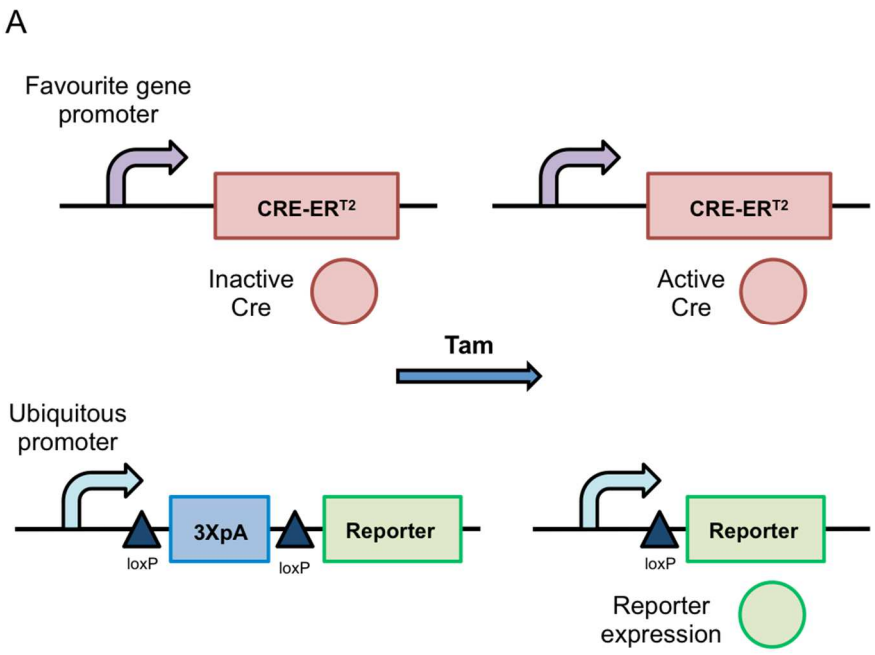

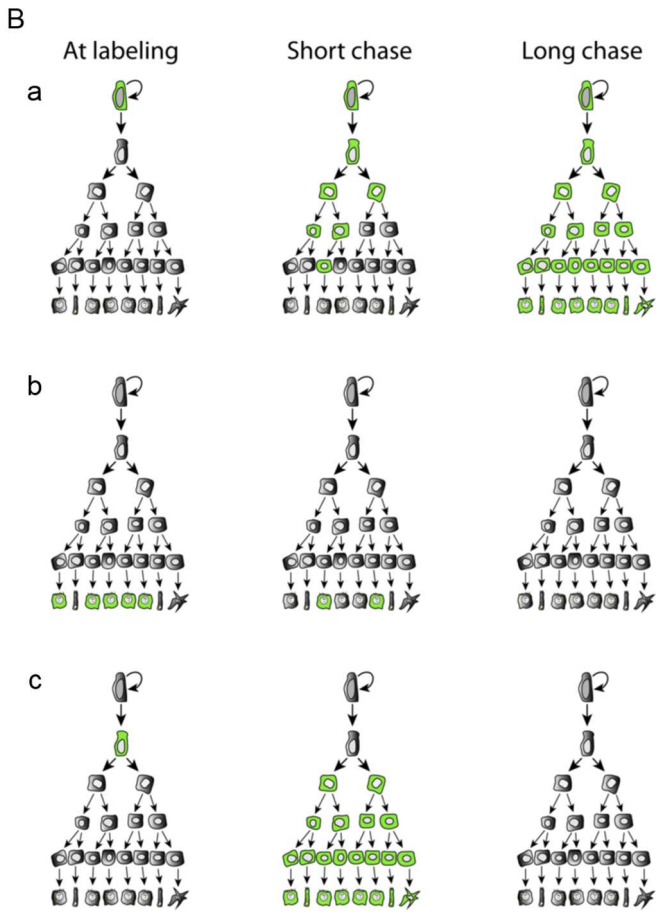

Figure 4: Schematic representation of a lineage tracing experiment. A. Components of the lineage tracing experiment based on Tamoxifen-driven Cre recombinase activation. B. (a) When the gene of interest marks SCs, all cells in the hierarchy will be permanently marked in the long term. (b) If the gene marks differentiated cells, the label will disappear as the mature cells die. (c) If the gene marks progenitor cells, the descendent lineages will be marked after a short follow up, but not after longer times. From (Grompe, 2012).

Notably in the intestine, the cells located in the crypt at the +4 position were long thought to be the true and only SCs (Potten, 1975). However, lineage tracing of cells expressing the WNT target Leucine-rich repeat containing G protein coupled Receptor 5 (*Lgr5*) clearly showed that cells at the bottom of the crypt, which are clearly distinct from the +4 cells, also act as SCs (Barker et al., 2007) (**Figure 5**). Intestinal stem cells (ISCs) will be discussed in more detail in the following sections.

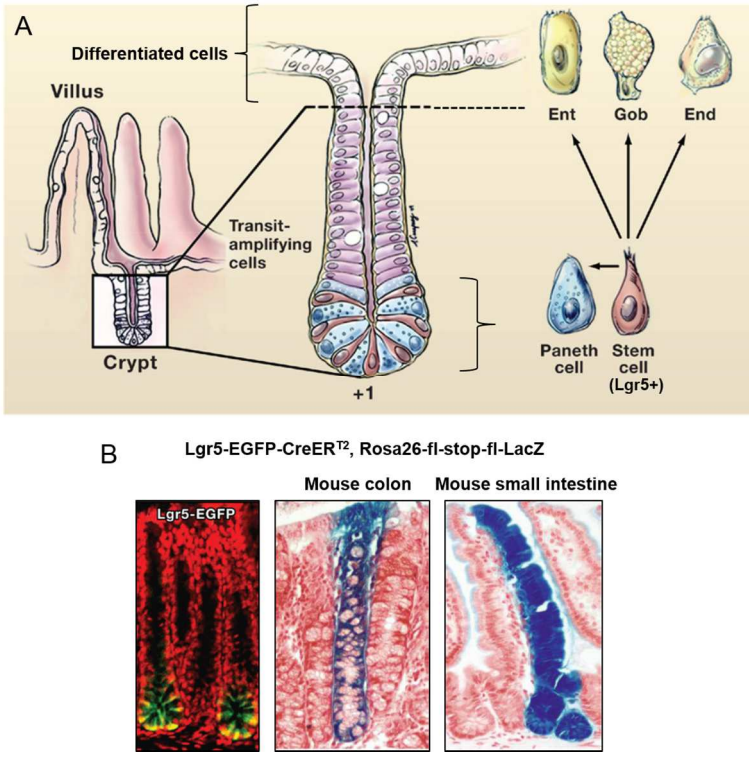

Figure 5: Lineage tracing from *Lgr5* expressing cells in mouse intestine. A Hierarchical organization of the intestinal epithelium: *Lgr5*+ cells reside at the bottom of the crypts and give rise to all the differentiated cells that populate the epithelium. B. Lineage tracing of *Lgr5*+ cells in colon and small intestine of *Lgr5-eGFP-CreERT2, Rosa26-fl-stop-fl-LacZ* mice. From (Barker et al., 2007; Fuchs, 2009).

1.2.4 Clonogenic cultures

Despite the evident advantages of the lineage tracing, the cost in resources and time of generation of these mutant transgenic mice is a limiting step of this approach.

The recent establishment of *in vitro* 3D SC culture models represents a more rapid and economic tool to assess the clonogenic potential of certain cell populations, and also to perform detailed studies on the pathways involved in the SC biology and tissue architecture. The principle behind this approach resides in the isolation and culture of the cell population of interest. SCs are commonly cultured in a 3D matrix in the presence of cocktails of growth factors and inhibitors that mimic the SC niche of the tissue of origin. Only SCs are able to sustain the culture for extended periods of time. Moreover, the 3D SC culture should allow the formation of mini-organoids composed by all the types of cells deriving from the SC and resembling the hierarchical organization of the tissue of origin (Barker et al., 2010; Dong et al., 2013; Jung et al., 2011; Sato et al., 2009, 2011a) (**Figure 6**).

The major caveat of this approach is the possibility that SCs could require unknown signals. It is plausible that the culture conditions could bias and select the growth of a subpopulation that is not representative of the SC population of origin. In this regard, the combination of *in vivo* and *in vitro* approaches is recommended.

Finally, it's worth mentioning that most of the functional approaches to study SC populations described above are based on the isolation of cells from the tissue of origin. The selection of a specific marker or combinations of markers to isolate the SCs has crucial importance and it has been a controversial field. In fact, the use of different markers can lead to the isolation of different populations

with different features, but may not necessarily enrich for SCs. In this regard, the identification of pathways and gene programs specific for certain cell populations together with the establishment of purification techniques based on Fluorescence Activated Cell Sorting (FACS) have allowed further refinement of the assays mentioned above.

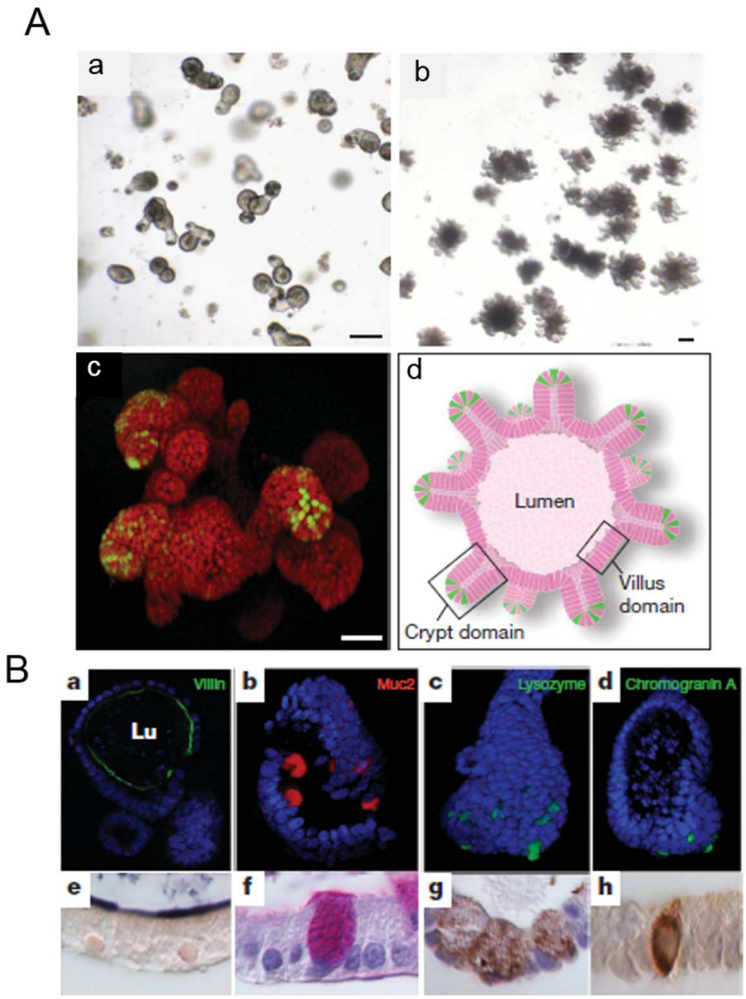

Figure 6: Establishment of an intestinal crypt culture system. A. (a-b) Single isolated crypts (left panel) efficiently form large organoids within 14 days (right panel). (c) Three-dimensional reconstructed confocal image after 3 weeks in culture. *Lgr5-GFP* stem cells (green) are localized at the tip of crypt-like domains. (d) Schematic representation of an intestinal organoid, consisting of a central lumen lined by villus-like epithelium and several surrounding crypt-like domains. B. Confocal images (a-d) and stained paraffin sections (e-h) of single intestinal SC-derived organoids reveal the presence of all the differentiated lineages. From (Sato et al., 2009).

2. The mammalian intestine as model for adult SC biology

2.1 Anatomy of the intestine

The intestinal tract is a tubular structure that connects the end of the stomach to the anus. It is anatomically and functionally divided into two main parts: the small intestine and the large intestine or colon (**Figure 7 A**). The small intestine is composed of duodenum, jejunum and ileum, and is responsible for the final steps of digestion as well as being the primary site of food uptake. The colon exerts the function of water absorption and stool compaction for excretion.

The intestinal tube is organized as concentric layers around a central lumen (**Figure 7 B**). The first layer in contact with the lumen is the mucosa or epithelium. Besides representing a barrier from mechanical and biological insults, the intestinal epithelium exerts the functions of absorption and secretion. The intestinal epithelium is monostratified and is folded into tubular crypts (crypts of Lieberkühn) that invaginate into the underlying mesenchyme. Contrary to the colon, the small intestinal epithelium also possesses finger-like structures that protrude into the lumen (villi) to maximize the intestinal surface area for absorption (**Figure 7 C**). The second layer is termed *lamina propria* and is composed of connective tissue and stromal cells. The third layer, the submucosa, contains blood vessels, nerves, lymphatic noduls and myofibroblasts. It is separated from the *lamina propria* by a thin muscle layer (*muscularis mucosae*) and is externally enveloped by a thicker smooth muscle layer, *tunica muscularis externa*, which is involved in peristaltic motions (**Figure 7 B**).

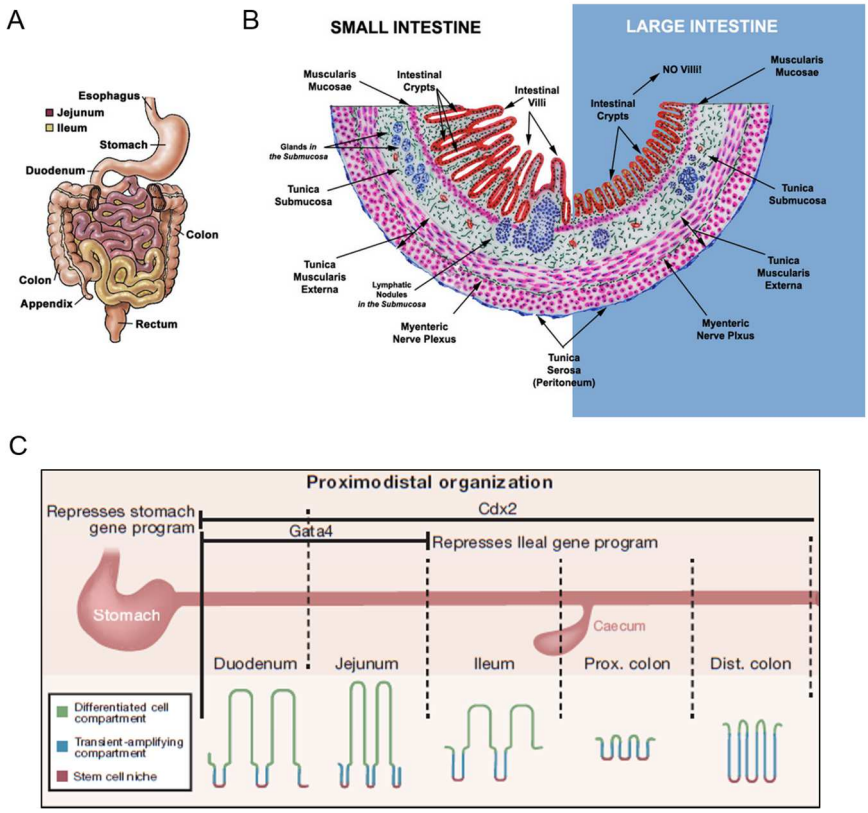

Figure 7: Anatomy of the intestinal tract. A Anatomy of the intestinal tract (http://www.yoursurgery.com/ProcedureDetails.cfm?BR=1&Proc=49). B. Representation of a transverse section of the small intestine and colon (http://www.vetmed.vt.edu/education/curriculum/vm8054/Labs/Lab19/Lab19.htm). C. Representation of the intestinal epithelium organization along the proximo-distal axis. From (Clevers and Batlle, 2015).

2.2 Self renewal in the intestinal epithelium

As mentioned before, the inner surface of the intestinal tube is lined by a simple epithelial monolayer. Cells in the monolayer are exposed to a harsh environment and thus the adult epithelium must undergo rapid renewal to maintain optimal function.

Regeneration relies in a small group of adult SCs that reside at the bottommost position of the crypts of Lieberkühn. Functional differentiated cells occupy positions close to the lumen where they are required for the main functions of the intestinal tract, absorption, compaction and excretion of intestinal contents. To maximize these functions, the intestinal tube displays distinct morphologies along the proximo-distal axis. The small intestine is arranged in crypts and villi, whereas the colon consists only of crypts (**Figure 8 A, B**).

Despite their distinctive morphologies, epithelial cell types of both the small intestine and colon are organized following a bottom-to-top axis into three compartments: the SC compartment that is located at the crypt base, the transient-amplifying (TA) compartment that occupies the middle portion of the crypts, and the differentiation zone, which expands from the top third of the crypt to the tip of the villus (**Figure 8 A, B**).

Renewal of the epithelial monolayer is a continuous process throughout the life span of an individual. Regeneration relies upon the activity of adult SCs that regularly divide to produce TA cells that are highly proliferative progenitors. The nascent TA cells divide 2-3 times and gradually commit to the absorptive or secretory cell lineages while migrating upwards towards the base of the villi

(Marshman et al., 2002). The differentiated cells continue migrating upwards along the villi until they reach the tip and die.

More than 300 million new epithelial cells must be generated daily in the small intestine to compensate for the high rate of cell death on the villi. The entire epithelial cell renewal cycle takes 3-5 days (Karam, 1999). Paneth cell turnover is the only exception. In fact, these cells are renewed every 3-6 weeks from secretory cell progenitors located at the base of the TA compartment. These progenitors mature into fully differentiated Paneth cells while following a downward migratory path to the crypt bottom (Ireland et al., 2005; Karam, 1999).

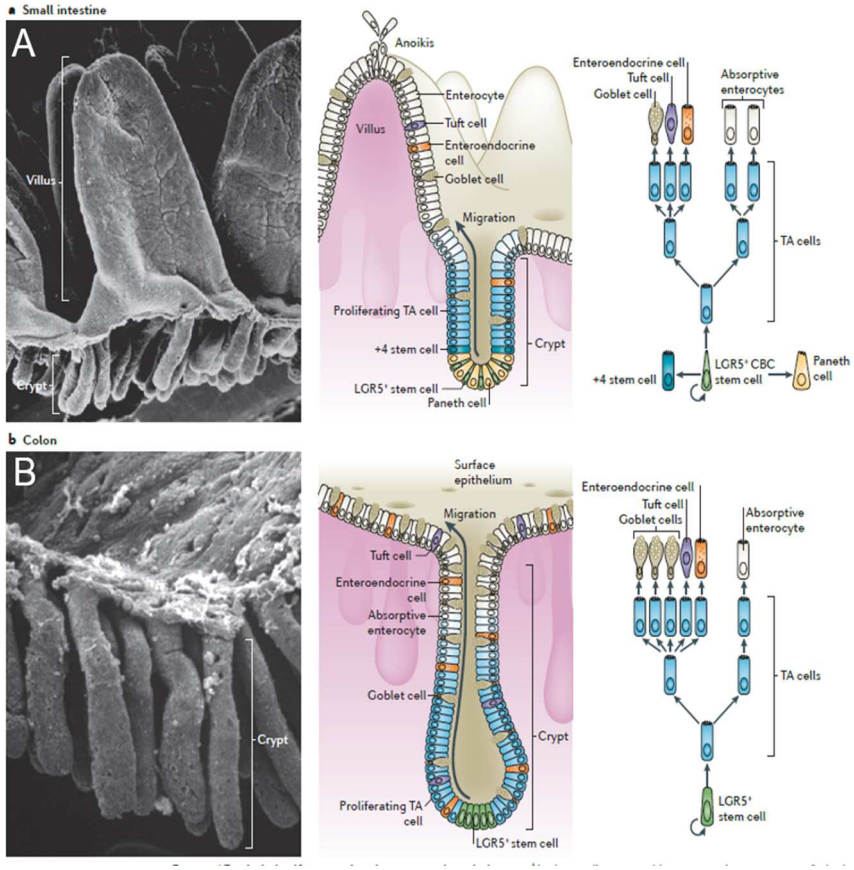

Figure 8: Epithelial self-renewal in the intestinal epithelium. A. Scanning electron micrograph of the small intestine (left panel). Longitudinal representation of the crypt-villus axis (central panel). Hierarchical organization of the intestinal epithelial cells (right panel). B. Scanning electron micrograph of the colon (left panel). Longitudinal representation of the crypt-villus axis (central panel). Hierarchical organization of the colon epithelial cells (right panel). From (Barker, 2014).

2.3 Differentiated cell types composing the intestinal epithelium

2.3.1 Cell types of epithelial origin

Seven differentiated cell types have been identified in the intestinal epithelium belonging to two main lineages, absorptive or secretory: Enterocytes, Goblet cells, Enteroendocrine cells, Paneth cells, Tuft cells, M cells and Cup cells (**Figure 9**) (Clevers and Batlle, 2015; van der Flier and Clevers, 2009; Neutra, 1998; Schonhoff et al., 2004; Takashima et al., 2013).

Absorptive lineage:

- Enterocytes (or columnar cells) constitute more than 80% of the epithelium. They are highly polarized cells carrying an apical brush border that is responsible for absorbing and transporting nutrients across the epithelium (Takashima et al., 2013).

Secretory lineage:

- Goblet cells secrete protective mucins that are required for the movement and expulsion of gut contents (Karam, 1999). The proportion of goblet cells increases from the duodenum (4%) to the colon (16%).

- Paneth cells reside at the crypt base and have a function in innate immunity since there are able to secrete granules containing specific proteins like lysozymes, antimicrobials, and defensins. Paneth cells are the only differentiated intestinal epithelial cell type that migrates downward to the crypt bottom. This compartmentalization is achieved through guidance mediated by tyrosine kinase receptors EPHB2 and EPHB3 (Batlle et al., 2002).

- Enteroendocrine cells are scattered as individual cells throughout the mucosa, representing approximately 1% of the epithelial cells. They coordinate gut functioning through specific peptide hormone secretion (Schonhoff et al., 2004).

- Tuft cells are rare cells that are believed to secrete prostanoids. These cells are characterized by Dclk1 (or Dcamkl1) gene expression (Gerbe et al., 2011; Gerbe, Brulin, Makrini, Legraverend, & Jay, 2009; Gerbe, Legraverend, & Jay, 2012).

- M cells or Microfold cells are situated over the Peyer's patches (PPs), which are intraepithelial pockets characterized by high density of antigen-presenting cells. The M cells exert an important role for the mucosa immunity since they transport antigens into the PPs (Neutra, 1998).

- Cup cells comprise up to 6% of epithelial cells in the ileum. Their function is still unknown.

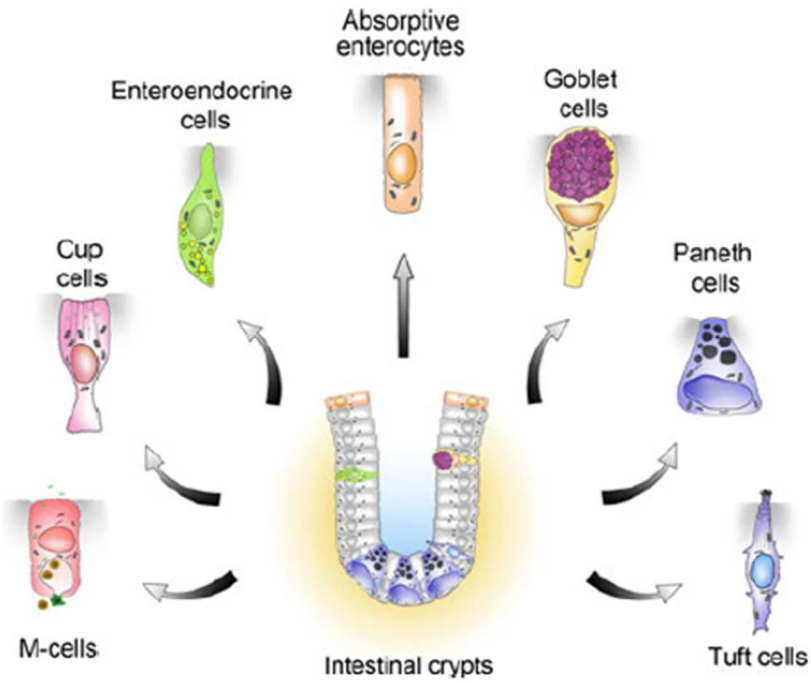

Figure 9: ISCs at the crypt bottom give rise to all the intestinal differentiated cell types. From (Gerbe et al., 2012).

2.3.2 Major cell types composing the intestinal lamina propria

The intestinal *lamina propria* (**Figure 10**) is composed of cells of mesenchymal origin, in addition to immune cells:

Mesenchymal cells:

- Myofibroblasts are cells that possess both fibroblast and smooth muscle cell characteristics, and are located in close contact with the epithelial cells. They mediate the information flow between the epithelium and the mesenchymal elements of the *lamina propria* through expression and secretion of cytokines, chemokines, growth factors, prostaglandins, and basal lamina/extracellular matrix molecules (Powell et al., 2005).

- Fibroblasts are the main component of the connective tissue. They synthesize extracellular matrix and collagen and play a critical role in tissue wound healing.

- Endothelial cells compose the intestinal microvasculature that provides oxygen and nutrients.

- Pericytes wrap around capillaries as single cells. They provide proteins to the vascular basement membrane, and communicate with the endothelial cells via paracrine signals. Together with the endothelium, pericytes contribute to angiogenesis and revascularization. Paracrine signals from pericytes can control contractility and permeability of the capillary. Pericytes and endothelial cells are in close contact in a similar way as the subepithelial myofibroblasts are with the intestinal epithelium (Bergers and Song, 2005).

- Bone marrow-derived stromal stem cells (MSCs) have been

shown to modulate the immune system through the secretion of prostaglandin E2. Additionally, they aid vasculogenesis (Powell et al., 2011).

- Smooth muscle cells of the *muscularis mucosae* are responsible for peristaltic contractions. In particular, the Interstitial Cells of Cajal (ICC) have specialized contacts with both nerves and smooth muscle cells, allowing them to relay information from nerves to muscles (Al-Shboul, 2013).

Immune cells:

- Resident Macrophages, Dendritic Cells (DC) and B/T Lymphocytes migrate in and out the tissue, providing constant immunosurveillance and antigen trafficking. These cells are normally in a resting state but, when the need arises, new monocytes and new lymphocytes are recruited from the circulation and lymphoid organs to trigger inflammation (Bogunovic et al., 2009; Smith et al., 2011).

Aside from their role as structural elements, mesenchymal cells also serve as resident sentinels that produce chemokines upon activation, initiating the recruitment of leukocytes to the site of tissue injury and inflammation (Pinchuk et al., 2007; Vogel et al., 2004).

All of these neighboring stromal cells are critical for the establishment and maintenance of the ISC niche by providing structural support and modulating the main pathways that regulate intestinal homeostasis.

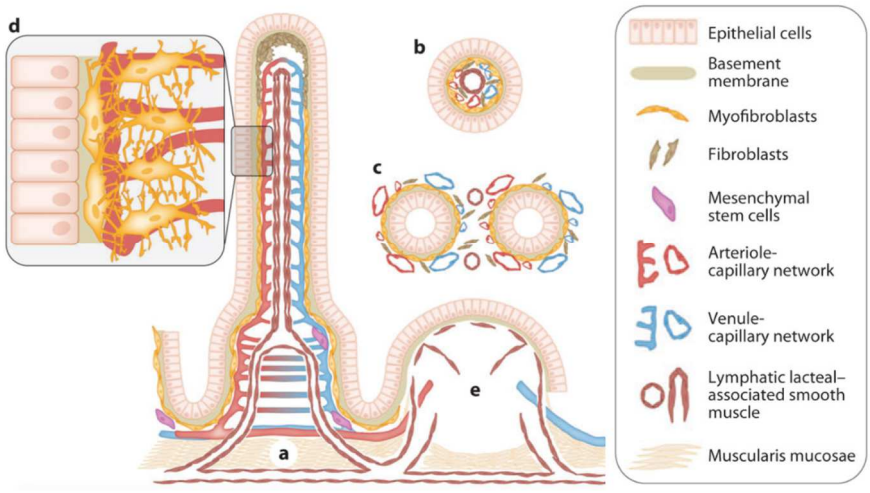

Figure 10: Epithelial and mesenchymal elements of the intestine. (a) Longitudinal representation of the crypt-villus axis showing the epithelium and the *lamina propria* composed of subepithelial myofibroblasts, pericytes of the capillaries, mesenchymal stem cells, and smooth muscle cells. Fibroblasts are shown mainly in the upper portion of the villus. (b-c) Cross sections through villus and crypts. (d) A higher-power depiction of the myofibroblasts and pericytes surrounding and supporting the capillaries. (e) A Peyer's patch with its vascular, lymphatic, and stromal elements. Lymphocytes, macrophages, dendritic cells, and polymorphonuclear leukocytes are not shown. From (Powell et al., 2011).

2.4 Signaling pathways regulating ISC homeostasis

The major pathways that regulate ISC homeostasis are: WNT, Notch, EGF and BMP/TGFβ signaling (**Figure 11**).

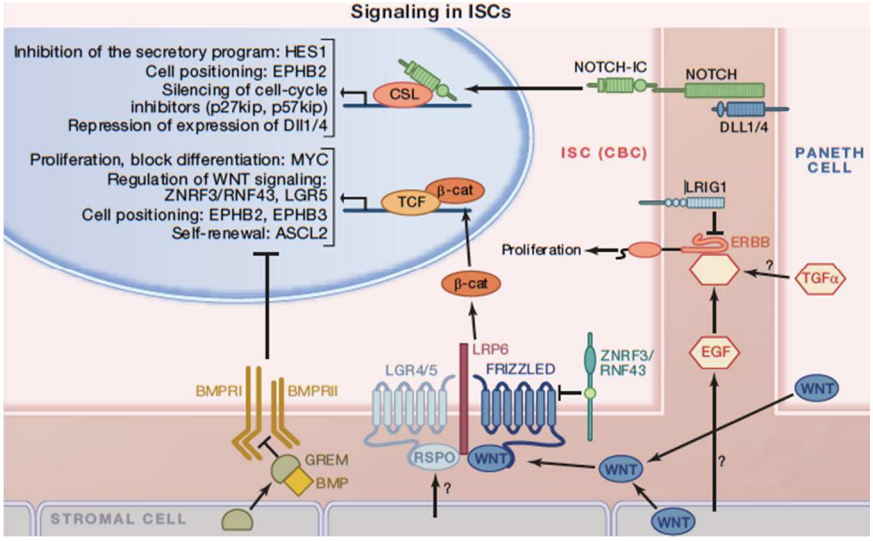

Figure 11: Major pathways regulating ISCs. A tight signaling network is established between SCs and the stroma to modulate the main pathways behind intestinal homeostasis. In particular, WNT, Notch and EGF signaling promote stemness and proliferation. On the other side, BMP signaling counteracts proliferation and promotes differentiation. From (Clevers and Batlle, 2015)**.**

2.4.1 The WNT pathway

This pathway is highly conserved throughout the animal kingdom (Clevers, 2006). The central player in the canonical WNT pathway is β-catenin. In the absence of a WNT signal, β-catenin is targeted for phosphorylation and consequent proteasomal degradation. The β-catenin phosphorylation complex consists of the tumor suppressors AXIN and adenomatous polyposis coli (APC) and the constitutively active glycogen synthase kinase 3 (GSK3) and casein kinase I (CKI). When WNT ligands signal through their Frizzled and Low-density lipoprotein Receptor–related Protein (LRP) co-receptors, the destruction complex is inactivated. As a result, β-catenin is no longer degraded and accumulates in the cell. The subsequent translocation of β-catenin into the nucleus results in the binding of β-catenin to transcription factors of the T cell factor/lymphocyte enhancer factor (TCF/LEF) family. TCF/LEF-β-catenin forms an active transcriptional complex that activates expression of target genes. In the absence of a WNT signal, transcriptional repressors like Groucho bind TCF/LEF transcription factors (Cavallo et al., 1998) (**Figure 12**).

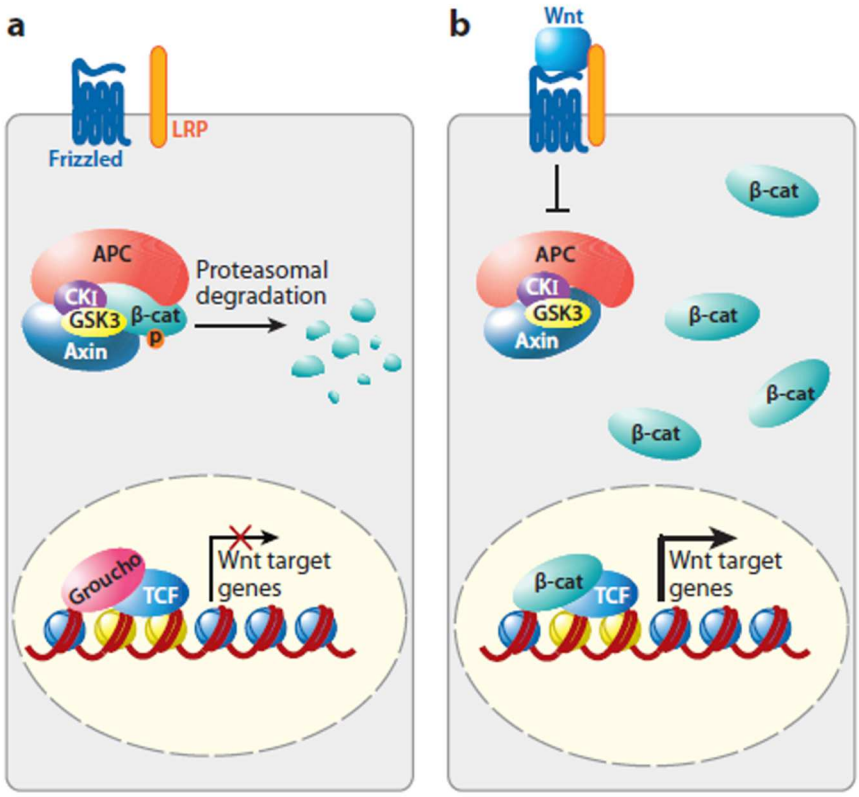

Figure 12: Components of the WNT signaling pathway. (a) In the absence of WNT stimulation, β-catenin levels in the cell are kept low through a destruction complex composed of APC, CKI, GSK3 and AXIN. This complex phosphorylates and targets β-catenin for proteasomal degradation. (b) In the presence of WNT ligands, they bind to Frizzled receptors and LRP co-receptors. Consequently, the destruction complex no longer targets β-catenin for proteasomal degradation and the β-catenin level rises, resulting in its translocation into the nucleus. Here β-catenin replaces Groucho on TCF transcription factors. Transcriptionally active β-catenin/TCF complex activates the expression of WNT target genes. From (van der Flier and Clevers, 2009).

This pathway represents the dominant force behind the proliferative activity of the intestinal epithelium as many functional studies confirm that the WNT pathway constitutes the master switch between proliferation and differentiation of the intestinal epithelial cells. In fact, a dramatic reduction of proliferative activity in the crypts has been observed upon deletion of *Tcf4* (Korinek et al., 1998), depletion of *β-catenin* (Ireland et al., 2004), and transgenic expression of the secreted WNT inhibitor Dickkopf-1 (*Dkk-1*) (Kuhnert et al., 2004). On the contrary, transgenic expression of the WNT agonist *R-spondin1* results in augmentation of crypt proliferation (Kim et al., 2005).

Besides the maintenance of proliferation, WNT signaling is also required for determining the correct cell positioning in the intestinal epithelium. This is achieved through the regulation of the distribution of the tyrosine kinase receptors EPHB2 and EPHB3, which are targets of the β-catenin/TCF complex. Genetic deletion of *EphB2* and *EphB3* generates defects in the compartmentalization of crypt cells leading to Paneth cell miss-positioning and intermingling of differentiated cells with progenitor cells (Batlle et al., 2002).

Paneth cells are a rich source of canonical WNTs (3, 6, 9b) and, interestingly, they use WNT signaling for their terminal maturation (van Es et al., 2005; Gregorieff et al., 2005; Sato et al., 2011b). The stromal niche also exerts an important role in intestinal WNT pathway regulation. Non-canonical WNTs (2b, 4, 5a, 5b) are secreted by the intestinal mesenchyme (Gregorieff et al., 2005) and subepithelial myofibroblasts support ISC growth by secreting R-spondins (Lei et al., 2014).
On the other hand, microarray analysis of micro-dissected tissue

demonstrated a stromal source for the WNT antagonists *Dkk-2*, *Dkk-3*, *Sfrp-1* and *Sfrp-2* (Li et al., 2007).
Therefore, mesenchymal cells have a key role in the regulation of WNT/β-catenin signaling, inducing this critical pathway in the stem and progenitor cells and preventing its abnormal activity in mature intestinal epithelial cells.

2.4.2 The Notch pathway

The Notch pathway plays a central function in intestinal cell fate decisions. Notch genes encode single transmembrane receptors that regulate a broad spectrum of differentiation processes during animal development (Artavanis-Tsakonas, 1999). Interaction of one of the four Notch receptors with any one of the five Notch ligands results in proteolytic cleavage of the receptor. The resulting free Notch intracellular domain (NICD) translocates into the nucleus where binds to the transcription factor RBP-Jκ (CSL or CBF1) to activate target gene transcription (Tamura et al., 1995).
Like WNT signaling, the Notch pathway is essential to maintain the crypt compartment in its undifferentiated and proliferative state. Inhibition of the Notch pathway in the intestinal epithelium by conditional deletion of the *Csl* gene or through pharmacological inhibitors results in the complete conversion of all epithelial cells into goblet cells (Milano et al., 2004). Gain of function through specific overexpression of a constitutively active Notch1 receptor in the intestinal epithelium results in the opposite effect, a depletion of goblet cells and a reduction in enteroendocrine and Paneth cell differentiation (Fre et al., 2005; Stanger et al., 2005). Thus, the Notch pathway controls absorptive versus secretory fate decisions in the intestinal epithelium.

In particular, the direct Notch target gene *Hes1* represses the expression of the transcription factor *Math1* (Jensen et al., 2000). Intestines from *Hes1* deficient animals show an increase in Paneth, goblet, and enteroendocrine cells and a decrease in absorptive enterocytes (Jensen et al., 2000; Suzuki et al., 2005). Intestinal *Math1* expression is required for commitment toward the secretory lineage because the epithelium of *Math1* mutant mice is populated only by enterocytes (Yang et al., 2001).

2.4.3 The EGF pathway

Epidermal Growth Factor (EGF) is the most described ligand of the family of EGF Receptors. These ligands exist as pro-proteins that are cleaved for their activation/secretion. When bound to their ligand, the EGFRs dimerize and transactivate their kinase domains. This active kinase domain is able to signal to several downstream effector pathways that overall result in mitogenic signals (Yarden and Shilo, 2007). In the case of the intestine, EGF is one of the major mitogens required for ISC growth (Sato et al., 2009).
LRIG1, a marker for stem and early TA cells, acts as a negative regulator of EGF signaling. Previous research has shown that genetic inactivation of this gene in mouse models leads to an increase in the size of the ISC population (Wong et al., 2012).

2.4.4 The BMP pathway

2.4.4.1 Components of canonical BMP signaling

Bone Morphogenetic Proteins (BMPs) represent the largest subgroup of the TGFβ superfamily. They account for nearly two thirds of the ligands of the TGFβ superfamily and are characterized by a high degree of promiscuity with regards to interactions between ligands and receptors (Kim and Choe, 2011; Mueller and Nickel, 2012). Dimeric BMP ligands (homo- or hetero-dimers) bind to two copies of a heteromeric signaling complex composed of BMP receptor 1 (BMPRI) and BMP receptor 2 (BMPR2) (**Figure 13**). There are five known BMP type 1 receptors: ALK1 (Acvrl1), ALK2 (ActRI), ALK3 (BMPRIA), ALK4 (ActRIb) and ALK6 (BMPRIB). Three BMP type 2 receptors have been shown to be bound by BMPs: BMPR2, ActRIIa and ActRIIb (Bragdon et al., 2011; Nohe, 2004). BMPs bind with different affinity to these receptors. The initial interaction occurs with the high affinity anchoring receptor that is the BMP type 1 receptor. Dimerization of the BMP type 1 and type 2 receptors results in the phosphorylation of the intracellular glycine/serine-rich domain (GS-box) in the BMP type 1 receptor by the BMP type 2 receptor. In the canonical BMP pathway, the activated BMP type 1 receptor recruits and phosphorylates the receptor-associated SMAD1, SMAD5 and SMAD8. Phosphorylated SMADs then form heteromeric complexes with a co-SMAD (SMAD4) and enter the nucleus where they interact with other transcription factors and regulate target gene expression such as the direct targets *ID1*, *ID2* and *ID3* (**Figure 13**) (Brazil et al., 2015).

2.4.4.2 Negative and positive regulators of BMP pathway

BMP activity can be regulated by extracellular modulators including Noggin (NOG), Gremlins (GREM1 and GREM2), Chordin (CHRD), and BMP and Activin Membrane-Bound Inhibitor (BAMBI). In particular, NOG (Groppe et al., 2002), GREM1/2 (Topol et al., 2000) and CHRD (Larraín et al., 2000) directly bind and dimerize with BMP ligands effectively blocking signal transduction upstream of the receptors (**Figure 13**). BAMBI acts as a decoy receptor as it resembles the BMP type 1 receptors but lacks the GS box. As a result, it sequesters ligands from active receptors inhibiting BMP signal transduction (Onichtchouk et al., 1999).

There are also BMP intracellular modulators such as SMAD6, SMAD7 and SMAD Ubiquitin Regulatory Factors (SMURF1 and SMURF2). SMAD6 (Imamura et al., 1997) and SMAD7 (Souchelnytskyi et al., 1998) are inhibitory SMADs as they can either mediate degradation of BMP type 1 receptors in the cytoplasm or interact with transcriptional repressors in the nucleus (Yan et al., 2009). SMAD7 blocks both BMP and TGFβ signaling, while SMAD6 acts specifically on the BMP pathway (Zhang et al., 2007). SMURF1 and 2 are ubiquitin ligases that are recruited by SMAD6 and SMAD7 to target both BMP type 1 receptors and SMAD1/5/8 for proteasomal degradation (Murakami et al., 2003). Interestingly, *SMAD6* is also a BMP target gene, denoting the existence of a feedback regulation of the pathway.

BMP co-receptors that act as positive regulators of the pathway also exist. These function by potentiating the interactions between BMP ligands and type 1 receptors. These co-receptors are Endoglin (CD105), TGFBR3 and DRAGON (Barbara et al., 1999; Kirkbride et al., 2008; Lee et al., 2008; Samad et al., 2005;

Yamashita et al., 1994)

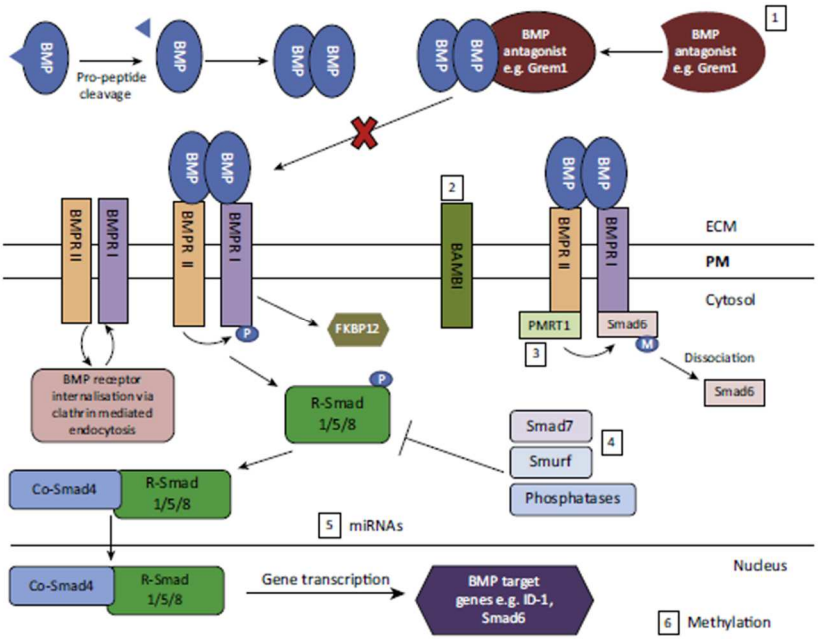

Figure 13: Components of canonical BMP pathway. BMPs are processed by peptidases to generate mature dimers. These dimers bind to two copies of the BMP type I and type II receptors, generating heterohexameric complexes that trigger the activation of the downstream pathway. Regulation of the BMP pathway can occur via binding of extracellular antagonists (1) or in the plasma membrane via the action of pseudo-receptors such as BAMBI (2). Smad1/5/8 phosphorylation can also be inhibited by SMAD6 binding to the receptors. SMAD6 can be inactivated by the action of PMRT1 methyltransferase (3). Additional regulation of BMP signaling occurs via ubiquitin ligases such as Smurf (4), via miRNA- (5) and via methylation- (6) mediated control of BMP gene expression. From (Brazil et al., 2015).

2.4.4.3 BMP pathway in intestinal homeostasis

The switch from proliferation to differentiation must be finely regulated along the crypt-villus axis. The activation of WNT, Notch and EGF pathways is required for the maintenance of the SC compartment. On the other hand, the WNT pathway must be counteracted at the top of the intestinal crypt in order to allow differentiation.

BMP signaling seems to play a major role in normal intestinal homeostasis by restricting WNT activity at the bottom of the crypts and promoting differentiation at the top (**Figure 14)**. Indeed, *in vivo* specific ablation of BMP signaling in the intestinal epithelium impairs terminal differentiation of the intestinal secretory lineage (Auclair et al., 2007), whereas full intestinal blockade of the BMP pathway results in ectopic SC niches in the villus and the eventual appearance of benign outgrowth called hamartomas (Haramis et al., 2004). As a confirmation of the above, *in vitro* ISC expansion requires inhibitors of BMP pathway such as NOG (Jung et al., 2011; Sato et al., 2009).

Active BMP signaling is commonly assessed by immune detection of phosphorylated SMAD1/5/8 and is observed within differentiated epithelial cells and throughout the stroma of the *lamina propria* (Haramis et al., 2004; Hardwick et al., 2008). *Kosinski et al.* (Kosinski et al., 2007) gave an explanation of the lack of active BMP signaling in the SC zone finding that myofibroblasts and *muscularis mucosae* cells in proximity to this zone secrete the BMP inhibitory molecules GREM1, GREM2, and CHRD1. Interestingly, a recent study has identified GREM1 as a marker of the cells of origin of the periepithelial intestinal mesenchyme, the intestinal reticular stem cells (iRSCs) (Worthley et al., 2015). A model has

been proposed in which cryptal myofibroblasts and *muscularis mucosae* cells, via localized secretion of BMP antagonists, create a low BMP gradient at the bottom of the crypt, contributing to the establishment of a SC niche where WNT signaling proceeds unopposed. As cells migrate up the crypt-villus axis, BMP levels increase, generating an environment that promotes epithelial differentiation (**Figure 14**).

In the normal intestinal epithelium the study of BMPs has mainly focused on BMP2, BMP4 and BMP7. BMP2 has been shown to be expressed in terminally differentiated epithelial cells of colon and small intestine, whereas BMP7 was localized to myofibroblasts adjacent to the most terminally differentiated epithelial cells. BMP4 expression has been detected in mesenchymal cells located around crypts and within villi in the small intestine (Batts et al., 2006; van Dop et al., 2009; Haramis et al., 2004; Hardwick et al., 2008; Kosinski et al., 2007).

In particular, Hedgehog (HH) signaling is the primary determinant of stromal BMP synthesis and thus contributes to the establishment of the epithelial SC niche (Sukegawa et al., 2000). Epithelial synthesis of HH proteins in the adult intestine is restricted to differentiated cells, ensuring a lower level of BMPs within the proliferative zone (**Figure 14**) (van den Brink, 2007; Shyer et al., 2015). Indeed, *Ihh* knockout mice display villus branching, aberrant crypt formation and increased epithelial proliferation (Kosinski et al., 2010). Conversely, constitutively active HH signaling results in premature enterocyte differentiation and depletion of SCs in the crypt (van Dop et al., 2009).

The dichotomy between WNT and BMP finely regulates the fate of

intestinal epithelial cells. Interestingly, it has been described that WNT signals in the SC niche induce nearby fibroblasts to produce the BMP antagonist GREM2, inhibiting differentiation and promoting expansion of SCs in their microenvironment (Klapholz-Brown et al., 2007). However it is not clear how BMP signaling manages to counteract the WNT-driven gene program. *Kosinski et al.* showed that treatment of normal intestinal cells with GREM1 enhanced WNT signaling, as determined by cytoplasmic and nuclear translocation of β-catenin and increased WNT target gene expression (Kosinski et al., 2007). It has also been described that BMPs can antagonize WNT signaling by stabilizing Phosphatase and Tensin homolog (PTEN), resulting in decreased AKT activity, which culminates in decreased nuclear β-catenin (Waite and Eng, 2003). Further, alternative SMAD-independent BMP signaling can occur when a BMP type 2 receptor initiates Mitogen-Activated Protein (MAP) kinase cascades (Miyazono et al., 2010).

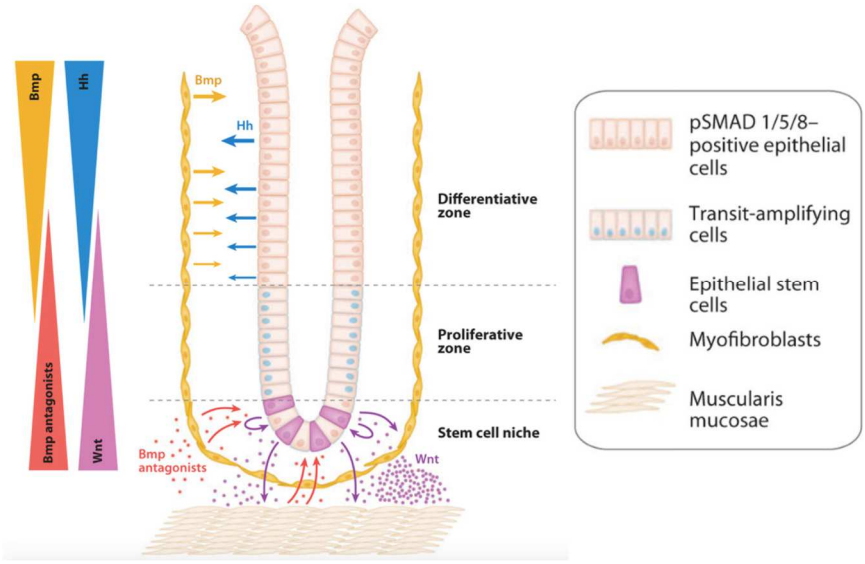

Figure 14: Epithelial-mesenchymal interactions orchestrate HH, BMP and WNT signaling in the intestinal crypt. HH proteins produced by differentiated epithelial cells trigger stromal BMP synthesis. Active BMP signaling within the differentiated compartment contributes to maintenance of the differentiated state. Within the SC niche, lack of HH signaling leads to reduced stromal BMP synthesis. Secretion of WNTs by Paneth cells and myofibroblasts, in addition to promote self-renewal of ISCs, may also induce synthesis and secretion of BMP inhibitors by the underlying myofibroblasts and *muscularis mucosae* cells. BMP antagonism within the SC niche would further enhance WNT signaling. From (Powell et al., 2011).

2.5 Identification of ISCs

2.5.1 Historical models of adult ISC identity

Over the past decades two models of ISC identity have competed: the “stem cell zone model” and the “+4 model” (**Figure 15**).

Based on pulse-chase experiments, the “stem cell zone model” proposed that the columnar cells at the base of the crypt (CBCs) were the stem cells (Bjerknes and Cheng, 1999; Cheng and Leblond, 1974). The authors described the CBCs as being actively phagocytic, clearing dead cells from the crypt base. Taking advantage of this property, they pulsed mice with tritiated thymidine and irradiated them. They observed that surviving CBCs contained radiolabelled phagosomes as a consequence of neighboring CBCs that had died. Initially, only CBCs were marked, but at later time points also the differentiated cells became radiolabelled. This was interpreted as CBCs being the common ancestor of the differentiated epithelial cells of the intestinal epithelium.

Yet for many years the accepted identity for the ISCs was that proposed in the “+4 model” (Potten, 1975). This model was based on label retaining experiments under the assumption that crypt cells capable of label retention (LRCs or label retaining cells) were ISCs. LRCs were located in the position “+4”, immediately above Paneth cells rather than at the crypt base and were also highly sensitive to ionizing radiation (Potten, 1977). This was a SC trait believed to ensure that long-lived cells would not survive DNA damage that could eventually lead to cancer.

2.5.2 Identification of Lgr5 as ISC marker and validation of CBCs as ISCs

After the cornerstone discovery that constitutive activation of the WNT pathway was the key driver of colorectal cancer (CRC) initiation (Korinek et al., 1997), the Clevers group investigated the physiological role of TCF4 by using engineered mouse models. They observed that the WNT signaling pathway was essential for the development and maintenance of the mouse intestine as *Tcf4* deficient mice died shortly after birth due to the lack of the proliferative compartment in the intestinal epithelium (Korinek et al., 1998). They also analyzed the transcriptional program driven by WNT signaling in CRC cells and observed that constitutive activation of WNT pathway leads to the initiation of tumorigenesis by the acquisition of a constitutive stem/progenitor gene program in crypt cells (Van de Wetering et al., 2002). Consequently, they analyzed in detail target genes of the WNT pathway to identify potential ISC restricted genes.

In 2007, the generation of a mouse carrying the knock-in allele *eGFP-ires-CreER*^{T2} under the promoter of the *Lgr5* gene allowed to visualize restricted *Lgr5* expression in CBC cells and to perform lineage tracing experiments *in vivo* that confirmed *Lgr5* as a *bona fide* ISC marker (see **Figure 5**) (Barker et al., 2007).
By using these *Lgr5-eGFP* knock-in mice, the Clevers group was consequently able to purify and expand single *Lgr5*+ cells *in vitro*, showing that *Lgr5*+ cells are the only clonogenic cells in the intestine (see **Figure 6**). In order to maintain these cultures, the authors confirmed that activation of WNT and EGF signaling was required, as well as the blockade of the BMP pathway (Sato et al., 2009).

2.5.3 Validation of "+4 cells" as ISCs

In support of the "+4 model", several genes have been reported to be specifically expressed in the "+4 SCs" (**Figure 15**). Although some of these markers have been validated by *in vivo* lineage tracing, many of them seem to mark epithelial cell populations distinct from the LRCs originally described by Potten. This may reflect the existence of phenotypically distinct SC populations residing at the +4 position. However, the validity of some of these candidate +4 SC markers remains controversial, due to the fact that some mouse models do not faithfully report the endogenous expression pattern of these candidate SC markers.

- BMI1: the *Bmi1* gene encodes a component of the polycomb repressor complex.
In situ hybridization (ISH) analyses documented *Bmi1* expression at the +4 position, which was confirmed using a *Bmi1-eGFP* reporter mouse model (Sangiorgi and Capecchi, 2008; Tian et al., 2012). *In vivo* experiments using a *Bmi1-ires-CreER^{T2}/R26R-lacZ* mouse model revealed the presence of a *Bmi1*+ reserve SC population harboring relatively quiescent and radiation resistant cells that can still repopulate the intestinal epithelium after ablation of *Lgr5*+ cells (Tian et al., 2012). Additionally, *in vivo* ablation of the *Bmi1*+ population led to crypt loss, and *Bmi1*+ cells could generate epithelial organoids in culture (Sangiorgi and Capecchi, 2008; Yan et al., 2012). Functionally, it has been demonstrated that BMI1 is necessary for ISC self-renewal by acting downstream of Notch (Lopez-Arribillaga et al., 2015).
However, further studies have documented a broad endogenous *Bmi1* expression throughout the proliferative zone of the crypt and

were not able to reproduce the intestinal lineage tracing of the original study (Itzkovitz et al., 2011; Muñoz et al., 2012).

- HOPX: The *Hopx* gene encodes an atypical homeobox protein and its expression at +4 position was shown with a *Hopx-lacZ* reporter mouse (Takeda et al., 2011). *Hopx*+ cells were relatively quiescent and radiation resistant, and they harbored the capacity to rapidly proliferate in response to irradiation. *In vivo* lineage tracing using a *Hopx-ires-CreER*^{T2} mouse model, showed that activation of the reporter gene at +4 position produced persistent, multipotent tracings throughout the intestine.
Comparative expression profiling of *Hopx*+ cells and their crypt base progeny showed that *Hopx*+ cell descendants have higher expression of *Lgr5* and other CBC markers. Conversely, organoid culture assays confirmed that isolated *Lgr5*+ CBCs give rise to *Hopx*+ cells *ex vivo* (Takeda et al., 2011). These observations support a model in which proliferating *Lgr5*+ SCs and quiescent *Hopx*+ SCs are located at distinct anatomical locations within the crypt and efficiently interconvert to ensure correct homeostasis. However, it should be noted that a different expression profile for *Hopx* was reported in a separate study (Muñoz et al., 2012).

- LRIG1: The *Lrig1* gene encodes a transmembrane receptor that functions as inhibitor of ERB proteins.
In vivo lineage tracing using an *Lrig1-ires-CreER*^{T2} mouse model generated long-term tracing typical of multipotent SCs throughout the small intestine (Powell et al., 2012). Reporter gene activation was mostly observed within positions +2 to +5, but also in the lower portion of the TA compartment. In the colon, *Lrig1* expression marked a small population of cells at the very bottom of the crypt, a

minority of which overlapped with *Lgr5*. The lineage tracing indicated that some but not all the *Lrig1*+ cells were cycling SCs contributing to daily epithelial homeostasis. The quiescent cells were induced to proliferate and were able to repopulate the colonic intestine following irradiation. An independent study also documented *Lrig1* as being expressed in a broad gradient, with extensive overlap with *Lgr5*+ CBC stem cells (Muñoz et al., 2012). These *Lrig1*+ cells were also shown to be actively proliferating.
Functionally, the *Lrig1* intestinal knockout showed crypt hyperplasia after birth with the expansion of the *Lgr5*+ compartment. This was linked to deregulated *ErbB* expression in the SC compartment.
Collectively, these studies suggest that LRIG1 regulates ERBB signaling in ISCs. However, its broad expression gradient in the crypts of the small intestine disqualifies it as a specific ISC marker.

- TERT: it is a catalytic subunit of the telomerase enzyme.
Elevated telomerase expression is considered to be a SC feature that protects against replication-induced senescence.
Using *Tert-GFP* reporter mice, predominantly quiescent *Tert*+ cells were detected at +4 position (Breault et al., 2008). *In vivo* lineage tracing showed that a small fraction of *Tert*+ crypt cells were cycling SCs contributing to daily epithelial homeostasis in both small intestine and colon (Montgomery et al., 2011). The other quiescent *Tert*+ cells could be activated after epithelial damage.
However, other studies detected TERT expression and telomerase activity in all proliferative cells of the crypt, with highest levels within *Lgr5*+ SCs (Itzkovitz et al., 2011; Schepers et al., 2011). This fits better with the idea that such elevated telomerase activity would probably benefit the highly proliferative *Lgr5*+ SCs.

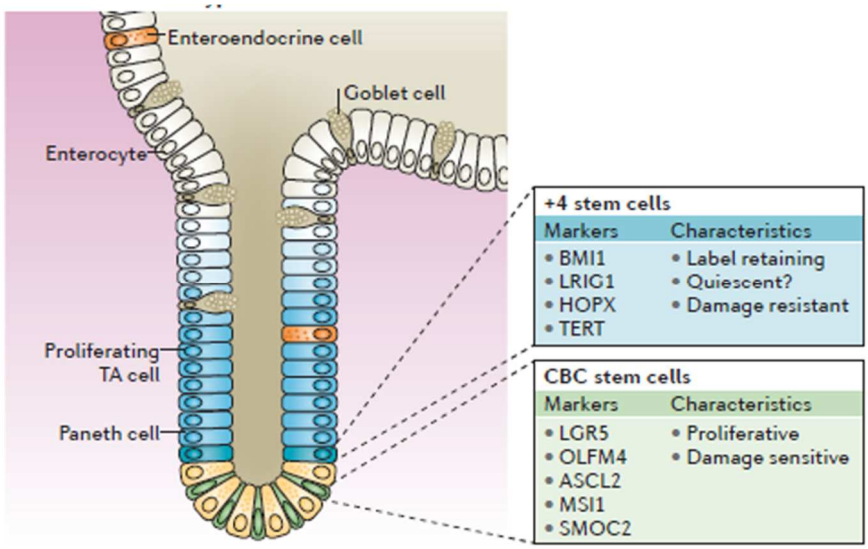

Figure 15: CBC stem cells and +4 stem cells. Summary of markers and characteristics defining CBC SCs and +4 SCs according to up to date studies. From (Barker, 2014).

2.5.4 Intestinal plasticity and models of epithelial regeneration

Despite all of the current tools, the true identity of adult ISCs is still controversial.

It has been demonstrated that *Lgr5*+ CBC cells ensure intestinal epithelial homeostasis under physiological conditions (Barker et al., 2007) (**Figure 16 A**). However, it has also been shown that the intestine can survive short-term loss of CBCs *in vivo*, suggesting the co-existence of distinct ISC pools in the niche or the ability of committed cells to be reconverted to SCs (Tian et al., 2012).

In order to reconcile opposing views, the "plastic model" for ISC identity has been proposed. This model suggests the existence of an ISC niche composed of a pool of active SCs (CBCs), involved in daily epithelial homeostasis, and a pool of quiescent "reserve" SCs that can be activated upon injury (**Figure 16 B, C**).

Reserve ISCs can be identified within *Bmi1*+ cells, since *in vivo* lineage tracing of *Bmi1*+ cells, following *Lgr5*+ CBC cells ablation, showed that *Bmi1*+ cells can repopulate the *Lgr5* SC pool (Tian et al., 2012). Nevertheless, *Bmi1*, as well as other "+4 markers", have been reported to have a broad expression pattern throughout the proliferative compartment of the crypt (Muñoz et al., 2012).

An alternative view considers the ability of progenitor (TA) cells to re-acquire SC identity upon loss of the *Lgr5*+ population (**Figure 16 B, D**). Indeed, *in vitro* experiments have demonstrated that exposure to WNT3A efficiently re-converted *Lgr5*- TA cells to *Lgr5*+ SCs (Sato et al., 2011b).

This model is supported by a separate study where histone *H2B-YFP* (yellow fluorescent protein) was used to identify and isolate LRCs in the small intestine. Authors observed a pool of LRCs presenting a mixed phenotype as they expressed markers of

Paneth cells, enteroendocrine cells, *Lgr5* and +4 SC markers. Under physiological conditions, these cells acted as progenitors of Paneth and enteroendocrine cells. Upon irradiation-induced damage, these LRCs were converted to cycling multipotent SCs contributing to epithelial regeneration (Buczacki et al., 2013) (**Figure 16 B, D**). As these LRCs were characterized as being a subpopulation of *Lgr5*+ cells and the intestinal epithelium is able to survive to *Lgr5*+ SC ablation, a further *Lgr5*- SC population should exist. An independent study suggested that Paneth cells (Roth et al., 2012) exhibited this capability although this observation was not confirmed in the study performed by *Buczacki et al.* The colonic epithelium, deprived from Paneth cells and LRCs, is also still able to survive acute *Lgr5*+ cells ablation, strongly suggesting the existence of a further *Lgr5*- SC population.

In particular, *Van Es et al* have shown that Notch ligand Delta-like1 (DLL1) positive cells residing at the +5 position physiologically represent the progenitors of the secretory lineage. Following *Lgr5*+ cells ablation, *Dll1*+ cells can convert into multipotent *Lgr5*+ cells and contribute to the regeneration of the epithelium (van Es et al., 2012) (**Figure 16 B, D**).

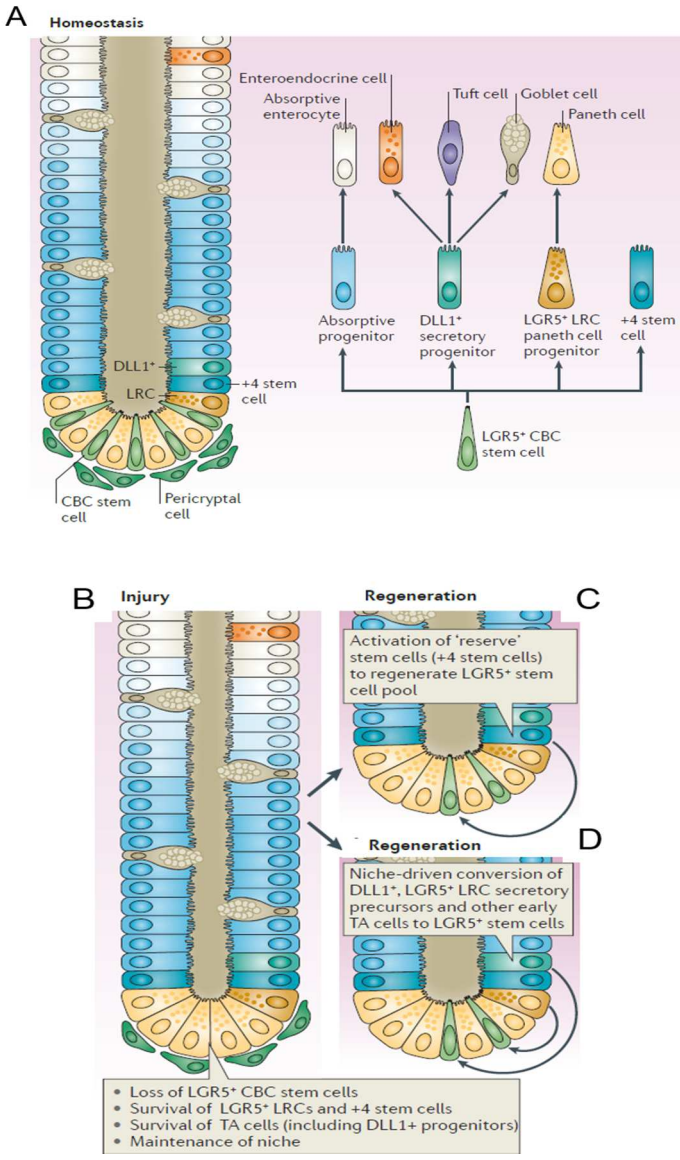

Figure 16: Model for intestinal epithelial regeneration. In this model, CBC cells are responsible for daily epithelial homeostasis (A) whereas more quiescent “reserve” SCs (+4 cells) can be activated following injury (B and C). This model also proposes that cells residing in lower positions of the TA compartment can acquire SC identity to ensure correct epithelial homeostasis in case of loss of the other SC populations (D). From (Barker, 2014).

3. Colorectal cancer (CRC)

3.1 Epidemiology of CRC

CRC is one of the most prevalent tumors being the second most diagnosed cancer worldwide in women and the third in men. Respectively, it is estimated to be the fourth and third most deadly cancer in women and men (www.cancer.gov).

North America and Europe are among the areas with the highest incidence rate. Moreover, CRC incidence rate is alarmingly increasing in Spain and other nations with historically low rates of CRC (Jemal et al., 2011).

More than 90% of all cases occur in individuals older than 50 years. Beside the older age, risk factors include high fat, alcohol or red meat intake, obesity, lack of physical activity and smoking (Watson and Collins, 2011).

3.2 TNM staging and disease management

The 5 year survival rate of CRC patients is related to the tumor stage at time of diagnosis, that to date is still the most robust predictor of clinical outcome (**Figure 17**).

The staging system is referred to the TNM (Tumor extent, Nodal involvement and presence of Metastases) system.

Stage 0 is the earliest detectable non-invasive malignant lesion and is confined to the mucosa layer. The only difference between stage 0 and I is that a stage I CRC has broken the mucosa layer, but has not penetrated the muscle layer. Both stage 0 and stage I CRCs are surgically resected and no adjuvant therapy is usually indicated. These patients have low risk of relapse and a survival rate of 90%.

Stage II CRCs display invasion through the muscle layer, the serosa and/or adjacent tissue. The treatment involves the resection of a portion of the colon (colectomy) and the use of chemotherapy alone or in combination with other drugs. These patients have a survival rate around 70%.

Stage III includes CRCs that have invaded the nearby lymph nodes but not distal organs, yet. The treatment includes resection of the local lymph nodes, colectomy and combined therapies.

The major cause of death in patients with CRC at stage II and III is disease relapse that can occur even years after the end of the therapy. Relapses occur in form of metastasis (preferentially in liver and lungs) and are due to the presence of disseminated cells that survived therapy.

Stage IV CRCs are large, invasive tumors that at the time of diagnosis have already disseminated to distant organs. When the tumors are unresectable, due to large metastasis or multiple metastases, the treatment involves a combination of therapies to shrink the tumor burden prior surgery. This may be followed by further drug combination treatments post-surgery. Tumors with incurable metastatic lesions are subjected to palliative treatments to improve the quality of life of the patient. Stage IV patients have a survival rate lower than 8%.

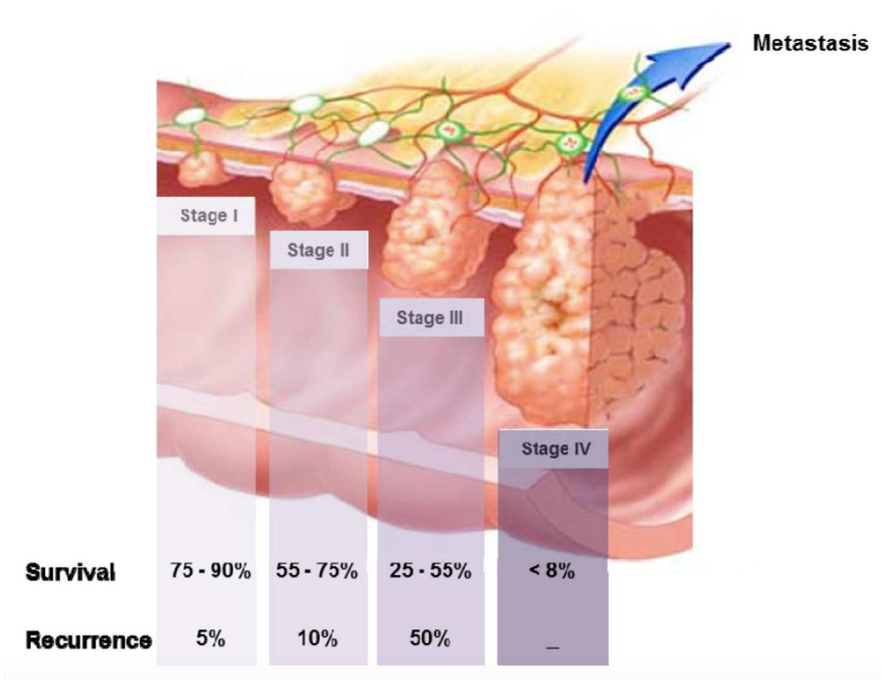

Figure 17: Overview of American Join Committee on Cancer TNM staging (7th ed.) for CRC. Survival and recurrence rate of the different stages of CRC.

3.3 Pathogenesis and genetics of CRC

Approximately 75% of patients with CRC acquire the disease sporadically, whereas around 25% of individuals with CRC have some family history suggesting a hereditary contribution (Burt, 2010).

The vast majority of CRCs are initiated by the uncontrolled growth of colon epithelial cells that give rise to glandular clusters called adenomas (**Figure 18**). Once an adenoma has acquired sufficient genetic aberrations to become malignant it is referred to as an adenocarcinoma, which is the most common type of CRC (95%). The progression from a benign lesion to a fully malignant CRC is a process that requires many years (Vogelstein, 1996). In particular, genetic characterization of various stages of CRC allowed Fearon and Vogelstein to propose a model of CRC progression based on the acquisition of successive genetic alterations (Fearon and Vogelstein, 1990) (**Figure 18**). This model suggests that colon tumors are formed due to progressive accumulation of genetic alterations and that, although a preferred sequence of these mutations exists, the kind of mutations is the determining factor of tumor biology rather than the order in which the mutations appear.
The earliest detectable lesions are aberrant crypt foci (ACF), which are usually associated with aberrant activation of the WNT signaling pathway. In 80% of the cases loss of function mutations in the tumor suppressor gene APC can be found (**Figure 18**). The pre-malignant lesions characteristically acquire further mutations through chromosomal instability (CIN). Over time, rapidly proliferating adenomas acquire further somatic mutations and progress toward malignancy. Most commonly, these further mutations hyper-activate key pro-tumorigenic pathways (KRAS,

BRAF, PI3K), and block tumor suppressor pathways (TGFβ/BMP, P53, PTEN) (Fearon and Vogelstein, 1990; Markowitz and Bertagnolli, 2009) (**Figure 18**).

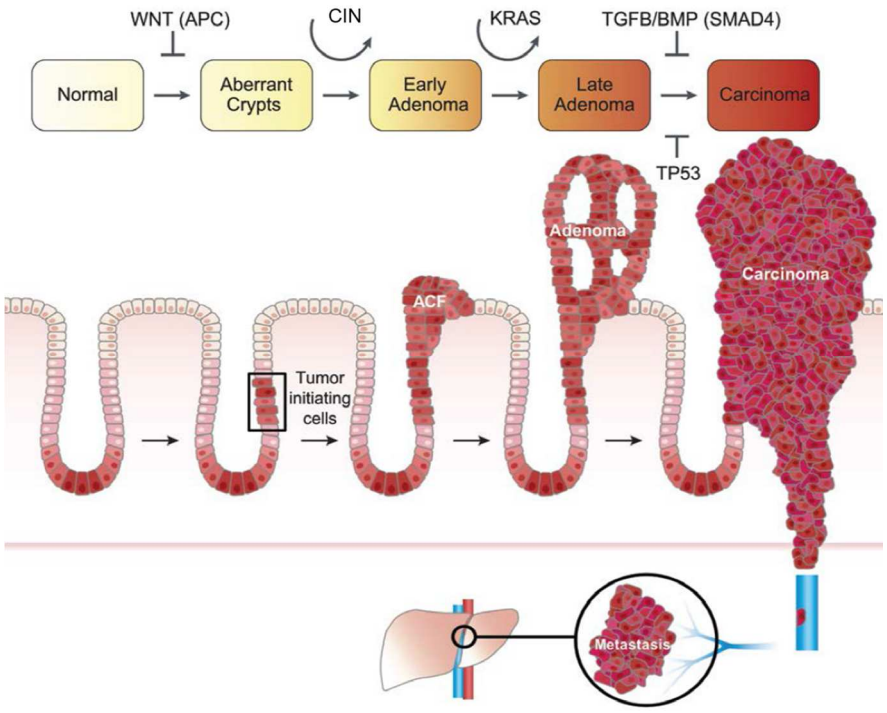

Figure 18: CRC progression. A Schematic representation of the major genetic events and tissue alterations leading to the acquisition of malignancy. Adapted from (Fearon and Vogelstein, 1990; Hardwick et al., 2008) and Batlle lab ©.

As previously mentioned, the mutations can be inherited or acquired.

75% of the cases of CRC are sporadic, which suggests a strong influence of the environment and ageing on promoting CRC (Kinzler and Vogelstein, 1996). Supporting the relevance of these two factors is the data that 65% of the cases are diagnosed in developed countries.

The remaining 25% of CRCs show hereditary components but only 5% of them are caused by known genetic mutations. The study of this kind of tumors has provided important mechanistic insights that have improved our knowledge about CRC initiation and progression.

- Familial adenomatous polyposis (FAP): is a hereditary syndrome characterized by the formation of hundreds benign polyps in the colon of the patients. As a consequence, patients are at high risk of developing CRC (Kinzler and Vogelstein, 1996). Genetic studies revealed the presence of inactivating mutations in one *APC* allele in the germline of most patients. Over time, as the wild-type *APC* allele is stochastically inactivated, the WNT pathway becomes deregulated leading to constitutive activation of β-catenin/TCF complex and to the appearance of polyps (Kinzler and Vogelstein, 1996).

- Hereditary non-polyposis colon cancer (HNPCC), also referred as Lynch Syndrome: is an autosomal dominant pathology that also enhances CRC risk (Kinzler and Vogelstein, 1996). The genetic analysis of these patients led to the identification of mutations in DNA repair genes *MLH1* and *MSH2*. This leads to microsatellite instability and the consequent generation of mutations in genes with nucleotide repeated sequences such as, amongst others, β-

catenin. Activating mutations in β-catenin also lead to constitutive activation of β-catenin/TCF activity.

- Juvenile Polyposis (JP): these patients possess germline mutations in either *BMPR1A* or *SMAD4*, thus affecting BMP and/or TGFβ pathways (Hardwick et al., 2008). Unlike FAP and HNPCC, JP patients develop cists filled polyps surrounded by non-dysplastic epithelium and abundant stroma (Daniels and Montgomery, 2007; Gammon et al., 2009). These lesions are called hamartomatous polyps and eventually can progress to adenomatous polyps. Thus, this autosomal dominant disease increases the risk of developing CRC (Brosens et al., 2007).

Loss of function mutations in *PTEN* have been found in patients with Bannayan Riley Ruvalcaba Syndrome (BRRS) and Cowden Syndrome (CS), which are even more rare polyposis syndromes characterized by the development of hamartomas (Edelman and Eng, 2010). A link between BMP and PTEN has already been proposed (Waite and Eng, 2003).

It has become increasingly clear that the mechanisms involved in these rare hereditary syndromes also participate in the development of sporadic CRC. Indeed, around 85% of sporadic CRCs present mutations in components of the WNT signaling pathway whereas about 10-15% displays defects in the DNA damage repair machinery.
On the other hand, it has been speculated that the TGFβ/BMP pathway could have a more prominent role during later stages of tumor progression, during the transition from benign status (adenoma) to malignant status (carcinoma) (Hardwick et al., 2008).

3.4 WNT pathway alterations in CRC and the connection to SC biology

As mentioned before, the WNT signaling pathway is the most commonly mutated pathway in CRC and the first and only genetic alteration observed in the earliest lesions. The genetic program driven by the β-catenin/TCF transcription complex in CRC was deciphered by generating CRC cell lines where the blockade of β-catenin/TCF activity could be induced. By studying the expression of a set of putative WNT target genes in mouse and human tissues, it was observed that both early CRC lesions and stem/progenitor cells of normal intestinal crypts expressed a similar genetic program, suggesting the acquisition of a stem/progenitor cell phenotype during tumorigenesis (Batlle et al., 2002; Van de Wetering et al., 2002).

WNT target genes are highly upregulated in CRC (Batlle et al., 2005; Van der Flier et al., 2007). Among them, *MYC* oncogene regulates downstream expression of a large subset of genes (Van de Wetering et al., 2002). Supporting this notion, *Myc* ablation is able to rescue the phenotype imposed by *Apc* deletion in mice (Sansom et al., 2007).

3.4.1 Identification of the adenoma stem cell (AdSC) hierarchy

Further to the identification of *Lgr5*+ ISCs, the Clevers group also identified the cells of origin of intestinal cancer (Barker et al., 2009). By deleting *Apc* either in ISCs or in their progeny (TA and differentiated cells), in genetic mouse models, they observed that only deletion of *Apc* in *Lgr5*+ ISCs resulted in the formation of adenomas, whereas *Apc* deficiency in *Lgr5*- cells mainly generated small aberrant crypt foci. This result suggested that *Lgr5*+ ISCs

represent the cells of origin of intestinal cancer (Barker et al., 2009).

Of note, despite nuclear β-catenin and *Myc* expression (hallmarks of active WNT signaling) are homogeneously distributed in the adenoma mass, only few cells residing at the base of adenoma glands retained *Lgr5* expression, suggesting the presence of an AdSC compartment and a hierarchical organization.

To explore this hypothesis, the Clevers group performed lineage tracing experiments from *Lgr5*+ cells in *Apc* null mice using the multicolor *Rosa26R-confetti* tracing allele (Schepers et al., 2012). Upon a first tamoxifen induction and consequent activation of the Cre recombinase in *Lgr5*+ cells, the confetti reporter recombines in a random fashion adopting one of the four possible fluorescent colors. Every active color remains associated to a silent color that can be activated upon a second induction of tamoxifen, resulting in a color switch (re-tracing) (**Figure 19 A**). Following 24 days of re-tracing, the newly labeled *Lgr5*+ cells reconstituted the adenomas and all cell types within it (**Figure 19 B**).

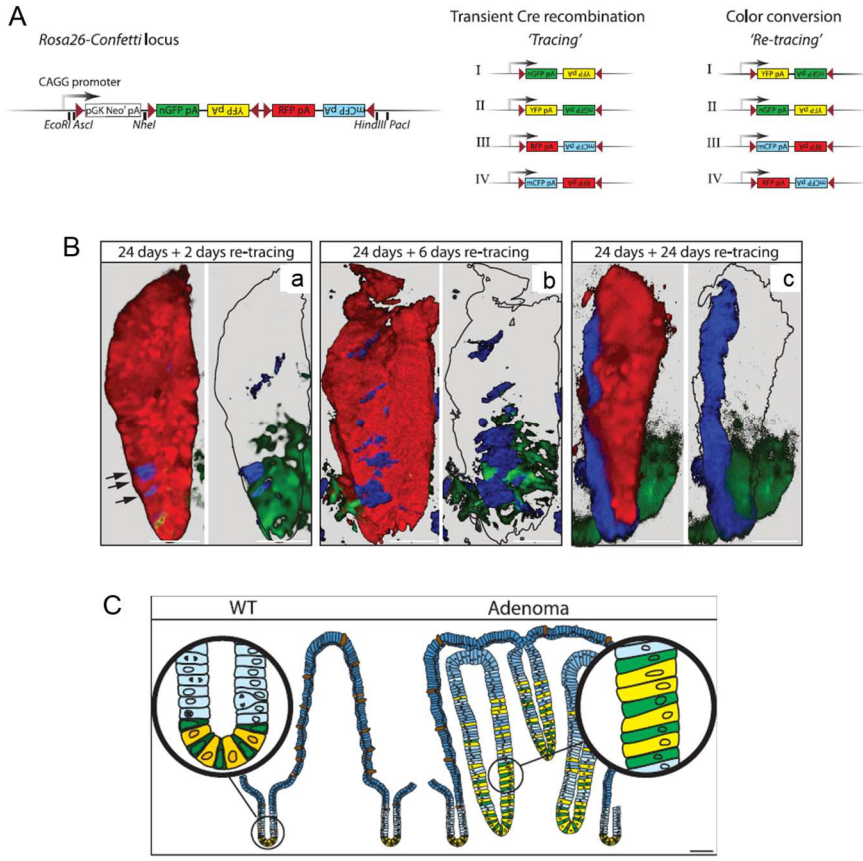

Figure 19: Lineage tracing from adenoma *Lgr5*+ cells. A. Possible outcomes of *Rosa26-Confetti* locus after the first tamoxifen induction (tracing) and the second tamoxifen induction (re-tracing). B. 24 days-adenoma shows a few *Lgr5*+ newly labeled cells (blue) 2 days after re-tracing (a). The newly labeled cells start repopulating the adenoma (b) and fully repopulate it after 24 days of re-tracing (c). *LGR5-EGFP* cells are shown in green. C. Adenomas maintain a hierarchical organization despite the SC compartment is expanded. *Lgr5*+ cells still reside at the bottom of adenoma gland intermingled with paneth cells. From (Schepers et al., 2012).

A different group identified Doublecortin-like kinase 1 (DCLK1) as a specific marker of AdSCs, but not normal ISCs (Nakanishi et al., 2013). They performed lineage tracing of *Dclk1*+ cells and observed that *Dclk1* marked post mitotic tuft cells in normal intestine, as already reported (Gerbe et al., 2009). Nevertheless, in adenomas, *Dclk1* marked a small proportion of *Lgr5*+ cells that could generate all the adenoma cell types. Targeted depletion of *Dclk1*+ cells from adenomas using an inducible diphtheria toxin allele resulted in adenoma collapse. The surrounding normal tissue remained unaffected (Nakanishi et al., 2013).

3.4.2 Colorectal cancer stem cells (CRC-SCs)

In the last two decades, the modern molecular genetics have allowed the identification of several genomic alterations as driving forces of tumor initiation and progression (Hanahan, 2000). These findings led to the proposal of the “clonal evolution model” that states that any cell clone within the tumor has the same potential to sustain the tumor, depending on the stochastic acquisition of genetic mutations that would give a selective advantage to grow. Thus, this model assumes that cells with the same genotype potentially have the same ability to sustain the tumor and the clonal evolution is explained as a stochastic process determined by the environment and driven by the competition between cell clones.

Nevertheless, in 1994 a study showed for the first time the presence of heterogeneity within genetically identical tumor cells. The authors purified cell subpopulation from human acute myeloid leukemia (AML) and observed that only one subpopulation was able to initiate and sustain the tumor when injected in immunocompromised mice (Lapidot et al., 1994). These findings

suggested the presence of a hierarchical organization in AML. In the follow-up study, the group demonstrated that these tumor initiating cells (TICs) retained the same gene program of hematopoietic stem cells (Bonnet and Dick, 1997).

These pioneer studies led to the proposal of the “cancer stem cell model” that states that the tumor, as well as the normal tissue, is hierarchically organized. Therefore, only a subset of cells retaining self-renewal ability and multipotency can sustain the tumor growth. Remarkably, this model identifies the cancer stem cells as real relevant therapeutic targets.

Since these initial studied performed in AML, other evidence has accumulated that supports the existence of a hierarchical organization in breast tumor (Al-Hajj et al., 2003; Liu et al., 2010), melanoma (Boiko et al., 2010; Schatton et al., 2008) and brain tumor (Chen et al., 2012).

The first studies showing evidence supporting colorectal cancer stem cells (CRC-SCs) were published in 2007 (Dalerba et al., 2007; O’Brien et al., 2007; Ricci-Vitiani et al., 2007). These studies identified CD133 and CD44 as markers of colon tumor initiating cells upon transplantation in immunodeficient mice. Yet, these analyses lack a deep investigation of these markers in the context of normal intestinal biology and it was unclear if they just segregated for a subset of aggressive tumor subpopulation, or if they really identified a cancer population at the base of the tumor hierarchy reminiscent of normal SCs. The above reasons and the inconsistency with follow-up studies (Kemper et al., 2010; Merlos-Suárez et al., 2011) disqualified these molecules as CRC-SC markers.

Due to the current lack of a good antibody against LGR5, our group identified an alternative ISC marker that could allow SC isolation from both mouse and human intestine. In particular, in 2011, we isolated human colon SCs and mouse small intestine SCs by using the receptor tyrosine kinase EPHB2 (Jung et al., 2011; Merlos-Suárez et al., 2011).

EPHB2 plays a crucial role in intestinal crypt cell positioning and migration as knockout mice for this receptor, or its ligand *EfnB1,* display loss of normal and tumor cell compartmentalization (Batlle et al., 2002; Cortina et al., 2007). In order to guide the crypt cell compartmentalization, WNT signaling drives EPHB2 expression along the crypt axis following a decreasing gradient from the bottom to the top (Batlle et al., 2002).

In normal intestine, isolated EPHB2^{high} cells from human colon expressed a similar gene program to that of mouse ISCs and strongly overlapped with the previous described signature of mouse *Lgr5*+ cells. Moreover, EPHB2^{high} cells could be expanded *in vitro* for extended periods of time maintaining multipotency (Jung et al., 2011).

In CRC, EPHB2^{high} cells were still enriched in ISC genes and identified a population of undifferentiated cells at the bottom of the tumor glands that possessed tumor initiation capability when injected into immunocompromised mice (Merlos-Suárez et al., 2011). This study demonstrated that CRC maintains a hierarchical organization that resembles that of the normal intestinal epithelium (**Figure 20**). Within the tumor, only the subset of cells retaining the ISC gene program was able to sustain the tumor, the CRC-SCs. Indeed, the expression level of ISC genes in CRC correlated with poor prognosis.

In the absence of a good commercial antibody for LGR5, EPHB2 represents the best marker, to date, to isolate normal and cancer ISCs, of both human and mouse origin.

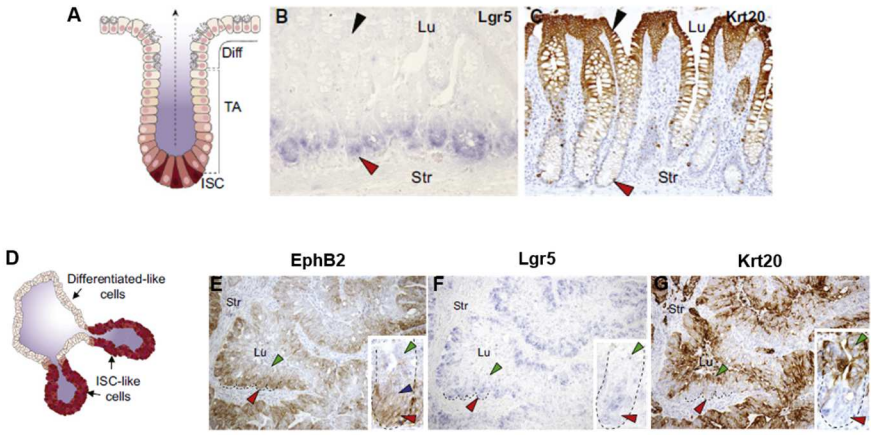

Figure 20: CRC resembles the hierarchical organization of normal intestine. A. Schematic representation of cell hierarchical organization in normal intestinal crypts. B. *LGR5* ISH identifies SCs at the base of the crypts. C. KRT20 immunohistochemistry (IHC) shows the differentiated cells at the top of the crypts, close to the intestinal lumen. SC and differentiation compartments are mutually exclusive in normal intestinal epithelium. D. Schematic representation of cell hierarchical organization in intestinal tumor glands. E. EPHB2 IHC shows decreasing expression gradient from the bottom to the top of tumor glands, identifying CRC-SCs (EPHB2^{high}), tumor TA cells (EPHB2^{medium}) and tumor differentiated cells (EPHB2$^{low/neg}$). F. *LGR5* ISH identifies the CRC-SC compartment. G. KRT20 IHC shows the differentiated compartment. SC and differentiation compartments are mutually exclusive in CRC. Black and green arrows indicate the differentiation compartment. Red arrows indicate the SC compartment. Blue arrow indicates the tumor proliferative compartment (EPHB2^{medium}). Str: stroma. Lu: lumen. From (Merlos-Suárez et al., 2011).

3.5 BMP pathway in CRC

As discussed in section 3.3, germline mutations in the BMP components *BMPR1A* and *SMAD4* lead to the formation of hamartomatous polyps (**Figure 21, bottom scheme**). This link is supported by a study conducted by the Clevers group where they demonstrated that silencing of BMP in the intestine by transgenic over-expression of *Noggin* in epithelial cells, resulted in the formation of Juvenile Polyposis-like polyps (Haramis et al., 2004).

Since epithelial BMP silencing is not enough to achieve this phenotype (Auclair et al., 2007), it has been suggested that juvenile polyps may develop through the so-called “landscaper mechanism” where an abnormal stromal microenvironment leads to neoplastic transformation of the adjacent epithelium. Two studies have demonstrated that specific mesenchymal BMP silencing, in fibroblasts and T cells respectively, leads to the formation of hamatomatous polyps (Beppu et al., 2008; Kim et al., 2006).

On the other hand, a study reported that the human Hereditary Mixed Polyposis Syndrome (HMPS), which is characterized by colon tumors of mixed morphology, is caused by a duplication of the *GREM1* locus resulting in ectopic epithelial expression of this BMP inhibitor (Jaeger et al., 2012). A recent follow-up study performed in mouse models confirmed that epithelial expression of GREM1 disrupts the homeostatic intestinal gradients, promoting the acquisition of SC properties in the *Lgr5*- compartment (Davis et al., 2015).

Although a debate exists regarding the locus driving Cre recombinase expression in the abovementioned studies to achieve specific BMP silencing in the stroma, it is clear the importance of BMP depletion in the development of hamartomas, regardless of

the compartment (epithelial or stromal) used to ablate it.
Interestingly, genetic alterations of the *BMPR1A* locus occur predominantly in the stroma of JP patients, whereas *SMAD4* mutations involve mainly the epithelium (Brosens et al., 2007).

In addition to JP patients, components of the BMP pathway (mainly *SMAD4* and *BMPR2*) have been found mutated in 70% of sporadic CRCs (Kodach et al., 2008). Histopathological analysis of adenoma and adenocarcinoma samples indicated that loss of BMP signaling preferentially occurs in the adenoma to carcinoma transition (Kodach et al., 2008) (**Figure 21, upper scheme**). This suggests a tumor suppressive role for BMP signaling during tumor progression rather than at tumor initiation, similarly to what has been described for TGFβ. Of note, since SMAD4 is a common component of TGFβ and BMP signaling pathways, the role of BMP in CRC has been historically understated in the literature.

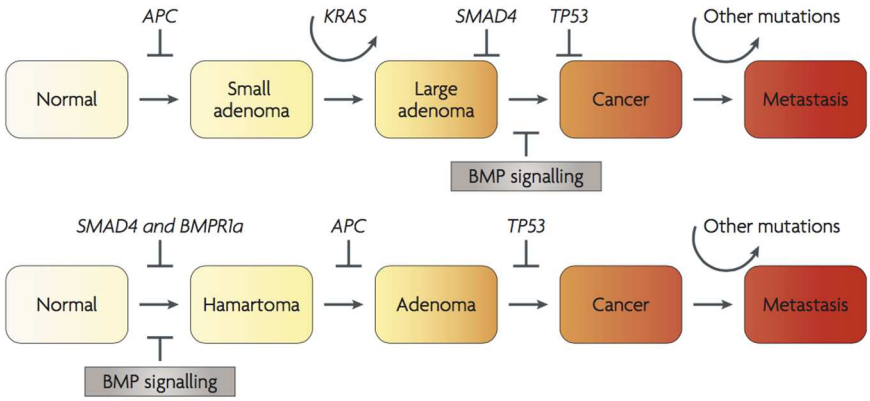

Figure 21: BMP pathway in adenoma to carcinoma progression. In sporadic CRC, blockade of BMP signaling is one of the molecular alterations involved in the acquisition of malignancy and the transition from adenoma to carcinoma (upper scheme). In JP patients, early loss of BMP signaling leads to the development of benign lesions (hamartomas) that predispose to loss of *APC* and adenomatous transformation (bottom scheme). From (Hardwick et al., 2008).

Strengthening the role of BMP in CRC, Genome Wide Association Studies (GWAS) of CRCs have identified four low-risk susceptibility variants mapping in genomic regions located near the locus encoding for the BMP pathway components *SMAD7*, *GREM1*, *BMP2*, *BMP4* and *BMP7* (Slattery et al., 2010; Tomlinson et al., 2011).

Importantly, BMP deregulation in CRC has also been detected at epigenetic level. Two studies performed in CRC cell lines and primary tumors reported that the promoters of *BMP2* and *BMP3* are hyper-methylated and consequently silenced in a high percentage of CRCs (Kodach et al., 2011; Loh et al., 2008). Indeed, treatment of CRC cell lines with statins, which are DNA methyltransferase (DNMT) inhibitors, re-activated BMP and induced tumor cell differentiation (Kodach et al., 2011).

Another study showed that BMP4 treatment of isolated CRC-SCs induced differentiation and increased response to chemotherapy by activating canonical pSMAD1/5/8 dependent- and non-canonical PI3K/PTEN dependent-BMP pathways. Only SMAD4-defective tumors, also harboring phosphoinositide 3-kinase (PI3K) activating mutations or phosphatase and tensin homolog (PTEN) loss of function mutations, were not responsive to BMP4 treatment (Lombardo et al., 2011).

4. GATA transcription factors

The transcription factors of the GATA family share two zinc finger domains that mediate not only the DNA binding through the core consensus sequence A/T GATA A/G, but also the interaction with other proteins (Maeda et al., 2005; Merika and Orkin, 1993). With a few exceptions, GATA1, GATA2 and GATA3 are mainly expressed in the hematopoietic system (Orkin, 1998), whereas GATA4, GATA5 and GATA6 are termed endodermal GATA factors (Kelley et al., 1993; Laverriere et al., 1994; Morrisey et al., 1996).

In general, GATA factors are broadly expressed in many tissues and can regulate cell expansion in addition to cell specification and differentiation, playing an essential role in determining cell fate.

Indeed, deregulation of GATA factors can lead to developmental disorders. In particular, *Gata3* null mice are embryonic lethal and display defects in hematopoiesis, spinal cord formation and show growth retardation (Pandolfi et al., 1995). *Gata4* ablation is early embryonic lethal due to defects in heart formation (Kuo et al., 1997; Molkentin et al., 1997). *Gata5* null mice are born with abnormalities in the genitourinary tract of females (Molkentin et al., 2000), whereas *Gata6* deficient mice die before gastrulation (Koutsourakis et al., 1999; Morrisey et al., 1998).

4.1 GATA factors in intestinal homeostasis

The study of GATA factors in intestine has been mainly focused on GATA4 and GATA6. These two factors are co-expressed in adult duodenum and jejunum. However, they present a different distribution in the ileum where GATA4 is expressed in differentiated cells of the villi and GATA6 in proliferative crypt cells and also in

mucous-secreting cells (Beuling et al., 2011; Bosse et al., 2006). In the colon, GATA6 is the only GATA factor expressed.

Given that *Gata4/6* constitutive knockout mice are lethal before birth, some groups have investigated their role in adult intestine by generating conditional knockout alleles in mice. Intestinal *Gata4* conditional knockout results in a shift of intestinal segment identity along the cefalocaudal axis (Beuling et al., 2010; Bosse et al., 2006). Loss of *Gata6* in adult intestine leads to defects in proliferation, migration and differentiated cell maturation (Beuling et al., 2012).

4.2 GATA factors in cancer

Given their important role in determining cell fate specification, GATA factors are involved in in the development of many human malignancies.

GATA1 is mutated in patients affected by Megakaryoblastic Leukemia (Wechsler et al., 2002). *GATA3* can harbor several mutations in breast cancer (Usary et al., 2004) and it has been involved in T cell lymphoma (Nawijn et al., 2001).

The abovementioned different expression of GATA4 and GATA6 in the ileum has suggested a potential oncogenic role for GATA6 and a tumor suppressive function for GATA4. Surprisingly, although *GATA4* and *GATA5* are not expressed in normal colon, they have been found silenced in cell lines and primary samples of CRCs through hyper-methylation of their promoters. Methylation did not correlate with CRC staging, suggesting that methylation could be an early event during disease progression. Consistently, *GATA4* and *GATA5* over-expression in CRC cell lines impaired proliferation and migration (Hellebrekers et al., 2009). On the other hand, high

levels of GATA4 correlate with poor prognosis in ovarian tumors (Anttonen et al., 2005), indicating that the role of GATA factors during tumorigenesis is context-dependent.

Similarly, a tumor suppressor role for GATA6 in astrocytoma has been proposed (Kamnasaran et al., 2007), yet *GATA6* upregulation has been detected in 50% of pancreatic carcinomas (Fu et al., 2008; Kwei et al., 2008). Moreover, GATA6 is highly expressed in the majority of CRC cell lines, adenomas and adenocarcinomas. In this context, GATA6 has been proposed to promote cell invasion by regulating urokinase plasminogen activator gene and also to prevent apoptosis by silencing 15-Lox-1 gene (Haveri et al., 2008; Shureiqi et al., 2007).

5. SPARC related modular calcium binding 2 (SMOC2)

5.1 SMOC2 is a novel member of the BM-40 protein family

SMOC2 is the last characterized member of the BM-40 protein family (Vannahme et al., 2003). These proteins are secreted extracellular matrix proteins sharing an extracellular calcium-binding (EC) domain and a follistatin-like (FS) domain (Vannahme et al., 2003) (**Figure 22**).

BM-40, also known as secreted protein acidic and rich in cysteine (SPARC) or Osteonectin, was the first member to be isolated originally from bone and subsequently found in a variety of other tissues (Lane and Sage, 1994; Termine et al., 1981). SPARC is the best characterized member of the family and it has been reported to participate in the regulation of cell-matrix interactions, influencing bone mineralization, wound repair and angiogenesis. In particular, *Sparc* deficient mice develop cataracts, and severe osteopenia (Delany et al., 2000; Gilmour et al., 1998; Yan et al., 2002). These mice also display defects in wound healing and in tissue remodeling (Basu et al., 2001; Bradshaw et al., 2002; Sangaletti et al., 2011; Savani et al., 2000).
In vitro experiments showed the ability of SPARC to inhibit cell adhesion, spreading and proliferation and to regulate the expression of proteins involved in matrix turnover (Brekken and Sage, 2000).

In general, the extracellular matrix (ECM) is a collection of extracellular molecules secreted by cells that provide structural and biochemical support to surrounding cells.
In particular, ECM proteins facilitate the communication between the cells and their microenvironment by directly binding to cell

surface integrins and receptors, or by mediating the binding of other growth factors (Bornstein, 2009). Thus, the ECM proteins can be involved in several physiological processes (cell migration, adhesion, proliferation, differentiation) (Engler et al., 2006) as well as pathological events (wound healing and fibrosis) (Schultz and Wysocki, 2009; Wight and Potter-Perigo, 2011).

The BM-40 protein family also includes SC1/hevin, QR1, tsc36/Flik/FRP, testican-1, -2, -3, and SMOC1 (**Figure 22**).
Interestingly, SMOC1 and SMOC2 represent a distinct subgroup of the family, as they share a common domain organization built from one FS domain, one EC domain, two thyroglobulin-like (TY) domains and a novel SMOC-specific domain without known homologs (Vannahme et al., 2003) (**Figure 22**).

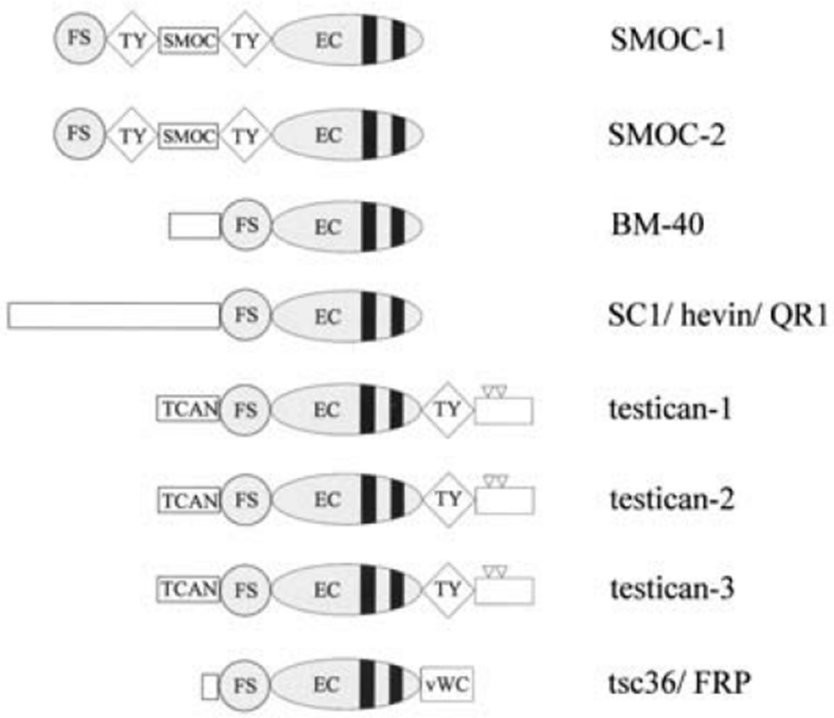

Figure 22: Domain organization of BM-40 proteins. FS: Follistatin-like domain. TY: Thyroglobulin-like domain. SMOC: Smoc protein-specific domain. TCAN: Testican-specific domain. EC: Extracellular calcium binding domain. Triangles indicate putative glycosaminoglycan-attachment sites. Black bars within the EC domain indicate calcium binding EF-hands motifs. From (Vannahme et al., 2003).

5.2 SMOC2 biological functions

Expression analysis from different tissues of adult mice indicates a broad expression of *Smoc2*. Indeed, *Smoc2* expression has been detected in brain, thymus, lung, heart, liver, kidney, spleen, testis, ovary and skeletal muscle (Vannahme et al., 2003).

Although its structural domains have been characterized, SMOC2 biological functions are still unknown.

In vitro analysis of its ability to bind to blood serum proteins showed that SMOC2 has strong binding affinity with vitronectin which is involved in cell adhesion, migration and proliferation and binds several extracellular and membrane proteins such as integrins (Novinec et al., 2008).

Experiments conducted with cell lines showed that SMOC2 promotes attachment and migration of keratinocytes (Maier et al., 2008), potentiates angiogenic effects of other growth factors (Rocnik et al., 2006), and promotes growth factor-induced fibroblast cell cycle progression through integrin linked kinase (ILK)-mediated induction of cyclin D1 (Liu et al., 2008).

SMOC proteins are abundant in vertebrates and SMOC-like proteins containing a conserved TY-EC domain pair were found throughout the animal kingdom (Novinec et al., 2006).

In *Drosophila Melanogaster*, the ortholog of *SMOC2* gene is called *Magu* (or *Pent*) and is required for germline stem cell renewal through the positive regulation of BMP pathway (Li and Tower, 2009; Zheng et al., 2011). In *Drosophila*, the BMP ortholog is called Decapentaplegic (*Dpp*) and represents an important morphogen regulating wing formation. In this context, Magu acts as an expander of Dpp gradient during disc growth (Hamaratoglu et al., 2011).

The *Xenopus* ortholog of human *SMOC1/2* (*XSmoc1*) is essential for correct development and acts as a BMP antagonist. Interestingly, XSmoc1 still antagonizes BMP activity in the presence of a constitutively active BMP receptor, indicating a mechanism of action downstream of the receptor. Authors provided evidences that XSmoc1 counteracted BMP activation at the level of SMAD1/5/8 phosphorylation, suggesting the existence of independent SMOC signaling (through a specific receptor or integrins) that converges with BMP signaling downstream the activated receptors (Thomas et al., 2009).

These studies provide clues supporting the involvement of SMOC proteins in the regulation of the BMP pathway. Moreover, in contrast with other known extracellular BMP regulators that directly bind to BMP ligands, SMOC proteins could be signaling and interfering with BMP through other receptors. Supporting this hypothesis, the above mentioned study by *Liu et al.* showed that SMOC2 interacts with αvβ1 and αvβ6 integrins and maintains ILK activity.

In another study, knockdown of *Smoc2* in *zebrafish* showed teeth abnormalities reminiscent of the human phenotype of oligo- and microdontia. Moreover, *Smoc2* depletion affected the expression of three major odontogenesis genes: *dlx2*, *bmp2*, and *pitx2* (Bloch-Zupan et al., 2011).

On the other hand, *Smoc1* null mice showed defects in ocular and limb development related to disturbed expression of genes involved in BMP signaling (Okada et al., 2011).

5.3 SMOC2 in cancer and diseases

At the moment we started this thesis, only one study reported SMOC2 implication in cancer. In particular, the authors showed that mutagenic hyper-activation of the small GTPase Ran induced oncogenic transformation through *SMOC2* up-regulation (Milano et al., 2012).

SMOC2 is also implied in other human diseases like Oligodontia and Vitiligo. Recessive oligondontia is linked to homozygous loss-of-function mutation in the *SMOC2* locus (Alfawaz et al., 2013; Bloch-Zupan et al., 2011). Other studies point to *SMOC2* as a risk locus for Vitiligo, a common autoimmune skin disorder (Alkhateeb et al., 2010; Birlea et al., 2010).

Results

Chapter 1: The transcription factor GATA6 enables self-renewal of colon adenoma stem cells by repressing BMP gene expression

Whissell G, Montagni E, Martinelli P, Hernando-Momblona X, Sevillano M, Jung P, et al. The transcription factor GATA6 enables self-renewal of colon adenoma stem cells by repressing BMP gene expression. Nat Cell Biol. 2014 Jul 22;16(7):695–707. DOI: 10.1038/ncb2992

Chapter 2: Functional characterization of the novel ISC gene *Smoc2*

1. Identification of the ISC gene *Smoc2*

Besides LGR5, the secreted protein Olfactomedin-4 (OLFM4) and transcription factor achaete scute-like 2 (ASCL2) are other widely used ISC markers (Schuijers, van der Flier, van Es, & Clevers, 2014; Laurens G. van der Flier et al., 2009b).
To date, *Ascl2* is the only ISC specific gene that has shown to be essential for ISC maintenance, as its conditional ablation leads to rapid loss of ISCs, whereas its overexpression results in ISC expansion (van der Flier et al., 2009).

As discussed in section 3.4.2 of the introduction, our group took advantage of the EPHB2 expression gradient to isolate $EPHB2^{high}$ (ISCs), $EPHB2^{medium}$ (TA cells) and $EPHB2^{low}$ (differentiated cells) fractions from the intestinal epithelium (**Figure 23**). We observed that $EPHB2^{high}$ human colon stem cells expressed a similar gene program to that of mouse ISCs and could be grown in culture for extended periods of time, while maintaining multipotency (Jung et al., 2011; Merlos-Suárez et al., 2011).

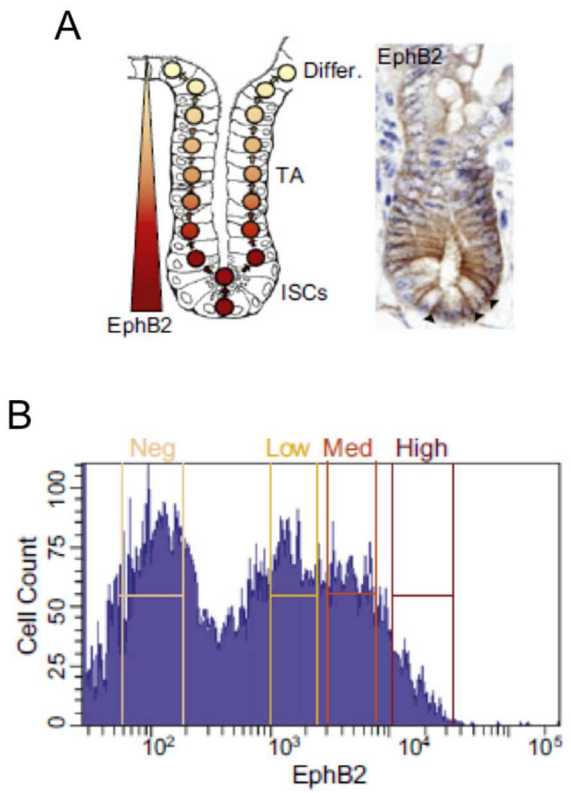

Figure 23: Sorting of intestinal epithelial cell populations based on EPHB2 expression. A. EPHB2 follows a decreasing expression gradient from the bottom to the top of the intestinal crypt. B. Representative FACS profile of EPHB2 expression in the intestinal epithelium. EPHB2 expression allows the identification of EPHB2^{high} (SCs), EPHB2^{medium} (TA cells) and EPHB2^{low} (differentiated cells) cell populations. From (Merlos-Suárez et al., 2011).

We then compared three ISC signatures: the EPHB2 ISC signature from mouse small intestine (Merlos-Suárez et al., 2011), the human EPHB2 colon SC signature (Jung et al., 2011) and the LGR5 signature from small intestine of *Lgr5-EGFP* mice obtained in our lab (**Figure 24 A**). By looking at these signatures, it was evident an over-representation of WNT target genes, strengthening the central role of WNT pathway in the ISC homeostasis. We focused our attention on the common genes among the three signatures, assuming that they could have an essential role in determining stemness. In particular, we found 3 already described ISC genes (*Lgr5*, *EphB3* and *Ascl2*) (Barker et al., 2007; Batlle et al., 2002; van der Flier et al., 2009; de Lau et al., 2011) and genes (*Apcdd1, Mex3a, Phgdh, Slco3a1, Smoc2*) still not related to ISC biology (**Figure 24 B**).

The reported involvement of SMOC2 in the regulation of the BMP morphogen pathway during invertebrate development (see section 5.2 of the introduction) together with the known relevance of BMP in the intestine, raised our interest in studying the role of SMOC2 in stemness and intestinal homeostasis. Moreover, our finding that *SMOC2* was still highly enriched in EPHB2^{high} CRC-SCs (Merlos-Suárez et al., 2011), strengthened our interest in characterizing its function in normal and pathological conditions.

A

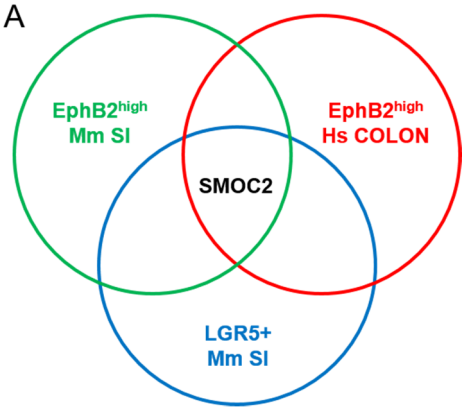

B

Gene	Described in ISC?	Known function in ISC?
Lgr5	yes	yes
Ascl2	yes	yes
EphB3	yes	yes
Apcdd1	no	no
Smoc2	yes	no
Mex3a	no	no
Phgdh	no	no
Slco3a1	no	no

Figure 24: Identification of the intestinal stem cell gene Smoc2. A. *Smoc2* is one of the common genes enriched in LGR5-derived and EPHB2-derived ISC signatures. B. Table with the common genes enriched in the three ISC signatures.

In parallel with our studies, the Clevers group generated gene expression and proteomic analysis of LGR5+ cells derived from *Lgr5-EGFP* mice (Muñoz et al., 2012). In particular, they used two independent microarray platforms (Affymetrix® and Agilent®) and Mass Spectrometry (MS)-based proteomics approach. Blue highlighted genes in the diagram are genes confirmed by at least two of these methods and represent the global mouse intestinal stem cell signature (**Figure 25 A**).

Consistently with our data, *Smoc2* was one of the most enriched genes in LGR5+ ISCs. Moreover, ISH analysis and *in vivo* lineage tracing of the *Smoc2* locus definitively established *Smoc2* as a novel ISC gene whose expression was restricted at the crypt base (Muñoz et al., 2012) (**Figure 25 B**).

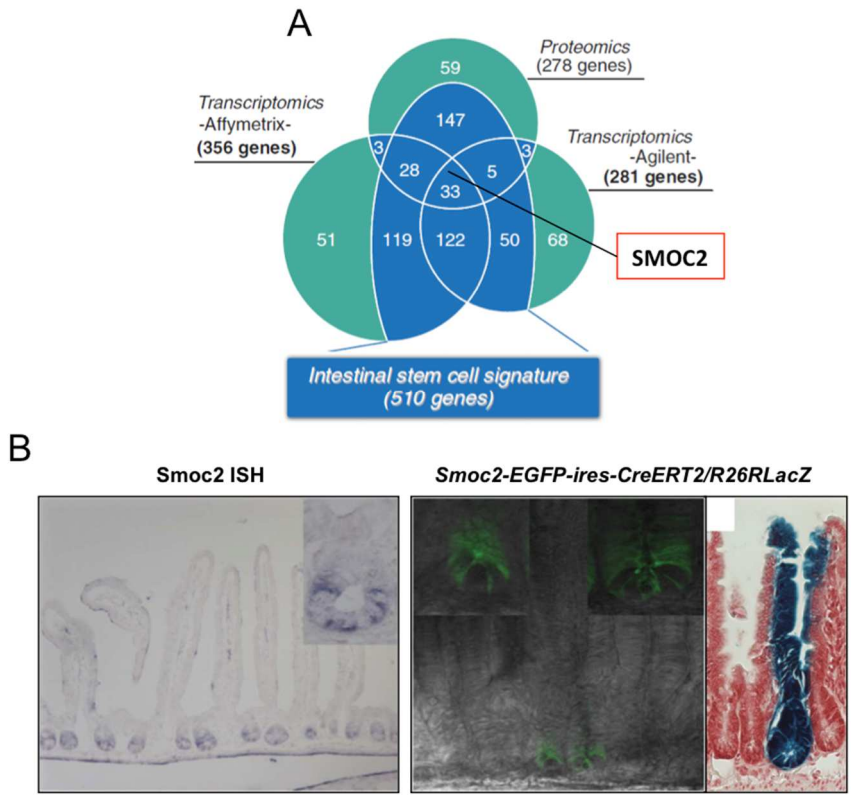

Figure 25: *Smoc2* marks intestinal stem cells *in vivo*. A. Proteomic and transcriptomic analyses of LGR5+ mouse ISCs identify *Smoc2* as one of the most enriched genes. D. *Smoc2* ISH of mouse small intestine (left panel); *Smoc2*-driven GFP expression at the bottom of intestinal crypts (central panel); lineage tracing of *Smoc2* expressing cells (right panel). From (Muñoz et al., 2012).

2. SMOC2 acts as a BMP inhibitor

As the literature reports the involvement of SMOC2 in the regulation of the BMP pathway in *Drosophila*, *Xenopus* and *Zebrafish*, we decided to analyze this possibility in mammalian cells. We first used HeLa cells, which are responsive to addition of BMPs.

Recombinant BMP2 and recombinant SMOC2 proteins were used in serum-free culture conditions. SMAD1/5/8 phosphorylation was assessed by Western Blot as readout of BMP activation downstream the BMP receptors. We observed strong SMAD1/5/8 phosphorylation already 20 minutes after rBMP2 addition and the SMAD1/5/8 phosphorylation was maintained over time (6 hours) (**Figure 26 A**). Recombinant SMOC2 was able to block the early BMP pathway activation, yet its inhibitory effect was lost over time. In order to exclude fast rSMOC2 degradation, we generated doxycycline-inducible SMOC2-FLAG HeLa cells. In this system, SMOC2 is produced upon doxycycline induction. We observed that both recombinant and overexpressed SMOC2 had the same dynamics of BMP repression, causing a delay in the activation more than a full blockade of the pathway (**Figure 26 A**).

Since our organ of interest is the intestine, we performed a similar experiment with SW480 cells. SW480 is a CRC cell line carrying a mutation on SMAD4. These cells are devoid of downstream BMP signaling but retain the response to BMP at the level of the receptors and SMAD1/5/8 phosphorylation. SW480s already presented high basal levels of pSMAD1/5/8 (**Figure 26 B**), probably as result of autocrine BMP signaling. On this cell line we performed response kinetics by treating the cells at different time points with recombinant SMOC2 (rSMOC2) and compared effects

to that of recombinant NOGGIN (rNOGGIN), which is a *bona fide* BMP inhibitor (Groppe et al., 2002). Since NOGGIN is composed of 232 amino acids and SMOC2 is composed of 457 amino acids, we tried to achieve an equivalent molecular amount of the two proteins by using rNOGGIN at a concentration of 100 ng/ml and rSMOC2 at a concentration of 200 ng/ml. We found that both recombinant proteins were able to counteract BMP pathway activation, although the effect of rSMOC2 was weaker and less persistent than that of rNOGGIN (**Figure 26 B**).

BMP pathway inhibition is required to culture and maintain ISCs *in vitro*. Using a specific cocktail of growth factors and inhibitors, it is possible to culture ISCs in 3D matrix. By doing so, their self-renewal capability can be preserved indefinitely and they can form intestinal organoids (“mini guts”) resembling the architecture of normal intestine with a stem, a proliferative and a differentiated compartment (Jung et al., 2011; Sato et al., 2009). In particular, rNOGGIN is commonly used to protect ISCs from BMP pathway activation. The removal of rNOGGIN from the culture dramatically impaired ISC growth and organoid formation (**Figure 26 C**). The addition of rSMOC2 to the medium partially rescued this phenotype, confirming that SMOC2 acts as a BMP inhibitor in intestinal cells, albeit with lower potency than NOGGIN.

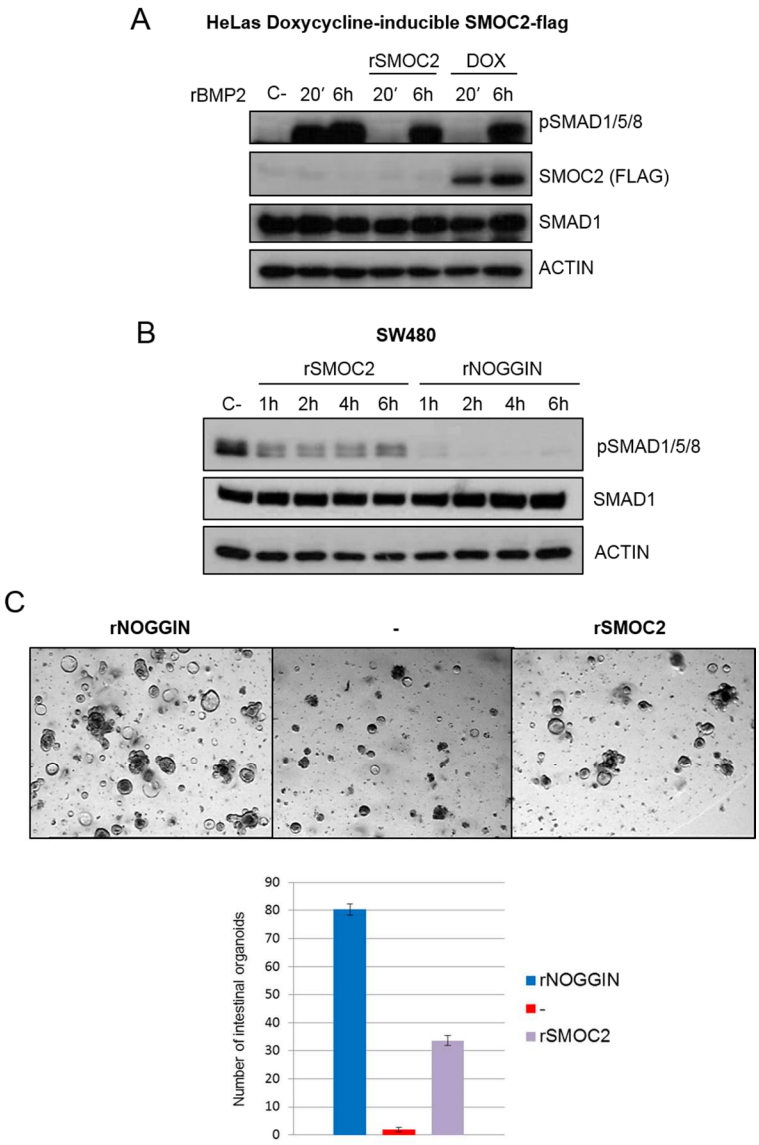

Figure 26: SMOC2 acts as a BMP inhibitor. A. Western blots of pSMAD1/5/8 in doxycycline-inducible SMOC2-flag HeLa cells treated with rBMP2 (25 ng/ml) and rSMOC2 (200 ng/ml). B. Kinetics of SMAD1/5/8 phosphorylation in SW480 treated with rSMOC2 (200 ng/ml) or rNOGGIN (100 ng/ml). C. Representative pictures showing the growth of intestinal crypts cultured with rNOGGIN or rSMOC2. Fully formed organoids were counted 5 days after crypt seeding and treatments. Data are mean ± SD of triplicates.

3. Characterization of intestinal *Smoc2* transgenic mouse

3.1 Generation of Villin-Smoc2 transgenic (TG) mouse

As described in section 2.4.4.3 of the introduction, BMP is one of the signaling mechanisms that determine the highly regular patterning of the intestinal epithelium into crypts and villi. Inhibition of BMP signaling by transgenic expression of *Noggin* results in the formation of numerous ectopic crypt units perpendicular to the crypt-villus axis. These changes of architecture phenocopy the intestinal histopathology of patients with the cancer predisposing syndrome Juvenile Polyposis (JP), including the frequent occurrence of intraepithelial neoplasia (Haramis et al., 2004).

We decided to confirm the role of SMOC2 as BMP inhibitor by generating an intestinal *Smoc2* transgenic mouse. In similar fashion than the experiments performed by the Clevers laboratory to study the function of NOGGIN *in vivo* (Haramis et al., 2004), we cloned the mouse *Smoc2* open reading frame downstream of a 9Kb fragment of the promoter of the *Villin1* gene, which drives robust expression of the transgene specifically in the intestinal epithelium (Pinto et al., 1999) (**Figure 27 A**). This construct was inoculated into oocytes by pronuclear injection by the mouse mutant facility at IRB Barcelona following standard techniques. This experiment yielded 36 mice, 8 of which had integrated *Villin-Smoc2* construct as assessed by PCR based genotyping on genomic DNA using specific primers (**Figure 27 B**). We established these founder transgenic mice by breeding with C57/Bl6 mice. All of them were fertile and transmitted the transgene to the progeny. We next analyzed *Smoc2* overexpression by quantitative PCR on intestinal extracts and three different lines expressing different levels of the transgene were selected for further studies (#127, #57, #13)

(**Figure 27 C**). We confirmed high *Smoc2* upregulation throughout the whole intestinal epithelium by ISH (**Figure 27 D**). Please note that in wild-type mice, expression of Smoc2 was restricted to the crypt base whereas in transgenic mice its expression extended throughout the crypt-villus axis. This pattern follows that of the *Villin1* gene (**Figure 27 D**).

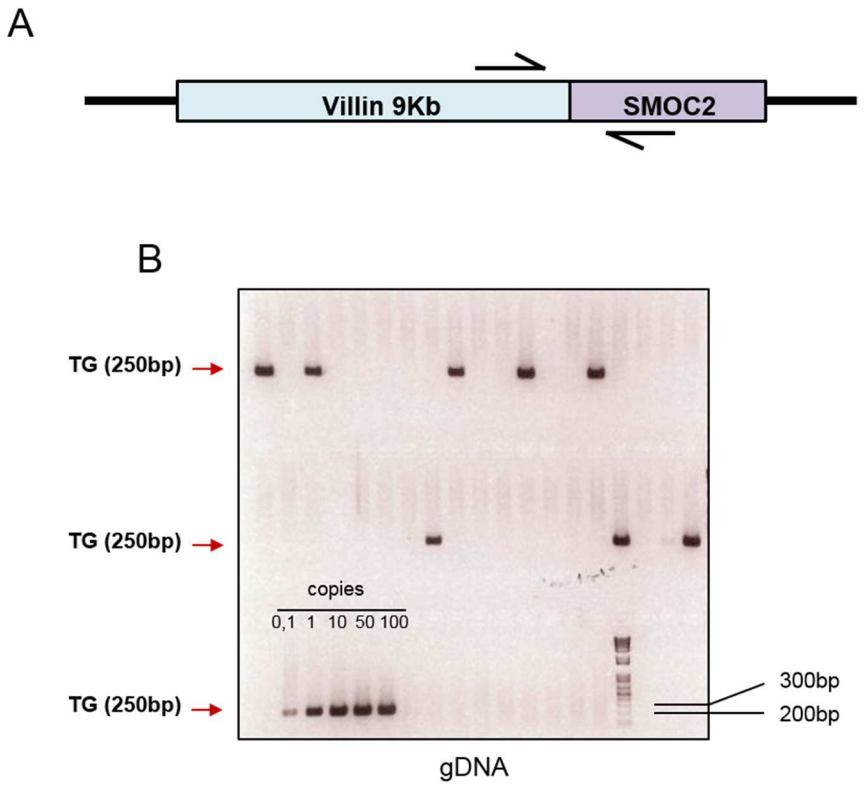

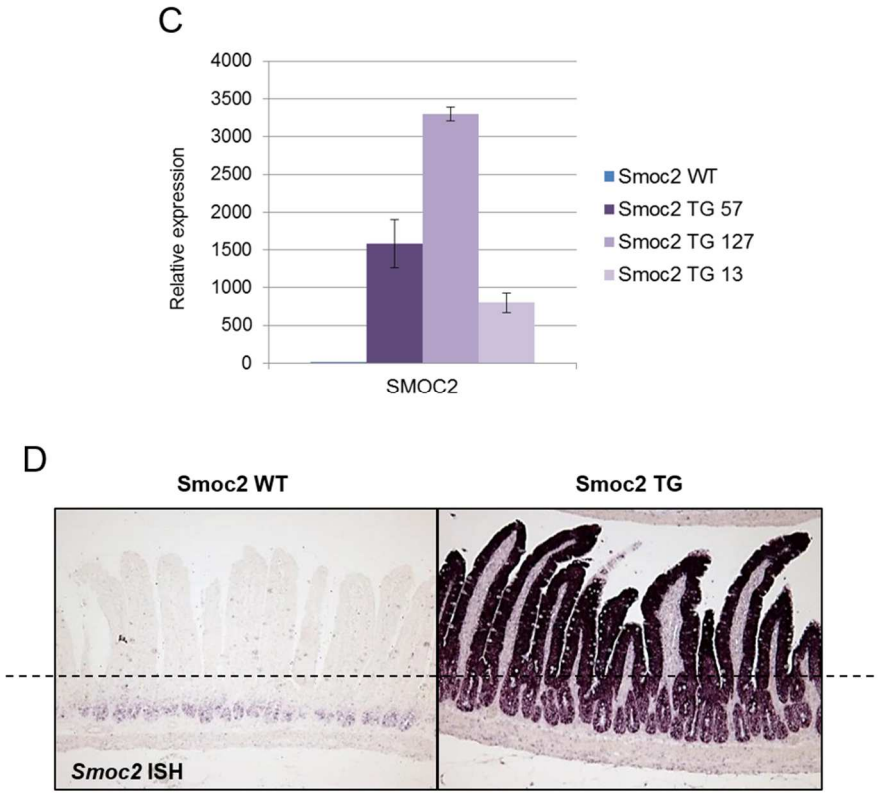

Figure 27: Generation of intestinal Smoc2 transgenic mouse. A. Structure of the *Villin-Smoc2* transgene. Black arrows indicate the location of the forward and reverse primers used for genotyping. B. Integration of *Villin-Smoc2* transgene was assessed by PCR. Copy-standards were used to assess the sensitivity of the PCR assay and estimate copy numbers. C. Representative RT-qPCR showing *Smoc2* expression in intestinal RNA extracts of three different *Smoc2* transgenic founders. D. Representative pictures showing detection of *Smoc2* mRNA in intestinal sections of *Smoc2* wild-type and transgenic mice. Dashed line indicates the crypt-villus boundary. Note that in *Smoc2* wild-type mice, *Smoc2* mRNA is restricted to the base of the crypts where ISCs reside. *Smoc2* transgenic mice display *Smoc2* expression throughout the whole epithelium. Magnification 10X.

3.2 Adult intestinal Smoc2 transgenic mice display intestinal gigantism

Macroscopic inspection upon necropsy of adult (12 weeks) mice revealed that the small intestine of transgenic mice was thicker than that of wild-type littermates (**Figure 28 A**). This feature was consistent in all the transgenic colonies and appeared more evident in colony #127 and #57. The total length of small intestine was not affected (**Figure 28 B**). No macroscopic differences were detected in transgenic colon. The other organs had normal gross appearance and size equivalent to wild-type littermates.

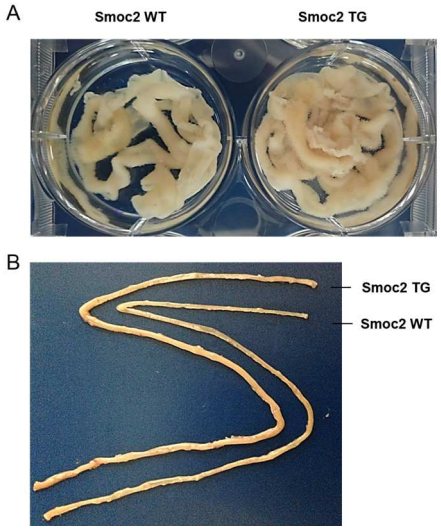

Figure 28: Transgenic intestines display increased thickness than wild-type intestines. Representative pictures of wild-type and transgenic small intestine. A. Transgenic small intestine is more voluminous than wild-type small intestine. B. The total length of transgenic small intestine is not affected.

Histological analysis revealed larger crypts and proportionally larger villi in transgenic small intestine compared to wild-type mice (**Figure 29 A**). The colon of transgenic mice had much larger crypts, as well (**Figure 29 B**). This denotes that the gigantism is present throughout the whole transgenic intestine and the absence of villi may make the phenotype macroscopically less evident in the colon. Moreover, there was evident abundant stromal cells and collagen deposition in the intravillus space of transgenic mice (**Figure 29 C**). These features were consistent among the different transgenic colonies and were more exacerbated in the colony #127 displaying the highest *Smoc2* over-expression.

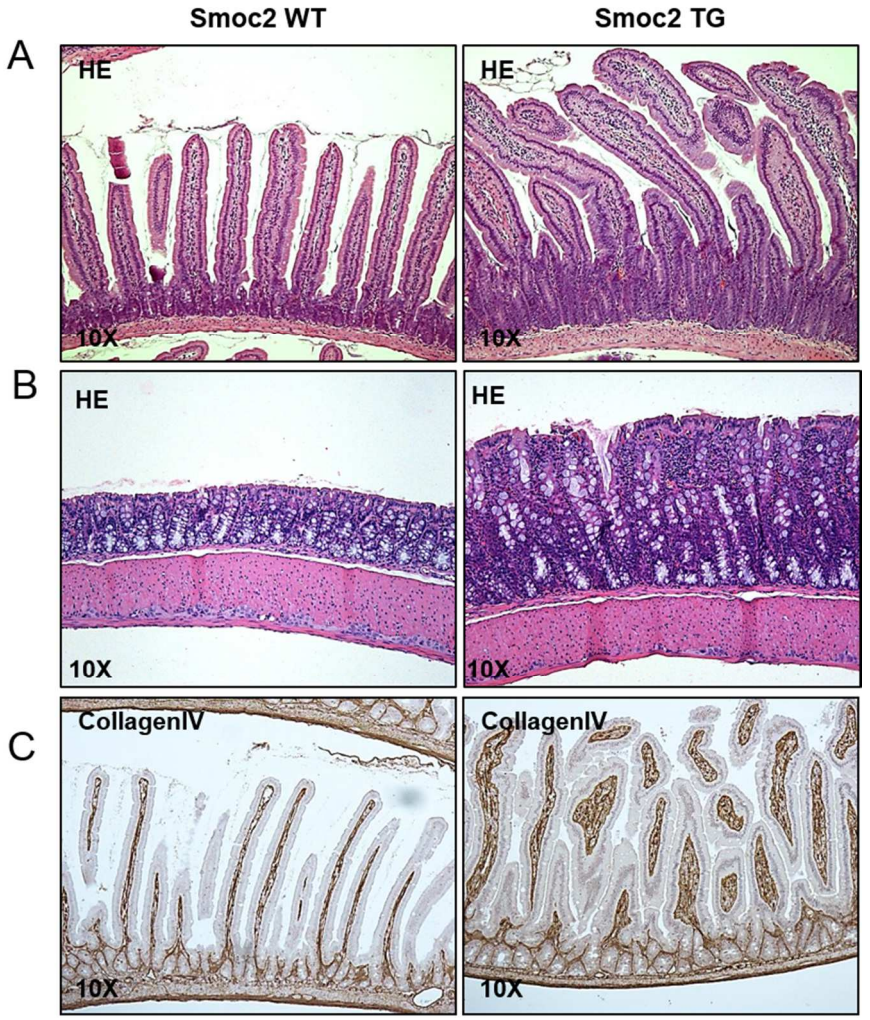

Figure 29: Histological characterization of *Smoc2* transgenic intestine. Hematoxilin/Eosin (HE) staining shows an overall gigantism in small intestine (A) and colon (B) of transgenic mice. C. CollagenIV staining shows increased collagen deposition in the intravillus space of transgenic small intestine (colony #127).

Cell size looked equivalent in transgenic and wild-type mice, suggesting that the increased size on the intestine triggered by *Smoc2* overexpression was due to increased number of cells.

To explore this, we performed quantitative analysis by taking several pictures of wild-type and littermate transgenic mice belonging to the three transgenic colonies. Thus, the result of these analyses represents an average between the different *Smoc2* transgenic colonies.

Overall, adult *Smoc2* transgenic mice displayed 1.6 fold larger villi than *Smoc2* wild-type littermates (**Figure 30 A, C**). Yet, crypts also contained 1.6 times more cells (**Figure 30 B, C**). We indeed found that transgenic mice contained about a 1.6 fold increase in proliferative (MKI67+) cells, thus confirming that overall proportions of the intestine were kept in transgenic mice (**Figure 31 A**). To study cell migration along crypt-villus axis we inoculated mice with BrdU so that all proliferative crypt cells were labeled. Then we assessed their positions along the crypt-villus axis after 72h (**Figure 31 B**). The speed of migration was also increased by about 1.6 fold respect to wild-type mice.

All these data suggest that *Smoc2* transgenic mice display an overall proportionate gigantism.

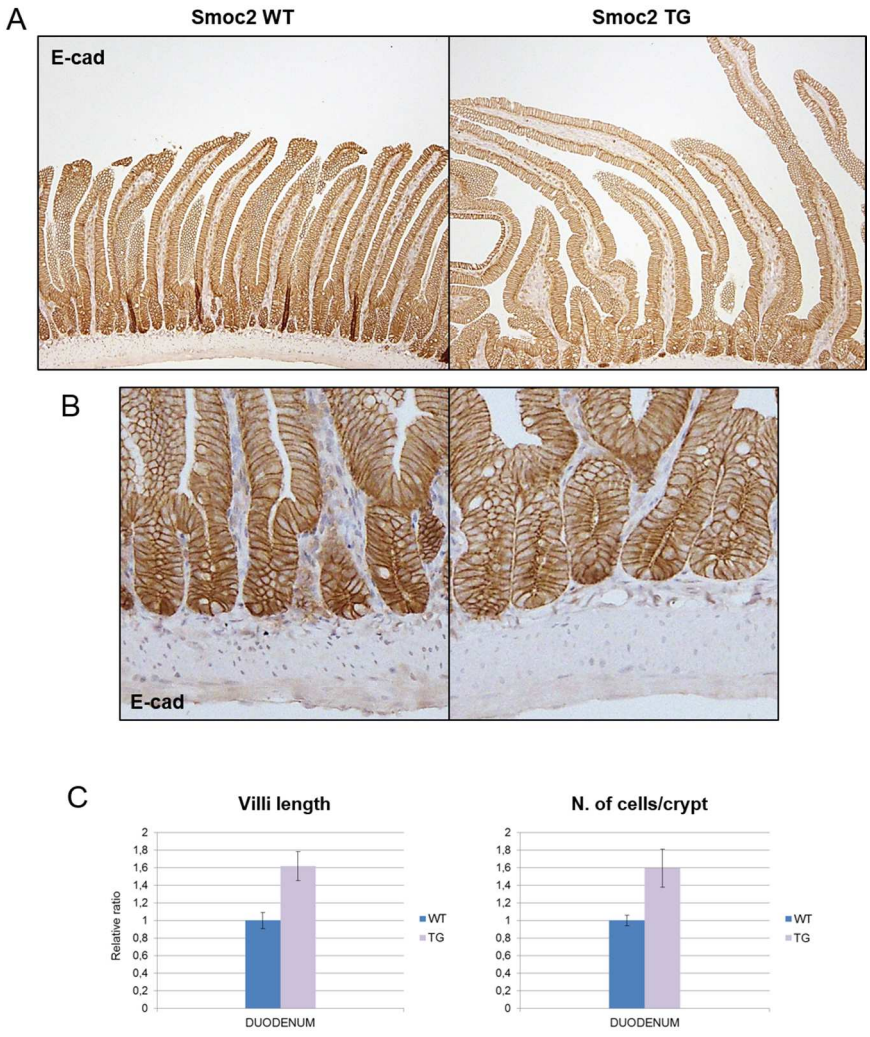

Figure 30: Transgenic mice display higher villi and larger crypts. Representative pictures of wild-type and transgenic mice showing comparisons of the villi length (A) and the crypt depth (B) (Colony #127). C. Quantification of villi length and number of cells per crypt in wild-type and transgenic mice. Data are mean ± SD of n=20 measurements deriving from the three transgenic colonies and wild-type littermates.

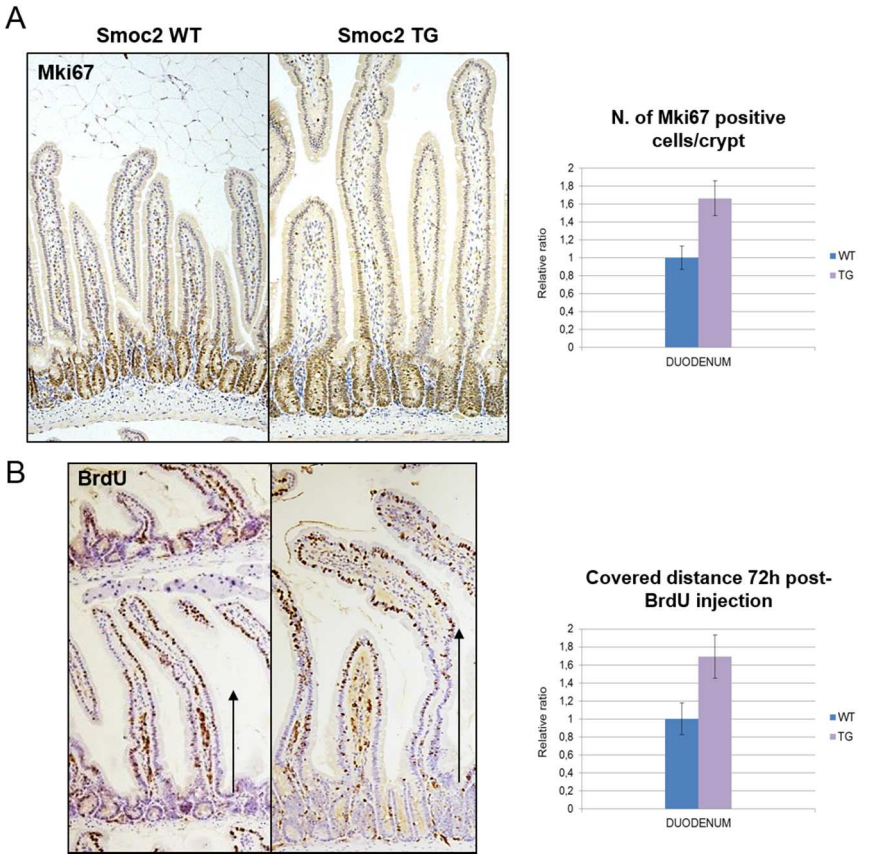

Figure 31: Proliferative compartment and speed of cell migration along the villus is proportionally increased in *Smoc2* transgenic. A. Representative pictures showing MKI67 positive cells in the proliferative compartment of the crypt (left panel) and quantification of the number of MKI67+ cells per crypt (right panel). B. Representative pictures showing BrdU positive cells 72 hours after injection (left panel). The very bright cells are the ones that were residing at the crypt-villus boundary at the moment of injection and were leaving the proliferative compartment to enter the differentiation compartment. These cells did not undergo many cell divisions and retained the whole labeling. Black arrows indicate the distance covered by the front of BrdU+ cells during 72 hours post-injection. Right panel shows the quantification. Data are mean ± SD of n=20 measurements. Duodenum, magnification 10X.

Cell differentiation towards the different lineages was unaffected in *Smoc2* transgenic mice as shown by ChromograninA (enteroendocrine cells) and PAS/Alcian blue (mucosecreting cells, enterocytes) staining (**Figure 32 A, B**). Less consistently than the observed gigantism, 30% of transgenic mice displayed Paneth cell miss-positioning (**Figure 32 C**). Nevertheless, the expression pattern of EPHB2, EPHB3 and EPHRINB1, whose distribution in the epithelium determines the correct cell positioning (Batlle et al., 2002), was also unaffected (**Figure 33**).

In the absence of evident defects in the EPHB-EPHRIN expression gradient, the observed Paneth cell miss-positioning could suggest the presence of an altered inflammatory status (Adolph et al., 2013).

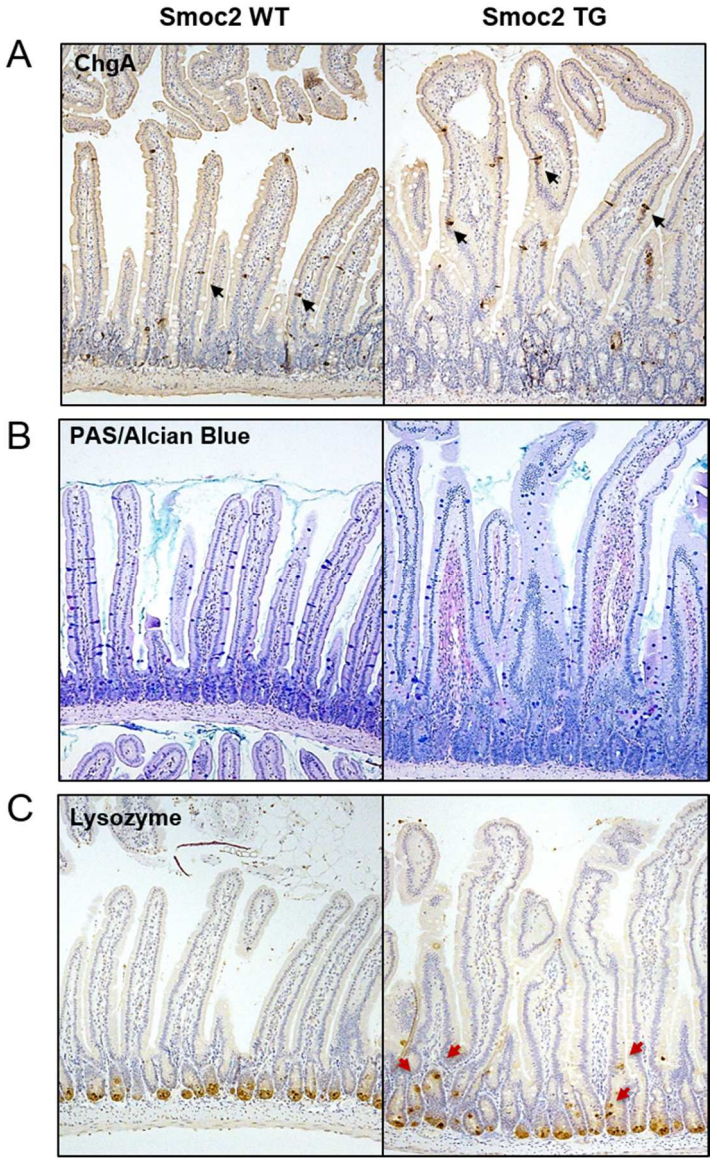

Figure 32: Differentiation lineages are not affected in *Smoc2* transgenic mice. A. Black arrows indicate ChromograninA positive cells (entoendocrine cells). B. Pas/Alcian Blue staining shows goblet cells and enterocytes in the villi. C. Lysozyme staining identifies Paneth cells in the crypt base of wild-type intestine and some miss-localized Paneth cells in transgenic intestine (red arrows). Duodenum, magnification 10X.

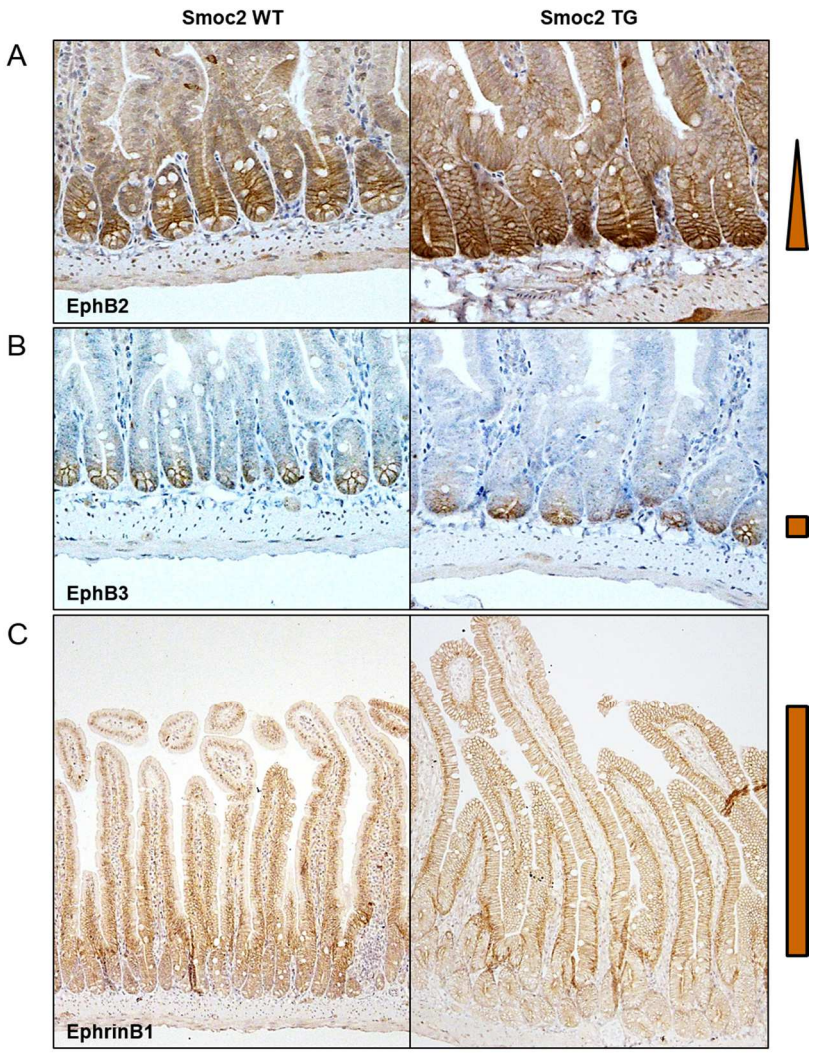

Figure 33: EPHRIN-EPHB expression in not altered in *Smoc2* transgenic mice. Representative pictures of EPHB2 (20X) (A), EPHB3 (20X) (B) and EPHRINB1 (10X) (C) IHC in the duodenum of *Smoc2* wild-type and transgenic mice. On the right, is shown the expected expression pattern.

Moreover, the levels and expression domain of the transcription factor MYC were equivalent in transgenic and wild-type mice (**Figure 34**).

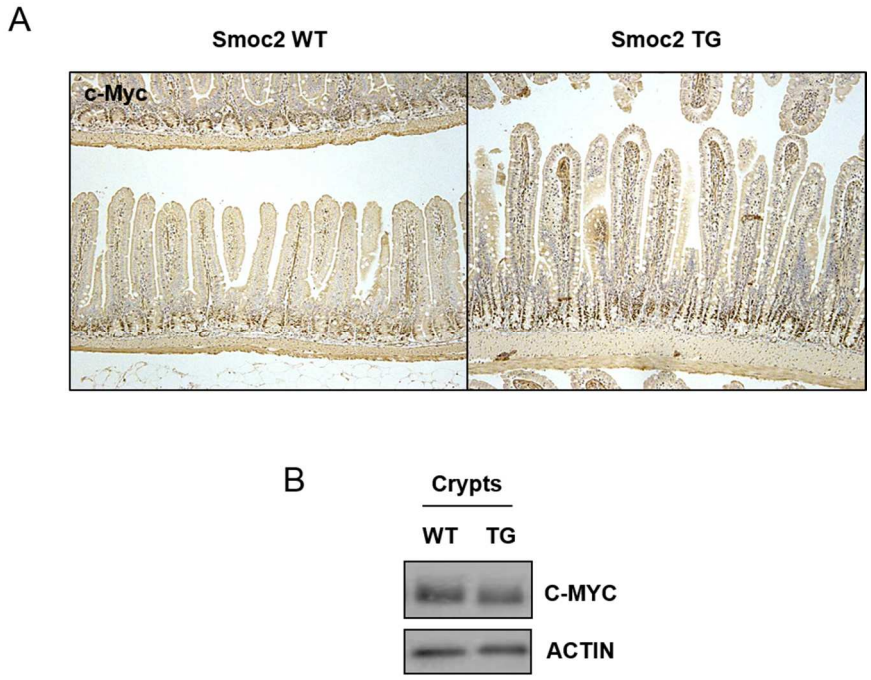

Figure 34: C-MYC expression is not altered in *Smoc2* transgenic mice. A. C-MYC IHC shows the expected expression pattern restricted to the proliferative compartment of the intestinal crypts in both wild-type and transgenic mice. Jejunum, magnification 10X. B. Western Blot analysis of C-MYC expression in protein extracts of *Smoc2* wild-type and transgenic crypts.

The *Villin* promoter drives expression of transgenes from embryonic day E16. To test whether overexpression of *Smoc2* had effects over the development of the intestine, we also analyzed the intestines of newborn mice (Postnatal day 1-P1). Macroscopically, the intestine of wild-type and transgenic newborn mice were identical. At this developmental stage (P1), crypts have not been formed yet. Then we analyzed the length of the villi and we found no differences between transgenic and wild-type littermates (**Figure 35**).

Altogether this data suggest that *Smoc2* overexpression affects organ size without affecting the overall organization of the underlying tissue. This phenomenon seems to occur during postnatal development.

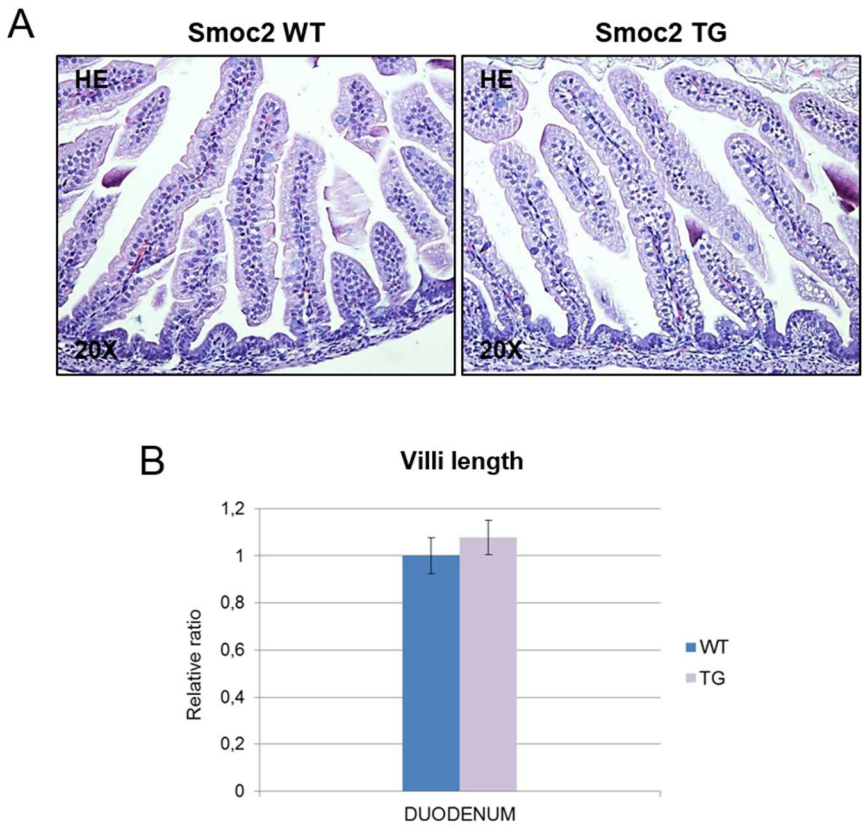

Figure 35: At P1 post-natal developmental stage the *Smoc2* wild-type and transgenic intestinal size is equal. A. Representative pictures of *Smoc2* wild-type and transgenic duodenum (#127) of P1 mice. B. Quantification of the length of the villi. Data are mean ± SD of n=10 for each genotype (transgenic #57 and #127).

3.3 Intestinal Smoc2 transgenic mice display strong inhibition of BMP signaling

We then studied the levels of BMP pathway activation in our *Smoc2* transgenic mice. Similarly to the effect of overexpression of *Noggin* in *Villin-Noggin* transgenic mice (Haramis et al., 2004), *Smoc2* overexpression triggered inhibition of BMP pathway, as shown by reduction in SMAD1/5 phosphorylation. Both epithelial and stromal cells of *Smoc2* transgenic mice were negative for p-SMAD1/5 (**Figure 36**). Of note, a few stromal cells located in the intravillus space at the tip of the villi that escaped from SMOC2 inhibitory effect. That is in line with recent findings suggesting maximum BMP signals at the villus tip (Shyer et al., 2015).
Overall, these data confirm the role of SMOC2 as inhibitor of BMP signaling pathway.

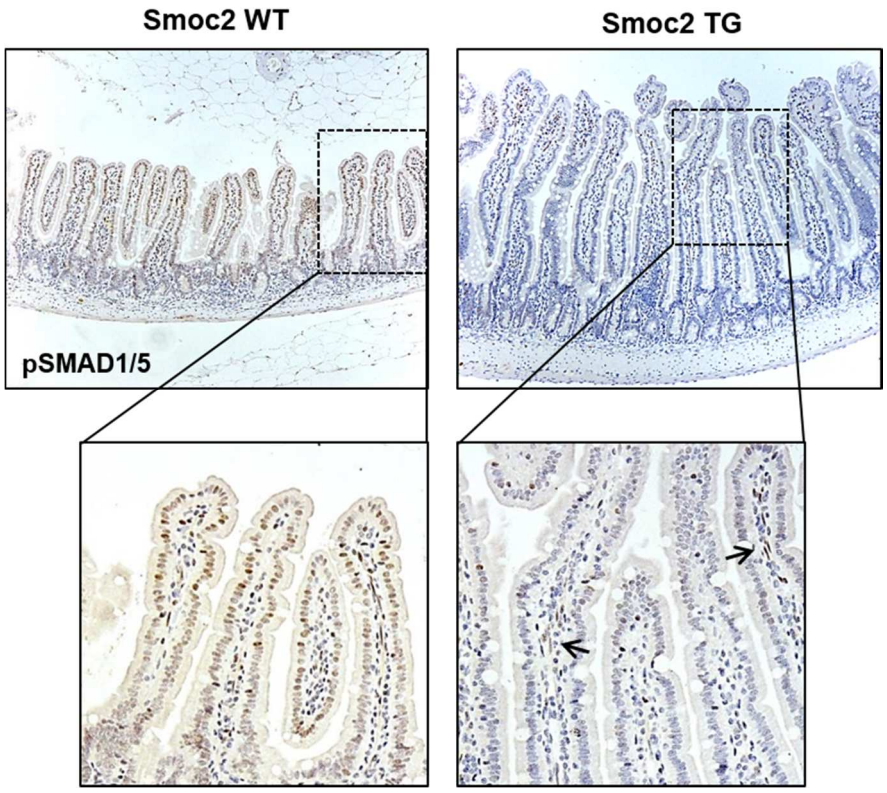

Figure 36: BMP signaling is strongly inhibited in *Smoc2* transgenic intestine. Representative pictures of pSMAD1/5 staining on tissue sections from *Smoc2* wild-type and transgenic (#127) mice. Duodenum, magnification 10X. Lower panels show the intravillus space at higher magnification. Black arrows indicate residual BMP activation in stromal cells of the villus tip in *Smoc2* transgenic mice.

3.4 Aged Smoc2 transgenic mice can develop Juvenile Polyposis-like polyps

We found that in old mice (8-10 months) the gigantism and the disorganization of stromal cells was exacerbated compared to young mice (2-3 months), suggesting that gigantism of the intestine progresses over time (**Figure 37**).

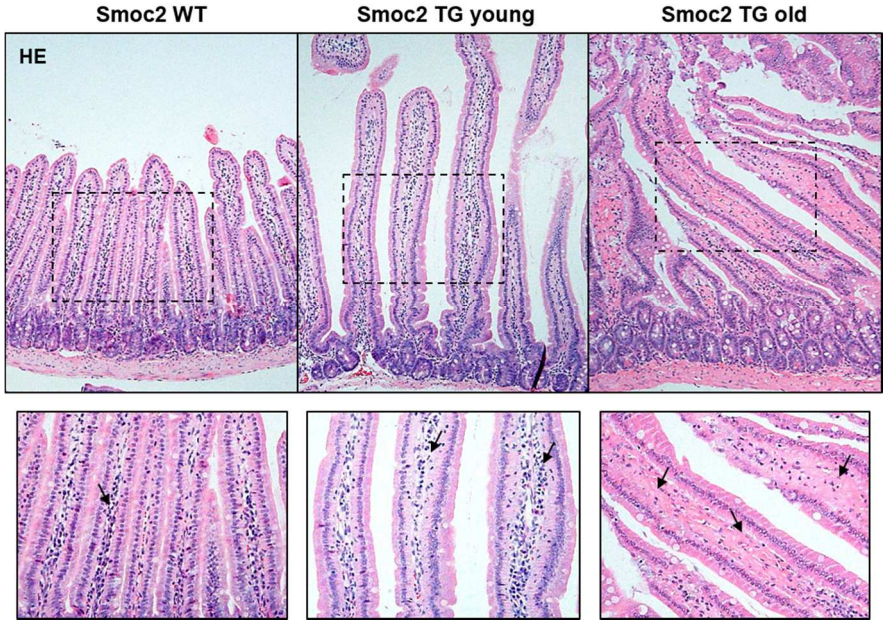

Figure 37: *Smoc2* transgenic phenotype increases by ageing. Representative pictures of *Smoc2* wild-type (left panel), young *Smoc2* transgenic (middle panel) and old *Smoc2* transgenic (right panel) duodenum. Dashed boxes are shown at higher magnification in the lower panels. Black arrows indicate the stromal cell composition in the intravillus space.

A large percentage of *Smoc2* transgenic mice displayed the presence of fecal blood and prolapses by ageing (**Figure 38 A, B**). Moreover, we noticed that 35% of old (5-10 months) transgenic mice deriving from colony #127 spontaneously developed polyps in the colon. At histological levels, these polyps appeared hyperplastic and presented the typical features of polyps arising in patients with Juvenile Polyposis syndrome, including the presence of big cysts and abundance of stromal cells (**Figure 39**). As expected, these polyps were mainly negative for SMAD1/5 phosphorylation (**Figure 39**).

A

B

Ageing mice from founder 127 (n=20)	
Presence of prolapse/fecal blood	50%
Polyp development	35%

Figure 38: *Smoc2* transgenic mice display prolapse by ageing. A. Representative pictures of the anus of old *Smoc2* wild-type and transgenic mice (10 months old). B. Percentages of old transgenic mice from colony #127 developing prolapse and polyps in the colon.

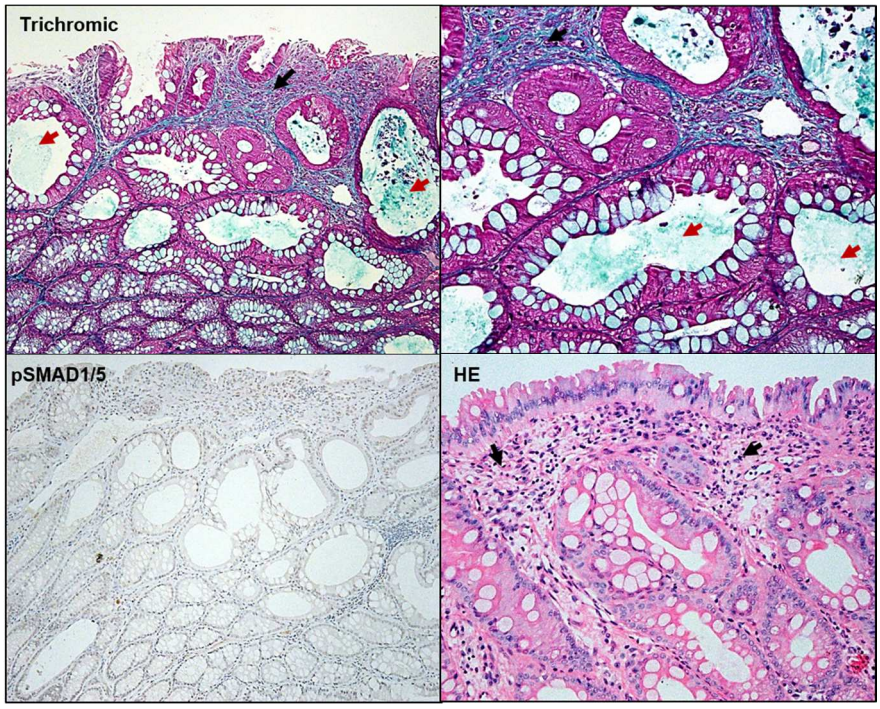

Figure 39: Old *Smoc2* transgenic mice develop benign hyperplastic polyps. Representative pictures of colonic hyperplastic polyps found in *Smoc2* transgenic colon. The upper panels show trichromic staining (left panel at 10X and right panel at 20X). Bottom right panel shows HE staining, at magnification 20X. Bottom left panel shows almost negative pSMAD1/5 staining (magnification 10X). Black arrows indicate abundant stroma infiltration. Red arrows indicate cysts.

Polyps developed by Juvenile Polyposis patients and by *Villin-Noggin* transgenic mice display no nuclear β-catenin accumulation. However, a fraction of these polyps develop aggressive features including dysplasia and WNT pathway activation (Brosens et al., 2011; Chow and Macrae, 2005). It has been described that hyperplastic polyps that arise as result of BMP signaling inhibition have increased chances to lose the *Apc* gene and evolve towards adenomatous polyps (see section 3.3 of the introduction). This process was reproduced in *Villin-Smoc2* transgenic mice. Embedded within hyperplastic polyps, we found areas of dysplasia and nuclear β-catenin accumulation that resemble classical adenomas (**Figure 40**).

From these results we conclude that *Smoc2* overexpression triggers a Juvenile Polyposis-like phenotype in mice. This phenotype is largely reminiscent of that present in *Villin-Noggin* transgenic mice (Haramis et al., 2004).

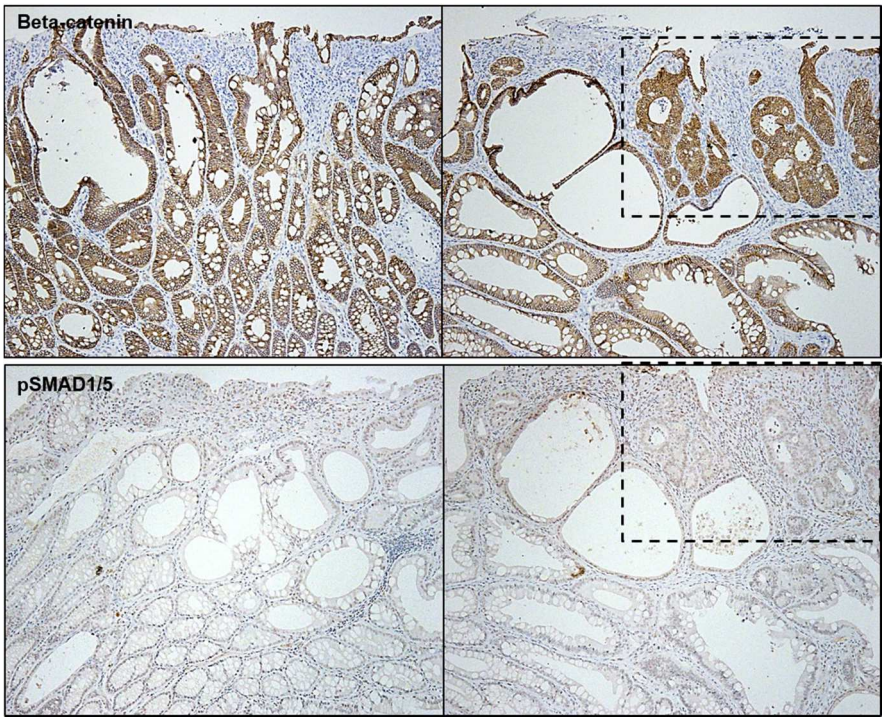

Figure 40: Benign hyperplastic polyps of *Smoc2* transgenic mice predisposes to adenoma transformation. Upper panels show β-catenin staining. The majority of the lesions are negative for nuclear β-catenin. Dashed box indicate adenomatous areas with nuclear β-catenin defining zones with mutagenic WNT activation. Lower panels show pSMAD1/5 staining. BMP signaling is strongly inhibited also in the adenomatous area (dashed box).

3.5 In vitro growth of Smoc2 transgenic intestinal crypts

We next explored whether gigantism present in the intestine of *Smoc2* transgenic mice was a cell-autonomous effect occurring in epithelial cells. To this end, we cultured intestinal crypts derived from *Smoc2* wild-type and transgenic mice. At the moment of seeding there was obvious difference in size between the crypts of the two genotypes. However, as the culture evolved, sizes of organoids were normalized (**Figure 41 A**). *Smoc2* wild-type and transgenic crypts formed organoids of equivalent dimensions despite the fact that *Smoc2* overexpression was kept in culture (**Figure 41 B**).

This observation suggests that the effect of *Smoc2* over crypt size is not cell autonomous and more likely depends on interaction with stromal cells.

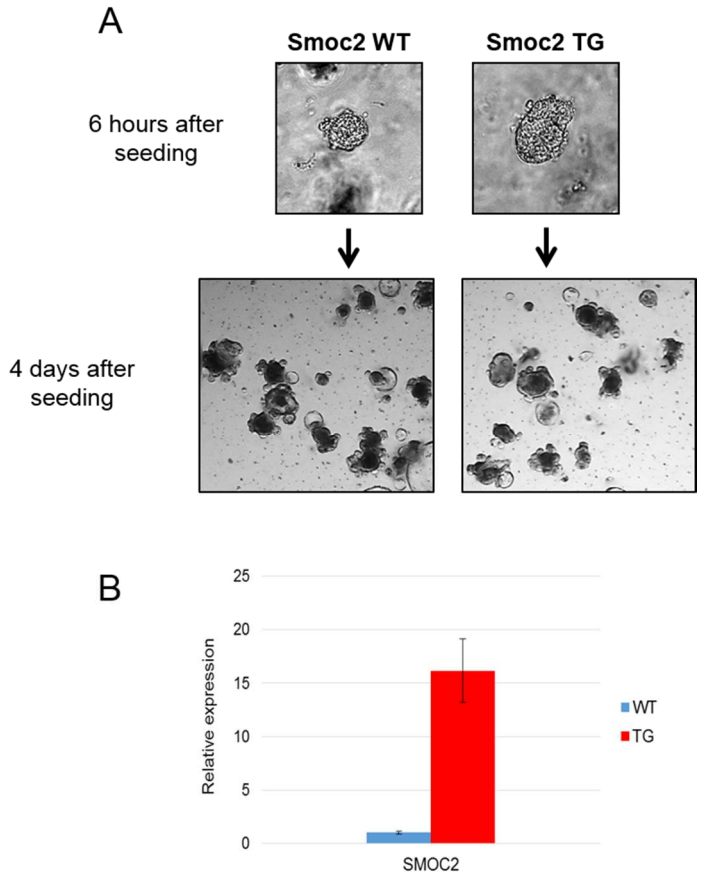

Figure 41: *In vitro* culture of intestinal crypts derived from *Smoc2* wild-type and transgenic mice. A. Representative pictures of *Smoc2* wild-type and transgenic intestinal crypts 6 hours after *ex vivo* extraction and 4 days after seeding. B. Representative RT-qPCR analysis of *Smoc2* expression in *Smoc2* wild-type and transgenic cultured crypts.

We next analyzed the *in vitro* growth of *Smoc2* wild-type and transgenic crypts and their dependency on BMP signaling. In the presence of rNOGGIN, *Smoc2* transgenic crypts grew to similar extent that crypts derived from wild-type mice (**Figure 42 A, B**). Removal of rNOGGIN induced a sharp loss of organoid growth. *Smoc2* overexpression facilitated organoid formation in this condition but it was not sufficient to fully rescue the effect (**Figure 42 A, B**). Of note, whereas levels of *Smoc2* transgenic overexpression *in vivo* are in the range of 800-3000 fold, transgenic crypts cultured *in vitro* expressed only 10 to 50 times more *Smoc2* than crypts derived from wild-type mice (**Figure 41 B**). This observation may suggest that intestinal epithelial cells require high SMOC2 levels to inhibit BMP signaling. These findings are also in line with the results obtained in cell lines (Section 2) indicating that SMOC2 has weaker activity than NOGGIN as BMP inhibitor.

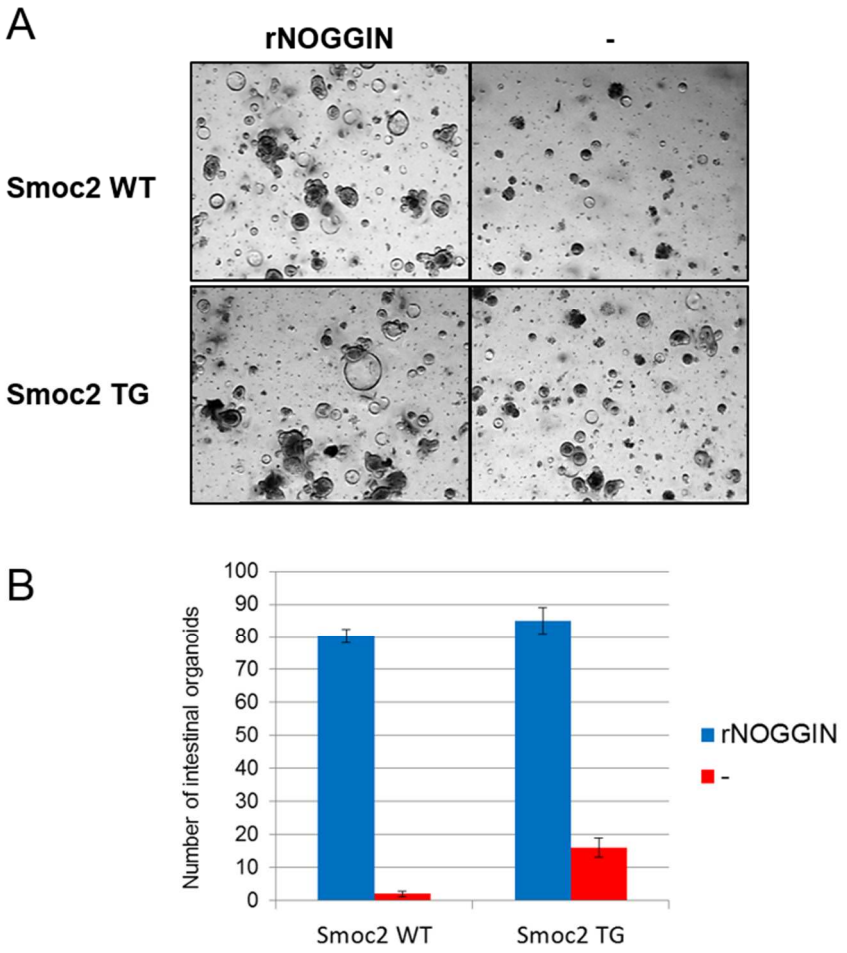

Figure 42: *In vitro* culture of *Smoc2* transgenic crypts displays dependency on BMP pathway inhibition. A. Representative pictures of *in vitro* cultured organoids derived from *Smoc2* wild-type and transgenic crypts in the presence or absence of rNOGGIN (100 ng/ml). B. Quantification of organoid formation. Formed organoids were counted 5 days after crypt seeding. Data are mean ± SD of triplicates.

3.6 Smoc2 overexpression enhances polyp formation and size in Apc mutant mice

We finally analyzed the effect of *Smoc2* overexpression during intestinal tumorigenesis. To this purpose, we crossed the *Smoc2* transgenic mice (#127 and #13) with Apc^{min} mice. Apc^{min} mice carry a truncating mutation at codon 850 of the *Apc* gene and spontaneously develop multiple adenomas in small intestine and colon (Moser et al., 1990).

Apc^{min}*, Smoc2* wild-type and transgenic mice where sacrificed at the age of 4 months and polyps were counted. *Smoc2* transgenic mice developed more polyps than *Smoc2* wild-type littermates and the phenotype was much more severe in colony #127 displaying the highest *Smoc2* overexpression (**Figure 43 A**). Indeed, the strength of the phenotype followed the extent of *Smoc2* overexpression in the different *Smoc2* transgenic colonies. Transgenic polyps were also larger (**Figure 43 A**). Histological analysis demonstrated robust BMP inhibition in adenoma arising in *Smoc2* transgenic mice (**Figure 43 B**).

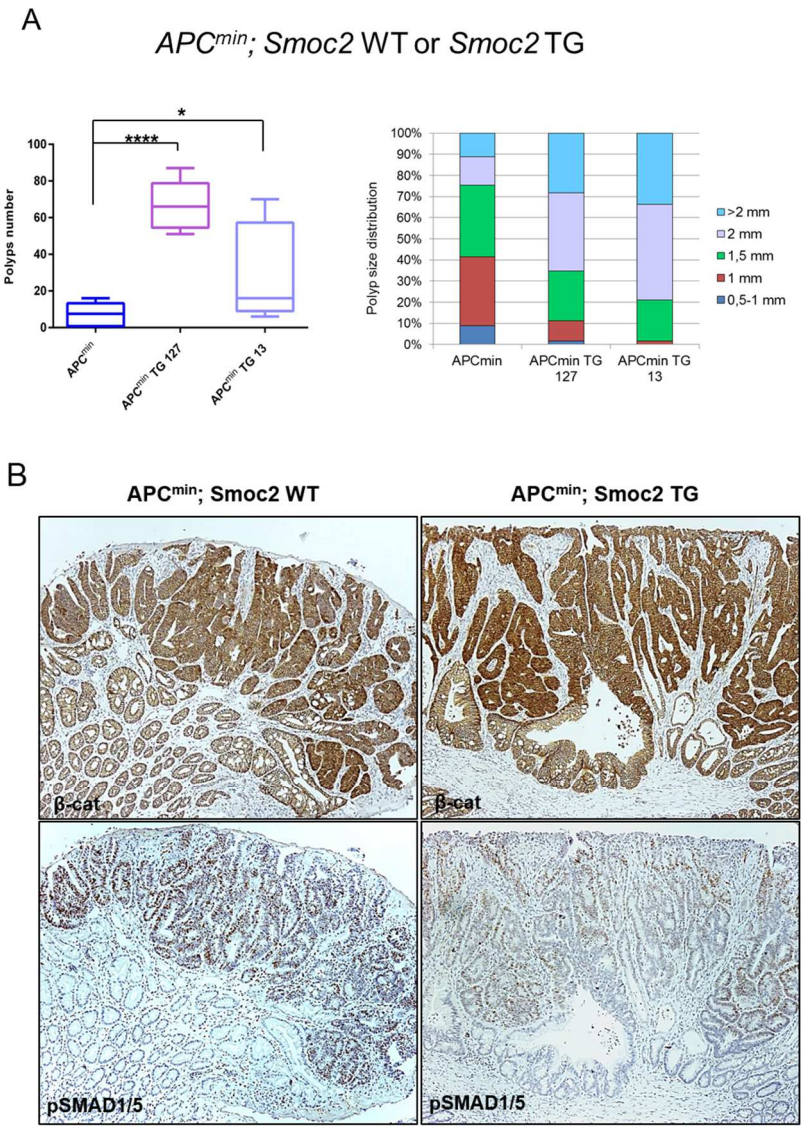

Figure 43: *Smoc2* overexpression enhances polyp formation in *Apc* mutant mice. A. Polyp counting (left panel) and polyp size distribution (right panel) in colon and small intestine of *Apc^{min}, Smoc2* wild-type and transgenic mice. Data are mean ± s.e.m of measurements (n=8-12 mice per genotype). Statistics are done by Student's *t*-test. ****P<0,0001; *P<0,05 B. β-catenin and pSMAD1/5 IHC in polyps of *APC^{min}, Smoc2* wild-type and *Smoc2* transgenic mice.

We also cultured adenoma stem cells (AdSCs) and tested the ability of rSMOC2 to block BMP pathway activation in these cells. Upon rNOGGIN removal or rBMP4 addition, Western Blot against pSMAD1/5/8 revealed that rSMOC2 was able to efficiently counteract BMP pathway activation in adenoma cultures at least at short time points after BMP induction (**Figure 44 A**). This effect triggered a significant rescue of adenoma organoid growth (**Figure 44 B, C**). We also observed significant inhibition in expression of BMP target genes such as *Apcdd1*, *Id1*, *Id3* and *Smad6* (**Figure 44 D**).

Overall, our results indicate that blockade of BMP signaling by *Smoc2* overexpression exacerbates the formation of adenomas induced by constitutive activation of the WNT pathway. These results are in concordance with a tumor suppressor role for BMP signaling in the intestine as previously shown (Whissell et al., 2014). Our data also point that upon overexpression, SMOC2 acts as a BMP inhibitor for intestinal epithelial cells.

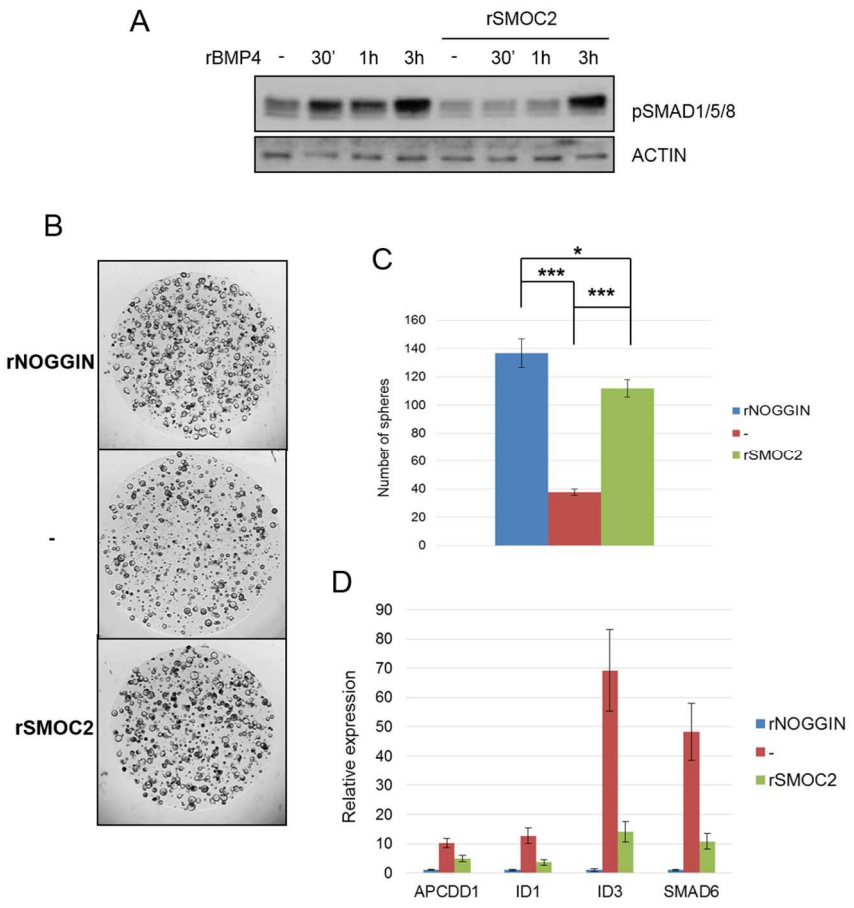

Figure 44: rSMOC2 protects AdSCs from BMP activation *in vitro.* A. Western blot of pSMAD1/5/8 on AdSCs treated with rBMP4 (25 ng/ml) and rSMOC2 (200 ng/ml). B. Representative pictures of spheres grown from AdSCs cultured with rNOGGIN (100 ng/ml) or rSMOC2 200 ng/ml). C. Quantification of sphere formation 6 days after sphere disaggregation and single cell seeding. Data are mean ± s.e.m. of triplicates. Statistics are done by Student's *t*-test. **P*<0,05; ****P*<0,001 D. BMP target gene expression detected by RT-qPCR on RNA extracts deriving from AdSCs cultured with rNOGGIN or rSMOC2.

4. Characterization of intestinal *Smoc2* conditional KO mouse

4.1 Generation of a Smoc2 conditional KO (cKO) allele

Based on our observations in transgenic mice, we hypothesized that SMOC2 could act as a BMP inhibitor in ISCs. Together with the other BMP inhibitors present in the niche, SMOC2 may contribute to maintain low BMP signaling levels in the ISC niche which is required for self-renewal. However, because SMOC2 appears to be a weaker BMP inhibitor than NOGGIN, experiments of overexpression in transgenic mice may also trigger non-specific effects.

To test the physiological roles of SMOC2 in intestinal epithelium homeostasis, we generated a new mouse model that enabled tissue specific ablation of *Smoc2* in adult mice (see methods for details). Briefly, we inserted by homologous recombination in mouse ES cells loxP sites flanking the second exon of the mouse *Smoc2* locus, which encodes the FS domain, a key functional domain of the protein shared by all members of BM-40 protein family (Vannahme et al., 2002) (**Figure 45 A**). Recombination of loxP sites will cause not only the deletion of exon 2 but also a frameshift and the introduction of a STOP codon in exon 4.

Correct targeting of this construct in ES cells was assessed by long-range PCR (LR-PCR), followed by Southern Blot (**Figure 45 B**). The positive clones were re-expanded and Neo cassette was removed by expressing FlpO recombinase. Clones with excised Neo cassette were identified by PCR. We then re-confirmed correct Neo cassette removal by Southern blot. The corrected targeted ES cell clones were then inoculated into blastocysts following standard protocols to obtain chimeric mice (see methods for details). Those were crossed with C57/Bl6 mice and offspring bearing the *Smoc2*

targeted allele were confirmed by standard genotyping (**Figure 45 C**). The *Smoc2* conditional KO mouse colony was then established and backcrossed to C57/Bl6 background for at least 6 generations before any experimental procedure.

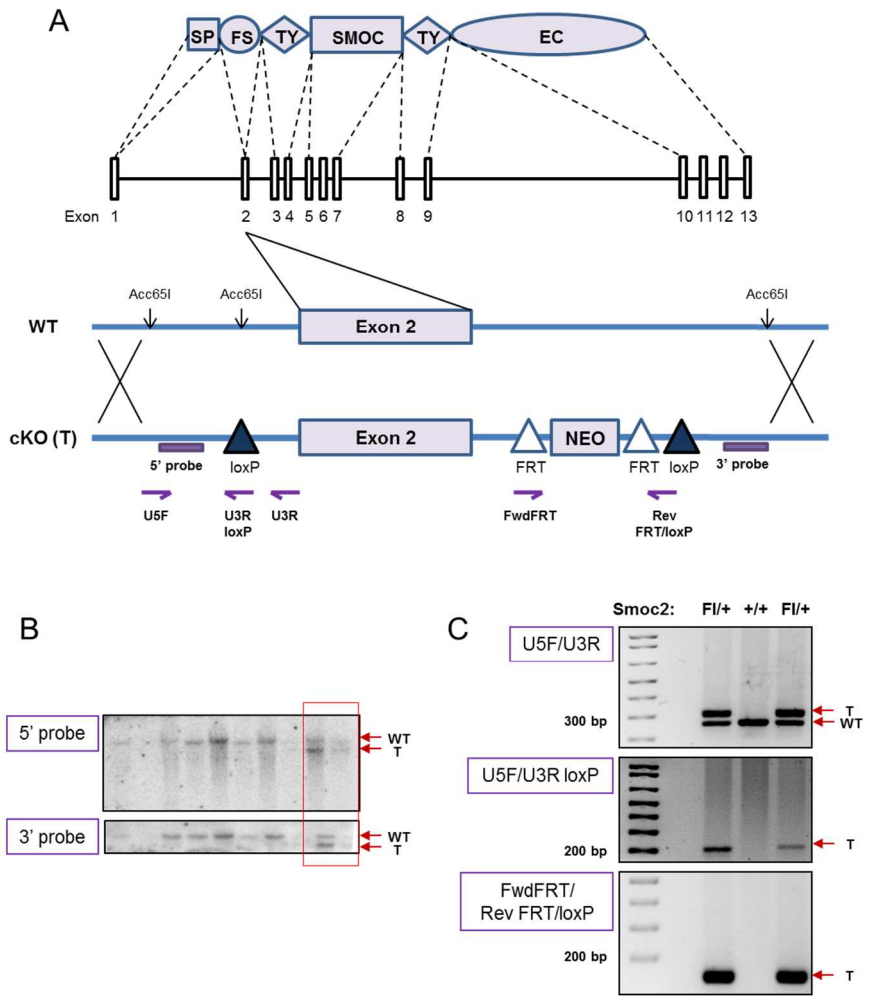

Figure 45: Generation of *Smoc2* conditional KO mouse. A. Schematic representation of mouse SMOC2 protein and *Smoc2* locus. LoxP sites are flanking the exon 2 in the targeted allele. Purple arrows indicate the position of the specific primers used for genotyping. B. Southern blots of the 5' and 3' region of *Smoc2* locus. 5' and 3' probes were used to assess gDNA after Acc65I digestion. C. PCR strategy to identify loxP and FRT sites. WT: wild-type allele; T: targeted allele.

4.2 Conditional ablation of Smoc2 in the intestinal epithelium

To ablate *Smoc2* expression in the intestinal epithelium we chose the well described *Villin Cre-ER^{T2}* transgenic mouse line. This *Cre* strain enables strong deletion of floxed genes in intestinal crypts and villi, including the ISC compartment (El Marjou et al., 2004).

Figure 46 shows the intestine-specific and inducible deletion of the exon 2 of *Smoc2* both at the level of gDNA and mRNA. Seven days after tamoxifen treatment the mRNA levels of *Smoc2* were reduced 100 fold in the intestinal epithelium of *Villin-CreER^{T2} Smoc2$^{flox/flox}$* mice (from here onwards called *Smoc2$^{\Delta IEC}$* mice) compared to *Villin-CreER^{T2} Smoc2$^{+/+}$* mice (from here onwards called *Smoc2^{CON}*).

We have been unable to detect *Smoc2* by Western Blot. Commercially available antibodies are either unable to detect the protein or they detect several unspecific bands of diverse sizes. Nevertheless, the strong decrease of *Smoc2* at the mRNA level suggests that the gene function is completely ablated in this mouse model.

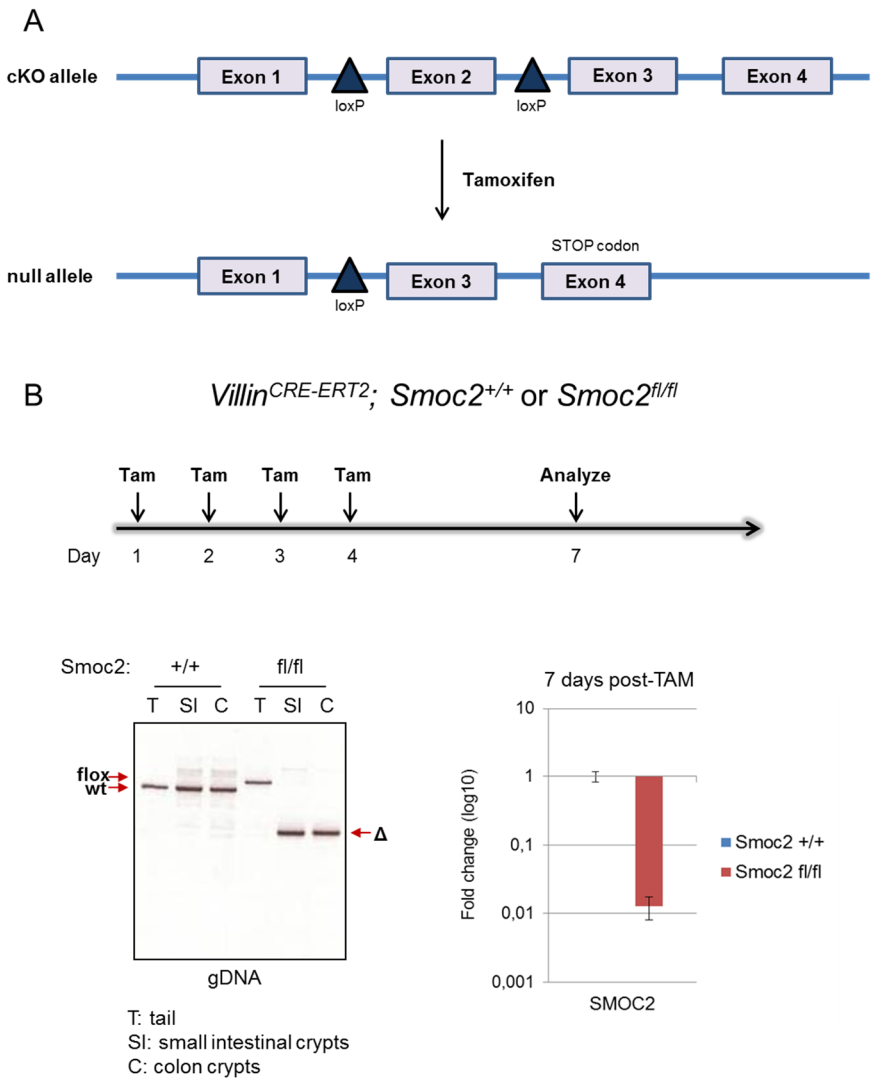

Figure 46: Intestinal deletion of *Smoc2*. A. Diagram of the targeted and the recombined allele of *Smoc2* cKO. B. Analysis of Tamoxifen injected mice bearing the *Villin Cre-ER*^{T2} transgene and either the wild-type or the floxed allele of *Smoc2*. The left panel shows the PCR on gDNA to assess recombination and the right panel shows the mRNA levels of *Smoc2* in purified intestinal crypts 7 days after tamoxifen injection. Data are mean ± SD of n=3 mice for each genotype.

4.3 BMP pathway is not altered in Smoc2 KO intestinal crypts

Several works indicate that the BMP pathway is kept off at the crypt base allowing the maintenance of the ISC compartment (Haramis et al., 2004; Kosinski et al., 2007). As the cells migrate upwards along the crypt-villus axis, they progressively encounter stronger BMP signals that trigger their differentiation.

Deletion of *Smoc2* in the intestinal epithelium did not cause changes in Inhibitor of Differentiation (*Id*) genes, which are BMP canonical targets genes (**Figure 47 A**). Moreover, we did not detect expression changes neither of *Lgr5* (**Figure 47 A**) nor of other known ISC markers (not shown). These experiments were performed on intestinal epithelial cells from purified crypts (see methods for details).

By IHC, we demonstrated that pSMAD1/5 showed negative staining in the crypts, as previously reported. *Smoc2* KO crypts did not display increased pSMAD1/5 staining (**Figure 47 B**).

All together, these data indicate that *Smoc2* depletion in intestinal epithelial cells does not alter BMP signaling.

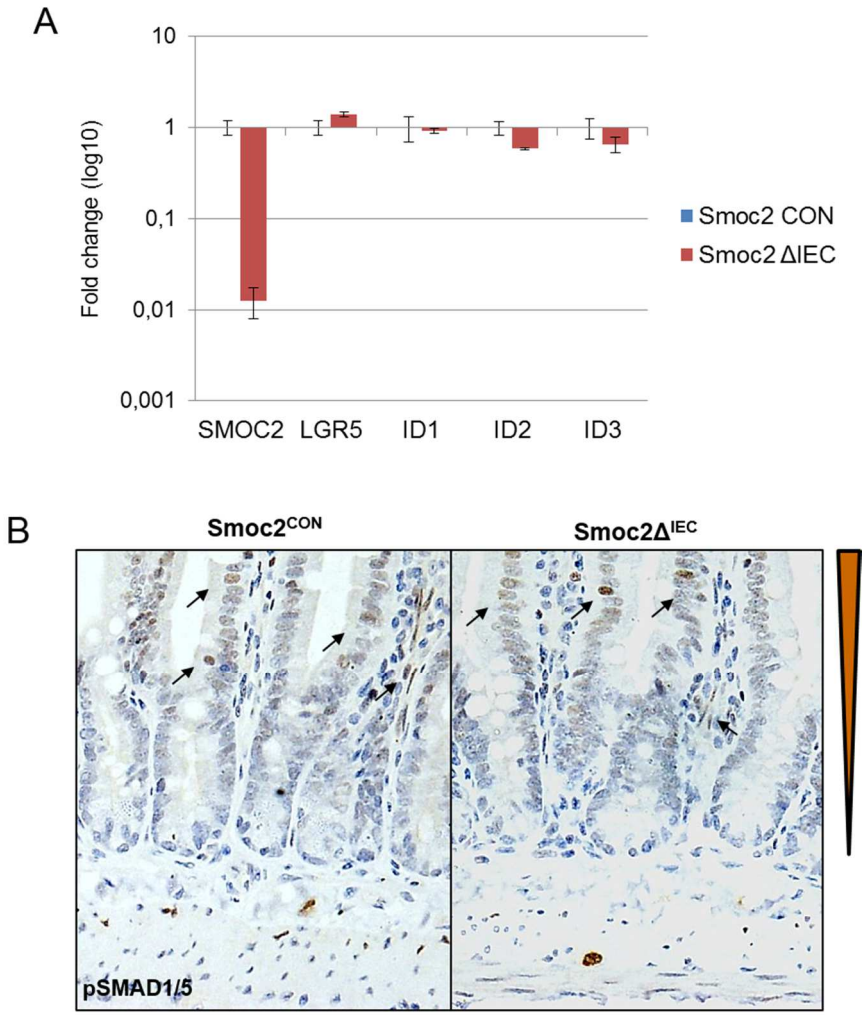

Figure 47: BMP pathway activation in intestinal crypts of *Smoc2$^{\Delta IEC}$* and *Smoc2^{CON}*. A. RT-qPCR analysis of expression of *Lgr5* and BMP target genes in intestinal crypts purified from *Smoc2$^{\Delta IEC}$* and *Smoc2^{CON}* mice 7 days after tamoxifen induction. Data are mean ± SD of n=3 mice for each genotype. B. IHC with pSMAD1/5 antibodies in intestinal crypts of adult *Smoc2$^{\Delta IEC}$* and *Smoc2^{CON}* mice. Black arrows indicate positive BMP signaling in the epithelial cells of the villus and in the stromal cells of the intravillus space. On the right, is shown the expected expression pattern.

4.4 Smoc2 epithelial depletion has no effect on intestinal biology

We next studied the overall architecture and the different cell compartments in the *Smoc2* KO intestinal epithelium. At the histological level, we could not find any obvious morphological or structural defects in *Smoc2*$^{\Delta IEC}$ mice when compared to their control littermates. EPHB2, a marker for stem cells and crypt progenitors showed the expected decreasing gradient from the crypt bottom to the top (**Figure 48 A**). MKI67 and KRT20 distinguished the proliferative from the differentiated compartment and presented a mutually exclusive expression pattern (**Figure 48 B, C**).

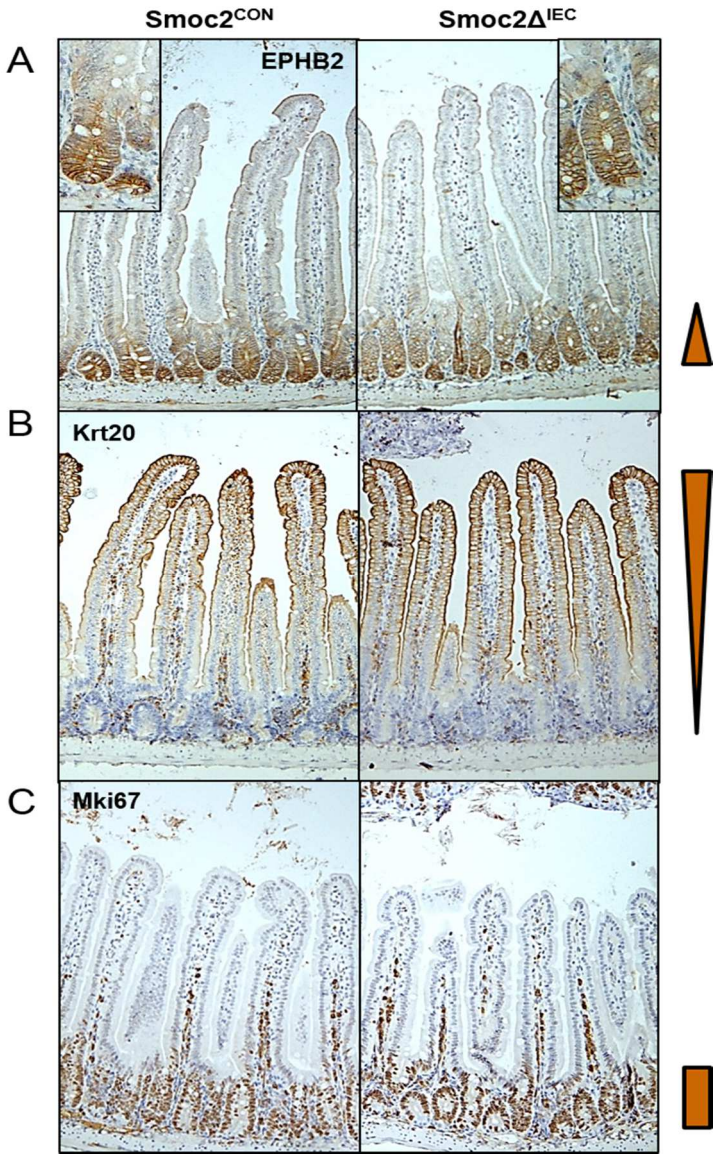

Figure 48: Impact of epithelial *Smoc2* depletion on intestinal homeostasis. A. EPHB2 IHC on intestinal sections of *Smoc2*$^{\Delta IEC}$ and *Smoc2*^{CON} mice. Insets show crypts at higher magnification. B. C. KRT20 and MKI67 IHC on intestinal sections of *Smoc2*$^{\Delta IEC}$ and *Smoc2*^{CON} mice. On the right, is shown the expected expression pattern. Duodenum, magnification 10X.

The *Villin-CreER*^{T2} driver does not enable full deletion of the floxed gene, resulting in a percentage of epithelial cells still retaining full expression of the floxed gene (El Marjou et al., 2004). In fact, we observed that *Smoc2* levels were strongly reduced (100 fold) after tamoxifen induction, but still detectable. This opens three possible scenarios: in the case that *Smoc2* depleted SCs would suffer a disadvantage from *Smoc2* loss, we should observe a progressive loss of *Smoc2* downregulation due to positive selection of *Smoc2* expressing cells that would repopulate the crypt; in the case that *Smoc2* depleted SCs would gain an advantage from *Smoc2* loss, these cells would replace the *Smoc2* expressing cells and we should observe increased reduction of *Smoc2* levels over time; in the case that *Smoc2* depletion would not give neither advantage nor disadvantage to the cells, we should expect stable *Smoc2* downregulation over time.

We then verified the extent and the persistency of *Smoc2* mRNA downregulation at early and late time points after tamoxifen induction in *Smoc2*$^{\Delta IEC}$ mice. We found that the gene deletion was stable over 7 months, suggesting that *Smoc2* deficient ISCs were neither negatively nor positively selected (**Figure 49**).

All these data pointed out that *Smoc2* is dispensable for normal intestinal homeostasis.

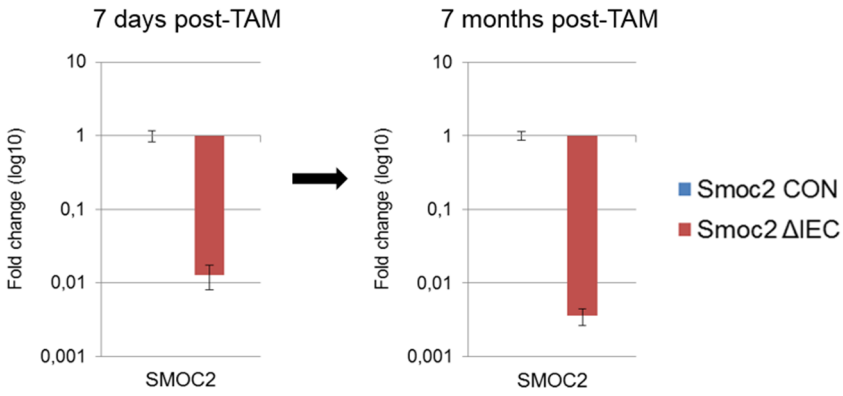

Figure 49: *Smoc2* downregulation in *Smoc2*$^{\Delta IEC}$ mice remains stable over time. mRNA levels of *Smoc2* were detected by RT-qPCR on RNA extracts of intestinal crypts purified from *Smoc2*$^{\Delta IEC}$ and *Smoc2*^{CON} mice 7 days and 7 months after tamoxifen injection. Data are mean ± SD of n=3 mice for each genotype.

4.5 Intestinal Smoc2 conditional KO in Apc mutant mice does not affect tumorigenesis

Our data demonstrate that specific *Smoc2* depletion in the epithelium does not affect the intestinal homeostasis *per se.* We then explored the role of SMOC2 during intestinal tumorigenesis.

Unpublished data from our lab demonstrate that the expression of *SMOC2* in intestinal cells is driven by β-catenin/TCF4 (Whissell, unpublished). Indeed, the inducible blockade of the WNT cascade in CRC cell lines defines specific WNT ON and WNT OFF gene programs, respectively characterized by genes that are activated by WNT (SC genes) and genes that are normally repressed by WNT (differentiation genes). We found that *SMOC2* was positively regulated by WNT (**Figure 50 A**).

Consistently, we observed that, upon mutagenic activation of WNT, *Smoc2* expression pattern in mouse *Apc* mutant crypts was expanded mirroring the expansion of the adenoma stem cell compartment (**Figure 50 B**).

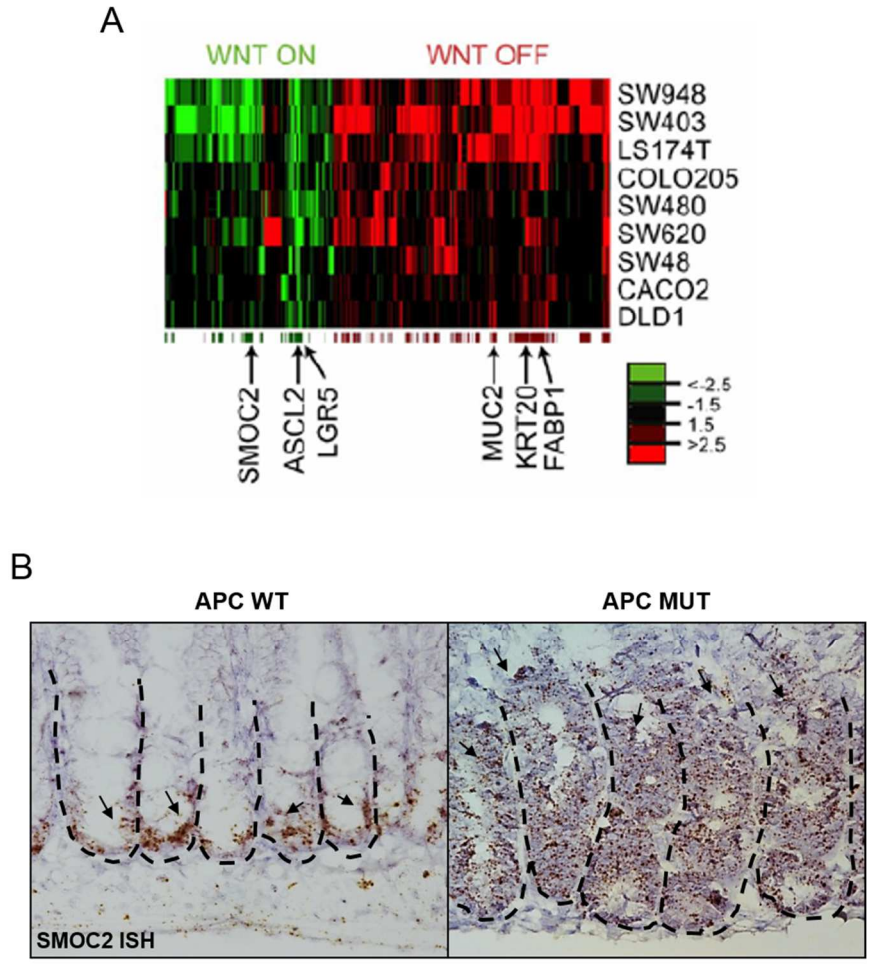

Figure 50: *Smoc2* is a WNT target gene upregulated during tumorigenesis. A. Cluster analysis showing relative changes in the expression levels of the WNT ON and the WNT OFF programs in CRC cell lines 36 hours after WNT blockade compared to control cells (Whissell, unpublished). Note that *SMOC2* is downregulated in the majority of CRC cell lines upon WNT blockade. B. Representative pictures of *Smoc2* ISH in *Apc* wild-type crypts and *Apc* mutant crypts. Black arrows indicate *Smoc2* expression restricted to the bottom of wild-type crypts and an expansion of *Smoc2* expression pattern upon mutagenic WNT activation.

To investigate SMOC2 function during tumorigenesis, we generated compound mice that carry *Smoc2 flox/flox* or wild-type alleles combined with an *Apc* floxed allele in heterozygosis (*Villin-CreER^{T2}; Smoc2$^{fl/fl}$* or *Smoc2$^{+/+}$; Apc$^{fl/+}$*) (**Figure 51 A**). In this setting, the *Villin-CreER^{T2}* driver triggers induction of the loss of one *Apc* allele in combination with loss of *Smoc2* in the whole intestinal epithelium. As it occurs in patients with FAP syndrome (see section 3.3 of the introduction), these mice develop loss of heterozygosity of the *Apc* locus spontaneously over time. This triggers the formation of intestinal adenomas.

Mice of the two genotypes presented identical survival curves and died within 10 months after tamoxifen induction (**Figure 51 B**). In a second experiment, we sacrificed the mice 4 months after induction with tamoxifen and we counted the total number of polyps developed in small intestine and colon of the two genotypes. As an average, control *Apc$^{fl/+}$* littermates (*Villin-CreER^{T2}; Smoc2$^{+/+}$; Apc$^{fl/+}$*) developed 25 polyps in the small intestine and colon (**Figure 51 C**). *Villin-creERT2; Smoc2$^{fl/fl}$; Apc$^{fl/+}$* developed equivalent number of adenomas. We neither observed differences in the size of the tumors that arose in both genotypes (**Figure 51 C**).

All together, these data imply that epithelial *Smoc2* expression is dispensable for intestinal homeostasis and that it is not required for the development of adenomas upon *Apc* inactivation.

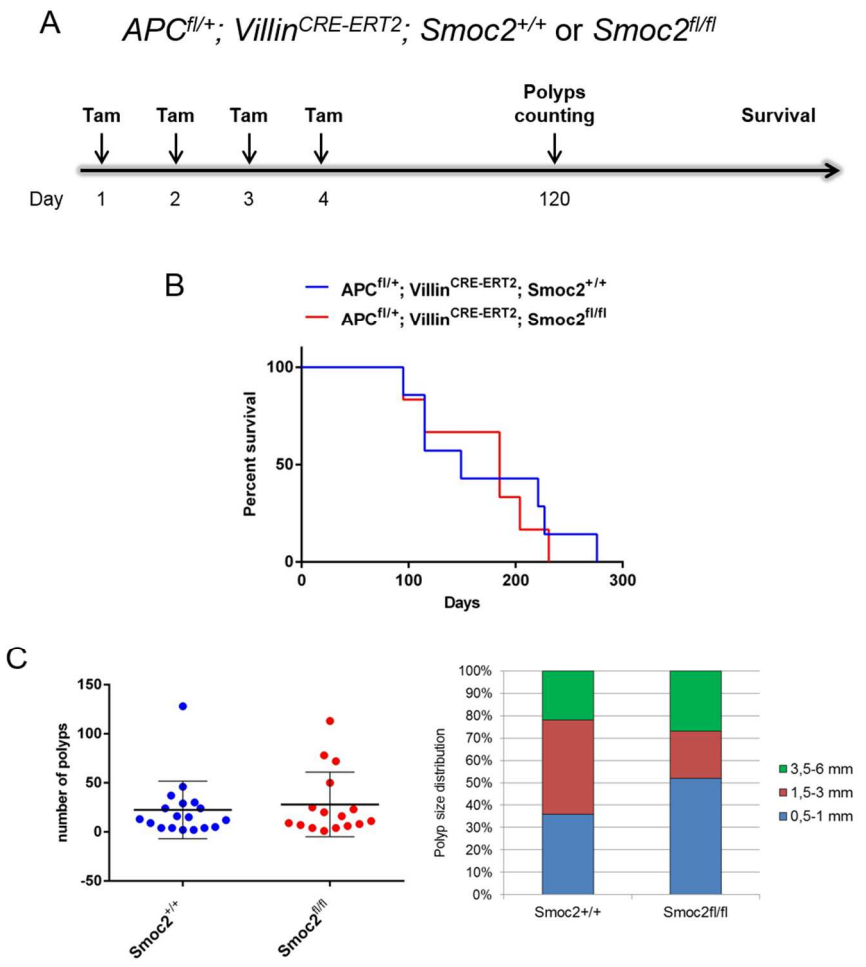

Figure 51: Effect of epithelial *Smoc2* depletion in *Apc* mutant mice. A. Experimental design. B. Survival curve of *Apc*$^{fl/+}$; *Villin-CreER*^{T2}; *Smoc2*$^{+/+}$ or *Smoc2*$^{fl/fl}$ mice after tamoxifen injection. N=7 *Smoc2*$^{+/+}$ mice; N=6 *Smoc2*$^{fl/fl}$ mice. Differences are not statistically significant. C. Polyp counting in small intestine and colon and polyp size distribution in *Apc*$^{fl/+}$; *Villin-CreER*^{T2}; *Smoc2*$^{+/+}$ or *Smoc2*$^{fl/fl}$ mice 4 months after tamoxifen injection. Each dot in the left panel represents one measurement for one mouse. N=18 *Smoc2*$^{+/+}$ mice; N=16 *Smoc2*$^{fl/fl}$ mice. Differences are not statistically significant.

4.6 A stromal Smoc2 source compensates downregulation of Smoc2 in the epithelium of Smoc2$^{\Delta IEC}$ mice

The complete lack of phenotype in the *Smoc2* mutant intestinal epithelium prompted us to investigate the possibility that an additional source of SMOC2 from stromal cells may compensate this deficiency. We thus investigated *Smoc2* expression in whole intestinal extracts of *Smoc2*$^{\Delta IEC}$ mice that include epithelial and stromal cells, such as fibroblasts, leukocytes, blood vessels, smooth muscle cells and nerve cells. Indeed, we observed that overall *Smoc2* mRNA levels did not change in the intestine of *Smoc2*$^{\Delta IEC}$ mice, suggesting the existence of a *Smoc2* extra-epithelial source (**Figure 52 A).** We next measured *Smoc2* specific gene expression in samples of homogenized total intestine compared to epithelium-depleted intestine (submucosa). For these experiments, we removed the epithelium by following the crypt extraction protocol described in the method section. We confirmed that the submucosa compartment showed high enrichment of general stroma genes (*Cd45*: pan-leukocyte marker; *Cd31*: endothelial marker; *IgfBP7*: fibroblast marker). Inversely, epithelial markers were lowly expressed in the submucosa (*EpCAM*: general epithelial marker; *Krt20, Aqp3, DefCR, Cryptidin*: epithelial differentiation markers; *Olfm4*: ISC marker). *Smoc2* mRNA level did not decrease upon removal of the epithelium, thus confirming the presence of a *Smoc2* extra-source that maintains high general *Smoc2* expression in the intestine of *Smoc2*$^{\Delta IEC}$ mice (**Figure 52 B).** The lack of a suitable SMOC2 antibody did not allow us to test this hypothesis on intestinal tissue sections by IHC or by Western Blot on total protein extracts. To overcome this limitation we used ISH, which showed high *Smoc2* mRNA enrichment in ISCs as well as in scattered cells in the submucosa layer (**Figure 52 C**). These

stromal *Smoc2* positive cells may likely represent fibroblast, endothelial cells, muscle cells or macrophages. Unfortunately, the resolution limits of this technique did not allow us to identify the precise cell types expressing *Smoc2* in the stroma.

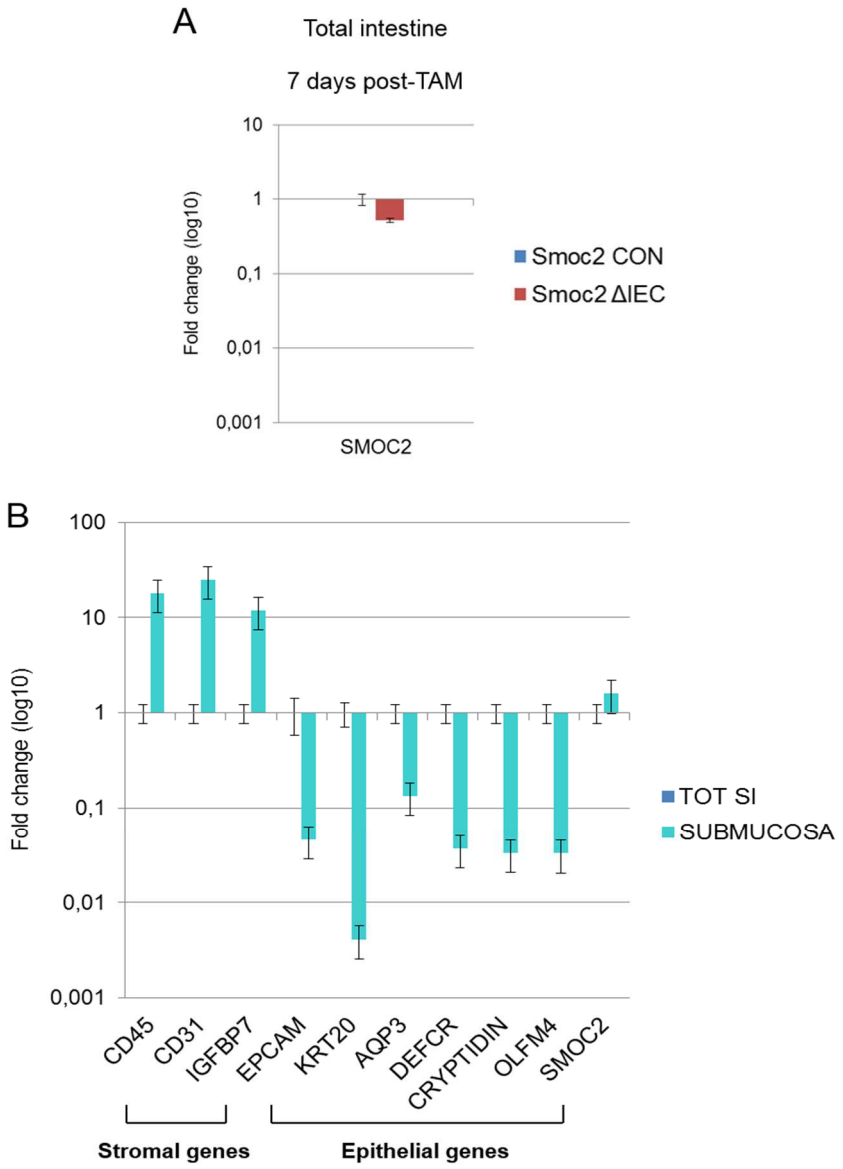

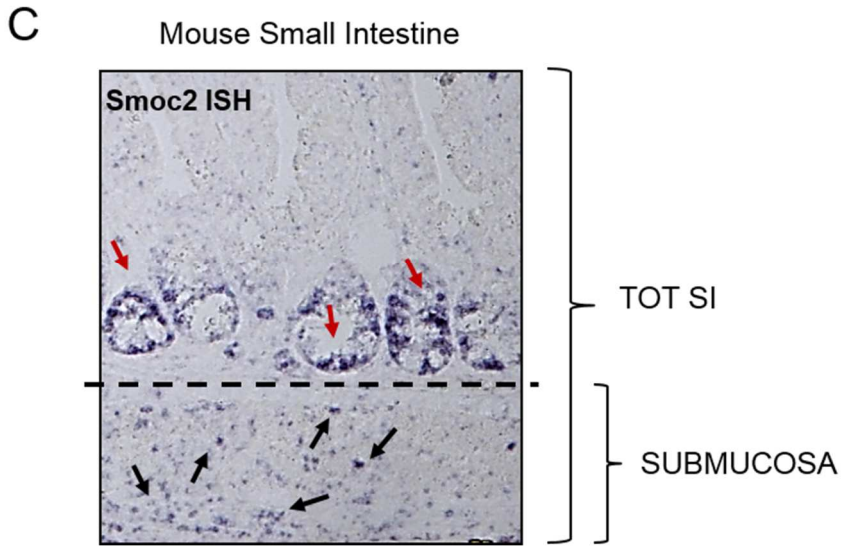

Figure 52: *Smoc2* extra-epithelial source. A. Detection of *Smoc2* expression by RT-qPCR on RNA extracts of total small intestine of *Smoc2*$^{\Delta IEC}$ and *Smoc2*^{CON} mice. Data are mean ± SD of n=3 mice for each genotype. B. Epithelial gene depletion and stromal gene enrichment in intestinal submucosa compared to total intestine. Genes were measured by RT-qPCR in total small intestine and in intestinal submucosa of *Smoc2* wild-type mice. Please note that *Smoc2* expression did not change in epithelium-depleted intestinal tissue. C. *Smoc2* mRNA detection in mouse intestinal section by ISH using a specific full length probe. Dashed line indicates the epithelium-submucosa boundary. Red arrows indicate *Smoc2* mRNA at the bottom of the intestinal crypts where ISCs reside. Black arrows indicate *Smoc2* positive cells in the submucosa.

We also dissected large polyps arising in *Villin-CreER^{T2}; Smoc2$^{fl/fl}$; Apc$^{fl/+}$* or in control *Villin-CreER^{T2}; Smoc2$^{+/+}$; Apc$^{fl/+}$* mice and analyzed *Smoc2* expression. We analyzed either the protruding part of the polyp, which is mainly composed by epithelial *Apc* mutant cells that express high levels of *Smoc2* as result of WNT pathway activation, or macro-dissected samples that include polyp plus submucosa (**Figure 53 A**). This experiment revealed large downregulation of *Smoc2* in the protruding region of polyps from *Villin-CreER^{T2}; Smoc2$^{fl/fl}$; Apc$^{fl/+}$* mice (**Figure 53 B**). In contrast, in samples that comprised polyp and submucosa, there was an evident compensation in *Smoc2* levels of about 10 fold (**Figure 53 B**).

Overall, these data suggest that stromal expression compensates *Smoc2* deficiency in epithelial cells. This compensation is complete in the normal intestine whereas it is less evident in large polyps that display a higher ratio of epithelial versus stromal cells.

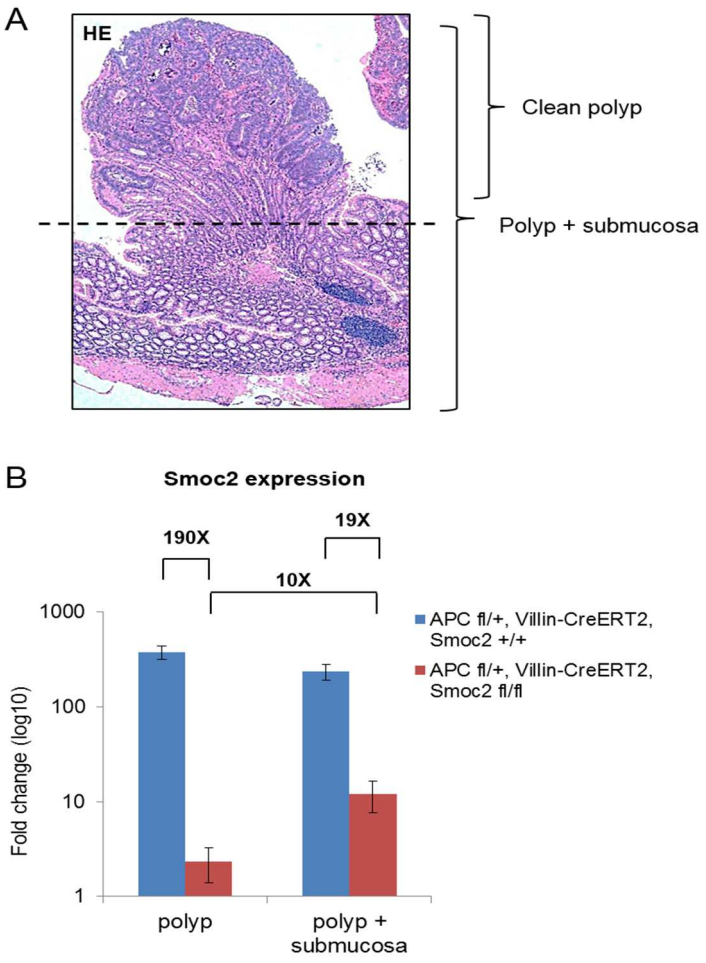

Figure 53: *Smoc2* extra-epithelial source in adenoma. A. HE staining of an adenomatous polyp composed of polyp glands plus the submucosa. B. *Smoc2* expression detected by RT-qPCR on RNA extracts deriving from the protruding part of the polyp alone or the polyp plus submucosa. Data are mean ± SD of n=3 mice for each genotype (*Villin-CreER^{T2}; Smoc2$^{+/+}$; Apc$^{fl/+}$* and *Villin-CreER^{T2}; Smoc2$^{fl/fl}$; Apc$^{fl/+}$*).

5. Characterization of *Smoc2* full KO mouse

5.1 Generation of Smoc2 null allele

Considering the lack of phenotype resulting from the conditional ablation of *Smoc2* in the adult intestinal epithelium and the possibility of compensation by stromal cells expressing *Smoc2*, we generated mice null for *Smoc2* in all tissues. To this end, we crossed *Smoc2*$^{flox/flox}$ mice with a transgenic *Sox2-Cre* line (Hayashi et al., 2002). This *Cre* line turned the conditional allele into a null allele in all the cells of the embryo including the germline. We selected mice bearing the *Smoc2Δ* allele in heterozygosis from this intercross and further breed them to obtain the *Smoc2* full KO mice (*Smoc2*$^{\Delta/\Delta}$). Mutant mice were identified by standard genotyping (**Figure 54**).

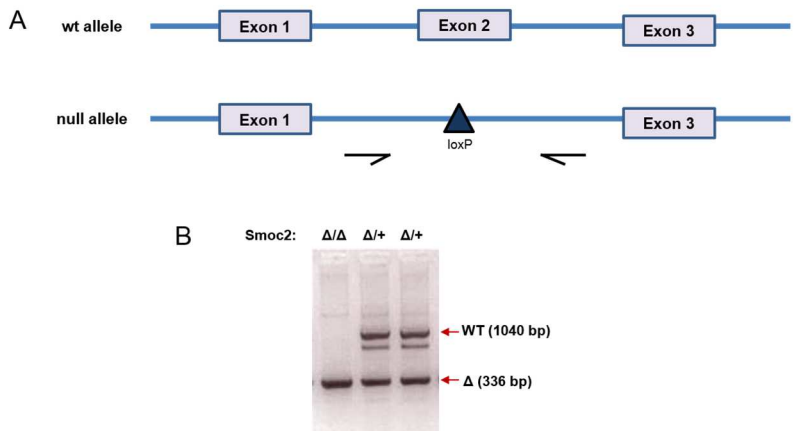

Figure 54: Generation of *Smoc2* full KO mouse. A. Diagram showing wild-type and null *Smoc2* alleles. Black arrows indicate the position of the specific primers used for genotyping. B. PCR to assess *Smoc2* null allele.

5.2 Complete Smoc2 ablation does not affect intestinal homeostasis

Smoc2$^{\Delta/\Delta}$ mice were born following mendelian ratio. Young and old mice did not display any gross abnormality and they were fertile. In order to confirm the lack of phenotype, we analyzed the intestine of *Smoc2*$^{+/+}$ and *Smoc2*$^{\Delta/\Delta}$ mice. Gross histological analysis revealed no obvious alteration in young or old *Smoc2* mutant mice (**Figure 55**).

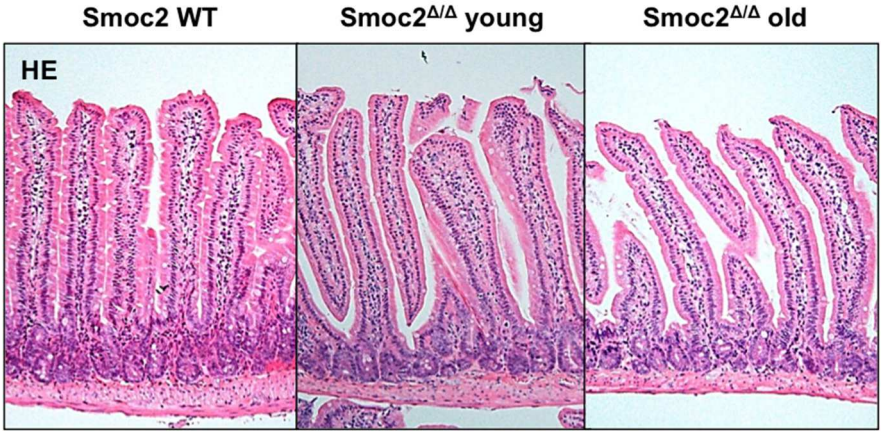

Figure 55: Old *Smoc2*$^{\Delta/\Delta}$ mice do not display histological alterations. Representative pictures showing HE of intestinal sections of *Smoc2*$^{+/+}$ (left panel), young *Smoc2*$^{\Delta/\Delta}$ (middle panel) and old *Smoc2*$^{\Delta/\Delta}$ (right panel) mice. Duodenum, magnification 10X.

Our quantitative analysis included length of the villi and the number of cells per crypt as well as the extent of proliferative compartment by counting MKI67 positive cells per crypt (**Figure 56**). We also assessed differentiation towards multiple lineages by ChromograninA staining (enteroendocrine cells), PAS/Alcian blue staining (mucosecreting cells and enterocytes), and Lysozyme staining (Paneth cells) (**Figure 57**). Finally, we measured cell migration along the crypt-villus axis. We did not find differences in any of these parameters in *Smoc2*$^{\Delta/\Delta}$ mice compared to *Smoc2*$^{+/+}$ littermates (**Figure 58**).

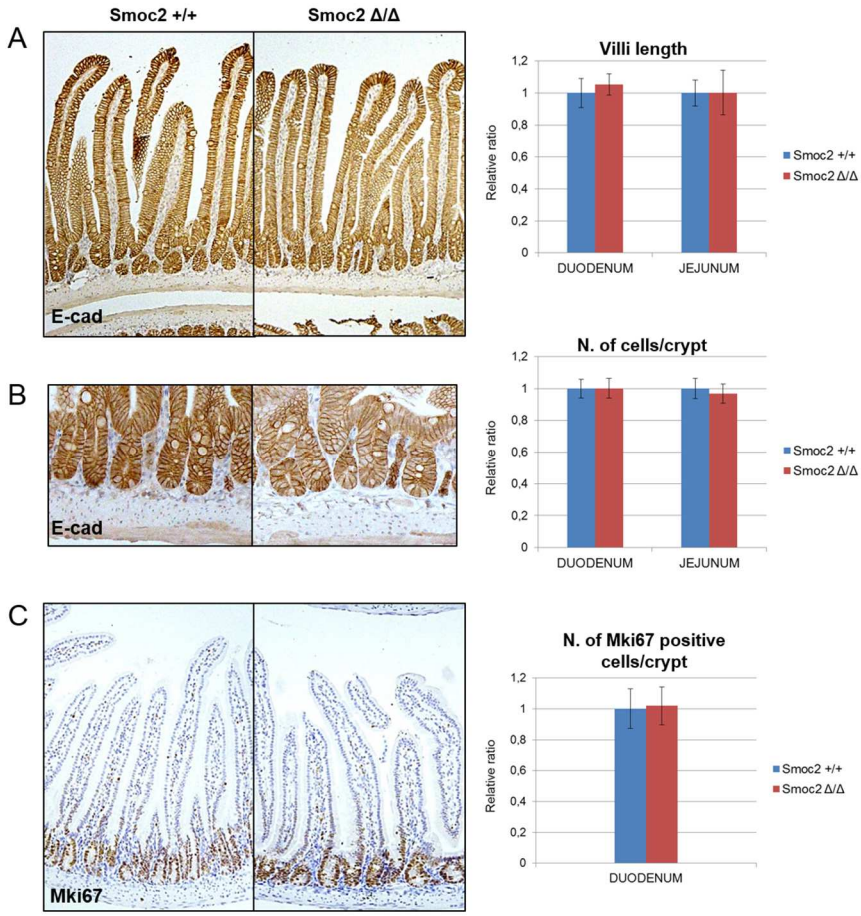

Figure 56: *Smoc2*$^{\Delta/\Delta}$ mice do not show intestinal abnormalities. A. Representative pictures of E-Cadherin staining in *Smoc2*$^{+/+}$ and *Smoc2*$^{\Delta/\Delta}$ intestinal sections (left panel). Duodenum, magnification 10X. Quantification (right panel) of the length of the villi. Data are mean ± SD of n=20 measurements for each genotype. B. Representative pictures of E-Cadherin staining in *Smoc2*$^{+/+}$ and *Smoc2*$^{\Delta/\Delta}$ intestinal crypts (left panel). Quantification (right panel) of the number of cells per crypt. Data are mean ± SD of n=20 measurements for each genotype. C. Representative pictures of MKI67 staining in *Smoc2*$^{+/+}$ and *Smoc2*$^{\Delta/\Delta}$ intestinal sections (left panel). Duodenum, magnification 10X. Quantification (right panel) of the number of MKI67 positive cells per crypt (proliferative cells). Data are mean ± SD of n=20 measurements for each genotype.

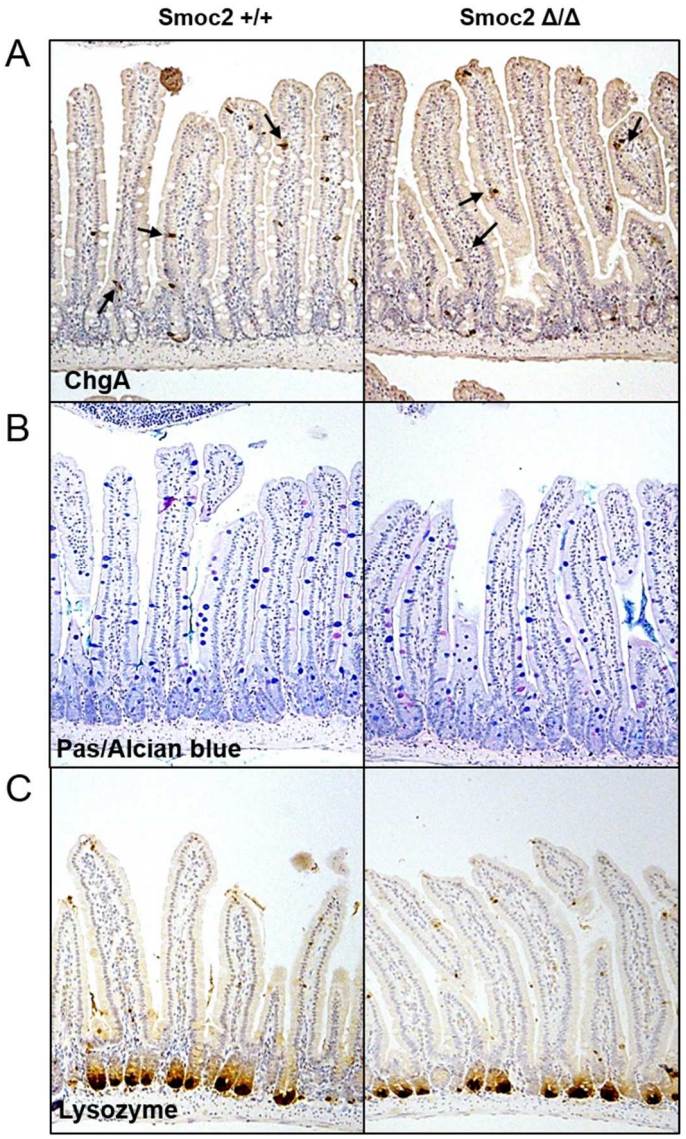

Figure 57: Differentiation towards multiple lineages is not affected in *Smoc2*$^{\Delta/\Delta}$ mice. Representative pictures of ChromograninA staining (enteroendocrine cells) (A), Pas/Alcian blue staining (goblet cells and enterocytes) (B) and Lysozyme staining (Paneth cells) (C) in intestinal sections of *Smoc2*$^{+/+}$ and *Smoc2*$^{\Delta/\Delta}$ mice. Black arrows indicate enteroendocrine cells. Duodenum, magnification 10X.

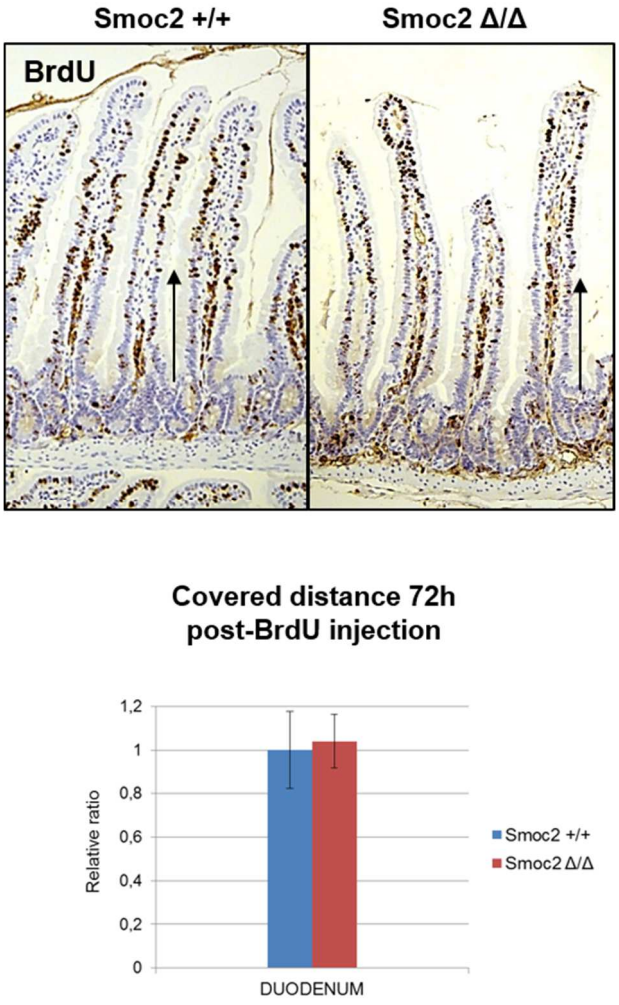

Figure 58: Cell migration along the crypt-villus axis is not affected in *Smoc2*$^{\Delta/\Delta}$ intestine. Representative pictures showing BrdU staining 72 hours post-injection in *Smoc2*$^{+/+}$ and *Smoc2*$^{\Delta/\Delta}$ duodenum. Black arrows indicate the equal distance covered by the BrdU positive cell front in both genotypes. Magnification 10X. Lower panel shows the quantification. Data are mean ± SD of n=20 measurements for each genotype.

The above results prompted us to search for compensation by *Smoc1* in the intestine of *Smoc2*$^{\Delta/\Delta}$ mice. Our data indicated that *Smoc1* was expressed at very low levels in the intestine, displaying cycle threshold (ct) value 33 compared to *Smoc2* (ct value: 25) (**Figure 59 A**). Moreover, its levels did not change upon deletion of *Smoc2* (**Figure 59 B**). *Sparc*, a related gene, was also expressed at equivalent levels in the intestine of *Smoc2*$^{\Delta/\Delta}$ mice compared to *Smoc2*$^{+/+}$ littermates (ct value: 28). We also measured intestinal BMP inhibitors (*Grem1, Grem2, Chordin*) in total intestine, which were expressed yet they did not change significantly in *Smoc2* deficient mice (ct value: 28) (**Figure 59 B**).

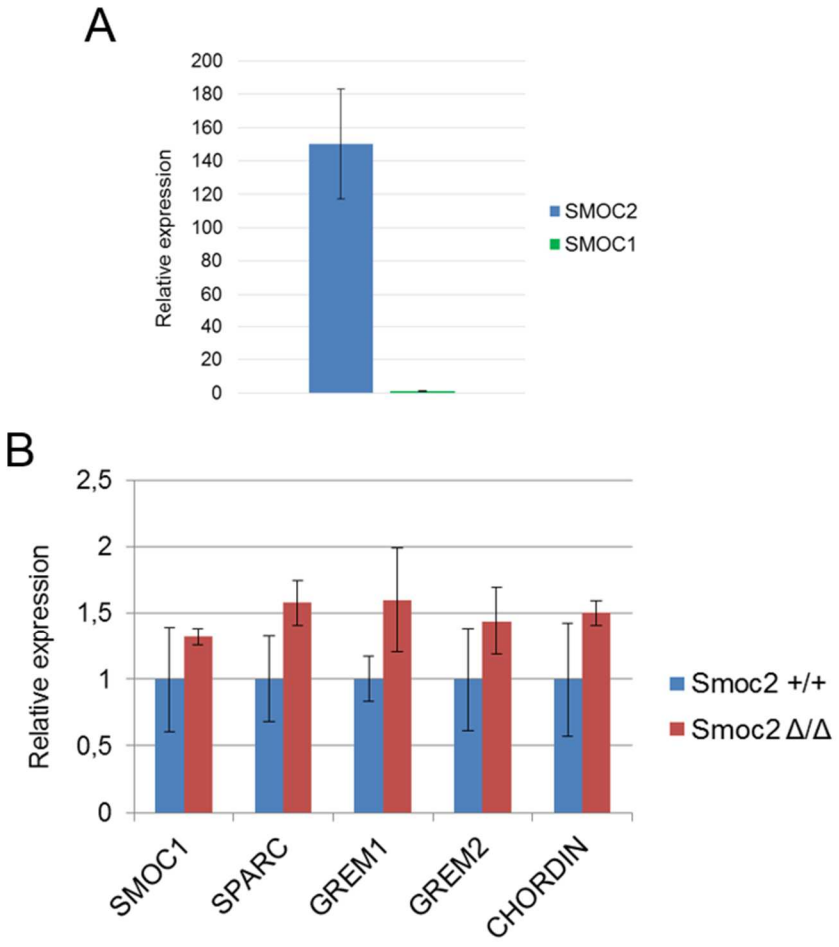

Figure 59: Expression levels of *Bm-40* related genes and BMP inhibitors in *Smoc2*$^{\Delta/\Delta}$ intestine. A. Comparison between *Smoc2* and *Smoc1* expression levels measured by RT-qPCR in total intestinal RNA extracts from wild-type mice. Note that *Smoc1* is 150 fold less expressed than *Smoc2*. Data are mean ± SD of n=3 mice for each genotype. B. Expression levels of *Bm-40* genes (*Smoc1* and *Sparc*) and known intestinal BMP inhibitors detected by RT-qPCR in total intestinal RNA extracts from *Smoc2*$^{+/+}$ and *Smoc2*$^{\Delta/\Delta}$ mice. Data are mean ± SD of n=3 mice for each genotype.

5.3 Full Smoc2 ablation does not affect intestinal BMP signaling

We first verified *Smoc2* mRNA levels in purified epithelial cells from crypts or whole tissue extracts of *Smoc2*$^{\Delta/\Delta}$ mice. As expected, *Smoc2* was barely detectable in both cases (**Figure 60 A, B**). We then measured expression levels of SC markers and BMP target genes. In purified epithelial cells from crypts we did not detect evident changes in BMP target gene expression (*Apcdd1, Id3*), in markers of stemness (*Lgr5*) or differentiation (*Krt20*) (**Figure 60 A**). BMP target gene expression was also unaffected in total intestine samples (*Id1, Id3, Apcdd1, Smad6*) (**Figure 60 B**).

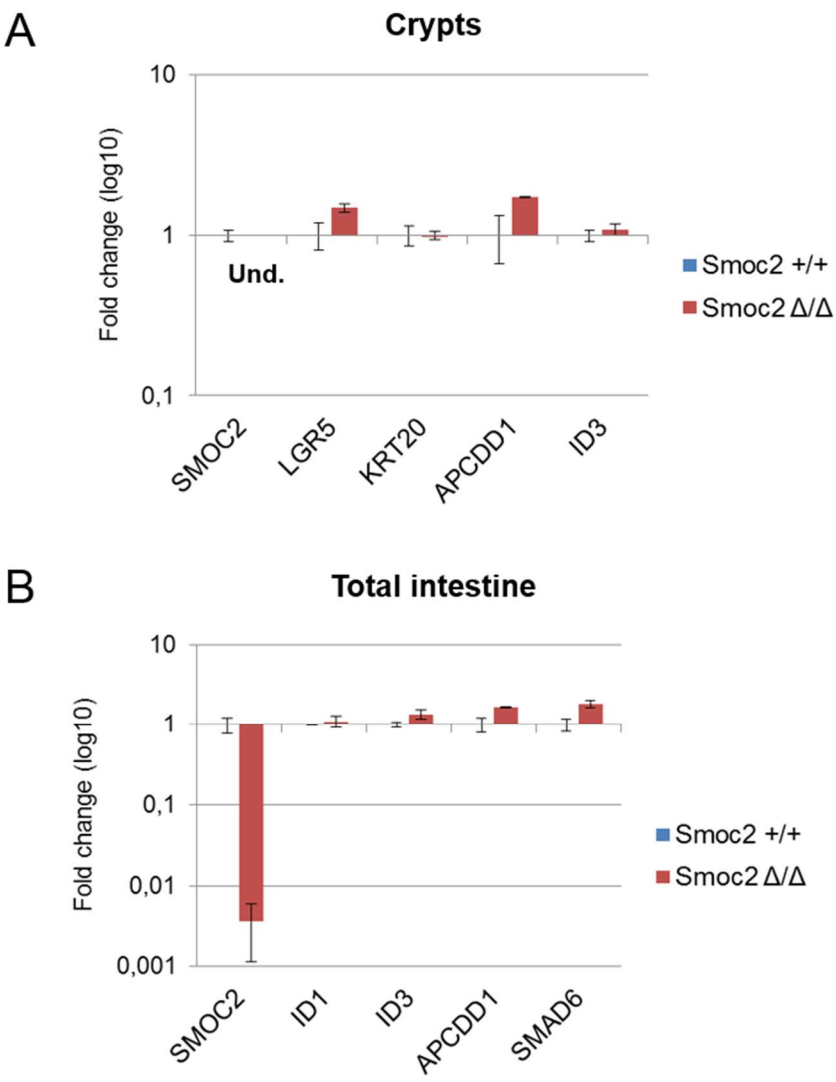

Figure 60: Complete *Smoc2* ablation does not affect intestinal BMP signaling. Gene expression analysis by RT-qPCR of purified intestinal crypt extracts (A) and total intestinal extracts (B) from *Smoc2*$^{+/+}$ and *Smoc2*$^{\Delta/\Delta}$ mice. Data are mean ± SD of n=3 mice for each genotype.

Furthermore, histological analysis showed equivalent pSMAD1/5 patterns in *Smoc2*$^{+/+}$ and *Smoc2*$^{\Delta/\Delta}$ mice. In both genotypes there was a decreasing gradient of BMP pathway activation from the tip of the villi towards the bottom of the crypts. In addition, some stromal cells located in the intravillus space present in both *Smoc2*$^{+/+}$ and *Smoc2*$^{\Delta/\Delta}$ intestines displayed positive pSMAD1/5 accumulation (**Figure 61**).

These observations imply that during adult intestinal homeostasis, *Smoc2* is dispensable for protecting ISCs from BMP pathway activation. We speculate that this is probably due to high abundance of other BMP inhibitors secreted by the stroma underlying the crypts (Kosinski et al., 2007).

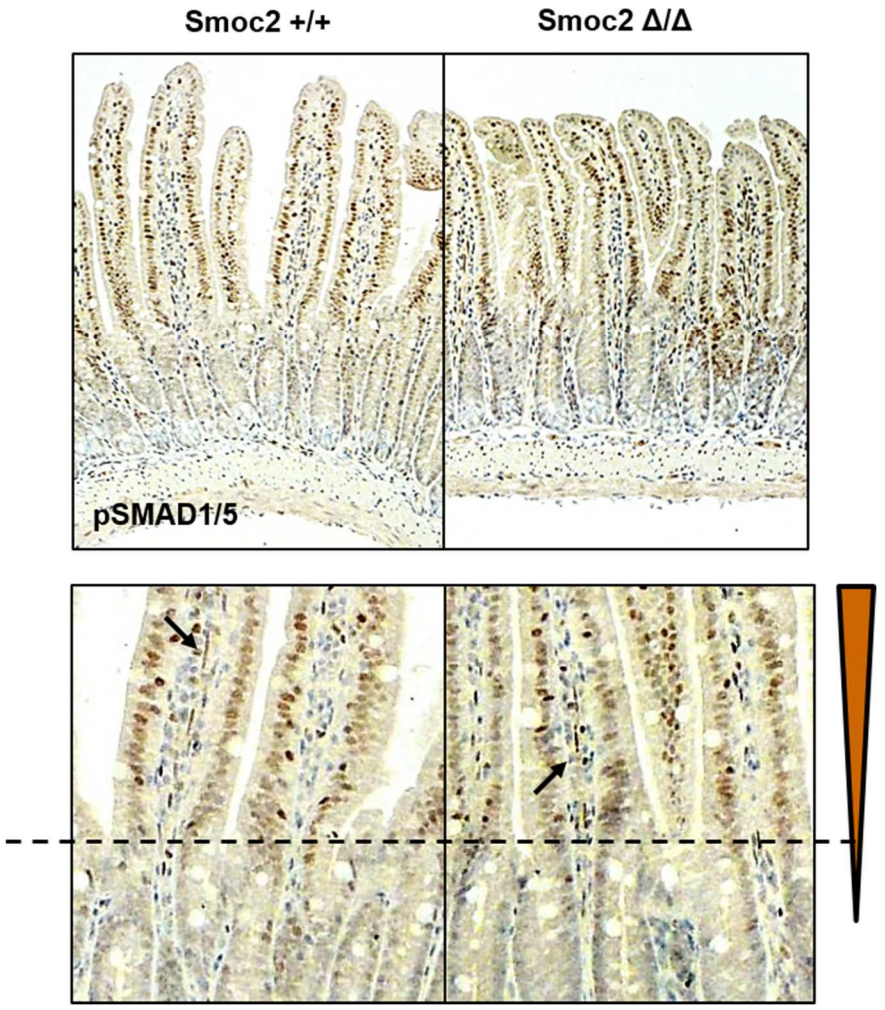

Figure 61: BMP signaling distribution is not affected in *Smoc2*$^{\Delta/\Delta}$ intestine. pSMAD1/5 staining on intestinal sections of *Smoc2*$^{+/+}$ and *Smoc2*$^{\Delta/\Delta}$ mice (upper panels). Jejunum, magnification 10X. Lower panels show the crypt-villus junction at higher magnification. Dashed line defines the crypt-villus boundary. Black arrows indicate scattered pSMAD1/5 positive cells in the intravillus space. On the right, is shown the expected pSMAD1/5 pattern in the epithelial cells.

5.4 Smoc2 depletion does not affect either BMP signaling or ISC self-renewal capability

To definitely confirm SMOC2 dispensability for ISC maintenance, we cultured intestinal crypts from *Smoc2*$^{+/+}$ and *Smoc2*$^{\Delta/\Delta}$ mice in 3D conditions. As already commented in section 2 and in the introduction, robust inhibition of BMP signals is required to culture ISCs. In the presence of rNOGGIN, *Smoc2*$^{+/+}$ and *Smoc2*$^{\Delta/\Delta}$ mouse-derived crypts were able to grow equally and were maintained over time (**Figure 62 A, B**). In order to exclude that rNOGGIN was masking the contribution of SMOC2, we followed organoid growth upon rNOGGIN dilution. We observed that the removal of rNOGGIN from the culture dramatically impaired the organoid growth and, upon rNOGGIN dilution, *Smoc2*$^{+/+}$ and *Smoc2*$^{\Delta/\Delta}$ organoids suffered equal growth reduction (**Figure 62 C**).
Our data indicate that in this context, the absence or presence of endogenous SMOC2 does not impinge on ISC growth.

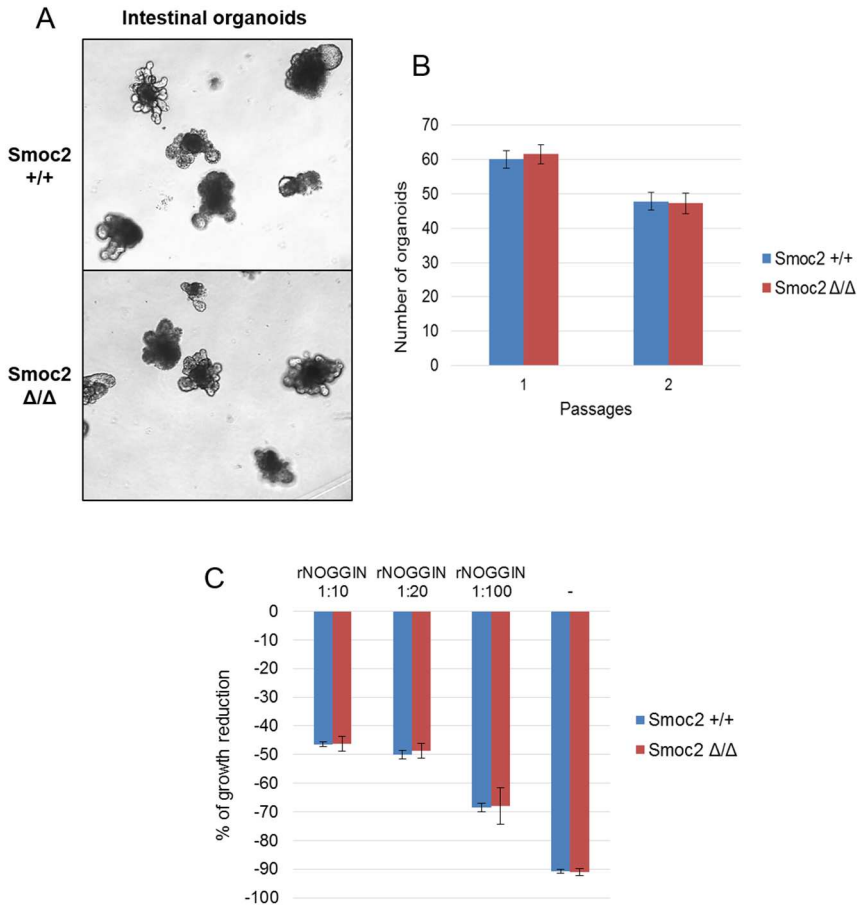

Figure 62: *In vitro* growth of ISCs derived from *Smoc2*$^{+/+}$ and *Smoc2*$^{\Delta/\Delta}$ mice. A. Representative pictures of organoids grown from *Smoc2*$^{+/+}$ and *Smoc2*$^{\Delta/\Delta}$ purified intestinal crypts in the presence of rNOGGIN. B. Assessment of clonogenic potential of *Smoc2*$^{+/+}$ and *Smoc2*$^{\Delta/\Delta}$ ISCs cultured with rNOGGIN (100ng/ml). Formed organoids were counted 5 days after disaggregation and seeding and the whole process was repeated over passaging. Data are mean ± SD of n=5 measurements for each genotype. C. Progressive reduction of organoid formation in *Smoc2*$^{+/+}$ and *Smoc2*$^{\Delta/\Delta}$ ISC cultures when subjected to increasing rNOGGIN dilutions. Data are mean ± SD of triplicates.

5.5 Full Smoc2 ablation in Apc mutant mice enhances survival and reduces polyp formation and size

Considering the lack of intestinal phenotypes resulting from full *Smoc2* deficiency, we decided to analyze the effect of *Smoc2* depletion in pathological settings. We generated *Villin-CreER^{T2}; Smoc2$^{\Delta\Delta}$; Apc$^{fl/+}$* mice and control *Villin-CreER^{T2}; Smoc2$^{+/+}$; Apc$^{fl/+}$* littermates. We challenged them with tamoxifen and performed survival and polyp formation studies (**Figure 63 A**). These experiments revealed a significant enhancement of survival in *Smoc2* deficient mice (**Figure 63 B**). Polyp counting confirmed reduced polyp number and size in *Smoc2$^{\Delta\Delta}$* mice (**Figure 63 C**).

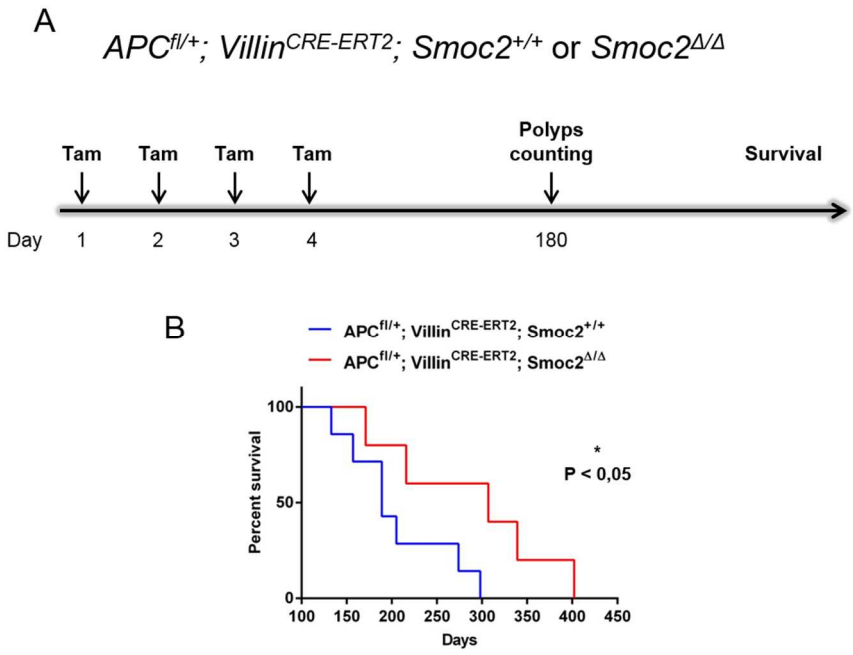

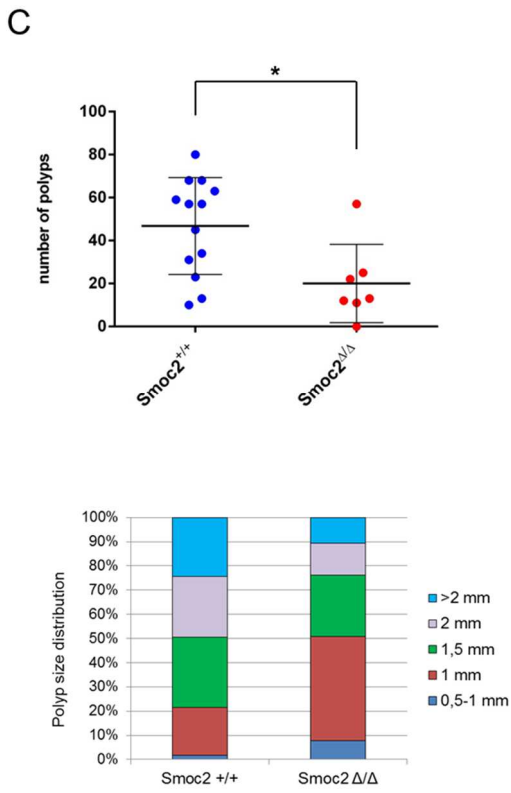

Figure 63: Effect of full *Smoc2* ablation in *Apc* mutant mice. A. Experimental design. B. Survival curve of *Villin-CreER^{T2}; Smoc2$^{\Delta\Delta}$; Apc$^{fl/+}$* mice and control *Villin-CreER^{T2}; Smoc2$^{+/+}$; Apc$^{fl/+}$* mice after tamoxifen injection. N=7 *Villin-CreER^{T2}; Smoc2$^{+/+}$; Apc$^{fl/+}$* mice and 6 *Villin-CreER^{T2}; Smoc2$^{\Delta\Delta}$; Apc$^{fl/+}$* mice. Statistics are done using the log-rank test. C. Polyp counting (upper panel) and polyp size distribution (bottom panel) in small intestine and colon of *Villin-CreER^{T2}; Smoc2$^{\Delta\Delta}$; Apc$^{fl/+}$* mice and control *Villin-CreER^{T2}; Smoc2$^{+/+}$; Apc$^{fl/+}$* mice 6 months after tamoxifen induction. Each dot in the upper panel represents one measurement (one mouse). Data are mean ± s.e.m. of n=13 *Villin-CreER^{T2}; Smoc2$^{+/+}$; Apc$^{fl/+}$* mice and 7 *Villin-CreER^{T2}; Smoc2$^{\Delta\Delta}$; Apc$^{fl/+}$* mice. Statistics are done by Student's *t*-test. **P*<0,05. Lower panel shows size distribution of all the polyps counted in the two genotypes and represented in the upper panel.

5.6 Effect of Smoc2 deficiency on inflammation

Inflammation exacerbates intestinal tumorigenesis in mouse models and in humans (Balzola et al., 2013; Zaki et al., 2011). Likewise, blockade of inflammatory pathways is linked to decreased incidence of CRC in patients and experimental models. We thus tested the intestinal inflammatory response in *Smoc2*$^{+/+}$ and *Smoc2*$^{\Delta/\Delta}$ mice. Treatment of mice with Dextran Sulfate Sodium (DSS) induces mechanical stress on colon epithelial surface, which triggers inflammation and colitis-like disease in the colon. This process progresses in specific steps: epithelium destruction, stromal infiltration and inflammation, *de novo* crypt formation and fission, repopulation and restoration of the normal epithelial layer. We subjected the mice to sub-lethal DSS exposure during five days. We assessed the efficiency of DSS-induced damage by checking appearance of fecal blood during the treatment. Subsequently, we tracked the recovery process by measuring the body weight loss and by analyzing the histology of the colonic mucosa at different time points (**Figure 64 A**). Three independent experiments showed that *Smoc2*$^{\Delta/\Delta}$ mice lost less weight and recovered faster than littermates *Smoc2*$^{+/+}$ mice (**Figure 64 C**). The histological analysis revealed that after five days of DSS treatment both genotypes presented an altered architecture of the intestinal epithelial layer. At this stage, there was no obvious inflammation (**Figure 64 B**) and all mice were positive to the fecal blood test. Two days after DSS removal, we observed massive stromal infiltration and inflammation in *Smoc2*$^{+/+}$ mice, whereas this response was attenuated in *Smoc2*$^{\Delta/\Delta}$ mice that had already undergone active intestinal regeneration and *de novo* crypt formation. Seven days after the removal of DSS from drinking

water, *Smoc2*$^{\Delta/\Delta}$ mice had almost fully recovered, whereas *Smoc2*$^{+/+}$ mice were still in the process of tissue reconstruction (**Figure 64 B**). These results imply that, upon damage, *Smoc2*$^{\Delta/\Delta}$ mice are less prone to undergo inflammation. We checked whether loss of *Smoc2* affects intestinal permeability, since an altered permeability could modulate the exposure of the mucosa to the gut microbiota and determine the extent of inflammation upon damage. To this end, we administered FITC-dextran by oral gavage and quantified the amount of absorbed FITC-dextran 4 hours later by measuring the correspondent absorbance in blood samples. Yet, we could not observe differences (**Figure 64 D**). We hypothesize that the resistance to DSS-induced colitis could be due to different recruitment or activation of pro-inflammatory cells at sites of damage.

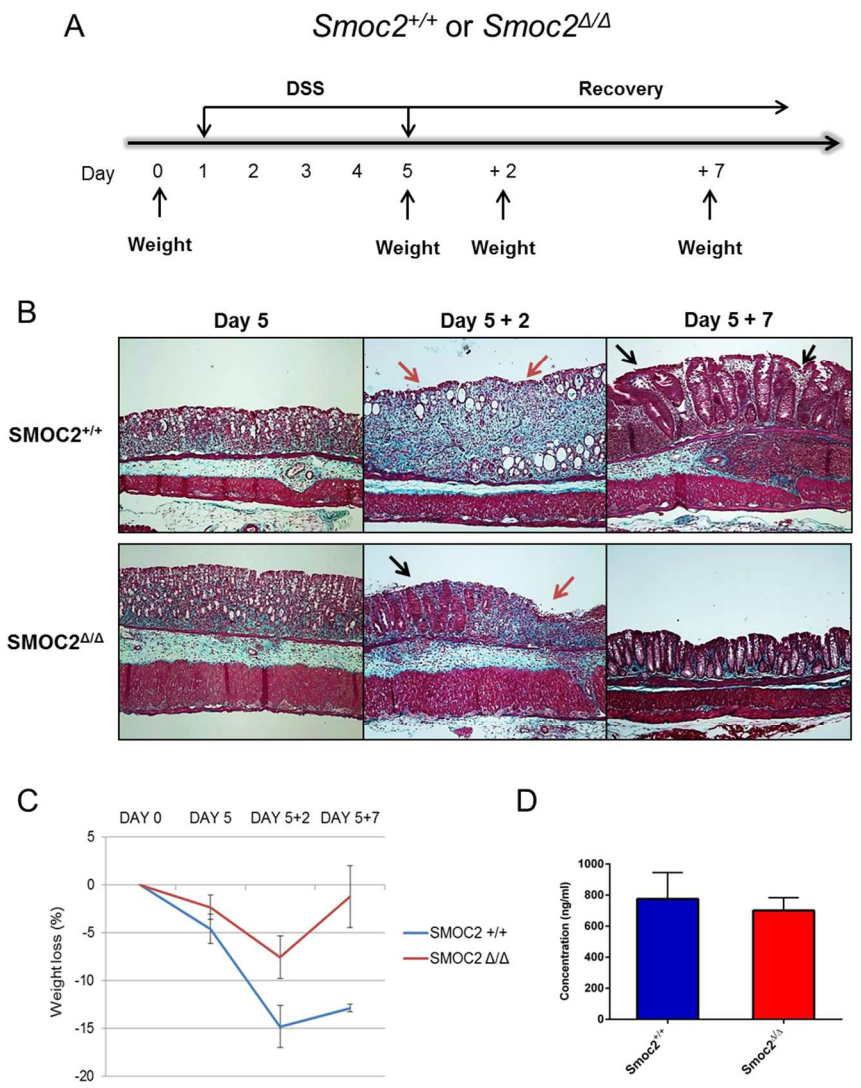

Figure 64: Full *Smoc2* ablation attenuates colonic colitis. A. Experimental design. B. Histological analysis of intestinal recovery after DSS removal. Red arrows indicate stromal infiltration at the inflamed sites. Black arrows indicate *de novo* crypt formation. C. Graphical representation of body weight loss. Data are mean ± SD of three independent experiments. N=10 mice per genotype per experiment. D. Measurement of intestinal permeability of healthy *Smoc2*$^{+/+}$ and *Smoc2*$^{\Delta/\Delta}$ mice. Data are mean ± s.e.m. of n=6 mice for each genotype.

5.7 BMP inhibition accelerates tumorigenesis and fully rescues polyp formation capability in Smoc2 full KO mice

We next returned to the analysis of tumorigenesis. In this case, we combined loss of *Apc* with short period of DSS treatment after tamoxifen induction (**Figure 65 A**). DSS-induced colitis in the *Apc* mutated background increases tumor burden in the colon and has the advantage of shortening the duration of the experiment. This setting also enables to study the combined effects of *Smoc2* loss in tumorigenesis and inflammation. As shown in **Figure 65 B**, *Smoc2* ablation significantly extended mice survival in this experimental setting.

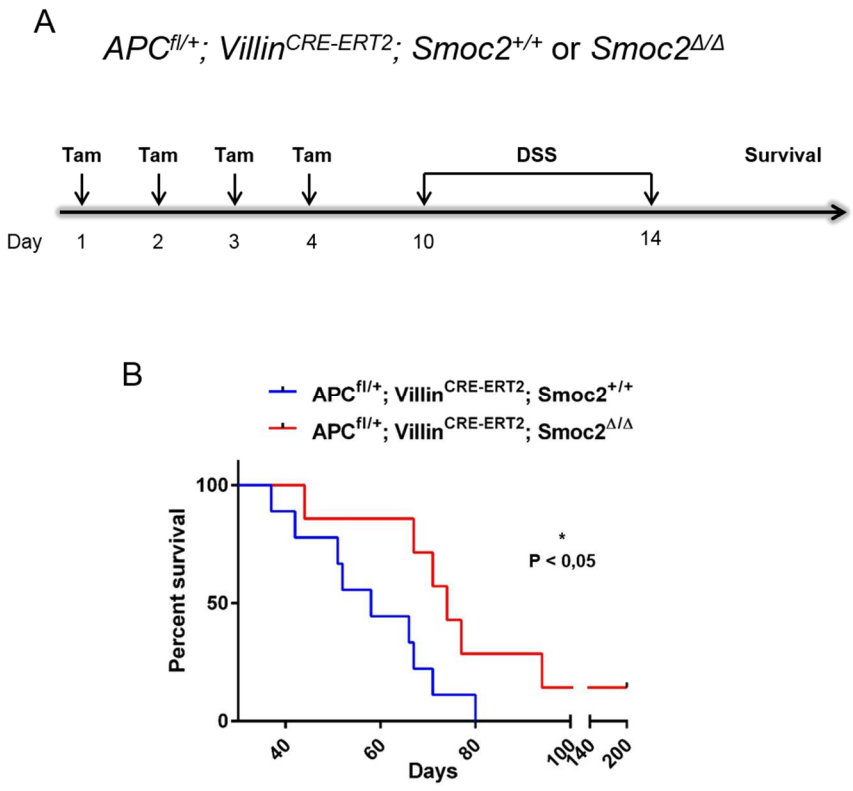

Figure 65: Effect of full *Smoc2* ablation in *Apc* mutant mice treated with DSS. A. Experimental design. B. Survival curve of *Villin-CreER^{T2}; Smoc2$^{\Delta\Delta}$; Apc$^{fl/+}$* mice and control *Villin-CreER^{T2}; Smoc2$^{+/+}$; Apc$^{fl/+}$* mice after tamoxifen injection and DSS treatment. N=9 *Villin-CreER^{T2}; Smoc2$^{+/+}$; Apc$^{fl/+}$* mice and 7 *Villin-CreER^{T2}; Smoc2$^{\Delta\Delta}$; Apc$^{fl/+}$* mice. Statistics are done using log-rank test.

In order to understand if the polyp reduction observed in *Apc*$^{flox/+}$, *Smoc2*$^{\Delta\Delta}$ mice is driven by BMP signaling upregulation, we repeated the previous experimental setting but introducing a new branch of LDN-193189 treatment. LDN-193189 is a specific BMPR1 inhibitor that has been previously used to inhibit systemically BMP signaling (Cuny et al., 2008; Yu et al., 2008) (see results-chapter 1). Treatment of control mice with LDN-193189 massively increased tumor burden and mice became moribund after 1 month approximately (**Figure 66 A, B**). IHC for pSMAD1/5 confirmed inhibition of BMP signaling (**Figure 66 C**). These results are consistent with a role for BMP signaling as a tumor suppressor during the onset of intestinal tumorigenesis as previously shown by us and several others (Haramis et al., 2004; Jaeger et al., 2012; Lombardo et al., 2011; Whissell et al., 2014).

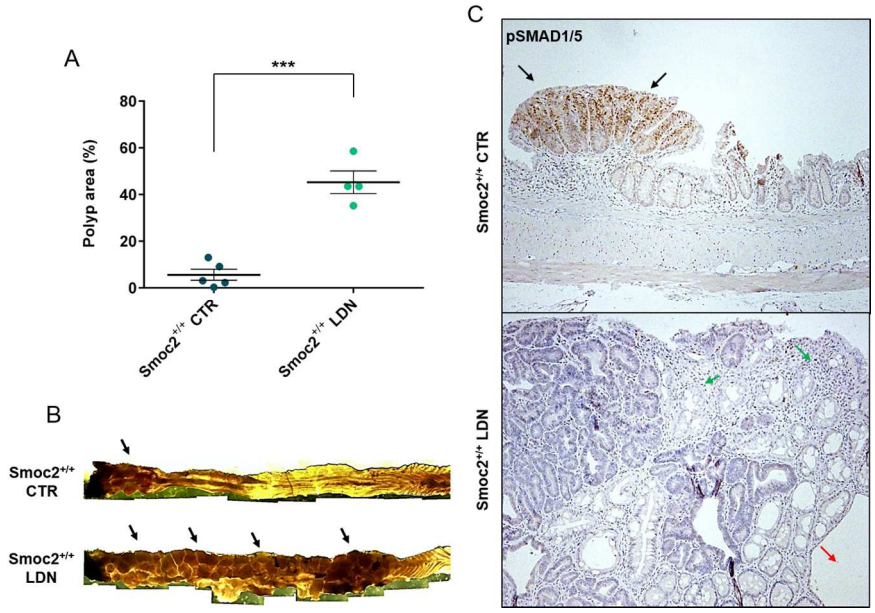

Figure 66: Blockade of BMP signaling accelerates colon tumorigenesis. A. Quantification of adenomatous area in the colon of *Villin-CreER^{T2}; Apc$^{fl/+}$* mice with or without LDN-193189 treatment following tamoxifen and DSS administration. All the mice were sacrificed 1 month after tamoxifen injection, when the LDN-treated ones became moribund. Each dot represents one mouse. Data are mean ± s.e.m. of n=5 untreated mice and n=4 LDN-treated mice. Statistics are done by Student's *t*-test. ****P*<0,001 B. Representative pictures of untreated and LDN-treated colon. Black arrows indicate tumor burden. C. pSMAD1/5 IHC on control and LDN-treated mice. Note the presence of small pSMAD1/5 positive polyps in untreated mice (upper panel) whereas LDN-treated mice (lower panel) display big polyps negative for BMP signaling. Black arrows indicate pSMAD1/5 positive polyp in the colon of untreated mice. Green arrows and red arrow respectively indicate stromal infiltration and the presence of cysts in LDN-treated mice, features resembling juvenile polyps. Magnification 10X.

Based on these results, we decided to sacrifice LDN-treated mice at 1 month whereas untreated mice were analyzed 1 further month later to enable polyp growth (**Figure 67 A**). As shown in previous experiments, untreated *Villin-CreER^{T2}; Smoc2$^{\Delta\Delta}$; Apc$^{fl/+}$* mice developed fewer tumors than control littermates (**Figure 67 B, C**). Interestingly, *Villin-CreER^{T2}; Smoc2$^{\Delta\Delta}$; Apc$^{fl/+}$* and *Villin-CreER^{T2}; Smoc2$^{+/+}$; Apc$^{fl/+}$* mice treated with LDN-193189 developed equivalent numbers of tumors (**Figure 67 B, C**).

Thus, SMOC2 acts as a tumor promoter in the intestine by blocking BMP signaling.

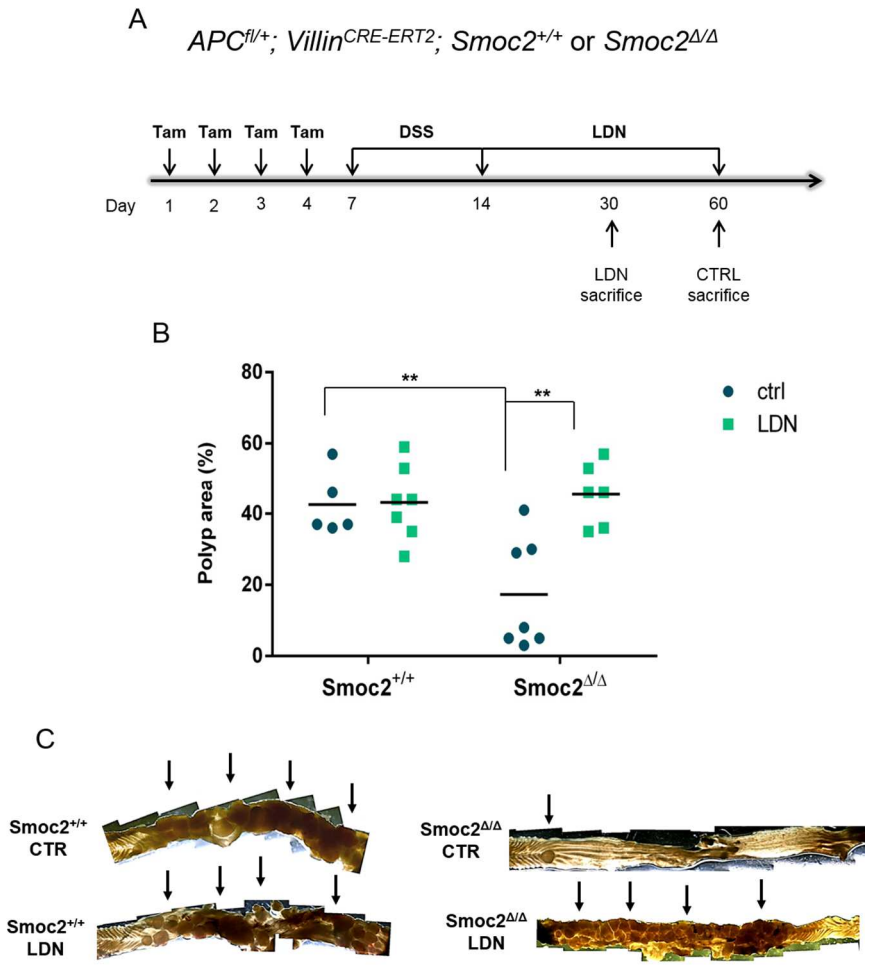

Figure 67: BMP drives the reduction in tumorigenesis of *Smoc2*$^{\Delta/\Delta}$ mice. A. Experimental design. B. Calculation of the adenomatous area in the colon of *Villin-CreER*^{T2}*; Smoc2*$^{\Delta/\Delta}$*; Apc*$^{fl/+}$ mice and control *Villin-CreER*^{T2}*; Smoc2*$^{+/+}$*; Apc*$^{fl/+}$ mice after tamoxifen, DSS and LDN treatment. Each dot represents one mouse. Data are mean ± s.e.m. of n=5 to 7 mice for each genotype and treatment. Statistics are done by Student's *t*-test. ***P*<0,01 C. Representative pictures of the colon of the four different conditions. LDN-treated mice were sacrificed 1 month after tamoxifen induction, whereas untreated mice were sacrificed 2 months after tamoxifen induction. Black arrows indicate tumor burden.

5.8 Smoc2$^{\Delta/\Delta}$ adenomas do not display increased BMP activation or reduction of AdSC compartment

It has been proved that the cells of origin of intestinal adenomas are LGR5 positive ISCs (Barker et al., 2009). In turn, adenomas contain a population of LGR5 expressing cells at the base of the adenoma glands that act as *bona fide* tumor stem cells (i.e. Adenoma Stem Cells). We thus repeated the analysis of tumor formation but depleting *Smoc2* specifically in ISCs. To this end, we used the *Lgr5-GFP-IRES-CreER^{T2}* driver that also allows tracking ISCs and adenoma stem cells (AdSCs) *in vivo* by means of GFP knock-in downstream the *Lgr5* promoter. For this experiments we compared *Lgr5-CreER^{T2}; Smoc2$^{\Delta/\Delta}$; Apc$^{fl/fl}$* mice with *Lgr5-CreER^{T2}; Smoc2$^{+/+}$; Apc$^{fl/fl}$* mice (**Figure 68 A**). As expected, we observed strong reduction in tumor burden in *Smoc2$^{\Delta/\Delta}$* mice (**Figure 68 B**). However, the size and distribution of AdSC compartment in *Smoc2* deficient polyps were identical to that of control mice, as shown by GFP staining (**Figure 68 C**). Likewise, we did not observe expansion of pSMAD1/5 positive compartment in *Smoc2$^{\Delta/\Delta}$* polyps, which was restricted to an area close to the lumen as we previously described (Whissell et al., 2014). It thus appears that the BMP gradient is maintained in *Smoc2* mutant polyps. Therefore, the bottom adenoma glands where AdSCs reside remain protected from BMP signaling in both genotypes (**Figure 68 C**). These data suggest that the adenoma epithelial compartment may not be the direct target of SMOC2-driven BMP inhibition.

A


APC fl/fl; LGR5 CRE-ERT2; Smoc2 +/+ or Smoc2 Δ/Δ
Tam 1:10
DSS
Counting
Day
1
7
11
60

B

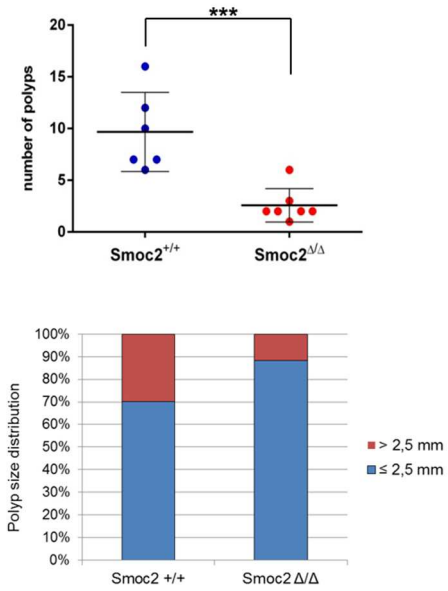
***
number of polyps
20
15
10
5
0
Smoc2 +/+
Smoc2 Δ/Δ
Polyp size distribution
100%
90%
80%
70%
60%
50%
40%
30%
20%
10%
0%
Smoc2 +/+
Smoc2 Δ/Δ
> 2,5 mm
≤ 2,5 mm

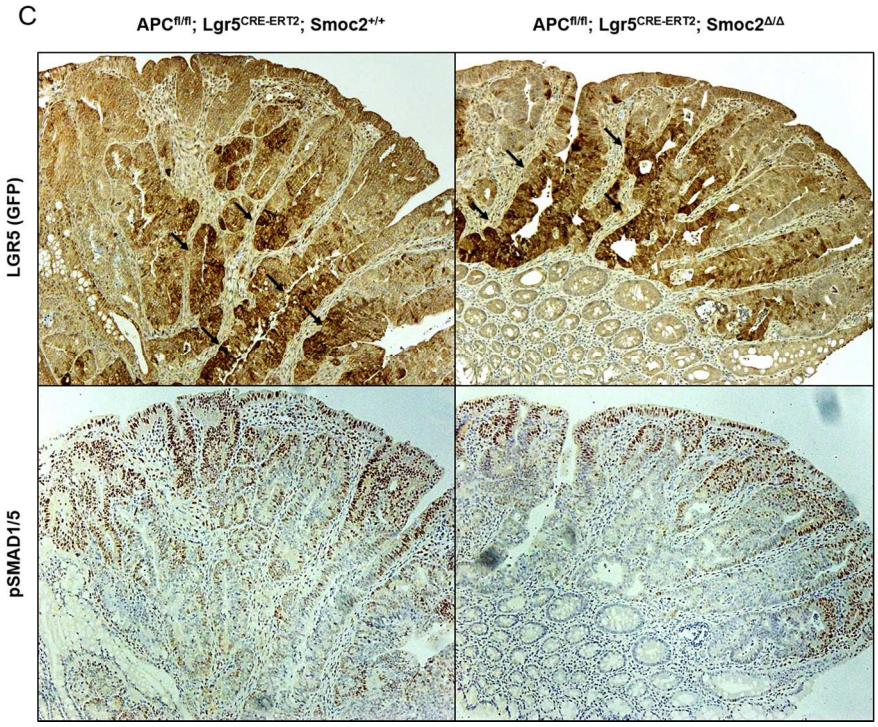

Figure 68: BMP and AdSC compartment are not altered in *Smoc2*$^{\Delta/\Delta}$ mice. A. Experimental design. B. Polyp counting (upper panel) and size distribution (lower panel) in the colon of *LGR5-GFP-CreER*^{T2}*; Smoc2*$^{\Delta/\Delta}$*; Apc*$^{fl/fl}$ mice and control *LGR5-GFP-CreER*^{T2}*; Smoc2*$^{+/+}$*; Apc*$^{fl/fl}$ mice sacrificed 2 months after tamoxifen injection and DSS treatment. Each dot in the upper panel represents one mouse. Data are mean ± s.e.m. of n=6 *LGR5-GFP-CreER*^{T2}*; Smoc2*$^{+/+}$*; Apc*$^{fl/fl}$ mice and 7 *LGR5-GFP-CreER*^{T2}*; Smoc2*$^{\Delta/\Delta}$*; Apc*$^{fl/fl}$ mice. Statistics are done by Student's *t*-test. ***P<0,001 C. Representative pictures of GFP IHC (*Lgr5-GFP*) (upper panels) and pSMAD1/5 IHC (lower panels) in polyps of *LGR5-GFP-CreER*^{T2}*; Smoc2*$^{\Delta/\Delta}$*; Apc*$^{fl/fl}$ mice and control *LGR5-GFP-CreER*^{T2}*; Smoc2*$^{+/+}$*; Apc*$^{fl/fl}$ mice. Black arrows in the upper panels indicate GFP positive cells corresponding to the AdSC compartment at the bottom of the adenoma glands adjacent to the stroma. In both genotypes, PSMAD1/5 stains the differentiated compartment of adenomas which is negative for GFP staining.

5.9 Smoc2 proficient and deficient AdSCs are equally sensitive to BMP pathway activation

In both *Smoc2*$^{+/+}$ and *Smoc2*$^{\Delta/\Delta}$ adenoma cultures, we observed considerable growth reduction upon rNOGGIN removal and consequent BMP pathway activation (**Figure 69 B**). In the absence of rNOGGIN, AdSCs clonogenic potential was progressively reduced as shown by loss of organoid forming capability over passaging in both genotypes (**Figure 69 C**). In concordance with this result, BMP target genes were equally upregulated in *Smoc2*$^{+/+}$ and *Smoc2*$^{\Delta/\Delta}$ adenoma cultured in the absence of rNOGGIN (**Figure 69 D**). These data suggest that endogenous *Smoc2* ablation does not exacerbate AdSC response to BMP activation. That leads us to conclude that SMOC2 does not exert a relevant role in protecting AdSCs from BMP and make us exclude adenoma epithelial cells as a major SMOC2 responsive target.

Based on this finding, we can assert that SMOC2 does not act in a cell-autonomous manner. It may rather impinge on adenoma growth through the inhibition of BMP in other stromal cell subpopulations that in turn could affect adenoma initiation and growth.

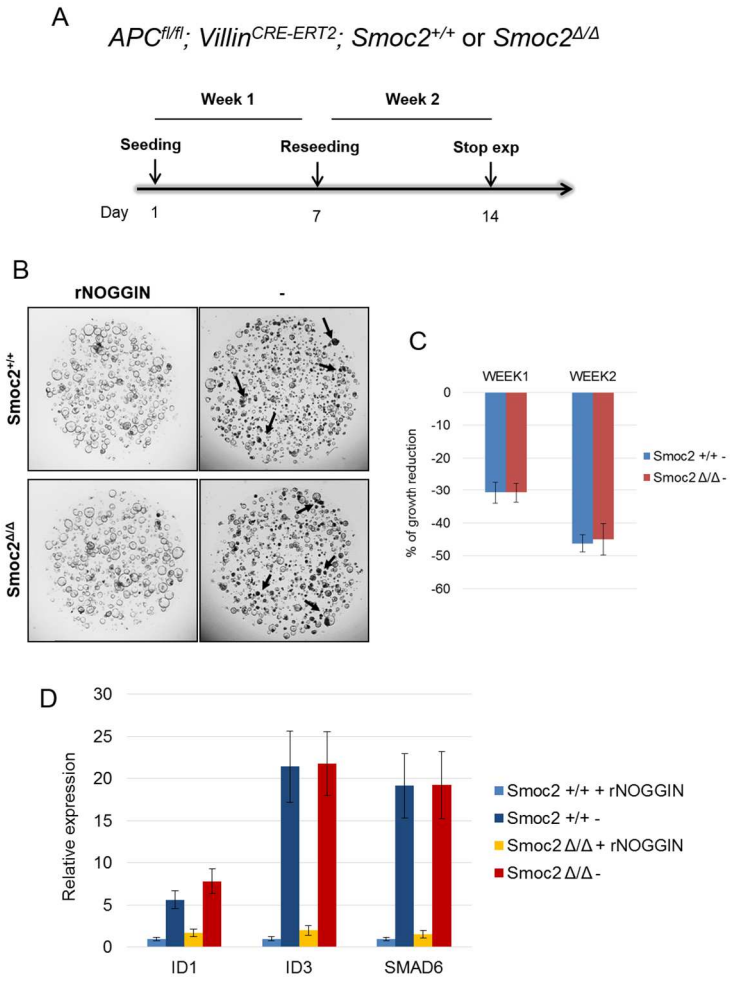

Figure 69: *Smoc2* deficient AdSCs are not more sensitive to BMP exposure *in vitro*. A. Experimental design. B. Representative pictures of colonic AdSC cultures derived from *Villin-CreER^{T2}; Smoc2$^{\Delta\Delta}$; Apc$^{fl/fl}$* mice and control *Villin-CreER^{T2}; Smoc2$^{+/+}$; Apc$^{fl/fl}$* mice recombined *in vivo* with tamoxifen. Upon rNOGGIN removal, AdSCs from both genotypes undergo growth reduction. Overall, the adenoma spheres are smaller and black arrows indicate apoptotic spheres. C. Progressive loss of AdSC clonogenic capability upon rNOGGIN removal from both *Smoc2$^{+/+}$* and *Smoc2$^{\Delta\Delta}$* adenoma cultures. Data are mean ± SD of triplicates. D. RT-qPCR analysis of BMP target gene expression in *Smoc2$^{+/+}$* and *Smoc2$^{\Delta\Delta}$* AdSCs cultured with or without rNOGGIN.

5.10 Gene expression analysis of stromal subpopulations sorted from Smoc2$^{+/+}$ and Smoc2$^{\Delta/\Delta}$ polyps

Our *in vitro* experiments demonstrate that epithelial cells are not the major direct targets of SMOC2 pro-tumorigenic effect. In addition, our preliminary analysis of DSS-induced colitis suggests a role for SMOC2 in controlling inflammation.

Important to understand the rationale behind the experiments described below is the fact that previous published data had shown that SMOC2 synergizes with vascular endothelial growth factor to stimulate endothelial angiogenesis *in vitro* (Rocnik et al., 2006). Furthermore, while we were developing these experiments, a manuscript revealed that the member of the SMOC2 family, SMOC1, binds directly the TGFβ auxiliary receptor Endoglin (CD105) and promotes endothelial cell proliferation and angiogenesis (Awwad et al., 2015). In addition, a previous study had also reported the capacity of SPARC to interact with Endoglin (Rivera and Brekken, 2011). Endoglin is a TGFβ binding protein expressed on the surface of endothelial cells. Loss-of-function mutations in the human Endoglin gene (*ENG*) cause Hereditary Hemorrhagic Telangiectasia (HHT1), a disease characterized by vascular malformations (Damjanovich et al., 2011). Moreover, mice lacking *Eng* die from defective vascular development (Li et al., 1999).

However, Endoglin expression is not restricted to endothelial cells. It has been reported that although Endoglin is absent from peripheral blood monocytes, it is expressed in differentiated monocytes (Lastres et al., 1992).

These data prompted us to focus on the response of stromal cells to *Smoc2* deficiency, particularly CD105+ cells. We studied different cells types present in adenomas arising in *Villin-CreER^{T2}; Smoc2$^{\Delta\Delta}$; Apc$^{fl/+}$* mice and control *Villin-CreER^{T2}; Smoc2$^{+/+}$ Apc$^{fl/+}$* mice. For these experiments, we macroscopically dissected large adenomas and we enzymatically dissociated them to single cells. We them labeled cells with specific surface markers and subsequently proceeded with FACS isolation. In particular, we purified epithelial cells (EpCAM+/CD45-/CD105-), CD105 expressing endothelial cells (EpCAM-/CD45-/CD105+), CD105 expressing immune cells (EpCAM-/CD45+/CD105+) and general leukocyte populations (EpCAM-/CD45+/CD105-). Because of the low numbers of cells obtained from these samples, we used a method to amplify cDNA that has been developed by the Functional Genomics core facility at our institution (Gonzalez-Roca et al., 2010). The robustness and reliability of this amplification method has been widely validated and used in previous studies by the Genomics core facility and by our laboratory (Calon et al., 2012).

By RT-qPCR analysis of amplified material we confirmed the enrichment for the markers used for cell sorting in the different cell fractions (*Cd105*, *Cd45*, *EpCAM*). Please note that each marker was upregulated between 10 and 1000 fold in each particular population, which validates this methodology (**Figure 70**).

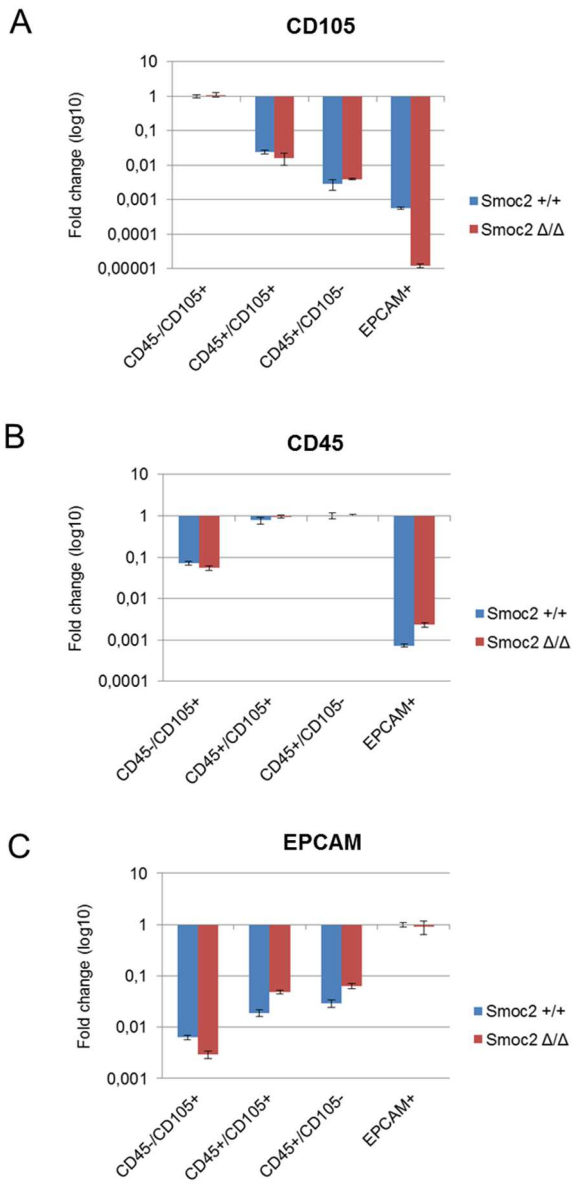

Figure 70: *Cd105*, *Cd45* and *EpCAM* expression in sorted cell population from adenomas of *Smoc2*$^{+/+}$ and *Smoc2*$^{\Delta/\Delta}$ mice. *Cd105* (A), *Cd45* (B) and *EpCAM* (C) expression was assessed by RT-qPCR on the different populations purified from *Smoc2*$^{+/+}$ and *Smoc2*$^{\Delta/\Delta}$ adenomas. For each fraction, data are mean ± SD of n=2 mice for each genotype.

We also characterized the identity of the CD45+/CD105+ and CD45-/CD105+ cell populations. CD45+/CD105+ expressed elevated levels of differentiated tissue resident macrophage marker genes compared to general leukocyte CD45+/CD105- fraction. Those include *Cx3cr1*, *Cd206*, *Cd11c* and *Cd68*. On the contrary, *Gr1*, which is a marker of undifferentiated monocytes was relatively less expressed on CD45+/CD105+ (**Figure 71 A**).

The CD45-/CD105+ cells expressed elevated levels of *Cd31*, a specific marker for endothelial cells (**Figure 71 B**). Therefore, CD45+/CD105+ cells were enriched in macrophages whereas CD45-/CD105+ fraction was composed of endothelial cells.

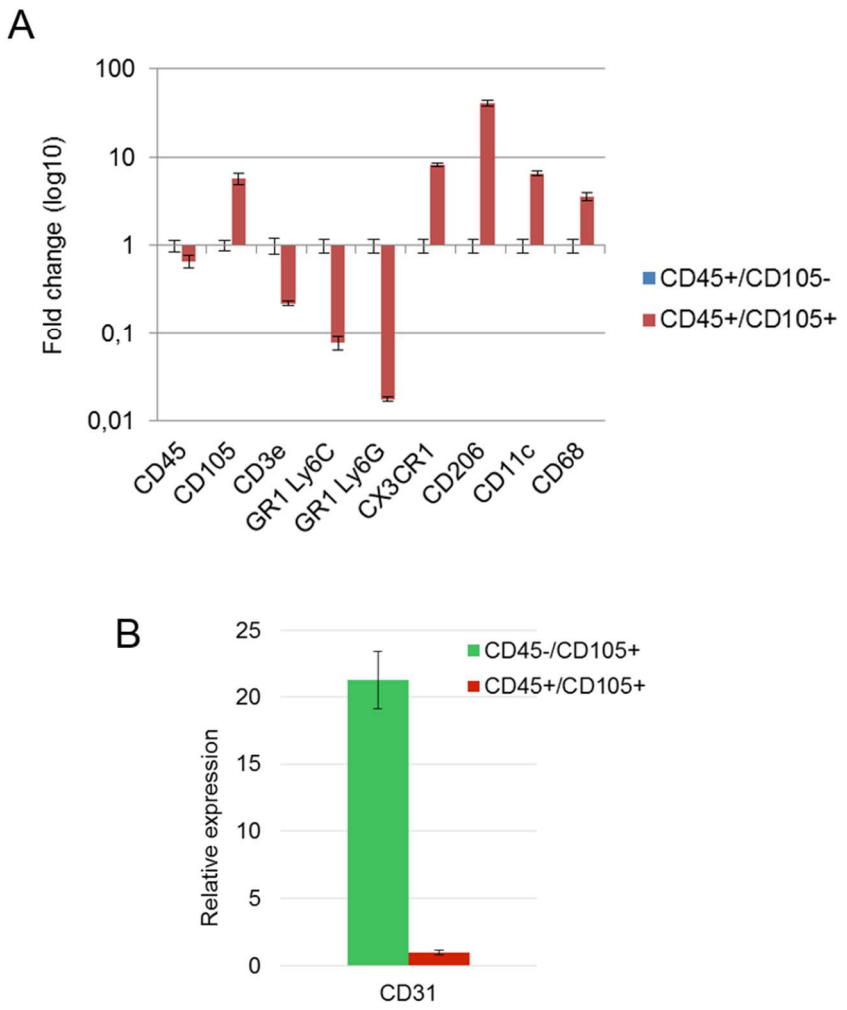

Figure 71: Characterization of CD45+/CD105+ and CD45-/CD105+ cell populations. A. Comparison of gene expression between CD45+/CD105+ and CD45+/CD105- cell populations derived from *Smoc2* wild-type adenomas. B. Detection of *Cd31* expression in Endoglin-expressing cell populations (CD45-/CD105+ and CD45+/CD105+) derived from *Smoc2* wild-type adenomas. Gene expression was assessed by RT-qPCR analysis.

Finally we found that *Smoc2* was almost undetectable in CD45+/CD105- fraction. On the contrary, *Smoc2* was highly expressed in CD105 positive cell populations, both CD45-/CD105+ and CD45+/CD105+ (**Figure 72**). This finding confirmed our previous observations suggesting that *Smoc2* was expressed in stromal cells. These stromal populations co-express Endoglin (CD105+) and appear to be tissue resident macrophages and endothelial cells.

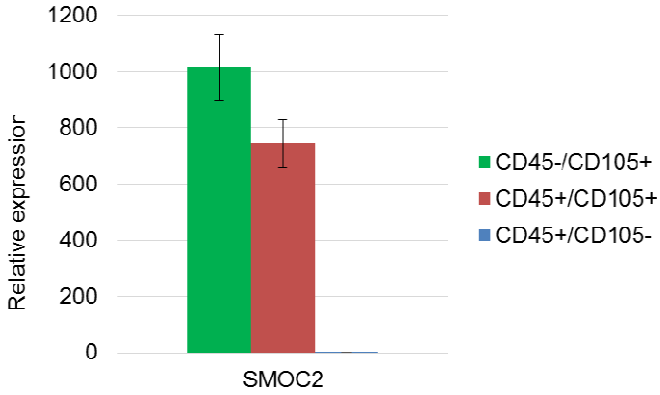

Figure 72: *Smoc2* expression in sorted cell populations. *Smoc2* expression was assessed by RT-qPCR in the cell populations sorted from *Smoc2* wild-type adenomas.

As already mentioned, we tested several commercial antibodies against SMOC2 and none of them allowed the detection of the protein neither by Western Blot nor by IHC. The recent publication by *Shvab et al.* showed nice SMOC2 staining in ISCs of human samples of normal mucosa and CRC. Neither this antibody showed SMOC2 specific signal in mouse samples. Nevertheless, the analysis of SMOC2 IHC on human samples revealed stromal SMOC2 positive cells besides the expected positive SCs. In particular, anatomopathologists from Hospital del Mar in Barcelona confirmed strong SMOC2 signal in SCs and immune cells resident in the tissue and inside the blood vessels. The shape and the distribution of these cells resembled those of macrophages. Furthermore, intermediate signal was detected in endothelial and nerve cells. Fibroblasts and muscle cells were classified negative for SMOC2 expression (**Figure 73**). These observations confirm our findings achieved by purification of cell populations and detection of *Smoc2* mRNA levels by RT-qPCR.

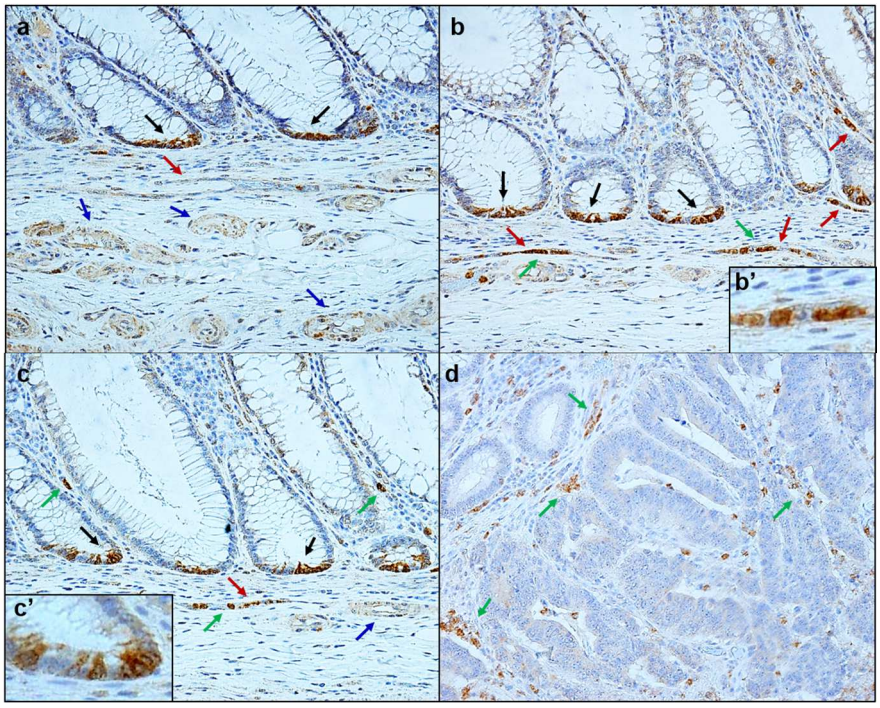

Figure 73: SMOC2 expression in human samples of normal intestinal mucosa and CRC. IHC showing SMOC2 expression in human intestinal normal mucosa (a, b, c) and CRC (d) at magnification 20X. Panel c' and b' respectively show higher magnification of SMOC2 positive ISCs and SMOC2 positive immune cells inside a blood vessel. Black arrows indicate SMOC2 positive SCs at the base of normal intestinal crypts. Blue arrows indicate intermediate SMOC2 signal in nerves. Red arrows indicate intermediate SMOC2 signal in endothelial cells of blood vessels. Green arrows indicate tissue resident macrophages or monocytes in the blood vessels.

5.11 Expression profiling of CD105+ cell populations

We next compared the global expression profiles of CD45-/CD105+ and CD45+/CD105+ cell populations isolated from *Villin-CreER^{T2}; Smoc2$^{\Delta/\Delta}$; Apc$^{fl/+}$* adenomas and control *Villin-CreER^{T2}; Smoc2$^{+/+}$ Apc$^{fl/+}$* adenomas. To this end, we hybridized samples in duplicate (i.e. purified populations obtained from 2 mice of each genotype) on Affymetrix® microarrays.

Principal Component Analysis (PCA) showed high segregation between the two fractions and similar identity between duplicates (**Figure 74**).

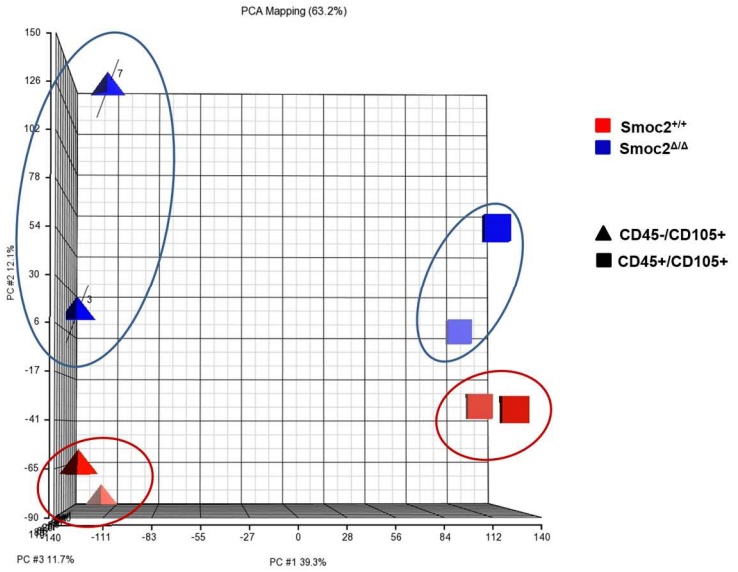

Figure 74: Gene expression profile of CD45-/CD105+ and CD45+/CD105+ cell populations sorted from *Smoc2$^{+/+}$* and *Smoc2$^{\Delta/\Delta}$* adenomas. PCA of CD45-/CD105+ and CD45+/CD105+ cell populations sorted from *Smoc2$^{+/+}$* and *Smoc2$^{\Delta/\Delta}$* adenomas and profiled on Affymetrix® microarrays. N=2 for each genotype and fraction.

In CD45+/CD105+ cells, we identified 77 genes consistently upregulated and 44 genes consistently downregulated in *Villin-CreER^{T2}; Smoc2$^{\Delta/\Delta}$; Apc$^{fl/+}$* mice compared to control *Villin-CreER^{T2}; Smoc2$^{+/+}$; Apc$^{fl/+}$* mice (cutoff: 2 fold; $p<0.05$). In CD45-/CD105+ cells, we identified 27 genes consistently upregulated and 102 genes consistently downregulated in *Villin-CreER^{T2}; Smoc2$^{\Delta/\Delta}$; Apc$^{fl/+}$* mice compared to control *Villin-CreER^{T2}; Smoc2$^{+/+}$; Apc$^{fl/+}$* mice (cutoff: 2 fold; $p<0.05$). Top genes for each comparison are listed in the following tables.

Downregulated genes in Smoc2$^{\Delta/\Delta}$ CD45-/CD105+ cell population

Gene.Symbol	FC	P.Value
Cxcl9	-5,68	0,00
Mfap4	-4,74	0,00
Il1rl1	-4,43	0,09
Bmp7	-4,28	0,00
Il1rn	-4,14	0,00
Pdgfra	-4,03	0,00
Serpina3n	-3,88	0,06
Lgi2	-3,63	0,01
Fgfr2	-3,55	0,00
Col6a4	-3,41	0,01
Lama1	-3,37	0,00
Rgs2	-3,36	0,01
Sycn	-3,24	0,14
Rgs2	-3,22	0,01
Igf1	-3,18	0,02
Sprr1a	-3,16	0,10
Scube1	-3,10	0,00
Lamb3	-3,09	0,02
Col6a4	-3,04	0,01
Smoc1	-2,98	0,02
Fndc1	-2,89	0,00
Rbp4	-2,89	0,13
Tnfrsf9	-2,86	0,09
Cdca7l	-2,86	0,01
Ereg	-2,84	0,19
Rgs2	-2,78	0,01
Fgf7	-2,68	0,02
Sema3c	-2,66	0,02
Krt20	-2,66	0,14
Pdgfra	-2,64	0,07
Cwh43	-2,64	0,14
Foxf2	-2,63	0,00
Spon1	-2,61	0,00
Plau	-2,58	0,06
Lamc2	-2,58	0,15
Pcdh7	-2,55	0,00
Cldn4	-2,54	0,00
Gpm6b	-2,54	0,01
Igfbp5	-2,54	0,03
Ccrl1	-2,54	0,05
Ptgs2	-2,53	0,21
Inhba	-2,51	0,05
Spon1	-2,49	0,00
Muc3	-2,47	0,10
Wnt5a	-2,47	0,04
Bmp2	-2,45	0,08
Bmp5	-2,44	0,00
Dio2	-2,43	0,25
Lum	-2,41	0,05
Krt8	-2,41	0,11
Dsg2	-2,37	0,01
Mmp12	-2,35	0,19
Fzd2	-2,34	0,12
Pmepa1	-2,33	0,00
Tubgcp6	-2,31	0,00
Rnd3	-2,30	0,01
Nrg1	-2,30	0,03
Pcdh7	-2,29	0,01
Krt8	-2,29	0,10
Hgf	-2,27	0,01
Wnt5a	-2,27	0,01
Gpm6b	-2,26	0,08
Tmem190	-2,24	0,01
Aldh1a3	-2,22	0,11
Csgalnact1	-2,22	0,09
U90926	-2,22	0,00
Dpep1	-2,20	0,00
Atp1a3	-2,19	0,00
Ncam1	-2,18	0,00
Col12a1	-2,18	0,00
Tmem119	-2,16	0,01
Bmp4	-2,15	0,00
Col12a1	-2,14	0,00
Ptch1	-2,13	0,00
Dpt	-2,12	0,00
Cpxm2	-2,10	0,00
Sycn	-2,10	0,23
Grem1	-2,10	0,07
Akr1b8	-2,09	0,09
Aldh1a3	-2,09	0,09
Ckmt1	-2,08	0,00
Syt13	-2,08	0,01
Wls	-2,08	0,03
Hhip	-2,08	0,14
Dpep1	-2,07	0,01
Aldh1a3	-2,06	0,31
Ptges	-2,06	0,15
Sema3c	-2,05	0,00
Ptgfrn	-2,05	0,01
Mmp9	-2,04	0,03
Srprb /// Trf	-2,04	0,00
Wfdc2	-2,03	0,18
Tubb4a	-2,03	0,00
Lrp1	-2,02	0,07

Gm14446	-2,02	0,08
Ccdc80	-2,02	0,00
Fosb	-2,01	0,29
Serpina3g	-2,01	0,02
Vegfa	-2,01	0,06
Serpind1	-2,01	0,01
Smox	-2,01	0,02
Egln3	-2,00	0,00
Gna13	-2,00	0,00

Upregulated genes in Smoc2$^{\Delta/\Delta}$ CD45-/CD105+ cell population

Gene.Symbol	FC	P.Value
Lyz1	5,05	0,06
Defa4	4,72	0,13
Defa-rs2	4,61	0,16
Cox8a	4,57	0,00
Defa15	4,34	0,16
H2-Aa	4,19	0,00
Cldn2	3,17	0,17
S100a8	3,05	0,06
Spink4	2,69	0,09
Cers6	2,60	0,01
S100a9	2,45	0,08
Idh1	2,44	0,00
Lyz2	2,37	0,04
Spock2	2,30	0,30
Slc30a2	2,17	0,24
Atp1b1	2,16	0,18
Galnt15	2,15	0,04
Flt4	2,15	0,01
Tigd3	2,12	0,00
Lyve1	2,09	0,01
Insig1	2,08	0,01
Pcdh17	2,06	0,02
Rnf157	2,05	0,01
Sephs2	2,02	0,00
Wfdc18	2,02	0,01
Adi1	2,01	0,04
Gimap8	2,01	0,13

Downregulated genes in Smoc2$^{\Delta/\Delta}$ CD45+/CD105+ cell population

Gene.Symbol	FC	P.Value
Mcpt1	-7,08	0,15
Igkv6-15	-5,30	0,13
Saa1	-4,81	0,04
Mcpt2	-4,81	0,12
Ppbp	-4,72	0,00
Ccl1	-4,29	0,16
Klrc1	-4,03	0,00
Gzmb	-3,98	0,03
Saa1	-3,06	0,04
Cp	-2,97	0,01
Zg16	-2,95	0,00
Col1a1	-2,91	0,02
Folr2	-2,69	0,00
Spic	-2,69	0,00
Dmbt1	-2,63	0,30
Zg16	-2,63	0,01
Cbr2	-2,61	0,00
Fcrla	-2,53	0,09
Fap	-2,46	0,00
Tpsab1	-2,45	0,14
Col1a1	-2,45	0,02
Ccl22	-2,43	0,05
Col1a2	-2,39	0,05
Fcrls	-2,37	0,00
Cxcl13	-2,35	0,09
Igfbp5	-2,34	0,20
Ccl4	-2,33	0,05
Apold1	-2,28	0,08
F2r	-2,28	0,02
Crabp2	-2,27	0,00
Hspa1b	-2,17	0,11
Nkg7	-2,16	0,17
Slc2a3	-2,12	0,00
Col3a1	-2,11	0,02
Mmp9	-2,10	0,02
Rbm39	-2,10	0,12
Lypd8	-2,10	0,23
Prkar1b	-2,09	0,00
Col6a1	-2,08	0,03
Fosb	-2,08	0,01
Maf	-2,07	0,00
Timp1	-2,05	0,04
Ccl3	-2,04	0,04
Cp	-2,01	0,04
Fpr1	-2,01	0,05

Upregulated genes in Smoc2$^{\Delta/\Delta}$ CD45+/CD105+ cell population

Gene.Symbol	FC	P.Value
Igk-V1/v9-120	5,82	0,17
Hbb-b2	5,46	0,02
Apcdd1	4,76	0,07
Igk-V21	4,55	0,22
Dsp	3,65	0,00
Igh-VJ558	3,64	0,13
Plagl1	3,25	0,06
Apcdd1	3,01	0,14
Mt4	3,00	0,03
Lgr5	2,84	0,10
Ang4	2,83	0,13
Mmp15	2,81	0,01
Mal2	2,75	0,00
Tenm4	2,73	0,01
Cyb561	2,65	0,00
Mpzl2	2,55	0,01
Reg3g	2,55	0,00
Lamb3	2,54	0,00
Reg3b	2,53	0,43
Ptn	2,52	0,14
Fat1	2,52	0,02
Foxa3	2,51	0,01
Ddr1	2,51	0,00
Cep170b	2,49	0,00
Nav2	2,49	0,00
Sox9	2,47	0,01
Atp1b1	2,47	0,00
Defa-rs7	2,46	0,32
Mpzl2	2,40	0,00
Tsc22d1	2,39	0,00
Wif1	2,39	0,01
Cdc20	2,38	0,02
Pvrl3	2,37	0,00
Cldn2	2,37	0,00
Slc30a2	2,35	0,11
Krt18	2,35	0,00
Dsp	2,33	0,00
Lmo7	2,25	0,00
Dsg2	2,24	0,00
Lama5	2,24	0,00
Reg4	2,23	0,24
Ppap2a	2,22	0,03
Neo1	2,22	0,00
Nkd1	2,21	0,03
Fam83h	2,21	0,01

Rrm2	2,19	0,00
Cdh13	2,19	0,08
Alox12	2,18	0,02
Ctxn1	2,18	0,01
Prox1	2,17	0,04
Syne4	2,15	0,05
Gm9817	2,14	0,02
Gpc4	2,13	0,02
Prom1	2,12	0,00
Nhsl1	2,12	0,09
Spink3	2,12	0,19
Krt7	2,09	0,00
Mmp7	2,09	0,27
Trip13	2,09	0,00
Aldh1l1	2,09	0,00
Perp	2,09	0,04
Rnf43	2,08	0,02
Ppap2a	2,07	0,02
Irf6	2,06	0,03
Cd24a	2,05	0,01
Fgfr4	2,04	0,04
Elovl6	2,04	0,00
Sectm1a	2,03	0,05
Cd24a	2,03	0,00
Dsg2	2,03	0,00
Iigp1	2,03	0,18
Vwa2	2,03	0,02
Atp1b1	2,02	0,03
Cdh13	2,01	0,12
Asprv1	2,01	0,06
Sox21	2,01	0,00
Mid1	2,00	0,00
Cldn4	2,00	0,01

Gene Set Enrichment Analysis (GSEA) revealed that *Smoc2* deficiency in CD45+/CD105+ cells negatively correlated with chemokine signaling pathway, natural killer cell-mediated cytotoxicity, T cell migration and dendritic cell differentiation (**Figures 75 A**). In CD45-/CD105+ cells, lack of *Smoc2* was negatively correlating with extracellular matrix organization and Insulin-like Growth Factor (IGF) receptor signaling pathway (**Figures 75 B**).

These data suggest that the lack of *Smoc2* triggers multiple responses in Endoglin positive populations of adenomas.

A **CD45+/105+_Smoc2$^{\Delta/\Delta}$ vs Smoc2$^{+/+}$**

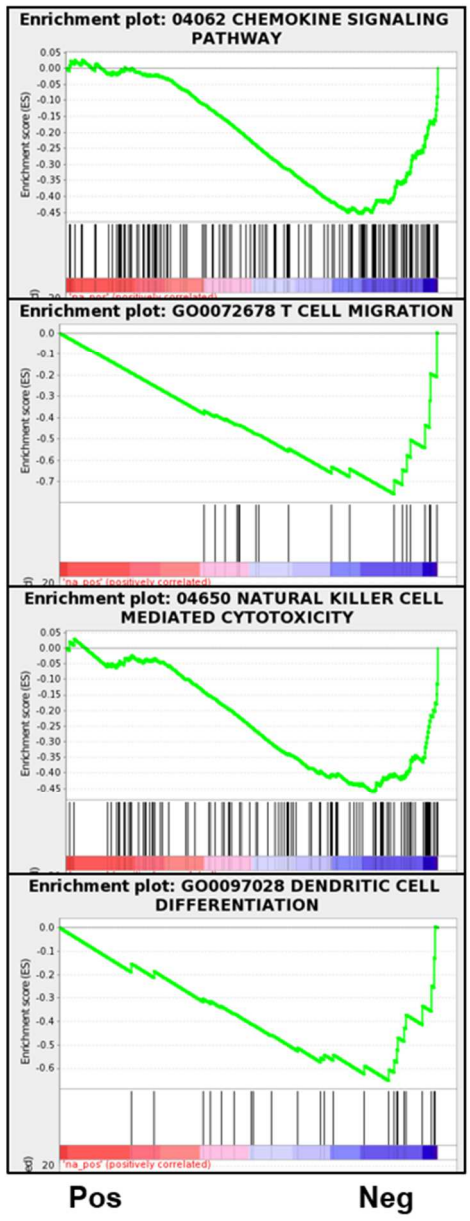

ES: -0,45
NES: -2,06
P-value: 0,0

ES: -0,75
NES: -2,24
P-value: 0,0

ES: -0,46
NES: -1,94
P-value: 0,0

ES: -0,65
NES: -2,02
P-value: 0,0

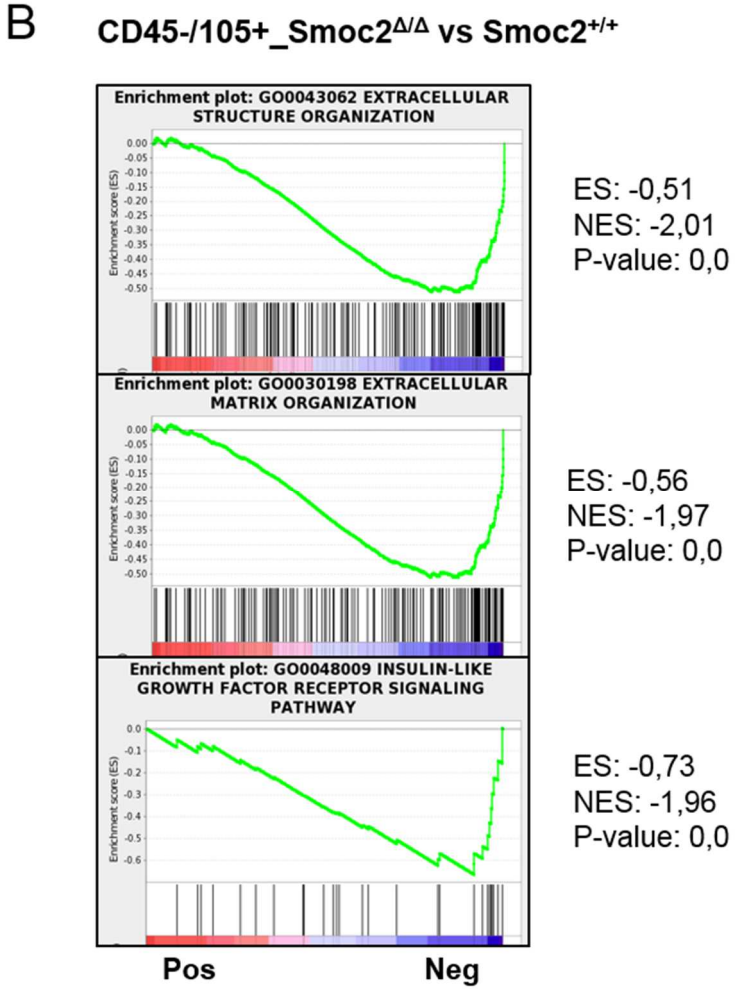

Figure 75: GSEA of profiled CD45+/CD105+ and CD45-/CD105+ cell populations sorted from *Smoc2*$^{+/+}$ and *Smoc2*$^{\Delta/\Delta}$ adenomas. A. CD45+/CD105+ cells from *Smoc2*$^{\Delta/\Delta}$ adenomas negatively associate with inflammation related processes (such as chemokine signaling, natural killer cell cytotoxicity, T cell migration and dendritic cell differentiation) compared to *Smoc2*$^{+/+}$ adenomas B. CD45-/CD105+ cells from *Smoc2*$^{\Delta/\Delta}$ adenomas negatively correlate with extracellular matrix remodeling processes and IGFR signaling pathway. Pos: positive correlation; Neg: negative correlation.

5.12 IGF1 is downregulated in Smoc2 deficient CD45-/CD105+ cells through BMP signaling

Among the pathways silenced in cells lacking *Smoc2*, we focused our attention on the IGF1 pathway. The rationale is the following: first, changes in *Igf1* may explain the enlarged intestines present in *Smoc2* transgenic mice. Second, IGF1 could act as a mitogen for AdSCs. Third, IGF1 plays important roles in regulation of inflammatory response (Heemskerk et al., 1999). The expression profiling experiments described above indicated that in CD45-/CD105+ cells purified from adenomas, lack of *Smoc2* induced downregulation of *Igf1* as well as of other genes regulating IGF1 signaling (IgfBP5). We thus sought to confirm these findings. To this end, we purified CD45-/CD105+ cells from an additional cohort of mice (n=4) following the methodology described above. We included in this experiment mice treated acutely with the BMPR1 inhibitor LDN-193189. RT-qPCR analysis showed increased levels of canonical BMP target genes such as *Id1* and *Smad6* in *Smoc2* deficient cells. In turn, levels of these BMP target genes were reduced in *Smoc2*$^{\Delta\Delta}$ cells obtained from mice treated with LDN-193189 (**Figure 76 A**). We also confirmed the observation that *Igf1* mRNA levels were downregulated in CD45-/CD105+ cells that lacked *Smoc2*. Consistently with regulation by the BMP pathway, treatment with LDN-193189 induced a large upregulation of *Igf1* (**Figure 76 B**).

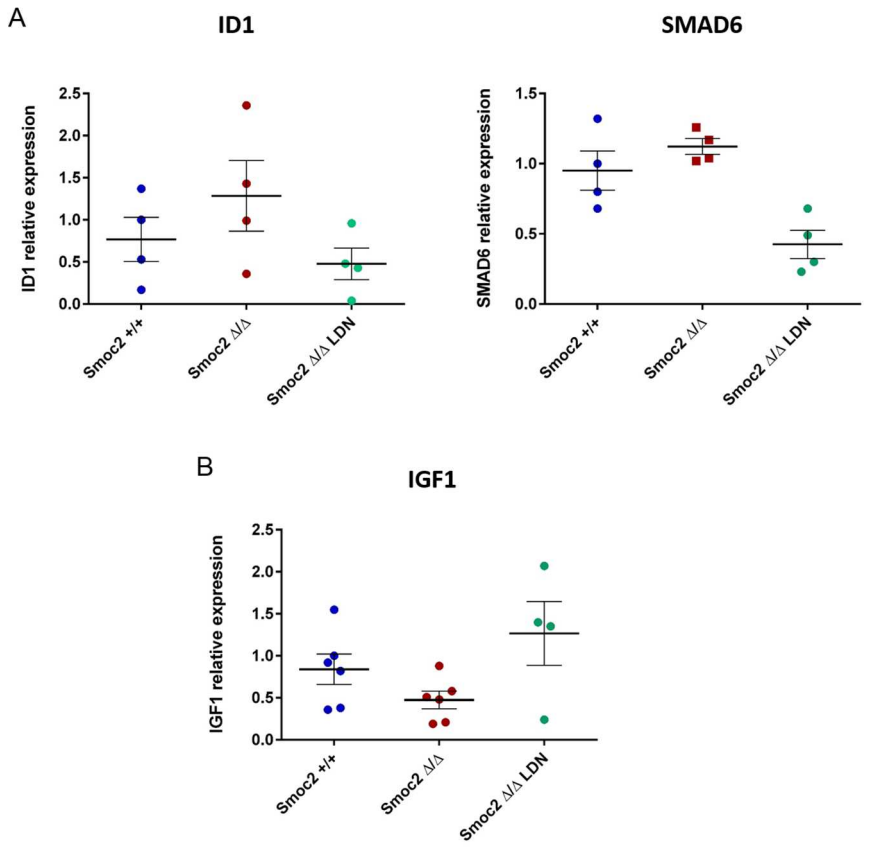

Figure 76: Gene expression analysis of CD45-/105+ cell population purified from *Smoc2*$^{+/+}$ and *Smoc2*$^{\Delta/\Delta}$ adenomas. A. BMP target gene expression was detected by RT-qPCR in CD45-/105+ cells sorted from *Smoc2*$^{+/+}$ and *Smoc2*$^{\Delta/\Delta}$ adenomas. B. *Igf1* expression was detected by RT-qPCR in CD45-/105+ cells sorted from *Smoc2*$^{+/+}$ and *Smoc2*$^{\Delta/\Delta}$ adenomas. Each dot represents one measurement deriving from a pool of polyps of one mouse. Data are mean ± s.e.m.

5.13 IGF1 does not have a direct effect on adenoma growth

IGF1 is a primary mediator of the effects of Growth Hormone (GH). GH is made in the anterior pituitary gland, is released into the blood stream, and then stimulates the liver to produce IGF1. IGF1 then stimulates systemic body growth, and has growth-promoting effects on almost every cell in the body.

Its primary action is mediated by binding to its specific receptor, the insulin-like growth factor 1 receptor (IGF1R), which is present on many cell types in many tissues. Binding to the IGF1R, a receptor tyrosine kinase, initiates intracellular signaling. Upon several external and internal stimuli, IGF1 can be produced by extra-systemic sources, especially tissue resident macrophages and endothelial cells.

Since endothelial CD105+ cells derived from *Smoc2*$^{\Delta/\Delta}$ polyps displayed a reduction in *Igf1* expression possibly mediated by BMP signaling, we wondered if reduced IGF1 production by these stromal cells could be the direct cause of the reduced adenoma growth observed in *Smoc2*$^{\Delta/\Delta}$ mice. To test this possibility, we cultured adenomas from *Villin-CreER*^{T2}*; Apc*$^{fl/fl}$ mice as organoids in the presence of recombinant IGF1 (rIGF1). Because EGF and Insulin are included in the media, we also set experiments in which we removed these supplements. Contrary to what was expected, we could not observe any growth promotion by rIGF1. Even in the absence of Insulin and EGF, rIGF1 failed to support adenoma growth (**Figure 77 A**). Cell stimulation with IGF1 can generally trigger three possible outcomes: cell proliferation through MAPK pathway, cell migration through RAC signaling and enhancement of cell survival through PI3K/AKT pathway (Stewart and Rotwein, 1996). Western Blot against pAKT showed a mild increase of AKT

phosphorylation in AdSCs upon rIGF treatment (**Figure 77 B**). These preliminary data suggest that, in the context of intestinal adenomas, IGF1 has no direct mitogenic effect on epithelial cells. Most likely, IGF1 must impinge on adenoma growth by modulating the survival pathway or through different mechanisms that involve the stroma.

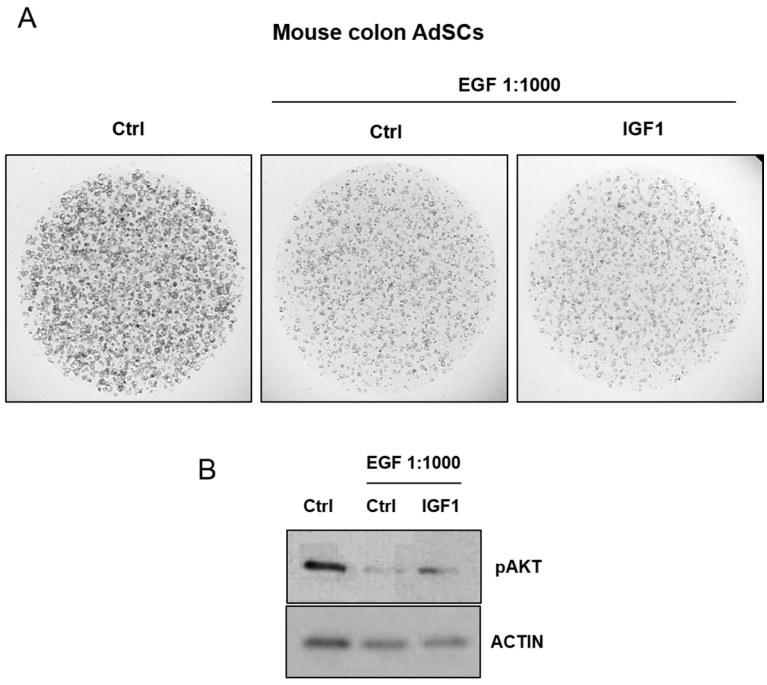

Figure 77: IGF1 effect on AdSC culture. A. Mouse colon AdSCs were purified from a *Villin-CreER^{T2}; APC$^{fl/fl}$* mouse injected *in vivo* with tamoxifen and cultured in the absence of insulin. The addition of diluted EGF (50 pg/ml compared to control 50ng/ml) in the media determined an evident reduction of the growth that was not rescued by rIGF1 addition (100ng/ml). B. Western Blot on cultured AdSCs shows mild enhancement of AKT phosphorylation in the presence of rIGF1.

Discussion

Chapter 1: The transcription factor GATA6 enables self-renewal of colon adenoma stem cells by repressing BMP gene expression

In normal mucosa, *Lgr5*+ cells reside at the base of the crypt and are able to both self-renew and give rise to all cell lineages of the intestinal tract throughout life (Barker et al., 2007). In a follow-up study, *Lgr5*+ cells were pinpointed as the cells of origin of CRC (Barker et al., 2009). In adenomas, *Lgr5*+ cells localize at the base of tumor glands and behave as AdSCs giving rise to the rest of tumor differentiated cell types that reside in closer proximity to the intestinal lumen (Schepers et al., 2012). Data from our laboratory support that late stage CRCs also rely on tumor SC for long term growth (Merlos-Suárez et al., 2011). Researchers are focusing great efforts on understanding the main pathways and regulators imposing hierarchies in benign and malignant lesions of the colon.

Screening for genes that regulate stemness in CRC

We used a bioinformatic approach based on the algorithm ARACNe to identify regulators of the tumor stem cell phenotype. In particular, we focused on genes directly associated to *LGR5*. An shRNA screening of *LGR5* neighbors in the ARACNe network led to the identification of the transcription factor GATA6 as positive regulator of *LGR5* expression in CRC cells. By ChIP-seq analysis we showed direct binding of GATA6 to the *LGR5* proximal promoter. Consistent with our findings, previous work had also shown that modulation of GATA6 directly affects *LGR5* expression

in differentiating embryonal carcinoma P19 cells (Alexandrovich et al., 2008).

Additionally, we also showed that GATA6 regulated the expression of another ISC gene *Cldn2*. Previous transcriptomic analysis had shown enrichment of *Cldn2* in mouse (Muñoz et al., 2012) and human (Jung et al., 2011) ISCs. We demonstrated that the protein levels of CLDN2 are highly restricted to ISCs and AdSCs. In adenoma, CLDN2 expression mirrors the expression pattern of *Lgr5*. As CLDN2 is a tight junction protein localized in the cell surface, it may represent a novel ISC marker for normal and tumor stem cell isolation and characterization. Several studies positively correlate CLDN2 to cancer severity (Dhawan et al., 2011; Kinugasa et al., 2007). *CLDN2* has been found upregulated in CRC and correlates with cancer progression (Dhawan et al., 2011). Moreover, CLDN2 has been shown to play a key role in the tropism of metastatic breast cancer cells. In particular, CLDN2 allows breast cancer cells to adhere to hepatocytes and home to the liver (Tabaries et al., 2011). Interestingly, a recent study showed that invasion and migration of CRC cell lines was decreased by *GATA6* knockdown and enhanced by aberrant *GATA6* expression that was associated with metastasis and poor overall survival (Shen et al., 2013). These observations suggest an interesting functional connection between CRC-SCs and liver metastasis.

Gata6 deficiency impairs the expansion of AdSCs through upregulation of BMP pathway

A considerable amount of evidence indicates that BMP signaling counteracts WNT signaling in the intestinal crypt. BMP signals along the crypt axis triggers cell differentiation (Auclair et al., 2007;

Haramis et al., 2004; Kosinski et al., 2010). Molecules secreted by the stromal cells underlying the crypt base maintain low levels of BMP signaling and functional SC compartment. Inversely, loss of this inhibitory effect in the upper region of the crypt triggers BMP activation and consequent epithelial cell differentiation (Haramis et al., 2004; Kosinski et al., 2007). Consistent with these observations, BMP inhibitors are required for the long-term culture of normal mouse and human ISC (Jung et al., 2011; Sato et al., 2009). In cultured AdSCs, we showed that recombinant BMP2 or BMP4 or *Gata6* deletion resulted in BMP target upregulation and loss of self-renewal. By supplementing culture media with the BMP antagonists DMH1 or NOGGIN, we re-established AdSC clonogenicity. These data demonstrates that the transcription factor GATA6 controls BMP signaling.

In vivo, BMP4 has been shown to be expressed in the epithelial compartment of mouse small intestinal adenomas and it was proposed to exert an autocrine protective function to limit self-renewal and tumor progression (Farrall et al., 2012). Our study confirmed that, upon aberrant WNT activation, the BMP pathway is activated in colon adenomas. Furthermore, we reported that BMP pathway activation does not follow a homogeneous pattern but it was switched on in the upper third of the adenoma glands. Reminiscent of normal intestine, the stromal cells underlying the base of adenoma glands may secrete BMP inhibitors that maintain AdSCs protected from BMP. As well as in normal intestine, BMP may be one of the major signaling pathways imposing cell compartmentalization and a SC hierarchy. In *Gata6* deficient adenoma, these compartments were perturbed as evidenced by an expansion of pSMAD1/5/8 and ID1 positive cell front into the AdSC

compartment. *Gata6* deficiency enforced BMP pathway activation at the base of adenoma glands, reducing the size of the AdSC compartment, demonstrated by decreased expression of ISC markers (*Lgr5*, CLDN2, EPHB3). As a consequence, *Apc* mutant *Gata6* null mice displayed reduced tumor growth and enhanced survival. Consistently, polyp formation in *Gata6* null mice was rescued by LDN-193189-induced BMP inhibition.

Linking BMP signaling, *Gata6* expression and CRC susceptibility

By ChIP-seq analysis, we showed that GATA6 positively regulates *BMP4* expression in CRC cells by direct binding to distal enhancer regions of the *BMP4* locus. One of these regions mapped to an SNP (rs1957636) which had been previously associated to CRC susceptibility (Tomlinson et al., 2011). We focused on this GATA6-bound *BMP4* enhancer region and confirmed direct GATA6 interaction by chromosome conformation capture experiments. Remarkably, in the same region, we identified binding sequences also for β-catenin/TCF4 complex. RT-qPCR and ChIP-seq analysis performed in *GATA6* deficient CRC cell line indicated that β-catenin/TCF4 and GATA6 inversely regulated *BMP4* expression by competing for the binding to the same *BMP4* enhancer region.

We hypothesize that the presence of SNPs at these regulatory regions could modulate the transcriptional circuit regulated by GATA6 and consequent BMP4 levels, influencing the expansion of AdSCs during tumorigenesis. Therefore, SNPs in the GATA6-bound *BMP4* enhancer region could be associated to CRC susceptibility. We further inspected linkage disequilibrium blocks at this genomic location and identified three more SNPs (rs1951674,

rs713424 and rs728425) located within GATA6-binding and in linkage disequilibrium with rs1957636. Although, these SNPs do not modify GATA6 core binding sequences themselves, the binding of GATA6 co-factors could be affected. In fact, GATA6 interaction with other transcription factors as well as epigenetic factors could explain the broad variety of divergent roles exerted by GATA6 depending on the cellular context, developmental and disease stage.

WNT/BMP regulatory interaction in CRC

We show that GATA6 can act as transcriptional repressor (*BMP4*) and transcriptional activator (*LGR5*) by binding to distal enhancer regions (*BMP4*) or to proximal promoters (*LGR5*). By doing so, GATA6 represses or promotes WNT target genes (*BMP4* and *LGR5* respectively) in adenoma, adding complexity to the WNT/BMP dichotomy. *BMP4* was already found to be a WNT target gene in CRC cell lines (Kim et al., 2002; Scholer-Dahirel et al., 2011; Van de Wetering et al., 2002). In turn, activated BMP signaling counteracts WNT signaling through mechanisms that have still not been deeply explored. It has been reported that conditional *Smad4* deletion in *Apc* mutant mice increased tumor burden as consequent abrogation of BMP-mediated regulation of β-catenin expression (Freeman et al., 2012). In our study we provide evidence of a WNT/BMP regulatory interaction by reporting high upregulation of WNT inhibitor genes (*Apcdd1*, *Dkk2*, *Dkk3*, *Nkd1*, *Notum*, *Wif1* and *Znrf3)* in response to BMP activation in *Gata6* null AdSC culture. Adding complexity to this regulatory network, *Apcdd1* is also a WNT target gene restricted to ISCs (Jung et al., 2011; Merlos-Suárez et al., 2011; Muñoz et al., 2012) and it has been reported to have a negative impact on WNT signaling

activation (Shimomura et al., 2010). All the other WNT inhibitors have been reported to act upstream the WNT receptor. Therefore, it is unlikely that they exert a major role in suppressing tumorigenesis in our model system where aberrant WNT signaling activation is caused by a loss-of-function *Apc* mutation. Fittingly, we observed that neither addition of recombinant WNT3a in the media nor overexpression of *Lgr5* could rescue the growth of *Gata6* null AdSCs. All the gathered observations indicate flexibility of BMP and WNT signaling pathway that can reciprocally modulate the output of their gene programs depending on the context.

Histological analysis of BMP signaling has associated the loss of BMP activation at the adenoma to carcinoma transition. Fittingly, 70% of CRCs display loss-of-function BMP pathway mutations, whereas sporadic adenomas generally do not present BMP alterations (Kodach et al., 2008). In agreement with these observations, BMP ligands have been shown to impinge growth of CRC cell lines that are still responsive to BMP signaling (Beck et al., 2006; Hardwick et al., 2008, 2004). Moreover, *Lombardo et al.* showed that BMP4 induces differentiation of CRC-SCs and increases their sensitivity to chemotherapy in mouse xenografts (Lombardo et al., 2011). In the normal intestine and pre-malignant lesions, BMP acts as a molecular break to maintain correct tissue homeostasis and impede SC over-growth. Supporting this notion, silencing of BMP in epithelial and stromal intestinal compartments lead to Juvenile Polyposis, a syndrome that predisposes to CRC (Beppu et al., 2008; Haramis et al., 2004; Kim et al., 2006). Thus, *GATA6* expression in adenomas might be a determining factor to maintain low levels of BMP signaling and enable disease progression.

Chapter 2: Functional characterization of the novel ISC gene *Smoc2*

After the identification of the gene program regulating intestinal SCs (Korinek et al., 1997), the current major effort of researchers in the field is addressing the role of specific markers in determining stemness. The second chapter of this thesis focuses on the functional characterization of *Smoc2*, a novel ISC gene. At the beginning of this study, we identified the gene by comparing three published ISC signatures based on EPHB2 and *Lgr5*-GFP cell sorting from mouse and human intestinal epithelium (Jung et al., 2011; Merlos-Suárez et al., 2011; Muñoz et al., 2012). During the development of this thesis, the Clevers group provided definitive proof that *Smoc2* marks ISCs *in vivo* (Muñoz et al., 2012). We will now discuss the different lines of evidence we gathered for the function of this novel ISC marker.

SMOC2 in the regulation of BMP pathway

At the moment we started to investigate the function of SMOC2, several studies had reported a role of Smoc2 in the modulation of the BMP morphogen gradient during Drosophila, Zebrafish and Xenopus development (Bloch-Zupan et al., 2011; Hamaratoglu et al., 2011; Thomas et al., 2009). Importantly, BMP is one of the major pathways orchestrating adult intestinal homeostasis by opposing to the WNT pathway (Kosinski et al., 2007) (see section 2.4.4.3 of the introduction). We initially hypothesized that SMOC2 could be a factor secreted by the ISCs to negatively regulate BMP signaling in the ISC niche, and ensure ISC maintenance. Interestingly, our laboratory found that *SMOC2* is positively regulated by WNT pathway (Whissell, unpublished). Thus, we

predicted that SMOC2 could be an important SC factor in the dichotomy between WNT and BMP signals that maintain the balance for correct intestinal homeostasis. In order to address the role of SMOC2 in the regulation of the BMP pathway in mammals, we first confirmed SMOC2-mediated BMP inhibition in mammalian cell lines and intestinal primary cultures. However SMOC2 showed a weaker effect than the *bona fide* BMP inhibitor NOGGIN. These results provided the first indication supporting a role of SMOC2 as BMP inhibitor in intestinal epithelial cells. We then generated mouse models in order to study the specific effect of *Smoc2* upregulation and *Smoc2* depletion in adult intestine.

Characterization of *Smoc2* transgenic mouse

The definitive proof demonstrating the importance of BMP inhibition to maintain the undifferentiated state at the intestinal crypt base was given by a study performed by the Clevers group (Haramis et al., 2004). Authors demonstrated that BMP silencing in the intestine by transgenic overexpression of the BMP inhibitor *Noggin* in the epithelium led to the formation of ectopic proliferative crypts in the differentiated compartment. Three month old mice developed benign hamartomas resembling human Juvenile Polyposis Syndrome. These lesions can progress and eventually become adenomatous. In a similar fashion, we generated mice overexpressing *Smoc2* throughout the whole intestinal epithelium. Consistently with our *in vitro* data, *Smoc2* transgenic mice displayed BMP inhibition in epithelial and stromal intestinal cells. Aged (5-10 months) *Smoc2* transgenic mice with very high *Smoc2* overexpression spontaneously developed JP-like hamartomas and some adenomas. Strengthening a role for SMOC2 during tumorigenesis, we found that *Smoc2* overexpression in mice

lacking one *Apc* allele exacerbated the development of adenomas. These results confirmed the BMP inhibitory effect exerted by SMOC2. In addition, *in vivo* results also support a weaker effect of SMOC2 compared to NOGGIN. This finding is consistent with our *in vitro* experiments. These observations could be explained by possibly different inhibitory mechanism adopted by the two proteins. Whereas it has been demonstrated that NOGGIN specifically blocks BMP activation by directly binding and sequestering BMP ligands (Groppe et al., 2002), the mechanism of action of SMOC2 is unknown. Although the main functional domains composing SMOC2 have been characterized based on their homology with those of other known proteins (Vannahme et al., 2003), their function remains speculative (Vannahme et al., 2002) and no proof of specific interaction with other proteins has been demonstrated. Most likely, SMOC2 could interfere with BMP activation downstream of the BMP receptor by signaling through independent receptors or integrins and converging with the BMP pathway at the level of pSMAD1/5/8. In fact, it has been shown that SMOC2 is still able to counteract SMAD1/5/8 phosphorylation in the presence of a constitutive active BMP type 1 receptor (Thomas et al., 2009). Moreover, it has been reported the capacity of SMOC2 to enhance cell cycle progression by binding to αvβ1 and αvβ6 integrins and by signaling through ILK (Liu et al., 2008).

The above evidences open to the possibility that SMOC2 could have broader functions not only restricted to the inhibition of BMP. Supporting this notion and contrary to the observation in *Noggin* transgenic mice (Haramis et al., 2004), *Smoc2* transgenic mice did not display ectopic crypts along the villi and correct intestinal homeostasis was apparently maintained. Instead, mice developed

gigantism affecting all the cell compartments of small intestinal and colonic epithelium. Interestingly, a study reported the crucial role of drosophila BMP (Dpp) in driving the scaling of the wing imaginal disc under the guidance of SMOC2 (Pent) (Ben-Zvi et al., 2011). Scaling is a general property of developmental systems that ensure the proportionate adjustment of signaling patterns with the organ size. The proportionate gigantism displayed by *Smoc2* transgenic mice led us to speculate an involvement of SMOC2 in developmental organ scaling. Nevertheless, the histological analysis of the intestine of new born *Smoc2* transgenic mice did not show any size abnormality, even though the *Villin* promoter drives the overexpression of *Smoc2* transgene already from embryonic day E16. On the contrary, *Smoc2* transgenic mice were born normal. The gigantism is clearly evident in 2 months old mice and is exacerbated in older mice, suggesting a progressive evolution of the SMOC2-driven phenotype.

We further investigated the effect of *Smoc2* overexpression on self-renewal and clonogenic potential of ISCs by culturing in 3D matrix *Smoc2* wild-type and transgenic purified crypts. In the absence of BMP inhibition in the culture, *Smoc2* overexpression provoked a mild enhancement of ISC growth rate that was not sufficient to sustain the culture over time. Surprisingly, *Smoc2* overexpression in cultured transgenic crypts was in the range of 20-50 fold instead of the massive *Smoc2* overexpression detected *in vivo* (up to 3000 fold). This observation could explain the failure of *Smoc2* transgenic ISCs to sustain their growth in culture in the absence of BMP inhibition. It also suggests a weak BMP-inhibitory activity of SMOC2 and provides an explanation for the requirement of high SMOC2 abundance to achieve full BMP blockade. Importantly, we

observed that the original difference in size of *Smoc2* transgenic intestinal crypts was not maintained in culture, since *Smoc2* wild-type and *Smoc2* transgenic purified crypts gave rise to organoids of equal size in the presence of strong BMP inhibition. This observation suggests again that *Smoc2* overexpression *in vitro* may not be sufficient to sustain the phenotype. On the other hand, this observation opens the possibility that the gigantism of the intestinal epithelium is not due to a cell-autonomous effect but rather depends on the contribution of stromal components responsive to SMOC2.

Characterization of *Smoc2* conditional KO mouse

Our experiments with *Smoc2* transgenic mice demonstrate that high levels of SMOC2 inhibit BMP activation in the intestine and cause a predisposition for adenoma growth. Nevertheless, *Smoc2* transgenic overexpression throughout the whole intestinal epithelium does not represent a physiological condition and therefore can lead to non-specific effects. In order to address the physiological role of SMOC2 in the intestinal epithelium, we generated *Smoc2* conditional KO mice where we could induce specific *Smoc2* ablation in the adult intestinal epithelium. Gene expression and histological analysis did not reveal any alteration in intestinal homeostasis of *Smoc2* intestinal epithelial KO mice. Moreover, BMP signaling was not affected.

Given the fact that *Smoc2* is a target of WNT signaling and as a result it is upregulated upon mutagenic WNT activation during tumor initiation, we decided to study the effect of *Smoc2* depletion in the intestinal epithelium of *Apc* mutant mice. We could not observe any difference in mice life span and in the incidence of

polyp burden in *Smoc2* intestinal epithelial KO mice compared to control wild-type mice. Surprisingly, we found that the Smoc2 levels in total intestine did not decrease in *Smoc2* intestinal epithelial KO mice. This first observation together with further analysis confirmed the presence of an extra-epithelial source of SMOC2 that contributes to *Smoc2* expression following *Smoc2* depletion in the epithelium. We proved this compensatory effect both in normal intestine and in the tumorigenic setting. These results suggest the lack of a SMOC2 epithelial cell-autonomous effect. Instead, they suggest that the maintenance of physiological SMOC2 levels in the intestinal crypt niche may ensure the correct intestinal homeostasis, regardless the source of SMOC2 (epithelial or stromal).

Characterization of *Smoc2* null mouse

In order to overcome the compensatory effect driven by stromal SMOC2 secretion, we generated *Smoc2* null mice. These mice presented almost undetectable *Smoc2* both in the epithelium and in total intestine. Yet, we could not detect any alteration in intestinal homeostasis. Supporting our findings, the Clevers group reported that homozygous *Smoc2* knock-in mice, constituting functional *Smoc2* null mice, did not show any intestinal nor gross non-intestinal phenotype (Muñoz et al., 2012). Furthermore, intestinal BMP signaling remained unaffected in *Smoc2* null intestine. It has been reported that BMP inhibitors are secreted by the stromal cells underlying the intestinal crypts to protect ISCs from BMP exposure (Kosinski et al., 2007). We sought to investigate the expression levels of these known intestinal BMP inhibitors (*Grem1, Grem2, Chordin*) as well as of SMOC2 related genes (*Smoc1, Sparc*). At transcriptional level, *Smoc2* was the most highly expressed among

these genes in total intestine, whereas the levels of these genes were not altered in *Smoc2* null intestine. These data suggest that these genes are not upregulated in response to *Smoc2* ablation, yet their basal levels can be sufficient to compensate the lack of SMOC2 and maintain low BMP signaling in the SC niche. In order to analyze the effect of SMOC2 loss on ISC maintenance in the absence of compensatory molecules, we cultured intestinal crypts purified from *Smoc2* null and wild-type mice. We observed equal growth rate in the presence of BMP inhibition and equal progressive growth reduction upon BMP exposure. These results definitively demonstrate epithelial SMOC2 dispensability for ISC maintenance.

As described in chapter 1 of the result section (Whissell et al., 2014), *BMP4* is upregulated in response to mutagenic WNT activation and exerts a protective role against adenoma progression. However, AdSCs are still protected from this massive BMP activation by stromal BMP inhibitors present in the tumor SC niche. In this context, the balance between BMP promoting and inhibitory signals can determine the extent of tumorigenic progression. Therefore, we sought to address the effect of complete *Smoc2* ablation in the intestine of *Apc* mutant mice. We observed that full *Smoc2* deficiency enhanced survival of *Apc* mutant mice by reducing the polyp burden, suggesting a pro-tumorigenic role of SMOC2. These findings support our previous results in *Smoc2* transgenic mice. Indeed, *Smoc2* overexpression enhances tumorigenesis whereas *Smoc2* deficiency has anti-tumorigenic effect. Consistent with this notion, a recent study showed preferential SMOC2 expression at the invasive front of CRC samples (Shvab et al., 2015). In this context, SMOC2 was

essential for L1CAM-mediated induction of aggressive/invasive properties. *SMOC2* upregulation induced a more mesenchymal-like phenotype and increased liver metastasis. Additionally, strengthening the relevance of SMOC2 in the tumorigenic process, we had previously found that *SMOC2* is one of the most enriched genes in CRC-SCs (Merlos-Suárez et al., 2011).

We investigated the role of SMOC2 during the first steps of tumorigenesis in the context of adenoma initiation and growth. We observed that complete *Smoc2* ablation reduced tumorigenesis in *Apc* mutant mice. On the contrary, *Smoc2* epithelial depletion had no effect on intestinal tumorigenesis of *Apc* mutant mice, although *Smoc2* KO macroadenomas displayed strong *Smoc2* downregulation as result of the consequent increase of the ratio between epithelial (*Smoc2* deficient) and stromal (*Smoc2* proficient) compartments. This observation suggests that either residual SMOC2 in the conditional KO intestine is sufficient to sustain an effective pro-tumorigenic activity, or SMOC2 plays a crucial role at adenoma initiation. If this would be the case, then the complete lack of SMOC2 in *Smoc2* null mice should restrain the transition from small aberrant crypt lesions to large adenomas. On the contrary, *Smoc2* epithelial depletion in the intestine of conditional KO mice would be fully compensated by stromal SMOC2 secretion, ensuring tumor initiation and further progression.

Inflammation is a key factor during intestinal tumorigenesis. Indeed, the extent and the quality of the inflammatory events can strongly affect the tumorigenic process. An altered inflammatory status can contribute both to the first stage of neoplastic transformation (initiation) and enhance malignancy in later stage tumors (Candido

and Hagemann, 2013; Dobrovolskaia and Kozlov, 2005). Interestingly, we observed that Smoc2 null mice responded better than wild-type littermates to DSS-induced colonic colitis. Whereas we observed equivalent extent of the damage in the two genotypes following DSS treatment, *Smoc2* null mice were more prone to recover upon DSS removal. The histological analysis confirmed that *Smoc2* null intestine underwent less inflammation and regenerated faster than wild-type intestine. This result suggests that SMOC2 could exert a pro-inflammatory role. Interestingly, it has been reported that SPARC, a SMOC2 family member, exacerbated colonic inflammation by modulating macrophage recruitment (Ng et al., 2013). SPARC null mice displayed reduced inflammation and reduced macrophage recruitment following removal of DSS treatment.

All these evidences prompted us to investigate the effect of SMOC2 in a setting where we combine DSS treatment (which triggers inflammation) with loss of *Apc*. By using both *Villin-CreER^{T2} and Lgr5-GFP-CreER^{T2}* drivers, we observed enhancement of survival and reduction in polyp formation in *Smoc2* null mice. In order to address whether the anti-tumorigenic effect observed in *Smoc2* null mice was attributed to lack of BMP inhibition and consequent BMP signaling hyperactivation, we combined *Apc* depletion and DSS treatment with LDN-193189 administration. We observed that LDN-driven specific BMP inhibition accelerated the tumorigenic process in *Smoc2* wild-type mice and fully rescued adenoma formation in *Smoc2* null mice. This result demonstrates that BMP inhibition recovers adenoma formation capability in *Smoc2* null mice.

The above observation implies that SMOC2 acts by inhibiting BMP signaling during tumor formation. Yet, the histological analysis of *Smoc2* null adenomas showed neither an expansion of the BMP positive differentiated compartment nor a reduction of AdSC compartment. Therefore, we conclude that adenoma epithelial cells are not the direct targets of SMOC2-driven BMP regulation. In order to reinforce this result, we cultured in 3D matrix AdSCs derived from *Apc* mutant, *Smoc2* null or wild-type mice. In the presence of robust BMP inhibition in the culture media, AdSCs of the two genotypes showed equal clonogenic potential. Upon BMP exposure, *Smoc2* null and wild-type AdSCs suffered equal growth reduction and equivalent upregulation of BMP target genes. Therefore, lack of SMOC2 does not exacerbate the response of AdSCs to BMP activation, confirming that SMOC2 does not protect AdSCs from BMP but it must impinge on adenoma growth through another mechanism that likely involves stromal cells.

Of note, although the data gathered from *Smoc2* KO mice indicates that epithelial cells are not the major targets of endogenous SMOC2, *Smoc2* transgenic mice showed strong BMP signaling inhibition also in epithelial cells. Consistently, we observed that recombinant SMOC2 protein promoted *in vitro* growth of normal intestinal crypts as well as of AdSCs upon BMP exposure. We speculate that *in vitro* treatment with rSMOC2 provides a non-physiological amount of SMOC2 molecules that mimic the abundance of SMOC2 in the intestinal epithelium of transgenic mice. In both contexts, epithelial cells showed responsiveness to SMOC2. These data lead us to hypothesize that intestinal cells (epithelial and stromal) could have a “SMOC2-responsiveness threshold”, depending on SMOC2 protein abundance. Based on

our data, stromal cells are most likely the targets of endogenous SMOC2 activity.

SMOC2 is expressed by and target Endoglin (CD105) positive endothelial cells

We next focused our effort to understand the role of SMOC2 in the stromal component of adenomas. In particular, several studies correlating BM-40 proteins with vascular cell biology caught our attention. It has been already reported a role of SMOC2 in the stimulation of endothelial angiogenesis *in vitro* by synergizing with vascular endothelial growth factor (VEGF) (Rocnik et al., 2006). Moreover, *Sparc* null mice exhibited decreased pericyte-associated vessels in an orthotopic model of pancreatic cancer (Brekken et al., 2003). The same authors also demonstrated that SPARC promotes pericyte migration by binding to the TGFβ co-receptor Endoglin (CD105) and by diminishing TGFβ activity (Rivera and Brekken, 2011). Additionally, a very recent paper showed that SMOC1 is expressed by endothelial cells and promotes their proliferation by binding Endoglin in an autocrine fashion. In particular, they showed that SMOC1-Endoglin interaction blocked TGFβ signaling through ALK5 receptor and promoted BMP9/10 signaling through ALK1 receptor, thus inducing angiogenesis (Awwad et al., 2015).

Both the ALK1- and ALK5-mediated signaling can be activated within endothelium (Goumans et al., 2009). ALK1 phosphorylates target SMADs (SMAD1, SMAD5, and SMAD8) through a similar mechanism as ALK5 phosphorylates SMAD2 and SMAD3 (Chen and Massagué, 1999) (**Figure 78**).

The homodimeric Endoglin (CD105) lacks kinase activity but modulates BMP and TGFβ signaling. Endoglin not only interacts

with ALK1 to promote downstream SMAD1/5/8 activation, it also disrupts ALK5-mediated signaling (Goumans et al., 2003). Moreover, Endoglin is able to bind directly to BMPs (Scharpfenecker et al., 2007) (**Figure 78**).

The requirement of Endoglin for endothelial cell proliferation and survival is illustrated by the fact that endothelial cell lines could not be derived from homozygous Endoglin-deficient matrix-embedded endothelial cells (MEECs) (Lebrin et al., 2004). Conversely, overexpression of either wild-type *Endoglin* or *ALK1* increases cell proliferation in MEECs. Similar pro-angiogenic and pro-proliferative features of Endoglin are also evident in an *in vivo* model of angiogenesis involving retinal vasculature. *Endoglin* heterozygous deficiency impairs angiogenesis in this model, due to reduced proliferation of the endothelial cells compared to wild-type cells (Park et al., 2013). Mouse tumor models showed that lack of Endoglin expression facilitates migration through the endothelial cell barrier (Anderberg et al., 2013). This indicates that the Endoglin/ALK1 signaling axis is a key component for endothelial cell integrity. However, the ability of both ALK1 and ALK5 to exceptionally bind to TGFβ in the endothelium depending on the cell context, adds complexity regarding the possible outcomes of TGFβ/BMP signaling (Jonker, 2014; Scharpfenecker et al., 2007) (**Figure 78**).

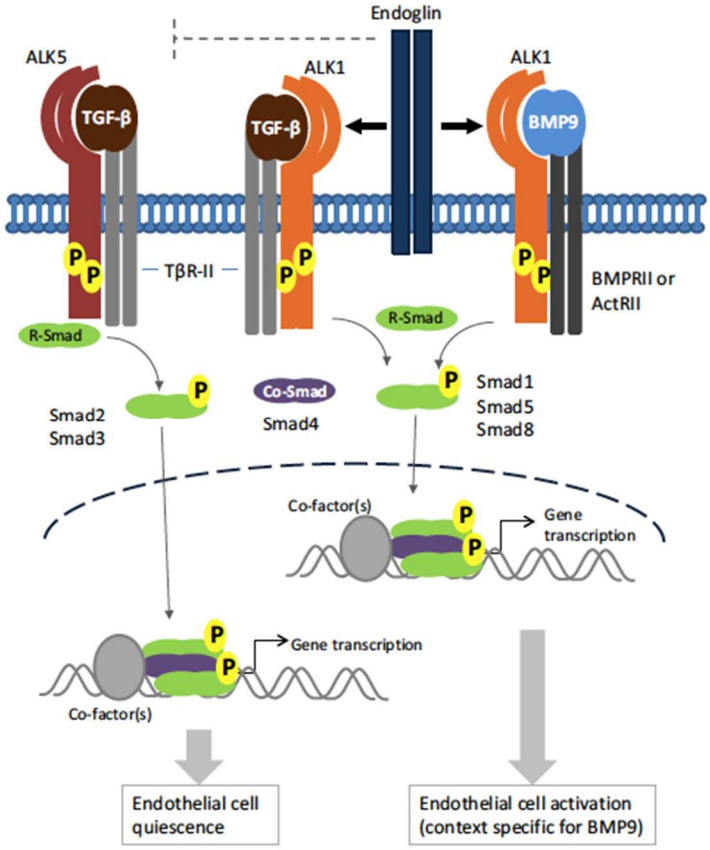

Figure 78: TGFβ and BMP9 signaling pathways involving Endoglin and ALK1 in endothelial cells. From (Jonker, 2014).

Endoglin is predominantly expressed on cellular lineages within the vascular system and is overexpressed on proliferating endothelial cells. Several studies indicate that Endoglin is involved in the development of blood vessels and that it represents a powerful marker of neovascularization in various types of tumors, including colon cancer (Minhajat et al., 2006a, 2006b; Saad et al., 2004). Indeed, Endoglin is emerging as a prime vascular target of anti-angiogenic cancer therapy (Jonker, 2014). However, Endoglin expression is not restricted to endothelial cells. It has been reported that although Endoglin is absent from peripheral blood monocytes, it is expressed in differentiated monocytes (Lastres et al., 1992) and smooth muscle cells (Ma et al., 2000; Mancini et al., 2009; Middleton et al., 2005).

Considering this interesting network involving BM-40 proteins and Endoglin-mediated regulation of TGFβ/BMP signaling in endothelial cells, we sought to purify Endoglin positive cells from *Smoc2* null and wild-type adenomas. In particular, we found two Endoglin positive cell populations: CD45-/CD105+ cells that represent endothelial cells, and CD45+/CD105+ cells which are enriched in specific markers of tissue resident macrophages. Interestingly, these two fractions expressed high levels of *Smoc2*. This finding is in line with previous observations regarding the existence of an extra-epithelial source of SMOC2. We then profiled the gene expression of these two cell populations purified from *Smoc2* null and wild-type adenomas. GSEA analysis showed negative correlation of *Smoc2* null Endoglin positive macrophages with several processes involved in inflammation. On the other hand, *Smoc2* null Endoglin positive endothelial cells showed negative correlation with genes related to ECM organization and IGF

receptor signaling pathway. It is known that inflammation is characterized by ECM remodeling to allow immune cells migration and recruitment, as well as by collagen deposition that can lead to fibrosis. We hypothesized that many of these events could be orchestrated by IGF1 that has been reported to be involved in several epithelial and stromal responses.

Connecting SMOC2 with IGF1 signaling

Our results indicate that lack of *Smoc2* induces upregulation of BMP signaling in adenoma endothelial cells, which in turn negatively regulate *Igf1* expression. By specific and acute blockade of BMP, endothelial *Igf1* expression was reestablished. These findings suggest a novel IGF1 regulatory circuit in adenoma endothelial cells which is mediated by BMP signaling and is perturbed upon *Smoc2* ablation.

IGF1 is essential for normal pre- and post-natal growth and development (Clemmons, 2007). Somatic growth in mammals is controlled by the regulated release of GH, which acts systemically through the controlled production of IGF1 by the liver. IGF1 then circulates to target organs acting in an endocrine manner (Le Roith et al., 2001). Yet, conditional liver-specific *Igf1* KO mice showed that abolished levels of liver *Igf1* mRNA and significant reduction in circulating IGF1 did not lead to differences in body weights. These study suggest that extra-hepatic sources of IGF1, acting in an autocrine/paracrine manner, are important for postnatal growth and development (Sjögren et al., 1999; Yakar et al., 1999).

Most IGF1 actions are mediated by its binding to the IGF1 receptor, a tyrosine kinase consisting of two heterodimers that has significant homology with the insulin receptor (Garrett et al., 1998).

Additionally, several proteins such as IGFBP1, IGFBP2, IGFBP3, IGFBP4, IGFBP5 and IGFBP6 may inhibit or potentiate IGF1 actions. IGF1 receptor signaling involves autophosphorylation and subsequent tyrosine phosphorylation of insulin receptor substrate (IRS) (Tsuruzoe et al., 2001). IRS serves as a docking protein and can activate multiple signaling pathways, including PI3K/AKT pathway and MAPK pathway (Le Roith et al., 2001; Saltiel and Kahn, 2001). The activation of these signaling pathways triggers differential biological processes, including cell growth, differentiation, migration, and survival (Stewart and Rotwein, 1996) (**Figure 79**).

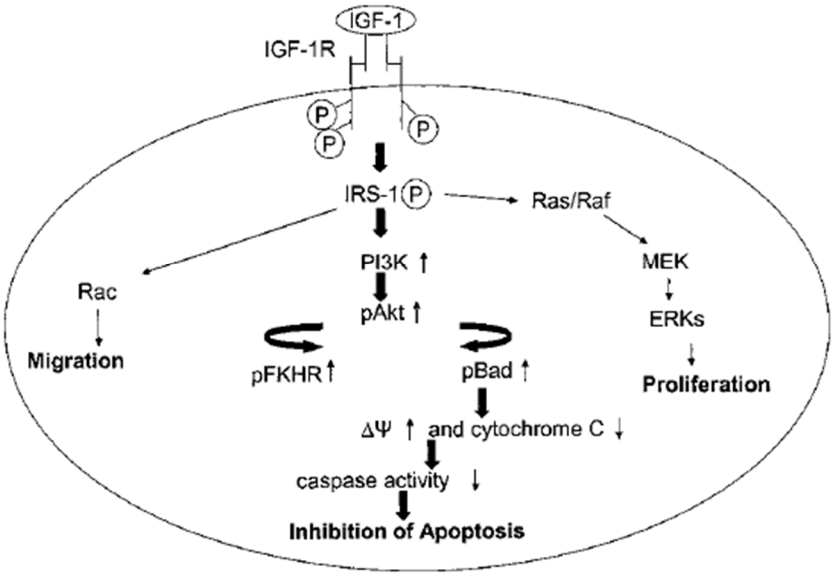

Figure 79: Possible outcomes of IGF1 signaling in the cell. From (Delafontaine et al., 2004).

IGF1 in blood vessels

Endothelial cells (ECs) are involved in IGF1 physiology and in turn they are targets of IGF1 actions. It has been reported that vascular smooth muscle cells (VSMCs) and ECs respectively express high and low levels of IGF1. The IGF1 receptor is highly expressed by both VSMCs and ECs from large and small vessels, suggesting that these cells are responsive to IGF1 (Delafontaine et al., 2004). Indeed, several studies report that IGF1 regulates migration and angiogenesis (Kondo et al., 2003; Nicosia et al., 1994; Shigematsu et al., 1999) and enhances inflammatory and vasodilatory responses in ECs (Che et al., 2002).

In particular, hypoxia is a major angiogenic stimulus, and hypoxia inducible factors (HIFs) regulate transcription of key angiogenic genes, including VEGF (Semenza, 2012). IGF1 stimulate *HIF1A* expression (Hoeben et al., 2004), and induces VEGF synthesis (Stearns et al., 2005; Warren et al., 1996). Interestingly, it has been reported that *Smoc2* was positively regulated by hypoxia in mesenchymal stem cells (Basciano et al., 2011). Furthermore, a recent study showed that both *Smoc2* and *Igf1* were upregulated in adipose tissue-derived stromal cells in response to serum deprivation (Tratwal et al., 2015), a condition that mimics in some aspects lack of vasculature and hypoxia.

Furthermore, there is substantial interest in the role of the IGF system in cardiovascular disease. Many studies suggest that IGF1 may be pro-atherogenic, because it promotes vascular smooth muscle cell proliferation and migration, and its expression is increased in atherosclerotic plaques (Clemmons, 2007). Interestingly, *Smoc2* was found upregulated during *neointima* formation in a rat carotid endarterectomy model, suggesting that

SMOC2 might be involved in the progression of atherosclerosis (Nishimoto et al., 2002).

Up to date, no evidences about direct BMP-mediated regulation of IGF1 have been reported. Yet, the literature offers extensive studies regarding the role of BMP in EC functions. Beyond its importance in embryonic development, BMP pathway plays a crucial role in vascular disorders including hereditary hemorrhagic telangiectasia (HHT) and peripheral arterial hypertension (PAH) (Cai et al., 2012). Although the BMP family is often considered pro-angiogenic, several studies highlight how the context affects whether a BMP ligand acts as pro- or anti-angiogenic. Indeed, different EC types exhibit varying responses to the same BMP ligands. These differences may be due to the differential expression of co-receptors that mediate BMP internalization (Dyer et al., 2014). Recent studies have shown that the BMP pathway also affects processes such as the endothelial response to hypoxia and inflammatory stimuli (Kim et al., 2013), strengthening the significance of BMP pathway in maintaining vascular homeostasis.

In our experimental system, we found that ECs are target of SMOC2-driven BMP deregulation and source of IGF1. At histological level, we have no clear evidence pointing to affected EC proliferation and angiogenesis in *Smoc2* null adenomas. Nevertheless, our initial results indicate that several pro-mitogenic factors (*Fgf7, FgfR2, VegfA, Hgf*) appear downregulated in *Smoc2* null ECs. Further analysis will be required to assess the status of vascular cells in *Smoc2* null adenomas. We also hypothesize that endothelium-secreted IGF1 may also exert paracrine functions on other cell types.

IGF1 in epithelial cells

IGF1 has been demonstrated to have mitogenic effects on cultured intestinal epithelial cells (Duncan et al., 1994; Simmons et al., 1995, 1999). Evidences suggest that mesenchymal cells, including myofibroblasts and smooth muscle cells, are primary sources of locally expressed IGF1 in the intestine. Indeed, in the normal intestine, IGF1 is expressed in scattered cells in the pericryptal regions and the *lamina propria* (Pucilowska et al., 2000a; Winesett et al., 1995). Situations of increased growth of the mucosal epithelium, such as adaptive growth following bowel resection, are accompanied by increased local *Igf1* mRNA expression in mesenchymal cells in the *lamina propria* or *muscularis propria* (Mantell et al., 1995; Winesett et al., 1995; Zeeh et al., 1998; Zimmermann et al., 1993). These findings provide correlative evidence for paracrine actions of mesenchymal cell-derived IGF1 on the intestinal epithelium. *Smp8-Igf1* transgenic mice expressing rat *Igf1* under transcriptional control of the murine *alpha-Sma* promoter exhibit normal levels of circulating IGF1 and high levels of transgene expression in smooth muscle in the small intestine (Wang et al., 1997). These mice display increased length and weight of the small intestine associated with increased thickness of the *muscularis propria* (Wang et al., 1997). In a follow-up study, authors observed an increase in crypt cell mitosis and mucosal mass in the ileum of *Smp8-Igf1* mice. Therefore, local *Igf1* overexpression in intestinal mesenchymal cells has paracrine actions *in vivo* to stimulate growth of the mucosal epithelium (Williams et al., 2002). However, it is intriguing that this paracrine effect is limited to the ileum. Some studies suggest that locally expressed IGF1 may have segment-specific effects on mucosal growth (Gillingham et al., 2000). In a similar fashion, *Igf1*

transgenic mice driving the expression of the transgene in the epithelium (particularly in the villi) by used of the *Metallothionein 1* promoter, display increased intestinal mass with higher villus and deeper crypts (Ohneda et al., 1997) (**Figure 80**).

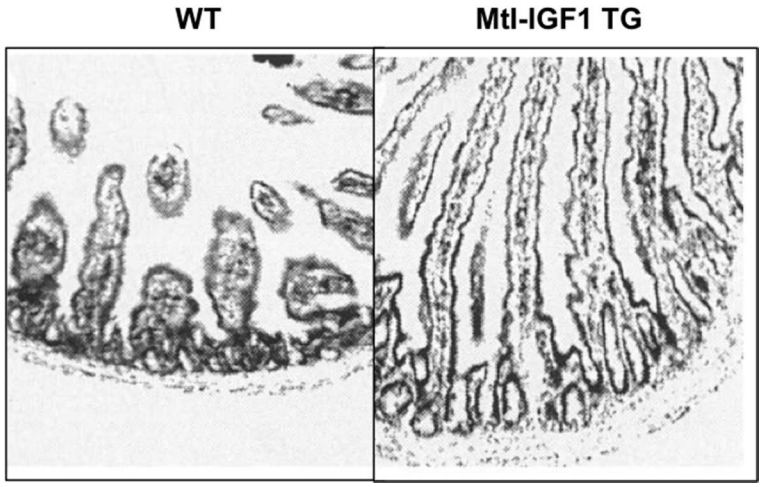

Figure 80: Histological sections (autoradiograph under bright field) of wild-type and *Mt1-Igf1* transgenic jejunum. From (Ohneda et al., 1997).

The above-described *Igf1* transgenic models resemble the *Smoc2* transgenic model in terms of general increase of mucosal mass. Therefore, we speculate that increased levels of stromal IGF1 driven by *Smoc2* overexpression could explain the proportionate gigantism observed in *Smoc2* transgenic mice.

The pro-proliferative effect of IGF1 prompted us to investigate the role of IGF1 on the growth of adenoma epithelial cells. Indeed, we hypothesized that reduced EC production of IGF1 in *Smoc2* null adenoma could negatively impinge on adenoma growth. However, we could not observe any growth promotion upon rIGF1 treatment. Further experiments are required to exclude or validate a direct IGF1 effect on adenoma epithelial cells.

The role of the IGF1 system on precancerous lesions (such as adenomatous polyps) has not been widely investigated. A recent study found a significant positive correlation between serum IGF1 and mucosal *IGF1R* mRNA in patients with adenomatous polyps (Zhang et al., 2013). IGF1 and its receptor may be activated before carcinogenesis, and may promote the growth and malignant transformation of adenomatous polyps. High levels of IGF1 have been also found in CRC patients (Jiang et al., 2014). Moreover, it has been reported that one SNP in *IGF2* significantly increased risk of development of distal adenoma (Levine et al., 2012). Furthermore, the IGF1 system has been involved in the hypoxia-induced cancer progression and metastasis (Guise, 2013; Nurwidya et al., 2014).

IGF1 in inflammation

The pathogenesis of CRC is associated to inflammation. Indeed, patients affected by Inflammatory Bowel Disease (IBD), a group of inflammatory conditions of colon and small intestine, have increased risk of developing CRC (Nieminen et al., 2014). Many evidences suggest a dual role for IGF1 during intestinal inflammation (Theiss et al., 2004). In a study aimed to analyze the relationship between serum levels of components of IGF1 system

and interleukins (IL1β and IL6) in IBD patients, authors found that IGF1 and IGFBP2 levels were co-related to ILs levels, disease activity and anatomical distribution (Street et al., 2004). A recent paper showed that epithelial-secreted IGF1 modulates the monocytes behavior to inhibit inflammation in intestine (Ge et al., 2015). Another study assessed *IGF1* mRNA and protein levels in Crohn's disease (CD) and ulcerative colitis (UC) using ISH and IHC (Lawrance et al., 2001). Authors observed that in CD, increased *IGF1* mRNA expression was transmural, affecting the full thickness of the bowel wall. In UC, *IGF1* increase was confined to the *lamina propria* and submucosa. In both cases, the distribution of IGF1 protein matched mRNA expression and coincided with the distribution of the inflammatory infiltrate. An increase in the collagen type 3 in both CD and UC also coincided with the inflamed sites. These findings suggest that IGF1 is involved in intestinal ECM remodeling in IBD. ECM remodeling is essential for regulating immune cell recruitment during inflammation. Interestingly, IGF1 plays a crucial role in the migration of macrophages at sites of inflammation (Furundzija et al., 2010). ECM organization and collagen deposition play also a crucial role during fibrosis. Fibrosis is associated to an irreversible healing response to chronic inflammation and injury (Speca et al., 2012). In particular, it involves *muscularis* overgrowth, excessive collagen deposition and mesenchymal cell hyperplasia within the *lamina propria*, *muscularis mucosa*, submucosa, *muscularis propria*, and serosa (Pucilowska et al., 2000b). While having potentially beneficial effects to promote mucosal repair and growth (Williams et al., 2001), considerable evidences suggest that local IGF1 can act in a paracrine and/or autocrine manner and mediate an excessive wound-healing response that leads to fibrosis during intestinal inflammation

(Pucilowska et al., 2000a; Simmons et al., 1999; Zimmermann et al., 1997).

IGF1 functions are broad and context-dependent. It is possible that SMOC2 regulates a variety of processes depending on the target cell type and on the context, as well. Our observations that *Smoc2* is expressed by and acts on ECs together with reported evidences that its levels are regulated by hypoxia and nutrient deprivation, lead us to speculate that SMOC2 may have an active role in angiogenesis and/or tumor cell intra- and extravasation during late stage events of tumorigenesis. In the context of tumor initiation, our current data indicate that SMOC2 could also regulate the tumor-associated inflammatory process through IGF1 that has been reported to be involved in ECM remodeling and immune cell recruitment (**Figure 81**).

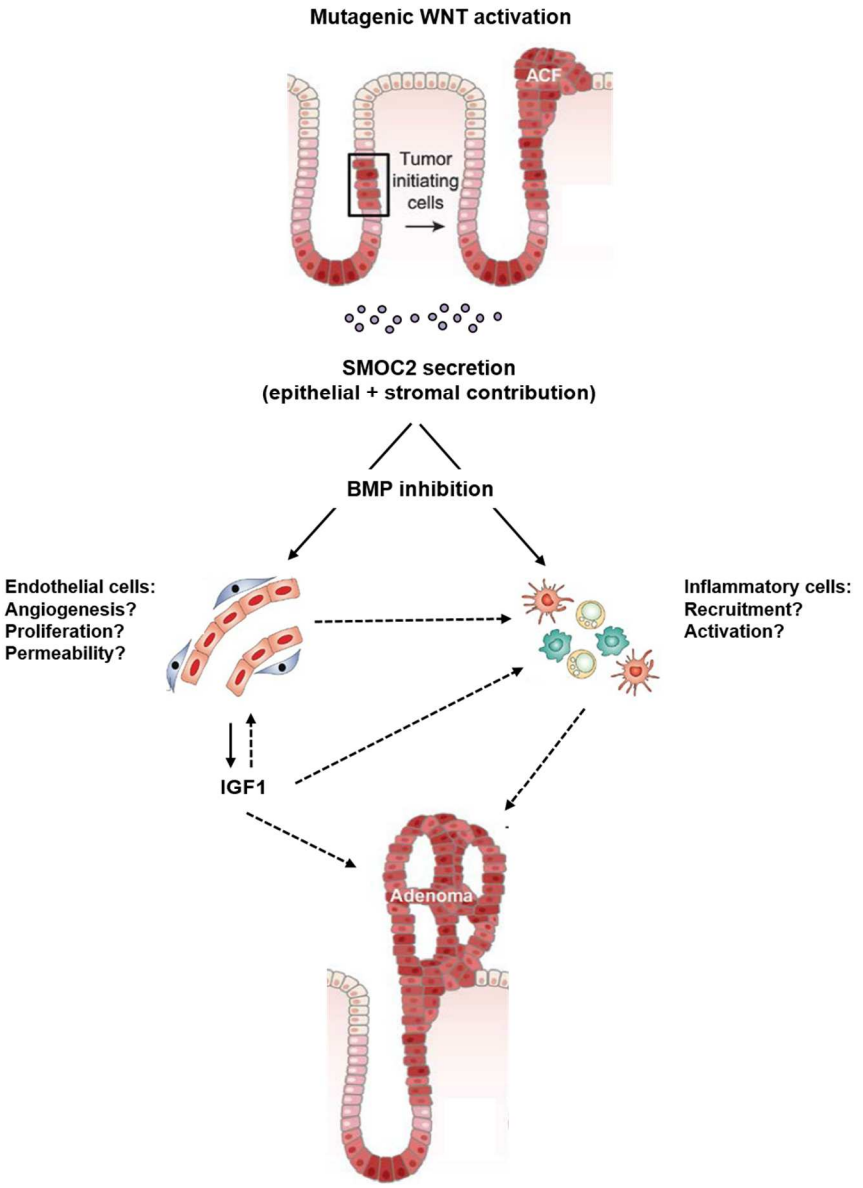

Figure 81: Working hypothesis for the biological function of SMOC2 during adenoma progression. Dashed arrows indicate hypothetical mechanisms that have still to be proved.

Conclusions

Chapter 1

1. The transcription factor GATA6 directly regulates *LGR5* expression.

2. GATA6 is the only GATA factor expressed in the colon.

3. *Gata6* deletion in an *Apc* null background leads to prolonged survival and a lower tumor burden.

4. *Gata6* deletion in colon AdSCs results in increased BMP signaling.

5. BMP inhibitors rescue the morphology and the proliferative and clonogenic potential of *Gata6* null adenoma organoids.

6. *In vivo*, mutagenic WNT activation induces protective activation of BMP pathway in the differentiated compartment of adenoma. *Gata6* null adenomas exhibit an expansion of BMP activation in the SC compartment.

7. *In vivo* treatment of mice with BMP inhibitor LDN-193189 increases tumor burden and rescues the *Gata6* null phenotype.

8. GATA6 regulates *BMP4* gene expression through distal enhancer elements.

9. GATA6 inhibits β-catenin/TCF4 binding to *BMP4* R.31 enhancer.

10. GATA6 competes with β-catenin/TCF4 complex for the regulation of BMP signaling during tumorigenesis.

Chapter 2

1. The analysis of human and mouse ISC signatures identifies *Smoc2* as a novel ISC gene.

2. SMOC2 acts as a BMP inhibitor in mammalian cell lines and primary intestinal cell cultures.

3. Transgenic *Smoc2* overexpression in intestinal epithelium leads to proportionate gigantism and triggers robust BMP inhibition in both epithelial and stromal compartments.

4. Aged *Smoc2* transgenic mice spontaneously develop hamartomatous polyps resembling those arising in patients with Juvenile Polyposis syndrome.

5. *Smoc2* overexpression in *Apc* mutant background enhances polyp formation.

6. Conditional *Smoc2* ablation in the intestinal epithelium does not affect either normal intestinal homeostasis or tumorigenesis in mice with an *Apc* mutant background.

7. A stromal source of SMOC2 maintains high SMOC2 levels upon epithelial *Smoc2* depletion.

8. Complete *Smoc2* depletion does not affect intestinal homeostasis or BMP signaling.

9. Intestinal SMOC2 is dispensable for ISC self-renewal and clonogenicity.

10. Complete *Smoc2* deficiency prolongs survival and decreases tumor burden in an *Apc* mutant background.

11. *Smoc2* null mice undergo less inflammation and recover faster after DSS-induced colitis.

12. Endogenous SMOC2 does not target epithelial cells and does not contribute to protect AdSCs from BMP activation.

13. In adenomas, *Smoc2* is expressed by Endoglin positive endothelial cells (CD105+/CD31+) and resident macrophages (CD105+/CD45+).

14. *Smoc2* null macrophages (CD105+/CD45+) show decreased levels of genes related to inflammation.

15. *Smoc2* null endothelial cells (CD105+/CD31+) show reduced expression of ECM related genes and of IGF1 pathway components.

16. BMP regulates *Igf1* mRNA levels in Endoglin-positive endothelial cells.

17. *In vitro* treatment with IGF1 does not promote AdSC proliferation.

General conclusions and perspectives

The unifying theme behind this thesis has been to understand stemness in the intestine, and how this is related to homeostasis and tumor initiation. In particular, we selected two genes, the *LGR5* transcriptional regulator *GATA6* and the novel ISC gene *SMOC2*, and studied their involvement in defining the stem cell phenotype. Both lines of investigation converged in the regulation of BMP signaling in intestine. In this thesis, we provide evidence that BMP is subjected to a complex regulatory network during tumor initiation. Also in the context of adenoma, WNT and BMP pathways interact and reciprocally modulate their outcomes, imposing hierarchies. Chapter 1 identifies a transcriptional regulatory circuit in the epithelium of adenoma where WNT and GATA6 compete for the regulation of BMPs. This newly discovered link between GATA6, BMP and WNT signaling pathways may have important implications to understand risk of CRC in the population. Moreover, dissecting the mechanisms that impose cell hierarchies on tumor cells may help to identify new therapeutic targets.

Chapter 2 is focused on addressing the role of the novel WNT target ISC gene *SMOC2*. Despite our first hypothesis, SMOC2 revealed to be dispensable for normal ISC maintenance and its expression was not only restricted to epithelial SC compartment. SMOC2 is secreted by both epithelial and stromal cells, with relevant functions in pathological settings. We have now started analyzing the functions of SMOC2 in endothelial cells and macrophages. The association between SMOC2, BMP signaling and IGF1 deserves further attention and it might reveal unexpected links between inflammation and tissue growth during colon tumor formation.

Methods

Standard cell culture and treatments

All cell lines were cultured in standard conditions in DMEM (Gibco), supplemented with 10% FBS (Gibco). For the lentivirus-transduced cells, puromycin (Invivogen, 2 µg/mL) was added to the standard media to select the stable expression of the transgene. For transgene induction Doxycycline (Sigma) was used at 1 µg/mL and left in the culture media for the intended time of the experiment. All the cell lines used in this study were obtained from the ATCC (HEK-293T, HeLa, SW480).

Human recombinant BMPs (Peprotech) were added at 25 ng/ml; human recombinant NOGGIN (Peprotech) was used at 100 ng/ml, human recombinant SMOC2 (R&D) was used at 200 ng/ml. Of note, rSMOC2 activation required 30 minutes of pre-incubation before adding rBMPs.

Lentivirus production and generation of HeLa cells over-expressing SMOC2

The entire human *SMOC2* ORF was amplified removing the stop codon and adding the FLAG-tag at the 3'. The *SMOC2-FLAG* construct was then amplified with Gateway adaptors and recombined into the pDONR221 vector. Finally, the *SMOC2-FLAG* was recombined into the lentiviral inducible vector pTRIPz Gateway.

All PCR reactions involved in the cloning were performed with the PFU Turbo polymerase (Agilent) following the manufacturer's instructions. All Gateway reactions were done following the manufacturer's protocol (Invitrogen).

To generate stable expressing HeLas, cells were infected with lentiviral particles that contained the DNA of *SMOC2-FLAG.* Replication-deficient lentiviral particles were produced in HEK-293T cells by cotransfection of *SMOC2-FLAG* construct with the viral envelope vector (pCAGGS_VSVG), packaging vector (pCAG_KGPIR) and retrotranscriptase vector (pCAG_RTR2) in the following proportions (Hanawa et al., 2002): 50% lentiviral vector containing *SMOC2-FLAG* construct, 10% envelope vector, 30% packaging vector and 10% retrotranscriptase vector. Total DNA content was 0.2 µg/cm2. Polyethylenimine (PEI) (Polysciences Inc.) was used as transfection reagent at 1 µg/cm2. DNA and PEI were mixed at 1:5 ratio and diluted in 150 mM NaCl up to 21 µl/cm2, incubated at room temperature for 20 minutes and added to HEK-293T cells. HEK-293T supernatant containing the viral particles was collected at 48h and 72h post-transfection, filtered through 0.22 µm filter and supplemented with 8 µg/ml polybrene (Fluka) before being added to the media of cells to be infected (0.1 ml/cm2 of virus supernatant). Cells were selected by resistance to puromycin (2 µg/ml).

Generation of the *Smoc2* conditional KO (cKO) mouse model

Mouse *Smoc2* gene is composed of 13 exons. To ensure the ablation of SMOC2 functionality, loxP sites were designed to flank the coding region of exon 2. The targeting vector was generated by Genebridges. The vector was verified by restriction enzyme digestion as well as sequencing. The vector was electroporated into W4 mouse embryonic stem cells (mESCs) and stably transfected cells were selected with G418. After this, single colonies were picked and triplicate plates of resistant clones were

generated. The clones were then screened by long range PCR by using the Sequal Prep Kit (Invitrogen). Positive clones were then expanded and further analyzed by Southern Blot to ensure correct and unique genomic integration. The clones verified by Southern were then transfected with an FlpO-bearing plasmid to remove the Neomycin resistance. Single clones were picked and screened by PCR for recombination and presence of both loxP sites. Positive clones were then expanded and analyzed by Southern once again to ensure the appropriate integration of the cassette, as well as to independently confirm the deletion of the Neomycin resistance cassette. Finally, positive clones were selected and blastocyst injection was done to generate chimeras. The chimeras with successful germline transmission were bred with C57/Bl6 mice and the offspring were used to generate the final colonies of mice.

Generation of *Smoc2* transgenic (TG) mouse

Mouse *Smoc2* ORF was amplified from *Smoc2* IMAGE cDNA clone 4191849 (Thermoscientific). NcoI restriction site was inserted before the ATG and NotI restriction site was inserted after the stop codon. *NcoI-Smoc2-NotI* construct was cloned in frame downstream of the last 2Kb *Villin* promoter fragment contained in a pGENT vector. The 2kb *Villin-Smoc2* construct was cut out with BamHI/NotI digestion and eventually cloned in a pBLUESCRIPT KS vector downstream of a 7Kb *Villin* promoter fragment. Mouse oocytes were injected with this plasmid carrying 9Kb *Villin-Smoc2* construct. The random integration of the transgene was assessed by genotyping the new born mice. We established several founder transgenic mouse colonies by breeding with C57/Bl6 mice.

Mouse models and genotyping

For inducible intestinal *Smoc2* deletion in the adult mouse, *Villin Cre-ER^{T2}; Smoc2$^{+/+}$* and *Villin Cre-ER^{T2}; Smoc2$^{fl/fl}$* mice were used. *Villin Cre-ER^{T2}* mice have been previously described and were obtained from Sylvie Robine.

For full *Smoc2* KO mice, *Sox2-Cre* mice were crossed with *Smoc2$^{flox/flox}$* mice to establish a *Smoc2* null (Δ) allele. The *Smoc2$^{Δ/+}$* mice were intercrossed and the *Sox2-Cre* was removed by selecting mice. *Sox2-Cre* mice have been previously described and were obtained from Ángel Nebreda.

For inducible intestinal tumorigenesis, *Villin Cre-ER^{T2}; Apc^{fll+}; Smoc2$^{+/+}$* and *Villin Cre-ER^{T2}; Apc$^{fl/+}$; Smoc2$^{fl/fl}$* or *Smoc2$^{Δ/Δ}$* mice were used.

In a similar experiment, inducible intestinal tumorigenesis was achieved by using *Lgr5 Cre-ER^{T2}; Apc^{fllfl}; Smoc2$^{+/+}$* and *Lgr5 Cre-ER^{T2}; Apc$^{fl/fl}$; Smoc2$^{Δ/Δ}$* mice. *Lgr5 Cre-ER^{T2}* mice have been previously described and were obtained from Hans Clevers.

For the study of tumorigenesis in *Smoc2* overexpressing mice, *APC^{min}; Smoc2 WT* and *APC^{min}; Smoc2 TG* mice were used.

For the study of adenoma growth *in vitro*, extracted crypts from *Villin Cre-ER^{T2}; Apc^{fllfl}; Smoc2$^{+/+}$* and *Villin Cre-ER^{T2}; Apc$^{fl/fl}$; Smoc2$^{Δ/Δ}$* mice were used.

All mice were genotyped with standard PCR protocols.

Mouse treatments

Tamoxifen (Sigma): tamoxifen was dissolved in 100% ethanol (1/10th of the final volume) at 55ºC. Once completely dissolved, solution was immediately combined with 9/10th of corn oil.

Villin CreER^{T2} mice received daily intraperitoneal injection of tamoxifen at a dose of 80 mg/kg body weight over a period of 4 days.

Lgr5 CreER^{T2} mice were injected once at a dose of 8 mg/kg body weight.

Dextran Sodium Sulfate (DSS) (Cymit Quimica): DSS was administered at 2% in drinking water over a period of 5 days.

LDN-193189 (Shanghai Biochem): LDN was dissolved in citric buffer (pH 3.1) at 3 mg/ml. Mice received two oral doses of LDN daily (morning and evening; 35 mg/kg body weight each). Controls received citric buffer alone with the same regime.

Bromodeoxyuridine (BrdU) (Sigma): BrdU was dissolved in HBSS and mice were injected with 125 mg/kg body weight 2 hours before sacrifice. Actively replicating cells were then detected by anti-BrdU immunohistochemistry.

Fluorescein isothiocyanate conjugated dextran (FITC-dextran) (Sigma): FITC-dextran was dissolved in PBS and administered by oral gavage at a dose of 44 mg/100g body weight.

Survival analysis

Kaplan-Meier survival curves were produced using the log rank test. Statistical analyses were performed using GraphPad Prism (GraphPad Software Inc.).

Colon tumor burden analysis

For the analysis of tumor burden, polyps were manually counted and the diameter was measured under the microscope the day after intestine fixation.

In LDN experiments, due to the massive uncountable polyp burden,

the percentage of tumor area was quantified as previously described in method section of Chapter 1 (Whissell et al., 2014).

Intestinal permeability assay

Intestinal permeability assay protocol was adapted from (Gupta and Nebreda, 2014, http://www.bio-protocol.org/e1289). Briefly, mice were food starved overnight. The morning after, FITC-dextran was administered by oral gavage (Bertola et al., 2013). After 4 hours, mice were anesthetized and blood was collected by intracardiac puncture. The blood was transferred to Microtainer SST tubes (BD) and the serum was separated following the manufacturer's instruction. Serum was diluted with an equal volume of PBS and 100ul of diluted serum were transferred to 96-well microplate (Corning) in duplicate. The FITC concentration in the serum was determined by spectrophoto-fluorimetry with an excitation of 485 nm and an emission of 528 nm using a standard curve generated with serially diluted FITC-dextran concentrations. Serum from mice not administered with FITC-dextran was used to determine background.

Immunohistochemistry (IHC)

Immunohistochemistry was performed as previously described in Chapter 1 (Whissell et al., 2014). Antibodies are listed in the following tables.

Masson's Trichromic staining was performed following manufacturer's protocol (DAKO AR17392-2).

Mouse *Smoc2 in situ* hybridization (ISH)

Paraffin sections of mouse intestine were de-waxed and hydrated

following standard procedures. Samples were then treated with 0.2 N HCl for 15 minutes at RT, washed 3 times in PBS and incubated for 15 minutes at 37ºC in Proteinase K (30 µg/ml in PBS). 0,2% glycine in PBS was added for 3 minutes to neutralize Proteinase K activity and samples were then washed 2 times in PBS. Sections were postfixed in 4% PFA for 10 minutes and washed 3 times in PBS. Histone acetylation was performed by incubating the samples 2 times for 5 minutes in a H_2O solution containing 1.5% triethanolamine, 0.15% HCl and 0.6% Acetic anhydride. Samples were then washed and prehybridized for 1h at 70ºC in prehybridization solution (50% Formamide, 5X SSC, 2% Blocking Reagent (Roche), 0.05% CHAPS, 5 mM EDTA, 50 µg/ml Heparin and 50 µg/ml yeast RNA). Full length *Smoc2* mRNA probe was diluted at 500 ng/ml in prehybridization solution and incubated for 24h at 68ºC. Post-hybridization washes were performed 3 times for 20 minutes in 50% Formamide/2X SSC at 65ºC. Sections were then rinsed in TBS-T buffer (0.1M Tris-HCl pH 7.5, 0.15M NaCl, 0.1% Tween20) and blocked for 30 minutes at RT in Blocking buffer (0.5% Blocking Reagent, 10% sheep serum in TBS-T). Sheep anti-DIG antibody (Roche) was diluted 1/5000 in blocking buffer and incubated overnight at 4ºC. Finally, samples were washed in TBS-T and then in NTM buffer (0.1M Tris pH 9.5, 0.1M NaCl, 0.05M MgCl2) and developed in NBT/BCIP solution (Roche) for 24-72h.

Figure 50 shows *Smoc2* ISH performed with RNAScope probe following manufacturer's protocol (Advanced Cell Diagnostics). Each dot represents a single target RNA molecule.

Mouse intestine measurements

Length of villi: intestinal pictures were taken at magnification 10X from at least 3 mice of the same genotype. 20 villi with intact transversal section were selected for each genotype. Length was measured using ImageJ.

Number of cells/crypt: Intestinal sections were stained with anti E-cadherin to highlight cell-cell boundary. Pictures were taken at 20X magnification. 20 crypts with intact transversal section were selected for each genotype. The number of cells per crypt was counted by using the ImageJ plugin “cell counter”.

Number of proliferative cells/crypt: Intestinal sections were stained with anti MKI67 to highlight proliferative cells. Pictures were taken at 20X magnification. 20 crypts with intact transversal section were selected for each genotype. The number of MKI67+ cells per crypt was counted by using the ImageJ plugin “cell counter”.

Cell migration speed: Mice were injected with BrdU and sacrificed after 72 hours. Pictures of intestinal sections were taken at 10X magnification. The distance covered by the BrdU positive cell front from the crypt-villus boundary was measured with ImageJ. 20 measurements for each genotype were performed.

Ex vivo intestinal crypt extraction and organoid culture

In order to culture normal mouse crypts, mouse small intestine was extracted and washed in HBSS. The tube was longitudinally opened and cut in 2 cm pieces. It was incubated in 8 mM EDTA in HBSS (Lonza) pH 8, during 5 minutes, at room temperature. After replacing EDTA with HBSS, the intestine was vigorously shaken and the supernatant discarded. EDTA incubation was repeated on ice for 20 minutes. After EDTA replacing with HBSS and shaking,

the supernatant containing the intestinal crypts was collected and filtered through a 100 μm strainer (BD Falcon). This step can be repeated until getting very clean crypt fractions. Intestinal crypts were seeded in 50 μl drops of matrigel (Corning) and cultured with Advanced DMEM/F12, Hepes, Glutamax, B27 and N2 supplements (Life Technologies), Rock inhibitor Y-27632 (Sigma; 10 μM), Normocin (Invivogen), rNOGGIN (Peprotech; 100 ng/ml), R-SPONDIN 1 (1 μg/ml) and EGF (Peprotech; 50 ng/ml).

In order to culture mouse colon adenoma, *Apc*$^{flox/flox}$ mice were injected with full Tamoxifen (Sigma) over a period of 2 days in order to achieve *Apc* gene ablation. Extracted colon was washed and cut in 2 cm pieces. Incubation with EDTA 8 mM (in HBSS) was performed at 37ºC for 15 minutes. After incubation, EDTA was replaced with HBSS. Following vigorous shaking, the supernatant containing colonic crypts was filtered through a 100 um strainer. The crypts were seeded in 50 μl drops of BME2 matrix (Amsbio) and cultured with basic adenoma medium: Advanced DMEM/F12, Hepes, Glutamax, B27 supplement, Rock inhibitor Y-27632, Normocin, rNOGGIN, EGF and TGFβ inhibitor LY (1 μM). For IGF1 treatment, it was used insulin-free B27 supplement (Life Technologies) and human rIGF1 (Peprotech; 100 ng/ml).

Organoid growth and clonogenic assay

Organoids formed from normal intestinal crypts were mechanically disaggregated with syringe and crypts were seeded in triplicates at the same concentration for each condition. After 5 days the number of formed organoids was manually counted.

Adenoma spheres were enzymatically disaggregated with trypsin-EDTA (Sigma) and the same number of single cells (12000-15000)

was seeded in triplicates. After one week, the number of formed spheres was counted. Clonogenic capability was assessed by repeating the previous steps over passaging.

Polyp disaggregation and staining

Polyps were minced with sterile blade and incubated for 30 minutes at 37ºC in HBSS with Collagenase IV 200 U/ml. Pieces were shaken every 5 minutes. Enzymatic reaction was stopped by adding 10% FBS and single cells were collected by sequential filtering through cell strainers of 100 µm, 70 µm and 40 µm. Cells were centrifuged, resuspended in 5 ml Ammonium Chloride (0.15M; Sigma) and incubated 5 minutes at room temperature to lyse the erythrocytes. After two washes in HBSS, cells were stained in HBSS 5% FBS with the proper conjugated antibodies for 30 minutes on ice in the dark. Antibodies are listed in the following tables. Dead cells were labeled with DAPI (Sigma Aldrich). Cells were selected in the FSC-A/ SSC-A dotplot to remove debris. The cells were then gated to exclude cellular aggregates in the FSC-A/ FSC-W dot plot. Single cells were selected for viability by excluding positive staining with DAPI. Specific polyp cell populations (2000 cells) were sorted using a FACS Aria 2.0 cell sorter (BD).

RNA extraction and gene expression analysis

For gene expression analysis of mouse intestinal organoids/spheres, 1-2 matrigel drops/condition were dissolved in TRIzol (Invitrogen). For gene expression analysis of purified mouse crypts, the crypt pellet was dissolved in TRIzol. After chloroform addition and centrifugation, the RNA from the aqueous phase was then purified with the RNA PureLink Kit (Ambion) and quantified by

Nanodrop. cDNA was produced with the High-Capacity cDNA Reverse Transcription kit (Applied Biosystems) following the manufacturer´s instructions.

RNA from polyp-sorted fractions (2000 cells) was isolated, amplified and converted into cDNA by using picoprofiling technique (Gonzalez-Roca et al., 2010) in the Genomics facility at IRB.

To assess changes in expression of selected genes, RT-qPCR was performed with their respective TaqMan probes or primers for SYBR Green. For TaqMan assays the TaqMan Universal PCR Master Mix (Applied Biosystems) was used. In the case of SYBR Green reactions the Power SYBR Master Mix (Applied Biosystems) was used. To calculate gene expression to a normalization gene the comparative threshold cycle method was used.

For global transcriptomic analysis, samples were hybridized in duplicate on Affymetrix® microarrays by the IRB Genomics facility.

Gene differential expression analysis and gene set enrichment analysis (GSEA) of differentially expressed genes was performed by the IRB Biostatistics core unit. For further details please refer to Methods of Chapter 1.

Protein extraction and Western Blot analysis

For protein expression analysis of mouse intestinal organoids/spheres, 2-3 matrigel drops were resuspended and incubated in cell recovery solution (BD Biosciences) for 30 minutes on ice to get rid of matrigel. After this, the cell pellet was resuspended in RIPA lysis buffer (50mM Tris-HCl, pH 7.5; 150nM NaCl; 1% NP-40; 0.1% SDS) supplemented with protease and phosphatase inhibitors (Sigma Aldrich) and sonicated with a Bioruptor for 5 minutes with cycles of 15s ON / 15s OFF. Cell lines

were lysed in RIPA buffer supplemented with protease and phosphatase inhibitors for 30 minutes on ice.

After centrifugation (13200 rpm, 15 minutes), the supernatant was kept as the protein extract. The samples were quantified with the Protein Assay (BioRad), based in the Bradford method, and normalized. Equal amounts of protein per sample were separated by standard SDS-PAGE and transferred to PVDF membranes. The membranes were incubated in TBS-T 0.1% supplemented with 5% milk or 5% BSA for 1 hour at RT to block unspecific antibody binding. Primary antibodies were incubated overnight at 4ºC. Primary antibodies are listed in the following tables. HRP-conjugated secondary antibodies were diluted 1/10000 in TBS-T 0.1% supplemented with 5% milk and incubated for 1 hour at RT with the membranes. After antibody incubation, membranes were washed at least 4 times with TBS-T 0.1% for 10 minutes. Immuno-complexes were visualized with ECL (Amersham).

Primary antibody Table

Primary Antibody	Manufacturer and reference	Dilution	Technique
pSMAD1/5/8	Cell Signaling 9511S	1:1000	WB
FLAG	Cell Signaling 2368	1:1000	WB
SMAD1	Abcam 33902	1:1000	WB
ACTIN-HRP	Abcam 20272	1:15000	WB
pAKT	Cell Signaling 4060P	1:1000	WB
β-CATENIN	Sigma 7207	1:100	IHC
pSMAD1/5	Cell Signaling 9516S	1:50	IHC
BRDU	Beckton 347580	1:500	IHC
CHGA	Abcam 45138	1:2000	IHC
MKI67	Novocastra Clone MM1	1:500	IHC
E-CADHERIN	BD 610182	1:400	IHC
COLLAGEN IV	Abcam 6586	1:200	IHC
GFP	ABCAM 6556-25	1:1000	IHC
KRT20	DAKO M7019	1:200	IHC
EPHB2	RD System AF467	1:200	IHC
EPCAM-FITC	Santa Cruz 53532	1:100	FACS

CD45-APC	eBioscience 17-0451-82	1:100	FACS
CD105-PE	eBioscience 12-1051-82	1:100	FACS

RT-qPCR Taqman probe Table

Gene	Taqman probe
SMOC2	Mm00491553_m1
LGR5	Mm00438890_m1
ID1	Mm00775963_g1
ID2	Mm00711781_m1
ID3	Mm00492575_m1
CD45	Mm01293568_m1
CD31	Mm00476702_m1
EPCAM	Mm00493214_m1
IGF1	Mm00439560_m1
IGFBP7	Mm03807886_m1
CD105	Mm00468256_m1
SPARC	Mm00486330_m1
SMOC1	Mm00491564_m1
SMAD6	Mm00484738_m1
APCDD1	Mm01257557_m1
OLFM4	Mm01320261_m1
CRYPTIDIN	Mm02524428_g1
AQP3	Mm01208559_m1
KRT20	Mm00508106_m1
DEFCR	Mm00655850_m1
B2M	Mm00437762_m1
ACTb	Mm00607939_s1

RT-qPCR Primer table

Gene	Primers 5'-3'
GREM1	FWD: CATACACTGTGGGAGCGTTG REV: GCTCCTTGGGAACCTTTCTT
GREM2	FWD: GTGGCTGTGCTGGTAAAGGT REV: TGTTGCTGCTACCATCCTTG
CHORDIN	FWD: TGCATCTGCTCTGAGAATGG REV: GAATATGCACGGGTGAAAGG
CD3e	FWD: CCTCAGCCTCCTAGCTGTTG REV: AGAGGGCACGTCAACTCTACA
GR1 Ly6C	FWD: CATAGAATTGATTGAGGACTC REV: GGGAACTGCTGCATTGCAGAGG
GR1 Ly6G	FWD: TACCTGCCCCTTCTCTGATG REV: AGATGGGAAGGCAGAGATTG
CX3CR1	FWD: CCTGTTATTTGGGCGACATT REV: CGAGGACCACCAACAGATTT
CD206	FWD: ATTGTGGAGCAGATGGAAGG REV: ATTTGCATTGCCCAGTAAGG
CD11c	FWD: TAGTTCCTGGGTGGTGGTTG REV: CAGTTGCCTGTGTGATAGCC
CD68	FWD: CCCTGTGTGTCTGATCTTGC REV: AGGATGGCAGGAGAGTAACG
GAPDH	FWD: CTTCACCACCATGGAGGAGGC REV: GGCATGGACTGTGGTCATGAG

Genotyping Primer Table

Gene	Primers 5'-3'
Smoc2 flox	FWD: ACATCAGTGACTTCCAGAGG REV: CGATAATAGCTGGCCATAAG
Smoc2 Δ	FWD: ACATCAGTGACTTCCAGAGG REV: GCCTAGCACGAAAGGGGTCCTGGG
Smoc2 TG	FWD: GCCAGTTTCCCTTCTTCCTC REV: GGCACAGAGTGGCTTCTGA

References

Adolph, T.E., Tomczak, M.F., Niederreiter, L., Ko, H.-J., Böck, J., Martinez-Naves, E., Glickman, J.N., Tschurtschenthaler, M., Hartwig, J., Hosomi, S., et al. (2013). Paneth cells as a site of origin for intestinal inflammation. Nature *503*, 272–276.

Al-Hajj, M., Wicha, M.S., Benito-Hernandez, A., Morrison, S.J., and Clarke, M.F. (2003). Prospective identification of tumorigenic breast cancer cells. Proc. Natl. Acad. Sci. U. S. A. *100*, 3983–3988.

Al-Shboul, O. a (2013). The importance of interstitial cells of cajal in the gastrointestinal tract. Saudi J. Gastroenterol. *19*, 3–15.

Alexandrovich, A., Qureishi, A., Coudert, A.E., Zhang, L., Grigoriadis, A.E., Shah, A.M., Brewer, A.C., and Pizzey, J.A. (2008). A role for GATA-6 in vertebrate chondrogenesis. Dev. Biol. *314*, 457–470.

Alfawaz, S., Fong, F., Plagnol, V., Wong, F.S.L., Fearne, J., and Kelsell, D.P. (2013). Recessive oligodontia linked to a homozygous loss-of-function mutation in the SMOC2 gene. Arch. Oral Biol. *58*, 462–466.

Alkhateeb, A., Marzouka, N.A.D., and Qarqaz, F. (2010). SMOC2 gene variant and the risk of vitiligo in Jordanian Arabs. Eur. J. Dermatology *20*, 701–704.

Anderberg, C., Cunha, S.I., Zhai, Z., Cortez, E., Pardali, E., Johnson, J.R., Franco, M., Páez-Ribes, M., Cordiner, R., Fuxe, J., et al. (2013). Deficiency for endoglin in tumor vasculature weakens the endothelial barrier to metastatic dissemination. J. Exp. Med. *210*, 563–579.

Anttonen, M., Unkila-Kallio, L., Leminen, A., Butzow, R., and Heikinheimo, M. (2005). High GATA-4 expression associates with aggressive behavior, whereas low anti-Mullerian hormone expression associates with growth potential of ovarian granulosa cell tumors. J Clin Endocrinol Metab *90*, 6529–6535.

Artavanis-Tsakonas, S. (1999). Notch Signaling: Cell Fate Control and Signal Integration in Development. Science (80-.). *284*, 770–776.

Auclair, B.A., Benoit, Y.D., Rivard, N., Mishina, Y., and Perreault, N. (2007). Bone Morphogenetic Protein Signaling Is Essential for Terminal Differentiation of the Intestinal Secretory Cell Lineage. Gastroenterology *133*, 887–896.

Awwad, K., Hu, J., Shi, L., Mangels, N., Abdel Malik, R., Zippel, N., Fisslthaler, B., Eble, J.A., Pfeilschifter, J., Popp, R., et al. (2015). Role of secreted modular calcium-binding protein 1 (SMOC1) in transforming growth factor β signalling and angiogenesis. Cardiovasc. Res. *106*, 284–294.

Balzola, F., Cullen, G., Ho, G.T., Hoentjen, F., and Russell, R.K. (2013). Intestinal inflammation targets cancer-inducing activity of the microbiota. Inflamm. Bowel Dis. Monit. *13*, 108.

Barbara, N.P., Wrana, J.L., and Letarte, M. (1999). Endoglin is an accessory protein that interacts with the signaling receptor complex of multiple members of the transforming growth factor-beta superfamily. J. Biol. Chem. *274*, 584–594.

Barker, N. (2014). Adult intestinal stem cells: critical drivers of epithelial homeostasis and regeneration. Nat. Rev. Mol. Cell Biol. *15*, 19–33.

Barker, N., van Es, J.H., Kuipers, J., Kujala, P., van den Born, M., Cozijnsen, M., Haegebarth, A., Korving, J., Begthel, H., Peters, P.J., et al. (2007). Identification of stem cells in small intestine and colon by marker gene Lgr5. Nature *449*, 1003–1007.

Barker, N., Ridgway, R.A., van Es, J.H., van de Wetering, M., Begthel, H., van den Born, M., Danenberg, E., Clarke, A.R., Sansom, O.J., and Clevers, H. (2009). Crypt stem cells as the cells-of-origin of intestinal cancer. Nature *457*, 608–611.

Barker, N., Huch, M., Kujala, P., van de Wetering, M., Snippert, H.J., van Es, J.H., Sato, T., Stange, D.E., Begthel, H., van den Born, M., et al. (2010). Lgr5+ve Stem Cells Drive Self-Renewal in the Stomach and Build Long-Lived Gastric Units In Vitro. Cell Stem Cell *6*, 25–36.

Basciano, L., Nemos, C., Foliguet, B., de Isla, N., de Carvalho, M., Tran, N., and Dalloul, A. (2011). Long term culture of mesenchymal stem cells in hypoxia promotes a genetic program maintaining their undifferentiated and multipotent status. BMC Cell Biol. *12*, 12.

Basu, A., Kligman, L.H., Samulewicz, S.J., and Howe, C.C. (2001). Impaired wound healing in mice deficient in a matricellular protein SPARC (osteonectin, BM-40). BMC Cell Biol. *2*, 15.

Batlle, E., Henderson, J.T., Beghtel, H., Van den Born, M.M.W., Sancho, E., Huls, G., Meeldijk, J., Robertson, J., Van de Wetering, M., Pawson, T., et al. (2002). β-catenin and TCF mediate cell positioning in the intestinal epithelium by controlling the expression of EphB/EphrinB. Cell *111*, 251–263.

Batlle, E., Bacani, J., Begthel, H., Jonkheer, S., Gregorieff, A., van de Born, M., Malats, N., Sancho, E., Boon, E., Pawson, T., et al. (2005). EphB receptor activity suppresses colorectal cancer progression. Nature *435*, 1126–1130.

Batts, L.E., Polk, D.B., Dubois, R.N., and Kulessa, H. (2006). Bmp signaling is required for intestinal growth and morphogenesis. Dev. Dyn. *235*, 1563–1570.

Beck, S.E., Jung, B.H., Fiorino, A., Gomez, J., Rosario, E. Del, Cabrera, B.L., Huang, S.C., Chow, J.Y.C., and Carethers, J.M. (2006). Bone morphogenetic protein signaling and growth suppression in colon cancer. Am. J. Physiol. Gastrointest. Liver Physiol. *291*, G135–G145.

Ben-Zvi, D., Pyrowolakis, G., Barkai, N., and Shilo, B.Z. (2011). Expansion-repression mechanism for scaling the Dpp activation gradient in drosophila wing imaginal discs. Curr. Biol. *21*, 1391–1396.

Beppu, H., Mwizerwa, O.N., Beppu, Y., Dattwyler, M.P., Lauwers, G.Y., Bloch, K.D., and Goldstein, A.M. (2008). Stromal inactivation of BMPRII leads to colorectal epithelial overgrowth and polyp formation. Oncogene *27*, 1063–1070.

Bergers, G., and Song, S. (2005). The role of pericytes in blood-vessel formation and maintenance. Neuro. Oncol. *7*, 452–464.

Bertola, A., Mathews, S., Ki, S.H., Wang, H., and Gao, B. (2013). Mouse model of chronic and binge ethanol feeding (the NIAAA model). Nat. Protoc. *8*, 627–637.

Beuling, E., Kerkhof, I.M., Nicksa, G.A., Giuffrida, M.J., Haywood, J., aan de Kerk, D.J., Piaseckyj, C.M., Pu, W.T., Buchmiller, T.L., Dawson, P.A., et al. (2010). Conditional Gata4 deletion in mice induces bile acid absorption in the proximal small intestine. Gut *59*, 888–895.

Beuling, E., Baffour-Awuah, N.Y.A., Stapleton, K.A., Aronson, B.E., Noah, T.K., Shroyer, N.F., Duncan, S.A., Fleet, J.C., and Krasinski, S.D. (2011). GATA factors regulate proliferation, differentiation, and gene expression in small intestine of mature mice. Gastroenterology *140*, 1219–1229.

Beuling, E., Aronson, B.E., Tran, L.M.D., Stapleton, K.A., ter Horst, E.N., Vissers, L.A.T.M., Verzi, M.P., and Krasinski, S.D. (2012). GATA6 Is Required for Proliferation, Migration, Secretory Cell Maturation, and Gene Expression in the Mature Mouse Colon. Mol. Cell. Biol. *32*, 3392–3402.

Birlea, S.A., Gowan, K., Fain, P.R., and Spritz, R.A. (2010). Genome-wide association study of generalized vitiligo in an isolated European founder population identifies SMOC2, in close proximity to IDDM8. J. Invest. Dermatol. *130*, 798–803.

Bjerknes, M., and Cheng, H. (1999). Clonal analysis of mouse intestinal epithelial progenitors. Gastroenterology *116*, 7–14.

Bloch-Zupan, A., Jamet, X., Etard, C., Laugel, V., Muller, J., Geoffroy, V., Strauss, J.P., Pelletier, V., Marion, V., Poch, O., et al. (2011). Homozygosity mapping and candidate prioritization identify mutations, missed by whole-exome sequencing, in SMOC2, causing major dental developmental defects. Am. J. Hum. Genet. *89*, 773–781.

Bogunovic, M., Ginhoux, F., Helft, J., Shang, L., Hashimoto, D., Greter, M., Liu, K., Jakubzick, C., Ingersoll, M.A., Leboeuf, M., et al. (2009). Origin of the Lamina Propria Dendritic Cell Network. Immunity *31*, 513–525.

Boiko, A.D., Razorenova, O. V, van de Rijn, M., Swetter, S.M., Johnson, D.L., Ly, D.P., Butler, P.D., Yang, G.P., Joshua, B., Kaplan, M.J., et al. (2010). Human

melanoma-initiating cells express neural crest nerve growth factor receptor CD271. Nature *466*, 133–137.

Bonnet, D., and Dick, J.E. (1997). Human acute myeloid leukemia is organized as a hierarchy that originates from a primitive hematopoietic cell. Nat. Med. *3*, 730–737.

Bornstein, P. (2009). Matricellular proteins: An overview. J. Cell Commun. Signal. *3*, 163–165.

Bosse, T., Piaseckyj, C.M., Burghard, E., Fialkovich, J.J., Rajagopal, S., Pu, W.T., and Krasinski, S.D. (2006). Gata4 is essential for the maintenance of jejunal-ileal identities in the adult mouse small intestine. Mol. Cell. Biol. *26*, 9060–9070.

Boyle, M., Wong, C., Rocha, M., and Jones, D.L. (2007). Decline in Self-Renewal Factors Contributes to Aging of the Stem Cell Niche in the Drosophila Testis. Cell Stem Cell *1*, 470–478.

Bradshaw, A.D., Reed, M.J., and Sage, E.H. (2002). SPARC-null mice exhibit accelerated cutaneous wound closure. J. Histochem. Cytochem. *50*, 1–10.

Bragdon, B., Moseychuk, O., Saldanha, S., King, D., Julian, J., and Nohe, a (2011). Bone morphogenetic proteins: a critical review. Cell Signal. *23*, 609–620.

Brazil, D.P., Church, R.H., Surae, S., Godson, C., and Martin, F. (2015). BMP signalling: agony and antagony in the family. Trends Cell Biol. *25*, 249–264.

Breault, D.T., Min, I.M., Carlone, D.L., Farilla, L.G., Ambruzs, D.M., Henderson, D.E., Algra, S., Montgomery, R.K., Wagers, A.J., and Hole, N. (2008). Generation of mTert-GFP mice as a model to identify and study tissue progenitor cells. Proc. Natl. Acad. Sci. U. S. A. *105*, 10420–10425.

Brekken, R.A., and Sage, E.H. (2000). SPARC, a matricellular protein: at the crossroads of cell-matrix. Matrix Biol. *19*, 569–580.

Brekken, R.A., Puolakkainen, P., Graves, D.C., Workman, G., Lubkin, S.R., and Sage, E.H. (2003). Enhanced growth of tumors in SPARC null mice is associated with changes in the ECM. J. Clin. Invest. *111*, 487–495.

Van den Brink, G.R. (2007). Hedgehog signaling in development and homeostasis of the gastrointestinal tract. Physiol. Rev. *87*, 1343–1375.

Brosens, L.A.A., van Hattem, A., Hylind, L.M., Iacobuzio-Donahue, C., Romans, K.E., Axilbund, J., Cruz-Correa, M., Tersmette, A.C., Offerhaus, G.J.A., and Giardiello, F.M. (2007). Risk of colorectal cancer in juvenile polyposis. Gut *56*, 965–967.

Brosens, L.A.A., Langeveld, D., van Hattem, W.A., Giardiello, F.M., and Offerhaus, G.J.A. (2011). Juvenile polyposis syndrome. World J. Gastroenterol. *17*, 4839–4844.

Buczacki, S.J. a, Zecchini, H.I., Nicholson, A.M., Russell, R., Vermeulen, L., Kemp, R., and Winton, D.J. (2013). Intestinal label-retaining cells are secretory precursors expressing Lgr5. Nature *495*, 65–69.

Burt, R.W. (2010). Colorectal cancer screening. Curr. Opin. Gastroenterol. *26*, 466–470.

Cai, J., Pardali, E., Sánchez-Duffhues, G., and ten Dijke, P. (2012). BMP signaling in vascular diseases. {FEBS} Lett. *586*, 1993–2002.

Calon, A., Espinet, E., Palomo-Ponce, S., Tauriello, D.V.F., Iglesias, M., Céspedes, M.V., Sevillano, M., Nadal, C., Jung, P., Zhang, X.H.F., et al. (2012). Dependency of Colorectal Cancer on a TGF-β-Driven Program in Stromal Cells for Metastasis Initiation. Cancer Cell *22*, 571–584.

Candido, J., and Hagemann, T. (2013). Cancer-related inflammation. J. Clin. Immunol. *33*.

Cavallo, R.A., Cox, R.T., Moline, M.M., Roose, J., Polevoy, G.A., Clevers, H., Peifer, M., and Bejsovec, A. (1998). Drosophila Tcf and Groucho interact to repress Wingless signalling activity. Nature *395*, 604–608.

Che, W., Lerner-Marmarosh, N., Huang, Q., Osawa, M., Ohta, S., Yoshizumi, M., Glassman, M., Lee, J.-D., Yan, C., Berk, B.C., et al. (2002). Insulin-like growth factor-1 enhances inflammatory responses in endothelial cells: role of Gab1 and MEKK3 in TNF-alpha-induced c-Jun and NF-kappaB activation and adhesion molecule expression. Circ. Res. *90*, 1222–1230.

Chen, Y.G., and Massagué, J. (1999). Smad1 recognition and activation by the ALK1 group of transforming growth factor-β family receptors. J. Biol. Chem. *274*, 3672–3677.

Chen, J., Li, Y., Yu, T.-S., McKay, R.M., Burns, D.K., Kernie, S.G., and Parada, L.F. (2012). A restricted cell population propagates glioblastoma growth after chemotherapy. Nature *488*, 522–526.

Cheng, H., and Leblond, C.P. (1974). Origin, differentiation and renewal of the four main epithelial cell types in the mouse small intestine. V. Unitarian Theory of the origin of the four epithelial cell types. Am. J. Anat. *141*, 537–561.

Chow, E., and Macrae, F. (2005). Review of juvenile polyposis syndrome. J. Gastroenterol. Hepatol. *20*, 1634–1640.

Claudinot, S., Nicolas, M., Oshima, H., Rochat, A., and Barrandon, Y. (2005). Long-term renewal of hair follicles from clonogenic multipotent stem cells. Proc. Natl. Acad. Sci. U. S. A. *102*, 14677–14682.

Clemmons, D.R. (2007). Modifying IGF1 activity: an approach to treat endocrine disorders, atherosclerosis and cancer. Nat. Rev. Drug Discov. *6*, 821–833.

Clevers, H., and Batlle, E. (2015). SnapShot: The Intestinal Crypt. Cell *152*, 1198–1198.e2.

Clevers, H., and Clevers, H. (2006). Wnt/beta-catenin signaling in development and disease. Cell *127*, 469–480.

Conboy, I.M., Conboy, M.J., Wagers, A.J., Girma, E.R., Weissman, I.L., and Rando, T.A. (2005). Rejuvenation of aged progenitor cells by exposure to a young systemic environment. Nature *433*, 760–764.

Corre, J., Mahtouk, K., Attal, M., Gadelorge, M., Huynh, A., Fleury-Cappellesso, S., Danho, C., Laharrague, P., Klein, B., Rème, T., et al. (2007). Bone marrow mesenchymal stem cells are abnormal in multiple myeloma. Leukemia.

Cortina, C., Palomo-Ponce, S., Iglesias, M., Fernández-Masip, J.L., Vivancos, A., Whissell, G., Humà, M., Peiró, N., Gallego, L., Jonkheer, S., et al. (2007). EphB-ephrin-B interactions suppress colorectal cancer progression by compartmentalizing tumor cells. Nat. Genet. *39*, 1376–1383.

Cuny, G.D., Yu, P.B., Laha, J.K., Xing, X., Liu, J.-F., Lai, C.S., Deng, D.Y., Sachidanandan, C., Bloch, K.D., and Peterson, R.T. (2008). Structure-activity relationship study of bone morphogenetic protein (BMP) signaling inhibitors. Bioorg. Med. Chem. Lett. *18*, 4388–4392.

Dalerba, P., Dylla, S.J., Park, I.K., Liu, R., Wang, X.H., Cho, R.W., Hoey, T., Gurney, A., Huang, E.H., Simeone, D.M., et al. (2007). Phenotypic characterization of human colorectal cancer stem cells. Proc. Natl. Acad. Sci. U. S. A. *104*, 10158–10163.

Damjanovich, K., Langa, C., Blanco, F.J., McDonald, J., Botella, L.M., Bernabeu, C., Wooderchak-Donahue, W., Stevenson, D.A., and Bayrak-Toydemir, P. (2011). 5'UTR mutations of ENG cause Hereditary Hemorrhagic Telangiectasia. Orphanet J. Rare Dis. *6*, 85.

Daniels, J., and Montgomery, E. (2007). Non-neoplastic colorectal polyps. Curr. Diagnostic Pathol. *13*, 467–478.

Davis, H., Irshad, S., Bansal, M., Rafferty, H., Boitsova, T., Bardella, C., Jaeger, E., Lewis, A., Freeman-Mills, L., Giner, F.C., et al. (2015). Aberrant epithelial GREM1 expression initiates colonic tumorigenesis from cells outside the stem cell niche. Nat Med *21*, 62–70.

Delafontaine, P., Song, Y.H., and Li, Y. (2004). Expression, Regulation, and Function of IGF-1, IGF-1R, and IGF-1 Binding Proteins in Blood Vessels. Arterioscler. Thromb. Vasc. Biol. *24*, 435–444.

Delany, A.M., Amling, M., Priemel, M., Howe, C., Baron, R., and Canalis, E. (2000). Osteopenia and decreased bone formation in osteonectin-deficient mice. J. Clin. Invest. *105*, 915–923.

Dhawan, P., Ahmad, R., Chaturvedi, R., Smith, J.J., Midha, R., Mittal, M.K., Krishnan, M., Chen, X., Eschrich, S., Yeatman, T.J., et al. (2011). Claudin-2 expression increases tumorigenicity of colon cancer cells: role of epidermal growth factor receptor activation. Oncogene *30*, 3234–3247.

Dobrovolskaia, M.A., and Kozlov, S. V (2005). Inflammation and cancer: when NF-kappaB amalgamates the perilous partnership. Curr. Cancer Drug Targets *5*, 325–344.

Dong, Q., Wang, D., Bandyopadhyay, A., Gao, H., Gorena, K.M., Hildreth, K., Rebel, V.I., Walter, C.A., Huang, C., and Sun, L.Z. (2013). Mammospheres from murine mammary stem cell-enriched basal cells: Clonal characteristics and repopulating potential. Stem Cell Res. *10*, 396–404.

Van Dop, W.A., Uhmann, A., Wijgerde, M., Sleddens-Linkels, E., Heijmans, J., Offerhaus, G.J., van den Bergh Weerman, M.A., Boeckxstaens, G.E., Hommes, D.W., Hardwick, J.C., et al. (2009). Depletion of the Colonic Epithelial Precursor Cell Compartment Upon Conditional Activation of the Hedgehog Pathway. Gastroenterology *136*.

Duncan, M.D., Korman, L.Y., and Bass, B.L. (1994). Epidermal growth factor primes intestinal epithelial cells for proliferative effect of insulin-like growth factor I. Dig. Dis. Sci. *39*, 2197–2201.

Duvillié, B., Attali, M., Aiello, V., Quemeneur, E., and Scharfmann, R. (2003). Label-retaining cells in the rat pancreas: Location and differentiation potential in vitro. Diabetes *52*, 2035–2042.

Dyer, L. a, Pi, X., and Patterson, C. (2014). The role of BMPs in endothelial cell function and dysfunction. Trends Endocrinol. Metab. 1–9.

Edelman, E., and Eng, C. (2010). PTEN Hamartoma Tumor Syndrome. In Management of Genetic Syndromes: Third Edition, pp. 661–675.

Engler, A.J., Sen, S., Sweeney, H.L., and Discher, D.E. (2006). Matrix Elasticity Directs Stem Cell Lineage Specification. Cell *126*, 677–689.

Van Es, J.H., Jay, P., Gregorieff, A., van Gijn, M.E., Jonkheer, S., Hatzis, P., Thiele, A., van den Born, M., Begthel, H., Brabletz, T., et al. (2005). Wnt signalling induces maturation of Paneth cells in intestinal crypts. Nat. Cell Biol. *7*, 381–386.

Van Es, J.H., Sato, T., van de Wetering, M., Lyubimova, A., Yee Nee, A.N., Gregorieff, A., Sasaki, N., Zeinstra, L., van den Born, M., Korving, J., et al. (2012). Dll1+ secretory progenitor cells revert to stem cells upon crypt damage. Nat. Cell Biol. *14*, 1099–1104.

Farrall, A.L., Riemer, P., Leushacke, M., Sreekumar, A., Grimm, C., Herrmann, B.G., and Morkel, M. (2012). Wnt and BMP signals control intestinal adenoma cell fates. Int. J. Cancer *131*, 2242–2252.

Fearon, E.R., and Vogelstein, B. (1990). A genetic model for colorectal tumorigenesis. Cell *61*, 759–767.

Ficara, F., Murphy, M.J., Lin, M., and Cleary, M.L. (2008). Pbx1 Regulates Self-Renewal of Long-Term Hematopoietic Stem Cells by Maintaining Their Quiescence. Cell Stem Cell *2*, 484–496.

Van der Flier, L.G., and Clevers, H. (2009). Stem cells, self-renewal, and differentiation in the intestinal epithelium. Annu Rev Physiol *71*, 241–260.

Van der Flier, L.G., Sabates-Bellver, J., Oving, I., Haegebarth, A., De Palo, M., Anti, M., Van Gijn, M.E., Suijkerbuijk, S., Van de Wetering, M., Marra, G., et al. (2007). The Intestinal Wnt/TCF Signature. Gastroenterology *132*, 628–632.

Van der Flier, L.G., van Gijn, M.E., Hatzis, P., Kujala, P., Haegebarth, A., Stange, D.E., Begthel, H., van den Born, M., Guryev, V., Oving, I., et al. (2009). Transcription Factor Achaete Scute-Like 2 Controls Intestinal Stem Cell Fate. Cell *136*, 903–912.

Fre, S., Huyghe, M., Mourikis, P., Robine, S., Louvard, D., and Artavanis-Tsakonas, S. (2005). Notch signals control the fate of immature progenitor cells in the intestine. Nature *435*, 964–968.

Freeman, T.J., Smith, J.J., Chen, X., Washington, M.K., Roland, J.T., Means, A.L., Eschrich, S.A., Yeatman, T.J., Deane, N.G., and Beauchamp, R.D. (2012). Smad4-mediated signaling inhibits intestinal neoplasia by inhibiting expression of beta-catenin. Gastroenterology *142*, 562–571.

Fu, B., Luo, M., Lakkur, S., Lucito, R., and Iacobuzio-Donahue, C.A. (2008). Frequent genomic copy number gain and overexpression of GATA-6 in pancreatic carcinoma. Cancer Biol. Ther. *7*, 1593–1601.

Fuchs, E. (2009). The Tortoise and the Hair: Slow-Cycling Cells in the Stem Cell Race. Cell *137*, 811–819.

Fuchs, E., and Chen, T. (2013). A matter of life and death: self-renewal in stem cells. EMBO Rep. *14*, 39–48.

Furundzija, V., Fritzsche, J., Kaufmann, J., Meyborg, H., Fleck, E., Kappert, K., and Stawowy, P. (2010). IGF-1 increases macrophage motility via PKC/p38-dependent alphavbeta3-integrin inside-out signaling. Biochem. Biophys. Res. Commun. *394*, 786–791.

Gammon, A., Jasperson, K., Kohlmann, W., and Burt, R.W. (2009). Hamartomatous polyposis syndromes. Best Pract. Res. Clin. Gastroenterol. *23*, 219–231.

Garrett, T.P., McKern, N.M., Lou, M., Frenkel, M.J., Bentley, J.D., Lovrecz, G.O., Elleman, T.C., Cosgrove, L.J., and Ward, C.W. (1998). Crystal structure of the first

three domains of the type-1 insulin-like growth factor receptor. Nature *394*, 395–399.

Ge, R.-T., Mo, L.-H., Wu, R., Liu, J.-Q., Zhang, H.-P., Liu, Z., Liu, Z., and Yang, P.-C. (2015). Insulin-like growth factor-1 endues monocytes with immune suppressive ability to inhibit inflammation in the intestine. Sci. Rep. *5*, 7735.

Gerbe, F., Van Es, J.H., Makrini, L., Brulin, B., Mellitzer, G., Robine, S., Romagnolo, B., Shroyer, N.F., Bourgaux, J.F., Pignodel, C., et al. (2011). Distinct ATOH1 and Neurog3 requirements define tuft cells as a new secretory cell type in the intestinal epithelium. J. Cell Biol. *192*, 767–780.

Gerbe, F., Legraverend, C., and Jay, P. (2012). The intestinal epithelium tuft cells: specification and function. Cell. Mol. Life Sci. *69*, 2907–2917.

Gerbe, F., Brulin, B., Makrini, L., Legraverend, C., and Jay, P. (2015). DCAMKL-1 Expression Identifies Tuft Cells Rather Than Stem Cells in the Adult Mouse Intestinal Epithelium. Gastroenterology *137*, 2179–2180.

Gillingham, M.B., Dahly, E.M., Carey, H. V, Clark, M.D., Kritsch, K.R., and Ney, D.M. (2000). Differential jejunal and colonic adaptation due to resection and IGF-I in parenterally fed rats. Am. J. Physiol. Gastrointest. Liver Physiol. *278*, G700–G709.

Gilmour, D.T., Lyon, G.J., Carlton, M.B.L., Sanes, J.R., Cunningham, J.M., Anderson, J.R., Hogan, B.L.M., Evans, M.J., and Colledge, W.H. (1998). Mice deficient for the secreted glycoprotein SPARC/osteonectin/BM40 develop normally but show severe age-onset cataract formation and disruption of the lens. EMBO J. *17*, 1860–1870.

Gonzalez-Roca, E., Garcia-Albéniz, X., Rodriguez-Mulero, S., Gomis, R.R., Kornacker, K., and Auer, H. (2010). Accurate Expression Profiling of Very Small Cell Populations. PLoS One *5*, e14418.

Goumans, M.-J., Liu, Z., and ten Dijke, P. (2009). TGF-beta signaling in vascular biology and dysfunction. Cell Res. *19*, 116–127.

Goumans, M.J., Valdimarsdottir, G., Itoh, S., Lebrin, F., Larsson, J., Mummery, C., Karlsson, S., and Ten Dijke, P. (2003). Activin receptor-like kinase (ALK)1 is an antagonistic mediator of lateral TGFβ/ALK5 signaling. Mol. Cell *12*, 817–828.

Gregorieff, A., Pinto, D., Begthel, H., Destrée, O., Kielman, M., and Clevers, H. (2005). Expression pattern of Wnt signaling components in the adult intestine. Gastroenterology *129*, 626–638.

Grompe, M. (2012). Tissue stem cells: New tools and functional diversity. Cell Stem Cell *10*, 685–689.

Groppe, J., Greenwald, J., Wiater, E., Rodriguez-Leon, J., Economides, A.N., Kwiatkowski, W., Affolter, M., Vale, W.W., Belmonte, J.C.I., and Choe, S. (2002).

Structural basis of BMP signalling inhibition by the cystine knot protein Noggin. Nature *420*, 636–642.

Guise, T.A. (2013). Breast cancer bone metastases: It's all about the neighborhood. Cell *154*, 957–958.

Hamaratoglu, F., de Lachapelle, A.M., Pyrowolakis, G., Bergmann, S., and Affolter, M. (2011). Dpp signaling activity requires pentagone to scale with tissue size in the growing drosophila wing imaginal disc. PLoS Biol. *9*.

HANAHAN, D. (2000). The Hallmarks of Cancer. Cell *100*, 57–70.

Hanawa, H., Kelly, P.F., Nathwani, A.C., Persons, D.A., Vandergriff, J.A., Hargrove, P., Vanin, E.F., and Nienhuis, A.W. (2002). Comparison of various envelope proteins for their ability to pseudotype lentiviral vectors and transduce primitive hematopoietic cells from human blood. Mol. Ther. *5*, 242–251.

Haramis, A.-P.G., Begthel, H., van den Born, M., van Es, J., Jonkheer, S., Offerhaus, G.J.A., and Clevers, H. (2004). De novo crypt formation and juvenile polyposis on BMP inhibition in mouse intestine. Science *303*, 1684–1686.

Hardwick, J.C., Kodach, L.L., Offerhaus, G.J., and van den Brink, G.R. (2008). Bone morphogenetic protein signalling in colorectal cancer. Nat. Rev. Cancer *8*, 806–812.

Hardwick, J.C.H., Van Den Brink, G.R., Bleuming, S.A., Ballester, I., Van Den Brande, J.M.H., Keller, J.J., Offerhaus, G.J.A., Van Deventer, S.J.H., and Peppelenbosch, M.P. (2004). Bone Morphogenetic Protein 2 Is Expressed by, and Acts Upon, Mature Epithelial Cells in the Colon. Gastroenterology *126*, 111–121.

Haveri, H., Westerholm-Ormio, M., Lindfors, K., Mäki, M., Savilahti, E., Andersson, L.C., and Heikinheimo, M. (2008). Transcription factors GATA-4 and GATA-6 in normal and neoplastic human gastrointestinal mucosa. BMC Gastroenterol. *8*, 9.

Hayashi, S., Lewis, P., Pevny, L., and McMahon, A.P. (2002). Efficient gene modulation in mouse epiblast using a Sox2Cre transgenic mouse strain. Gene Expr. Patterns *2*, 93–97.

Heemskerk, V.H., Daemen, M.A., and Buurman, W.A. (1999). Insulin-like growth factor-1 (IGF-1) and growth hormone (GH) in immunity and inflammation. Cytokine Growth Factor Rev. *10*, 5–14.

Hellebrekers, D.M.E.I., Lentjes, M.H.F.M., Van Den Bosch, S.M., Melotte, V., Wouters, K.A.D., Daenen, K.L.J., Smits, K.M., Akiyama, Y., Yuasa, Y., Sanduleanu, S., et al. (2009). GATA4 and GATA5 are potential tumor suppressors and biomarkers in colorectal cancer. Clin. Cancer Res. *15*, 3990–3997.

Hoeben, A., Landuyt, B., Highley, M.S., Wildiers, H., Van Oosterom, A.T., and De Bruijn, E.A. (2004). Vascular endothelial growth factor and angiogenesis. Pharmacol. Rev. *56*, 549–580.

Imamura, T., Takase, M., Nishihara, A., Oeda, E., Hanai, J., Kawabata, M., and Miyazono, K. (1997). Smad6 inhibits signalling by the TGF-beta superfamily. Nature *389*, 622–626.

Ireland, H., Kemp, R., Houghton, C., Howard, L., Clarke, A.R., Sansom, O.J., and Winton, D.J. (2004). Inducible Cre-Mediated Control of Gene Expression in the Murine Gastrointestinal Tract: Effect of Loss of beta-Catenin. Gastroenterology *126*, 1236–1246.

Ireland, H., Houghton, C., Howard, L., and Winton, D.J. (2005). Cellular inheritance of a Cre-activated reporter gene to determine Paneth cell longevity in the murine small intestine. Dev. Dyn. *233*, 1332–1336.

Itzkovitz, S., Lyubimova, A., Blat, I.C., Maynard, M., van Es, J., Lees, J., Jacks, T., Clevers, H., and van Oudenaarden, A. (2011). Single-molecule transcript counting of stem-cell markers in the mouse intestine. Nat. Cell Biol. *14*, 106–114.

Jaeger, E., Leedham, S., Lewis, A., Segditsas, S., Becker, M., Cuadrado, P.R., Davis, H., Kaur, K., Heinimann, K., Howarth, K., et al. (2012). Hereditary mixed polyposis syndrome is caused by a 40-kb upstream duplication that leads to increased and ectopic expression of the BMP antagonist GREM1. Nat. Genet. *44*, 699–703.

Jemal, A., Bray, F., Center, M.M., Ferlay, J., Ward, E., and Forman, D. (2011). Global Cancer Statistics: 2011. CA. Cancer J. Clin. *61*, 69–90.

Jensen, J., Pedersen, E.E., Galante, P., Hald, J., Heller, R.S., Ishibashi, M., Kageyama, R., Guillemot, F., Serup, P., and Madsen, O.D. (2000). Control of endodermal endocrine development by Hes-1. Nat. Genet. *24*, 36–44.

Jiang, B., Zhang, X., Du, L.L., Wang, Y., Liu, D.B., Han, C.Z., Jing, J.X., Zhao, X.W., and Xu, X.Q. (2014). Possible roles of insulin, IGF-1 and IGFBPs in initiation and progression of colorectal cancer. World J. Gastroenterol. *20*, 1608–1613.

Jones, D.L., and Wagers, A.J. (2008). No place like home: anatomy and function of the stem cell niche. Nat. Rev. Mol. Cell Biol. *9*, 11–21.

Jonker, L. (2014). TGF-β & BMP Receptors Endoglin and ALK1: Overview of their Functional Role and Status as Antiangiogenic Targets. Microcirculation *21*, 93–103.

Jordan, C.T., Guzman, M.L., and Noble, M. (2006). Cancer stem cells. N. Engl. J. Med. *355*, 1253–1261.

Jung, P., Sato, T., Merlos-Suárez, A., Barriga, F.M., Iglesias, M., Rossell, D., Auer, H., Gallardo, M., Blasco, M.A., Sancho, E., et al. (2011). Isolation and in vitro expansion of human colonic stem cells. Nat. Med. *17*, 1225–1227.

Kamnasaran, D., Qian, B., Hawkins, C., Stanford, W.L., and Guha, A. (2007). GATA6 is an astrocytoma tumor suppressor gene identified by gene trapping of mouse glioma model. Proc. Natl. Acad. Sci. U. S. A. *104*, 8053–8058.

Karam, S.M. (1999). Lineage commitment and maturation of epithelial cells in the gut. Front. Biosci. *4*, D286–D298.

Kelley, C., Blumberg, H., Zon, L.I., and Evans, T. (1993). GATA-4 is a novel transcription factor expressed in endocardium of the developing heart. Development *118*, 817–827.

Kemper, K., Sprick, M.R., De Bree, M., Scopelliti, A., Vermeulen, L., Hoek, M., Zeilstra, J., Pals, S.T., Mehmet, H., Stassi, G., et al. (2010). The AC133 epitope, but not the CD133 protein, is lost upon cancer stem cell differentiation. Cancer Res. *70*, 719–729.

Kim, M., and Choe, S. (2011). BMPs and their clinical potentials. BMB Rep. *44*, 619–634.

Kim, B.-G., Li, C., Qiao, W., Mamura, M., Kasprzak, B., Anver, M., Wolfraim, L., Hong, S., Mushinski, E., Potter, M., et al. (2006). Smad4 signalling in T cells is required for suppression of gastrointestinal cancer. Nature *441*, 1015–1019.

Kim, C.W., Song, H., Kumar, S., Nam, D., Kwon, H.S., Chang, K.H., Son, D.J., Kang, D.W., Brodie, S.A., Weiss, D., et al. (2013). Anti-inflammatory and antiatherogenic role of bmp receptor ii in endothelial cells. Arterioscler. Thromb. Vasc. Biol. *33*, 1350–1359.

Kim, J.S., Crooks, H., Dracheva, T., Nishanian, T.G., Singh, B., Jen, J., and Waldman, T. (2002). Oncogenic beta-catenin is required for bone morphogenetic protein 4 expression in human cancer cells. Cancer Res *62*, 2744–2748.

Kim, K.-A., Kakitani, M., Zhao, J., Oshima, T., Tang, T., Binnerts, M., Liu, Y., Boyle, B., Park, E., Emtage, P., et al. (2005). Mitogenic influence of human R-spondin1 on the intestinal epithelium. Science *309*, 1256–1259.

Kinugasa, T., Huo, Q., Higashi, D., Shibaguchi, H., Kuroki, M., Tanaka, T., Futami, K., Yamashita, Y., Hachimine, K., Maekawa, S., et al. (2007). Selective up-regulation of claudin-1 and claudin-2 in colorectal cancer. In Anticancer Research, pp. 3729–3734.

Kinzler, K., and Vogelstein, B. (1996). Lessons from Hereditary Review Colorectal Cancer. Cell *87*, 159–170.

Kirkbride, K.C., Townsend, T.A., Bruinsma, M.W., Barnett, J. V, and Blobe, G.C. (2008). Bone morphogenetic proteins signal through the transforming growth factor-beta type III receptor. J. Biol. Chem. *283*, 7628–7637.

Klapholz-Brown, Z., Walmsley, G.G., Nusse, Y.M., Nusse, R., and Brown, P.O. (2007). Transcriptional program induced by Wnt protein in human fibroblasts

suggests mechanisms for cell cooperativity in defining tissue microenvironments. PLoS One *2*.

Kodach, L.L., Wiercinska, E., de Miranda, N.F.C.C., Bleuming, S.A., Musler, A.R., Peppelenbosch, M.P., Dekker, E., van den Brink, G.R., van Noesel, C.J.M., Morreau, H., et al. (2008). The Bone Morphogenetic Protein Pathway Is Inactivated in the Majority of Sporadic Colorectal Cancers. Gastroenterology *134*.

Kodach, L.L., Jacobs, R.J., Voorneveld, P.W., Wildenberg, M.E., Verspaget, H.W., van Wezel, T., Morreau, H., Hommes, D.W., Peppelenbosch, M.P., van den Brink, G.R., et al. (2011). Statins augment the chemosensitivity of colorectal cancer cells inducing epigenetic reprogramming and reducing colorectal cancer cell "stemness" via the bone morphogenetic protein pathway. Gut *60*, 1544–1553.

Kondo, T., Vicent, D., Suzuma, K., Yanagisawa, M., King, G.L., Holzenberger, M., and Kahn, C.R. (2003). Knockout of insulin and IGF-1 receptors on vascular endothelial cells protects against retinal neovascularization. J. Clin. Invest. *111*, 1835–1842.

Korinek, V., Barker, N., Morin, P.J., van Wichen, D., de Weger, R., Kinzler, K.W., Vogelstein, B., and Clevers, H. (1997). Constitutive transcriptional activation by a beta-catenin-Tcf complex in APC-/- colon carcinoma. Science *275*, 1784–1787.

Korinek, V., Barker, N., Moerer, P., van Donselaar, E., Huls, G., Peters, P.J., and Clevers, H. (1998). Depletion of epithelial stem-cell compartments in the small intestine of mice lacking Tcf-4. Nat. Genet. *19*, 379–383.

Kosinski, C., Li, V.S.W., Chan, A.S.Y., Zhang, J., Ho, C., Tsui, W.Y., Chan, T.L., Mifflin, R.C., Powell, D.W., Yuen, S.T., et al. (2007). Gene expression patterns of human colon tops and basal crypts and BMP antagonists as intestinal stem cell niche factors. Proc. Natl. Acad. Sci. U. S. A. *104*, 15418–15423.

Kosinski, C., Stange, D.E., Xu, C., Chan, A.S., Ho, C., Yuen, S.T., Mifflin, R.C., Powell, D.W., Clevers, H., Leung, S.Y., et al. (2010). Indian hedgehog regulates intestinal stem cell fate through epithelial-mesenchymal interactions during development. Gastroenterology *139*, 893–903.

Koutsourakis, M., Langeveld, A., Patient, R., Beddington, R., and Grosveld, F. (1999). The transcription factor GATA6 is essential for early extraembryonic development. Development *126*, 723–732.

Kuhnert, F., Davis, C.R., Wang, H.-T., Chu, P., Lee, M., Yuan, J., Nusse, R., and Kuo, C.J. (2004). Essential requirement for Wnt signaling in proliferation of adult small intestine and colon revealed by adenoviral expression of Dickkopf-1. Proc. Natl. Acad. Sci. U. S. A. *101*, 266–271.

Kuo, C.T., Morrisey, E.E., Anandappa, R., Sigrist, K., Lu, M.M., Parmacek, M.S., Soudais, C., and Leiden, J.M. (1997). GATA4 transcription factor is required for ventral morphogenesis and heart tube formation. Genes Dev. *11*, 1048–1060.

Kwei, K.A., Bashyam, M.D., Kao, J., Ratheesh, R., Reddy, E.C., Kim, Y.H., Montgomery, K., Giacomini, C.P., Choi, Y. La, Chatterjee, S., et al. (2008). Genomic profiling identifies GATA6 as a candidate oncogene amplified in pancreatobiliary cancer. PLoS Genet. *4*.

Lane, T.F., and Sage, E.H. (1994). The biology of SPARC, a protein that modulates cell-matrix interactions. FASEB J. *8*, 163–173.

Lane, S.W., Williams, D. a, and Watt, F.M. (2014). Modulating the stem cell niche for tissue regeneration. Nat. Biotechnol. *32*, 795–803.

Lapidot, T., Sirard, C., Vormoor, J., Murdoch, B., Hoang, T., Caceres-Cortes, J., Minden, M., Paterson, B., Caligiuri, M.A., and Dick, J.E. (1994). A cell initiating human acute myeloid leukaemia after transplantation into SCID mice. Nature *367*, 645–648.

Larraín, J., Bachiller, D., Lu, B., Agius, E., Piccolo, S., and De Robertis, E.M. (2000). BMP-binding modules in chordin: a model for signalling regulation in the extracellular space. Development *127*, 821–830.

Lastres, P., Bellon, T., Cabañas, C., Sanchez-Madrid, F., Acevedo, A., Gougos, A., Letarte, M., and Bernabeu, C. (1992). Regulated expression on human macrophages of endoglin, an Arg-Gly-Asp-containing surface antigen. Eur. J. Immunol. *22*, 393–397.

De Lau, W., Barker, N., Low, T.Y., Koo, B.-K., Li, V.S.W., Teunissen, H., Kujala, P., Haegebarth, A., Peters, P.J., van de Wetering, M., et al. (2011). Lgr5 homologues associate with Wnt receptors and mediate R-spondin signalling. Nature *476*, 293–297.

Laverriere, A.C., MacNeill, C., Mueller, C., Poelmann, R.E., Burch, J.B.E., and Evans, T. (1994). GATA-4/5/6, a subfamily of three transcription factors transcribed in developing heart and gut. J. Biol. Chem. *269*, 23177–23184.

Lawrance, I.C., Maxwell, L., and Doe, W. (2001). Inflammation location, but not type, determines the increase in TGF-beta1 and IGF-1 expression and collagen deposition in IBD intestine. Inflamm. Bowel Dis. *7*, 16–26.

Lebrin, F., Goumans, M.-J., Jonker, L., Carvalho, R.L.C., Valdimarsdottir, G., Thorikay, M., Mummery, C., Arthur, H.M., and ten Dijke, P. (2004). Endoglin promotes endothelial cell proliferation and TGF-beta/ALK1 signal transduction. EMBO J. *23*, 4018–4028.

Lee, N.Y., Ray, B., How, T., and Blobe, G.C. (2008). Endoglin promotes transforming growth factor β-mediated Smad 1/5/8 signaling and inhibits endothelial cell migration through its association with GIPC. J. Biol. Chem. *283*, 32527–32533.

Lei, N.Y., Jabaji, Z., Wang, J., Joshi, V.S., Brinkley, G.J., Khalil, H., Wang, F., Jaroszewicz, A., Pellegrini, M., Li, L., et al. (2014). Intestinal subepithelial myofibroblasts support the growth of intestinal epithelial stem cells. PLoS One *9*.

Levine, A.J., Ihenacho, U., Lee, W., Figueiredo, J.C., Vandenberg, D.J., Edlund, C.K., Davis, B.D., Stern, M.C., and Haile, R.W. (2012). Genetic variation in insulin pathway genes and distal colorectal adenoma risk. Int. J. Colorectal Dis. *27*, 1587–1595.

Li, L., and Clevers, H. (2010). Coexistence of quiescent and active adult stem cells in mammals. Science *327*, 542–545.

Li, Y., and Tower, J. (2009). Adult-specific over-expression of the Drosophila genes magu and hebe increases life span and modulates late-age female fecundity. Mol. Genet. Genomics *281*, 147–162.

Li, D.Y., Sorensen, L.K., Brooke, B.S., Urness, L.D., Davis, E.C., Taylor, D.G., Boak, B.B., and Wendel, D.P. (1999). Defective angiogenesis in mice lacking endoglin. Science *284*, 1534–1537.

Li, X., Madison, B.B., Zacharias, W., Kolterud, A., States, D., and Gumucio, D.L. (2007). Deconvoluting the intestine: molecular evidence for a major role of the mesenchyme in the modulation of signaling cross talk. Physiol. Genomics *29*, 290–301.

Liu, H., Patel, M.R., Prescher, J.A., Patsialou, A., Qian, D., Lin, J., Wen, S., Chang, Y.-F., Bachmann, M.H., Shimono, Y., et al. (2010). Cancer stem cells from human breast tumors are involved in spontaneous metastases in orthotopic mouse models. Proc. Natl. Acad. Sci. U. S. A. *107*, 18115–18120.

Liu, P., Lu, J., Cardoso, W. V, and Vaziri, C. (2008). The SPARC-related factor SMOC-2 promotes growth factor-induced cyclin D1 expression and DNA synthesis via integrin-linked kinase. Mol. Biol. Cell *19*, 248–261.

Loh, K., Chia, J.A., Greco, S., Cozzi, S.J., Buttenshaw, R.L., Bond, C.E., Simms, L.A., Pike, T., Young, J.R., Jass, J.R., et al. (2008). Bone morphogenic protein 3 inactivation is an early and frequent event in colorectal cancer development. Genes Chromosom. Cancer *47*, 449–460.

Lombardo, Y., Scopelliti, A., Cammareri, P., Todaro, M., Iovino, F., Ricci-Vitiani, L., Gulotta, G., Dieli, F., De Maria, R., and Stassi, G. (2011). Bone morphogenetic protein 4 induces differentiation of colorectal cancer stem cells and increases their response to chemotherapy in mice. Gastroenterology *140*, 297–309.

Lopez-Arribillaga, E., Rodilla, V., Pellegrinet, L., Guiu, J., Iglesias, M., Roman, A.C., Gutarra, S., Gonzalez, S., Munoz-Canoves, P., Fernandez-Salguero, P., et al. (2015). Bmi1 regulates murine intestinal stem cell proliferation and self-renewal downstream of Notch. Development *142*, 41–50.

Ma, X., Labinaz, M., Goldstein, J., Miller, H., Keon, W.J., Letarte, M., and O'Brien, E. (2000). Endoglin is overexpressed after arterial injury and is required for transforming growth factor-beta-induced inhibition of smooth muscle cell migration. Arterioscler. Thromb. Vasc. Biol. *20*, 2546–2552.

Mackenzie, I.C., and Bickenbach, J.R. (1985). Label-retaining keratinocytes and Langerhans cells in mouse epithelia. Cell Tissue Res. *242*, 551–556.

Maeda, M., Ohashi, K., and Ohashi-Kobayashi, A. (2005). Further extension of mammalian GATA-6. Dev. Growth Differ. *47*, 591–600.

Maier, S., Paulsson, M., and Hartmann, U. (2008). The widely expressed extracellular matrix protein SMOC-2 promotes keratinocyte attachment and migration. Exp. Cell Res. *314*, 2477–2487.

Mancini, M.L., Terzic, A., Conley, B.A., Oxburgh, L.H., Nicola, T., and Vary, C.P.H. (2009). Endoglin plays distinct roles in vascular smooth muscle cell recruitment and regulation of arteriovenous identity during angiogenesis. Dev. Dyn. *238*, 2479–2493.

Mantell, M.P., Ziegler, T.R., Adamson, W.T., Roth, J.A., Zhang, W., Frankel, W., Bain, A., Chow, J.C., Smith, R.J., and Rombeau, J.L. (1995). Resection-induced colonic adaptation is augmented by IGF-I and associated with upregulation of colonic IGF-I mRNA. Am. J. Physiol. *269*, G974–G980.

El Marjou, F., Janssen, K.P., Chang, B.H.J., Li, M., Hindie, V., Chan, L., Louvard, D., Chambon, P., Metzger, D., and Robine, S. (2004). Tissue-specific and inducible Cre-mediated recombination in the gut epithelium. Genesis *39*, 186–193.

Markowitz, S.D., and Bertagnolli, M.M. (2009). Molecular Basis of Colorectal Cancer. N. Engl. J. Med. *361*, 2449–2460.

Marshman, E., Booth, C., and Potten, C.S. (2002). The intestinal epithelial stem cell. Bioessays *24*, 91–98.

Merika, M., and Orkin, S.H. (1993). DNA-binding specificity of GATA family transcription factors. Mol. Cell. Biol. *13*, 3999–4010.

Merlos-Suárez, A., Barriga, F.M., Jung, P., Iglesias, M., Céspedes, M.V., Rossell, D., Sevillano, M., Hernando-Momblona, X., Da Silva-Diz, V., Muñoz, P., et al. (2011). The intestinal stem cell signature identifies colorectal cancer stem cells and predicts disease relapse. Cell Stem Cell *8*, 511–524.

Middleton, J., Americh, L., Gayon, R., Julien, D., Mansat, M., Mansat, P., Anract, P., Cantagrel, A., Cattan, P., Reimund, J.M., et al. (2005). A comparative study of endothelial cell markers expressed in chronically inflamed human tissues: MECA-79, Duffy antigen receptor for chemokines, von Willebrand factor, CD31, CD34, CD105 and CD146. J. Pathol. *206*, 260–268.

Milano, J., McKay, J., Dagenais, C., Foster-Brown, L., Pognan, F., Gadient, R., Jacobs, R.T., Zacco, A., Greenberg, B., and Ciaccio, P.J. (2004). Modulation of Notch processing by gamma-secretase inhibitors causes intestinal goblet cell metaplasia and induction of genes known to specify gut secretory lineage differentiation. Toxicol. Sci. *82*, 341–358.

Milano, S.K., Kwon, W., Pereira, R., Antonyak, M.A., and Cerione, R.A. (2012). Characterization of a novel activated Ran GTPase mutant and its ability to induce cellular transformation. J. Biol. Chem. *287*, 24955–24966.

Minhajat, R., Mori, D., Yamasaki, F., Sugita, Y., Satoh, T., and Tokunaga, O. (2006a). Organ-specific endoglin (CD105) expression in the angiogenesis of human cancers. Pathol. Int. *56*, 717–723.

Minhajat, R., Mori, D., Yamasaki, F., Sugita, Y., Satoh, T., and Tokunaga, O. (2006b). Endoglin (CD105) expression in angiogenesis of colon cancer: Analysis using tissue microarrays and comparison with other endothelial markers. Virchows Arch. *448*, 127–134.

Miyazono, K., Kamiya, Y., and Morikawa, M. (2010). Bone morphogenetic protein receptors and signal transduction. J. Biochem. *147*, 35–51.

Molkentin, J.D., Lin, Q., Duncan, S.A., and Olson, E.N. (1997). Requirement of the transcription factor GATA4 for heart tube formation and ventral morphogenesis. Genes Dev. *11*, 1061–1072.

Molkentin, J.D., Tymitz, K.M., Richardson, J.A., and Olson, E.N. (2000). Abnormalities of the genitourinary tract in female mice lacking GATA5. Mol. Cell. Biol. *20*, 5256–5260.

Montgomery, R.K., Carlone, D.L., Richmond, C.A., Farilla, L., Kranendonk, M.E.G., Henderson, D.E., Baffour-Awuah, N.Y., Ambruzs, D.M., Fogli, L.K., Algra, S., et al. (2011). Mouse telomerase reverse transcriptase (mTert) expression marks slowly cycling intestinal stem cells. Proc. Natl. Acad. Sci. U. S. A. *108*, 179–184.

Morris, R.J., and Potten, C.S. (1994). Slowly cycling (label-retaining) epidermal cells behave like clonogenic stem cells in vitro. Cell Prolif. *27*, 279–289.

Morrisey, E.E., Ip, H.S., Lu, M.M., and Parmacek, M.S. (1996). GATA-6: a zinc finger transcription factor that is expressed in multiple cell lineages derived from lateral mesoderm. Dev Biol *177*, 309–322.

Morrisey, E.E., Tang, Z., Sigrist, K., Lu, M.M., Jiang, F., Ip, H.S., and Parmacek, M.S. (1998). GATA6 regulates HNF4 and is required for differentiation of visceral endoderm in the mouse embryo. Genes Dev. *12*, 3579–3590.

Morrison, S.J., and Kimble, J. (2006). Asymmetric and symmetric stem-cell divisions in development and cancer. Nature *441*, 1068–1074.

Moser, A.R., Pitot, H.C., and Dove, W.F. (1990). A dominant mutation that predisposes to multiple intestinal neoplasia in the mouse. Science *247*, 322–324.

Mueller, T.D., and Nickel, J. (2012). Promiscuity and specificity in BMP receptor activation. FEBS Lett. *586*, 1846–1859.

Muñoz, J., Stange, D.E., Schepers, A.G., van de Wetering, M., Koo, B.-K., Itzkovitz, S., Volckmann, R., Kung, K.S., Koster, J., Radulescu, S., et al. (2012). The Lgr5 intestinal stem cell signature: robust expression of proposed quiescent "+4" cell markers. EMBO J. *31*, 3079–3091.

Murakami, G., Watabe, T., Takaoka, K., Miyazono, K., and Imamura, T. (2003). Cooperative inhibition of bone morphogenetic protein signaling by Smurf1 and inhibitory Smads. Mol. Biol. Cell *14*, 2809–2817.

Nakanishi, Y., Seno, H., Fukuoka, A., Ueo, T., Yamaga, Y., Maruno, T., Nakanishi, N., Kanda, K., Komekado, H., Kawada, M., et al. (2013). Dclk1 distinguishes between tumor and normal stem cells in the intestine. Nat. Genet. *45*, 98–103.

Nawijn, M.C., Dingjan, G.M., Ferreira, R., Lambrecht, B.N., Karis, A., Grosveld, F., Savelkoul, H., and Hendriks, R.W. (2001). Enforced expression of GATA-3 in transgenic mice inhibits Th1 differentiation and induces the formation of a T1/ST2-expressing Th2-committed T cell compartment in vivo. J. Immunol. *167*, 724–732.

Neutra, M.R. (1998). Current concepts in mucosal immunity. V Role of M cells in transepithelial transport of antigens and pathogens to the mucosal immune system. Am. J. Physiol. *274*, G785–G791.

Ng, Y.L., Klopcic, B., Lloyd, F., Forrest, C., Greene, W., and Lawrance, I.C. (2013). Secreted Protein Acidic and Rich in Cysteine (SPARC) Exacerbates Colonic Inflammatory Symptoms in Dextran Sodium Sulphate-Induced Murine Colitis. PLoS One *8*.

Nicosia, R.F., Nicosia, S. V, and Smith, M. (1994). Vascular endothelial growth factor, platelet-derived growth factor, and insulin-like growth factor-1 promote rat aortic angiogenesis in vitro. Am. J. Pathol. *145*, 1023–1029.

Nieminen, U., Jussila, A., Nordling, S., Mustonen, H., and Färkkilä, M.A. (2014). Inflammation and disease duration have a cumulative effect on the risk of dysplasia and carcinoma in IBD: A case-control observational study based on registry data. Int. J. Cancer *134*, 189–196.

Nishimoto, S., Hamajima, Y., Toda, Y., Toyoda, H., Kitamura, K., and Komurasaki, T. (2002). Identification of a novel smooth muscle associated protein, smap2, upregulated during neointima formation in a rat carotid endarterectomy model. Biochim. Biophys. Acta - Gene Struct. Expr. *1576*, 225–230.

Nohe, A. (2004). Signal transduction of bone morphogenetic protein receptors. Cell. Signal. *16*, 291–299.

Novinec, M., Kordiš, D., Turk, V., and Lenarčič, B. (2006). Diversity and evolution of the thyroglobulin type-1 domain superfamily. Mol. Biol. Evol. *23*, 744–755.

Novinec, M., Kovačič, L., Škrlj, N., Turk, V., and Lenarčič, B. (2008). Recombinant human SMOCs produced by in vitro refolding: Calcium-binding properties and interactions with serum proteins. Protein Expr. Purif. *62*, 75–82.

Nurwidya, F., Takahashi, F., Kobayashi, I., Murakami, A., Kato, M., Minakata, K., Nara, T., Hashimoto, M., Yagishita, S., Baskoro, H., et al. (2014). Treatment with insulin-like growth factor 1 receptor inhibitor reverses hypoxia-induced epithelial–mesenchymal transition in non-small cell lung cancer. Biochem. Biophys. Res. Commun. *455*, 332–338.

O'Brien, C.A., Pollett, A., Gallinger, S., and Dick, J.E. (2007). A human colon cancer cell capable of initiating tumour growth in immunodeficient mice. Nature *445*, 106–110.

Ohneda, K., Ulshen, M.H., Fuller, C.R., D'Ercole, A.J., and Lund, P.K. (1997). Enhanced growth of small bowel in transgenic mice expressing human insulin-like growth factor I. Gastroenterology *112*, 444–454.

Okada, I., Hamanoue, H., Terada, K., Tohma, T., Megarbane, A., Chouery, E., Abou-Ghoch, J., Jalkh, N., Cogulu, O., Ozkinay, F., et al. (2011). SMOC1 is essential for ocular and limb development in humans and mice. Am. J. Hum. Genet. *88*, 30–41.

Onichtchouk, D., Chen, Y.G., Dosch, R., Gawantka, V., Delius, H., Massagué, J., and Niehrs, C. (1999). Silencing of TGF-beta signalling by the pseudoreceptor BAMBI. Nature *401*, 480–485.

Orkin, S.H. (1998). Embryonic stem cells and transgenic mice in the study of hematopoiesis. Int. J. Dev. Biol. *42*, 927–934.

Pandolfi, P.P., Roth, M.E., Karis, A., Leonard, M.W., Dzierzak, E., Grosveld, F.G., Engel, J.D., and Lindenbaum, M.H. (1995). Targeted Disruption of the Gata3 Gene Causes Severe Abnormalities in the Nervous-System and in Fetal Liver Hematopoiesis. Nat. Genet. *11*, 40–44.

Park, S., Dimaio, T. a, Liu, W., Wang, S., Sorenson, C.M., and Sheibani, N. (2013). Endoglin regulates the activation and quiescence of endothelium by participating in canonical and non-canonical TGF-β signaling pathways. J. Cell Sci. *126*, 1392–1405.

Pinchuk, I. V, Beswick, E.J., Saada, J.I., Suarez, G., Winston, J., Mifflin, R.C., Di Mari, J.F., Powell, D.W., and Reyes, V.E. (2007). Monocyte chemoattractant protein-1 production by intestinal myofibroblasts in response to staphylococcal enterotoxin a: relevance to staphylococcal enterotoxigenic disease. J. Immunol. *178*, 8097–8106.

Pinto, D., Robine, S., Jaisser, F., El Marjou, F., and Louvard, D. (1999). Regulatory sequences of the mouse villin gene that efficiently drive transgenic expression in immature and differentiated epithelial cells of small and large intestines. J. Biol. Chem. *274*, 6476–6482.

Potten, C.S. (1975). Kinetics and possible regulation of crypt cell populations under normal and stress conditions. Bull. Cancer *62*, 419–430.

Potten, C.S. (1977). Extreme sensitivity of some intestinal crypt cells to X and gamma irradiation. Nature *269*, 518–521.

Potten, C.S., and Hendry, J.H. (1975). Differential regeneration of intestinal proliferative cells and cryptogenic cells after irradiation. Int. J. Radiat. Biol. Relat. Stud. Phys. Chem. Med. *27*, 413–424.

Powell, A.E., Wang, Y., Li, Y., Poulin, E.J., Means, A.L., Washington, M.K., Higginbotham, J.N., Juchheim, A., Prasad, N., Levy, S.E., et al. (2012). The pan-ErbB negative regulator lrig1 is an intestinal stem cell marker that functions as a tumor suppressor. Cell *149*, 146–158.

Powell, D.W., Adegboyega, P.A., Di Mari, J.F., and Mifflin, R.C. (2005). Epithelial cells and their neighbors I. Role of intestinal myofibroblasts in development, repair, and cancer. Am. J. Physiol. Gastrointest. Liver Physiol. *289*, G2–G7.

Powell, D.W., Pinchuk, I. V, Saada, J.I., Chen, X., and Mifflin, R.C. (2011). Mesenchymal cells of the intestinal lamina propria. Annu. Rev. Physiol. *73*, 213–237.

Pucilowska, J.B., McNaughton, K.K., Mohapatra, N.K., Hoyt, E.C., Zimmermann, E.M., Sartor, R.B., and Lund, P.K. (2000a). IGF-I and procollagen alpha1(I) are coexpressed in a subset of mesenchymal cells in active Crohn's disease. Am. J. Physiol. Gastrointest. Liver Physiol. *279*, G1307–G1322.

Pucilowska, J.B., Williams, K.L., and Lund, P.K. (2000b). Fibrogenesis. IV. Fibrosis and inflammatory bowel disease: cellular mediators and animal models. Am. J. Physiol. Gastrointest. Liver Physiol. *279*, G653–G659.

Ricci-Vitiani, L., Lombardi, D.G., Pilozzi, E., Biffoni, M., Todaro, M., Peschle, C., and De Maria, R. (2007). Identification and expansion of human colon-cancer-initiating cells. Nature *445*, 111–115.

Rivera, L.B., and Brekken, R.A. (2011). SPARC promotes pericyte recruitment via inhibition of endoglin-dependent TGF-beta1 activity. J. Cell Biol. *193*, 1305–1319.

Rocnik, E.F., Liu, P., Sato, K., Walsh, K., and Vaziri, C. (2006). The novel SPARC family member SMOC-2 potentiates angiogenic growth factor activity. J. Biol. Chem. *281*, 22855–22864.

Le Roith, D., Bondy, C., Yakar, S., Liu, J.L., and Butler, A. (2001). The somatomedin hypothesis: 2001. Endocr. Rev. *22*, 53–74.

Roth, S., Franken, P., Sacchetti, A., Kremer, A., Anderson, K., Sansom, O., and Fodde, R. (2012). Paneth cells in intestinal homeostasis and tissue injury. PLoS One *7*.

Saad, R.S., Liu, Y.L., Nathan, G., Celebrezze, J., Medich, D., and Silverman, J.F. (2004). Endoglin (CD105) and vascular endothelial growth factor as prognostic markers in colorectal cancer. Mod. Pathol. *17*, 197–203.

Saltiel, A.R., and Kahn, C.R. (2001). Insulin signalling and the regulation of glucose and lipid metabolism. Nature *414*, 799–806.

Samad, T.A., Rebbapragada, A., Bell, E., Zhang, Y., Sidis, Y., Jeong, S.J., Campagna, J.A., Perusini, S., Fabrizio, D.A., Schneyer, A.L., et al. (2005). DRAGON, a bone morphogenetic protein co-receptor. J. Biol. Chem. *280*, 14122–14129.

Sangaletti, S., Tripodo, C., Cappetti, B., Casalini, P., Chiodoni, C., Piconese, S., Santangelo, A., Parenza, M., Arioli, I., Miotti, S., et al. (2011). SPARC oppositely regulates inflammation and fibrosis in bleomycin-induced lung damage. Am. J. Pathol. *179*, 3000–3010.

Sangiorgi, E., and Capecchi, M.R. (2008). Bmi1 is expressed in vivo in intestinal stem cells. Nat. Genet. *40*, 915–920.

Sansom, O.J., Meniel, V.S., Muncan, V., Phesse, T.J., Wilkins, J.A., Reed, K.R., Vass, J.K., Athineos, D., Clevers, H., and Clarke, A.R. (2007). Myc deletion rescues Apc deficiency in the small intestine. Nature *446*, 676–679.

Sato, T., Vries, R.G., Snippert, H.J., van de Wetering, M., Barker, N., Stange, D.E., van Es, J.H., Abo, A., Kujala, P., Peters, P.J., et al. (2009). Single Lgr5 stem cells build crypt-villus structures in vitro without a mesenchymal niche. Nature *459*, 262–265.

Sato, T., Stange, D.E., Ferrante, M., Vries, R.G.J., Van Es, J.H., Van Den Brink, S., Van Houdt, W.J., Pronk, A., Van Gorp, J., Siersema, P.D., et al. (2011a). Long-term expansion of epithelial organoids from human colon, adenoma, adenocarcinoma, and Barrett's epithelium. Gastroenterology *141*, 1762–1772.

Sato, T., van Es, J.H., Snippert, H.J., Stange, D.E., Vries, R.G., van den Born, M., Barker, N., Shroyer, N.F., van de Wetering, M., and Clevers, H. (2011b). Paneth cells constitute the niche for Lgr5 stem cells in intestinal crypts. Nature *469*, 415–418.

Savani, R.C., Zhou, Z., Arguiri, E., Wang, S., Vu, D., Howe, C.C., and DeLisser, H.M. (2000). Bleomycin-induced pulmonary injury in mice deficient in SPARC. Am J Physiol Lung Cell Mol Physiol *279*, L743–L750.

Scharpfenecker, M., van Dinther, M., Liu, Z., van Bezooijen, R.L., Zhao, Q., Pukac, L., Löwik, C.W.G.M., and ten Dijke, P. (2007). BMP-9 signals via ALK1 and

inhibits bFGF-induced endothelial cell proliferation and VEGF-stimulated angiogenesis. J. Cell Sci. *120*, 964–972.

Schatton, T., Murphy, G.F., Frank, N.Y., Yamaura, K., Waaga-Gasser, A.M., Gasser, M., Zhan, Q., Jordan, S., Duncan, L.M., Weishaupt, C., et al. (2008). Identification of cells initiating human melanomas. Nature *451*, 345–349.

Schepers, A.G., Vries, R., van den Born, M., van de Wetering, M., and Clevers, H. (2011). Lgr5 intestinal stem cells have high telomerase activity and randomly segregate their chromosomes. EMBO J. *30*, 1104–1109.

Schepers, A.G., Snippert, H.J., Stange, D.E., van den Born, M., van Es, J.H., van de Wetering, M., and Clevers, H. (2012). Lineage Tracing Reveals Lgr5+ Stem Cell Activity in Mouse Intestinal Adenomas. Science (80-.). *337*, 730–735.

Schofield, R. (1978). The relationship between the spleen colony-forming cell and the haemopoietic stem cell. Blood Cells *4*, 7–25.

Scholer-Dahirel, A., Schlabach, M.R., Loo, A., Bagdasarian, L., Meyer, R., Guo, R., Woolfenden, S., Yu, K.K., Markovits, J., Killary, K., et al. (2011). Maintenance of adenomatous polyposis coli (APC)-mutant colorectal cancer is dependent on Wnt/ -catenin signaling. Proc. Natl. Acad. Sci. *108*, 17135–17140.

Schonhoff, S.E., Giel-Moloney, M., and Leiter, A.B. (2004). Minireview: Development and differentiation of gut endocrine cells. Endocrinology *145*, 2639–2644.

Schuijers, J., van der Flier, L.G., van Es, J., and Clevers, H. (2014). Robust Cre-Mediated Recombination in Small Intestinal Stem Cells Utilizing the Olfm4 Locus. Stem Cell Reports.

Schultz, G.S., and Wysocki, A. (2009). Interactions between extracellular matrix and growth factors in wound healing. Wound Repair Regen. *17*, 153–162.

Semenza, G.L. (2012). Hypoxia-inducible factors in physiology and medicine. Cell *148*, 399–408.

Shen, F., Li, J., Cai, W., Zhu, G., Gu, W., Jia, L., and Xu, B. (2013). GATA6 predicts prognosis and hepatic metastasis of colorectal cancer. Oncol. Rep. *30*, 1355–1361.

Shigematsu, S., Yamauchi, K., Nakajima, K., Iijima, S., Aizawa, T., and Hashizume, K. (1999). IGF-1 regulates migration and angiogenesis of human endothelial cells. Endocr. J. *46 Suppl*, S59–S62.

Shimomura, Y., Agalliu, D., Vonica, A., Luria, V., Wajid, M., Baumer, A., Belli, S., Petukhova, L., Schinzel, A., Brivanlou, A.H., et al. (2010). APCDD1 is a novel Wnt inhibitor mutated in hereditary hypotrichosis simplex. Nature *464*, 1043–1047.

Shureiqi, I., Zuo, X., Broaddus, R., Wu, Y., Guan, B., Morris, J.S., and Lippman, S.M. (2007). The transcription factor GATA-6 is overexpressed in vivo and contributes to silencing 15-LOX-1 in vitro in human colon cancer. FASEB J. *21*, 743–753.

Shvab, A., Haase, G., Ben-Shmuel, A., Gavert, N., Brabletz, T., Dedhar, S., and Ben-Ze'ev, A. (2015). Induction of the intestinal stem cell signature gene SMOC-2 is required for L1-mediated colon cancer progression. Oncogene.

Shyer, A.E., Huycke, T.R., Lee, C., Mahadevan, L., and Tabin, C.J. (2015). Bending Gradients: How the Intestinal Stem Cell Gets Its Home. Cell *161*, 569–580.

Simmons, J.G., Hoyt, E.C., Westwick, J.K., Brenner, D.A., Pucilowska, J.B., and Lund, P.K. (1995). Insulin-like growth factor-I and epidermal growth factor interact to regulate growth and gene expression in IEC-6 intestinal epithelial cells. Mol. Endocrinol. *9*, 1157–1165.

Simmons, J.G., Pucilowska, J.B., and Lund, P.K. (1999). Autocrine and paracrine actions of intestinal fibroblast-derived insulin-like growth factors. Am. J. Physiol. *276*, G817–G827.

Sjögren, K., Liu, J.L., Blad, K., Skrtic, S., Vidal, O., Wallenius, V., LeRoith, D., Törnell, J., Isaksson, O.G., Jansson, J.O., et al. (1999). Liver-derived insulin-like growth factor I (IGF-I) is the principal source of IGF-I in blood but is not required for postnatal body growth in mice. Proc. Natl. Acad. Sci. U. S. A. *96*, 7088–7092.

Slattery, M.L., Herrick, J., Curtin, K., Samowitz, W., Wolff, R.K., Caan, B.J., Duggan, D., Potter, J.D., and Peters, U. (2010). Increased Risk of Colon Cancer Associated with a Genetic Polymorphism of SMAD7. Cancer Res *70*, 1479–1485.

Smith, P.D., Smythies, L.E., Shen, R., Greenwell-Wild, T., Gliozzi, M., and Wahl, S.M. (2011). Intestinal macrophages and response to microbial encroachment. Mucosal Immunol. *4*, 31–42.

Souchelnytskyi, S., Nakayama, T., Nakao, A., Morén, A., Heldin, C.H., Christian, J.L., and Ten Dijke, P. (1998). Physical and functional interaction of murine and Xenopus Smad7 with bone morphogenetic protein receptors and transforming growth factor-β receptors. J. Biol. Chem. *273*, 25364–25370.

Speca, S., Giusti, I., Rieder, F., and Latella, G. (2012). Cellular and molecular mechanisms of intestinal fibrosis. World J. Gastroenterol. *18*, 3635–3661.

Stanger, B.Z., Datar, R., Murtaugh, L.C., and Melton, D.A. (2005). Direct regulation of intestinal fate by Notch. Proc. Natl. Acad. Sci. U. S. A. *102*, 12443–12448.

Stearns, M., Tran, J., Francis, M.K., Zhang, H., and Sell, C. (2005). Activated ras enhances insulin-like growth factor I induction of vascular endothelial growth factor in prostate epithelial cells. Cancer Res. *65*, 2085–2088.

Stewart, C.E., and Rotwein, P. (1996). Growth, differentiation, and survival: multiple physiological functions for insulin-like growth factors. Physiol. Rev. *76*, 1005–1026.

Street, M.E., De'Angelis, G., Camacho-Hübner, C., Giovannelli, G., Ziveri, M.A., Bacchini, P.L., Bernasconi, S., Sansebastiano, G., and Savage, M.O. (2004). Relationships between serum IGF-1, IGFBP-2, interleukin-1beta and interleukin-6 in inflammatory bowel disease. Horm. Res. *61*, 159–164.

Sukegawa, A., Narita, T., Kameda, T., Saitoh, K., Nohno, T., Iba, H., Yasugi, S., and Fukuda, K. (2000). The concentric structure of the developing gut is regulated by Sonic hedgehog derived from endodermal epithelium. Development *127*, 1971–1980.

Suzuki, K., Fukui, H., Kayahara, T., Sawada, M., Seno, H., Hiai, H., Kageyama, R., Okano, H., and Chiba, T. (2005). Hes1-deficient mice show precocious differentiation of Paneth cells in the small intestine. Biochem. Biophys. Res. Commun. *328*, 348–352.

Tabaries, S., Dong, Z., Annis, M.G., Omeroglu, A., Pepin, F., Ouellet, V., Russo, C., Hassanain, M., Metrakos, P., Diaz, Z., et al. (2011). Claudin-2 is selectively enriched in and promotes the formation of breast cancer liver metastases through engagement of integrin complexes. Oncogene *30*, 1318–1328.

Takashima, S., Gold, D., and Hartenstein, V. (2013). Stem cells and lineages of the intestine: a developmental and evolutionary perspective. Dev. Genes Evol. *223*, 85–102.

Takeda, N., Jain, R., LeBoeuf, M.R., Wang, Q., Lu, M.M., and Epstein, J.A. (2011). Interconversion Between Intestinal Stem Cell Populations in Distinct Niches. Science (80-.). *334*, 1420–1424.

Tamura, K., Taniguchi, Y., Minoguchi, S., Sakai, T., Tun, T., Furukawa, T., and Honjo, T. (1995). Physical interaction between a novel domain of the receptor Notch and the transcription factor RBP-J kappa/Su(H). Curr. Biol. *5*, 1416–1423.

Termine, J.D., Kleinman, H.K., Whitson, S.W., Conn, K.M., McGarvey, M.L., and Martin, G.R. (1981). Osteonectin, a bone-specific protein linking mineral to collagen. Cell *26*, 99–105.

Terskikh, V. V., Vasiliev, A. V., and Vorotelyak, E.A. (2012). Label Retaining Cells and Cutaneous Stem Cells. Stem Cell Rev. Reports *8*, 414–425.

Theiss, A.L., Fruchtman, S., and Lund, P.K. (2004). Growth factors in inflammatory bowel disease: the actions and interactions of growth hormone and insulin-like growth factor-I. Inflamm. Bowel Dis. *10*, 871–880.

Thomas, J.T., Canelos, P., Luyten, F.P., and Moos, M. (2009). Xenopus SMOC-1 inhibits bone morphogenetic protein signaling downstream of receptor binding and

is essential for postgastrulation development in xenopus. J. Biol. Chem. *284*, 18994–19005.

Tian, H., Biehs, B., Warming, S., Leong, K.G., Rangell, L., Klein, O.D., and de Sauvage, F.J. (2012). A reserve stem cell population in small intestine renders Lgr5-positive cells dispensable. Nature *482*, 120–120.

Tomlinson, I.P.M., Carvajal-Carmona, L.G., Dobbins, S.E., Tenesa, A., Jones, A.M., Howarth, K., Palles, C., Broderick, P., Jaeger, E.E.M., Farrington, S., et al. (2011). Multiple common susceptibility variants near BMP pathway loci GREM1, BMP4, and BMP2 explain part of the missing heritability of colorectal cancer. PLoS Genet. *7*.

Topol, L.Z., Bardot, B., Zhang, Q., Resau, J., Huillard, E., Marx, M., Calothy, G., and Blair, D.G. (2000). Biosynthesis, post-translation modification, and functional characterization of Drm/Gremlin. J. Biol. Chem. *275*, 8785–8793.

Tratwal, J., Mathiasen, A.B., Juhl, M., Brorsen, S.K., Kastrup, J., and Ekblond, A. (2015). Influence of vascular endothelial growth factor stimulation and serum deprivation on gene activation patterns of human adipose tissue-derived stromal cells. Stem Cell Res. Ther. *6*, 62.

Tsuruzoe, K., Emkey, R., Kriauciunas, K.M., Ueki, K., and Kahn, C.R. (2001). Insulin receptor substrate 3 (IRS-3) and IRS-4 impair IRS-1- and IRS-2-mediated signaling. Mol. Cell. Biol. *21*, 26–38.

Usary, J., Llaca, V., Karaca, G., Presswala, S., Karaca, M., He, X., Langerød, A., Kåresen, R., Oh, D.S., Dressler, L.G., et al. (2004). Mutation of GATA3 in human breast tumors. Oncogene *23*, 7669–7678.

Vannahme, C., Smyth, N., Miosge, N., Gösling, S., Frie, C., Paulsson, M., Maurer, P., and Hartmann, U. (2002). Characterization of SMOC-1, a novel modular calcium-binding protein in basement membranes. J. Biol. Chem. *277*, 37977–37986.

Vannahme, C., Gösling, S., Paulsson, M., Maurer, P., and Hartmann, U. (2003). Characterization of SMOC-2, a modular extracellular calcium-binding protein. Biochem. J. *373*, 805–814.

Visnjic, D., Kalajzic, Z., Rowe, D.W., Katavic, V., Lorenzo, J., and Aguila, H.L. (2004). Hematopoiesis is severely altered in mice with an induced osteoblast deficiency. Blood *103*, 3258–3264.

Vogel, J.D., West, G.A., Danese, S., De La Motte, C., Phillips, M.H., Strong, S.A., Willis, J., and Fiocchi, C. (2004). CD40-Mediated Immune-Nonimmune Cell Interactions Induce Mucosal Fibroblast Chemokines Leading to T-Cell Transmigration. Gastroenterology *126*, 63–80.

Waite, K.A., and Eng, C. (2003). From developmental disorder to heritable cancer: it's all in the BMP/TGF-beta family. Nat. Rev. Genet. *4*, 763–773.

Wang, J., Niu, W., Nikiforov, Y., Naito, S., Chernausek, S., Witte, D., LeRoith, D., Strauch, A., and Fagin, J.A. (1997). Targeted overexpression of IGF-I evokes distinct patterns of organ remodeling in smooth muscle cell tissue beds of transgenic mice. J. Clin. Invest. *100*, 1425–1439.

Warren, R.S., Yuan, H., Matli, M.R., Ferrara, N., and Donner, D.B. (1996). Induction of vascular endothelial growth factor by insulin-like growth factor 1 in colorectal carcinoma. J. Biol. Chem. *271*, 29483–29488.

Watson, A.J.M., and Collins, P.D. (2011). Colon cancer: A civilization disorder. In Digestive Diseases, pp. 222–228.

Wechsler, J., Greene, M., McDevitt, M.A., Anastasi, J., Karp, J.E., Le Beau, M.M., and Crispino, J.D. (2002). Acquired mutations in GATA1 in the megakaryoblastic leukemia of Down syndrome. Nat. Genet. *32*, 148–152.

Van de Wetering, M., Sancho, E., Verweij, C., De Lau, W., Oving, I., Hurlstone, A., Van der Horn, K., Batlle, E., Coudreuse, D., Haramis, A.P., et al. (2002). The beta-catenin/TCF-4 complex imposes a crypt progenitor phenotype on colorectal cancer cells. Cell *111*, 241–250.

Whissell, G., Montagni, E., Martinelli, P., Hernando-Momblona, X., Sevillano, M., Jung, P., Cortina, C., Calon, A., Abuli, A., Castells, A., et al. (2014). The transcription factor GATA6 enables self-renewal of colon adenoma stem cells by repressing BMP gene expression. Nat. Cell Biol. *16*, 695–707.

Wight, T.N., and Potter-Perigo, S. (2011). The extracellular matrix: an active or passive player in fibrosis? AJP Gastrointest. Liver Physiol. *301*, G950–G955.

Williams, K.L., Fuller, C.R., Dieleman, L.A., DaCosta, C.M., Haldeman, K.M., Sartor, R.B., and Lund, P.K. (2001). Enhanced survival and mucosal repair after dextran sodium sulfate-induced colitis in transgenic mice that overexpress growth hormone. Gastroenterology *120*, 925–937.

Williams, K.L., Fuller, C.R., Fagin, J., and Lund, P.K. (2002). Mesenchymal IGF-I overexpression: paracrine effects in the intestine, distinct from endocrine actions. Am. J. Physiol. Gastrointest. Liver Physiol. *283*, G875–G885.

Winesett, D.E., Ulshen, M.H., Hoyt, E.C., Mohapatra, N.K., Fuller, C.R., and Lund, P.K. (1995). Regulation and localization of the insulin-like growth factor system in small bowel during altered nutrient status. Am. J. Physiol. *268*, G631–G640.

Wong, V.W.Y., Stange, D.E., Page, M.E., Buczacki, S., Wabik, A., Itami, S., van de Wetering, M., Poulsom, R., Wright, N.A., Trotter, M.W.B., et al. (2012). Lrig1 controls intestinal stem-cell homeostasis by negative regulation of ErbB signalling. Nat. Cell Biol. *14*, 401–408.

Worthley, D.L., Churchill, M., Compton, J.T., Tailor, Y., Rao, M., Si, Y., Levin, D., Schwartz, M.G., Uygur, A., Hayakawa, Y., et al. (2015). Gremlin 1 Identifies a

Skeletal Stem Cell with Bone, Cartilage, and Reticular Stromal Potential. Cell *160*, 269–284.

Yakar, S., Liu, J.L., Stannard, B., Butler, A., Accili, D., Sauer, B., and LeRoith, D. (1999). Normal growth and development in the absence of hepatic insulin-like growth factor I. Proc Natl Acad Sci U S A *96*, 7324–7329.

Yamashita, H., Ichijo, H., Grimsby, S., Morén, A., Ten Dijke, P., and Miyazono, K. (1994). Endoglin forms a heteromeric complex with the signaling receptors for transforming growth factor-β. J. Biol. Chem. *269*, 1995–2001.

Yan, K.S., Chia, L. a, Li, X., Ootani, A., Su, J., Lee, J.Y., Su, N., Luo, Y., Heilshorn, S.C., Amieva, M.R., et al. (2012). The intestinal stem cell markers Bmi1 and Lgr5 identify two functionally distinct populations. Proc. Natl. Acad. Sci. U. S. A. *109*, 466–471.

Yan, Q., Clark, J.I., Wight, T.N., and Sage, E.H. (2002). Alterations in the lens capsule contribute to cataractogenesis in SPARC-null mice. J. Cell Sci. *115*, 2747–2756.

Yan, X., Liu, Z., and Chen, Y. (2009). Regulation of TGF-beta signaling by Smad7. Acta Biochim. Biophys. Sin. (Shanghai). *41*, 263–272.

Yang, Q., Bermingham, N.A., Finegold, M.J., and Zoghbi, H.Y. (2001). Requirement of Math1 for secretory cell lineage commitment in the mouse intestine. Science *294*, 2155–2158.

Yarden, Y., and Shilo, B.-Z. (2007). SnapShot: EGFR signaling pathway. Cell *131*, 1018.

Yu, P.B., Deng, D.Y., Lai, C.S., Hong, C.C., Cuny, G.D., Bouxsein, M.L., Hong, D.W., McManus, P.M., Katagiri, T., Sachidanandan, C., et al. (2008). BMP type I receptor inhibition reduces heterotopic ossification. Nat. Med. *14*, 1363–1369.

Zaki, M.H., Lamkanfi, M., and Kanneganti, T.D. (2011). Inflammasomes and intestinal tumorigenesis. Drug Discov. Today Dis. Mech. *8*.

Zeeh, J.M., Mohapatra, N., Lund, P.K., Eysselein, V.E., and McRoberts, J.A. (1998). Differential expression and localization of IGF-I and IGF binding proteins in inflamed rat colon. J Recept Signal Transduct Res *18*, 265–280.

Zhang, R., Xu, G.-L., Li, Y., He, L.-J., Chen, L.-M., Wang, G.-B., Lin, S.-Y., Luo, G.-Y., Gao, X.-Y., and Shan, H.-B. (2013). The role of insulin-like growth factor 1 and its receptor in the formation and development of colorectal carcinoma. J. Int. Med. Res. *41*, 1228–1235.

Zhang, S., Fei, T., Zhang, L., Zhang, R., Chen, F., Ning, Y., Han, Y., Feng, X.-H., Meng, A., and Chen, Y.-G. (2007). Smad7 antagonizes transforming growth factor beta signaling in the nucleus by interfering with functional Smad-DNA complex formation. Mol. Cell. Biol. *27*, 4488–4499.

Zheng, Q., Wang, Y., Vargas, E., and DiNardo, S. (2011). Magu is required for germline stem cell self-renewal through BMP signaling in the Drosophila testis. Dev. Biol. *357*, 202–210.

Zhu, Y., Ghosh, P., Charnay, P., Burns, D.K., and Parada, L.F. (2002). Neurofibromas in NF1: Schwann cell origin and role of tumor environment. Science *296*, 920–922.

Zimmermann, E.M., Sartor, R.B., McCall, R.D., Pardo, M., Bender, D., and Lund, P.K. (1993). Insulinlike growth factor I and interleukin 1 beta messenger RNA in a rat model of granulomatous enterocolitis and hepatitis. Gastroenterology *105*, 399–409.

Zimmermann, E.M., Li, L., Hou, Y.T., Cannon, M., Christman, G.M., and Bitar, K.N. (1997). IGF-I induces collagen and IGFBP-5 mRNA in rat intestinal smooth muscle. Am. J. Physiol. *273*, G875–G882.